ACTA CARSOLOGICA

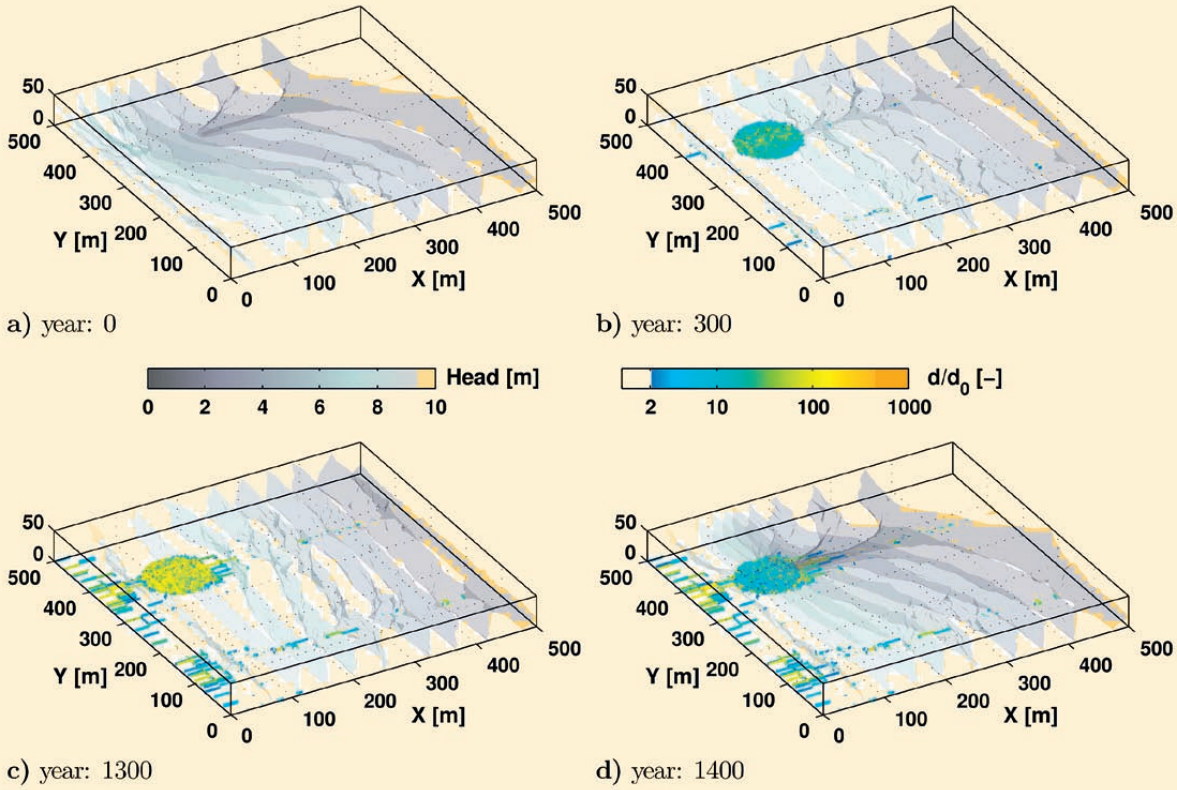

a) year: 0

b) year: 300

c) year: 1300

d) year: 1400

43/2–3 · 2014

ACTA CARSOLOGICA
ISSN 0583-6050

Naslov uredništva / Editor's address:
Inštitut za raziskovanje krasa ZRC SAZU - Karst Research Institute ZRC SAZU
SI - 6230 Postojna, Titov trg 2, Slovenija
Fax: +386 (0)5 700 19 99; e-mail: gabrovsek@zrc-sazu.si

Vsebina je prosto dostopna na spletnem naslovu / The content is freely available at: http://ojs.zrc-sazu.si/carsologica/

Sprejeto na seji IV. razreda SAZU 18. 2. 2014 in na seji predsedstva SAZU 25. 2. 2014.

Distribucija in prodaja / Ordering address:
Založba ZRC/ZRC Publishing
Novi trg 2, P.O.Box 306, SI-1001 Ljubljana, Slovenia
Fax: +386 (0)1 425 77 94; e-mail: zalozba@zrc-sazu.si; http://zalozba.zrc-sazu.si

Acta Carsologica izide trikrat letno / Acta Carsologica is published three times a year

Cena / Price
Posamezni izvod / Single Issue
Individual / Posameznik: 15 €
Institutional / Institucija: 25 €

Letna naročnina / Annual Subscription
Individual / Posameznik: 25 €
Institutional / Institucija: 40 €

Slika na naslovnici: Računalniška simulacija razvoja udornic (gl: Kaufmann *et al.*).

Cover figure: Computer Simulation of the collapse dolines development (see: Kaufmann *et al.*).

ACTA CARSOLOGICA

43/2–3
2014

SLOVENSKA AKADEMIJA ZNANOSTI IN UMETNOSTI
ACADEMIA SCIENTIARUM ET ARTIUM SLOVENICA
Razred za naravoslovne vede – Classis IV: Historia naturalis

ZNANSTVENORAZISKOVALNI CENTER SAZU
Inštitut za raziskovanje krasa – Institutum carsologicum

LJUBLJANA 2014

ACTA CARSOLOGICA je vključena / *is included into:* THOMSON SCIENTIFIC Science Citation Index Expanded, Journal Citation Reports – Science Edition, Zoological Records / Elsevier SCOPUS / Current Geographical Contents / *Ulrich's* Periodicals Directory / COS GeoRef / BIOSIS Zoological Record.

ACTA CARSOLOGICA izhaja s finančno pomočjo / *is published with the financial support of:*
Agencije za raziskovalno dejavnost RS / *Slovenian Research Agency in* Slovenske nacionalne komisije za UNESCO / *Slovenian National Commission for UNESCO*

CONTENTS

VSEBINA

INTERVIEW WITH JEAN NICOD, THE KEY FIGURE OF FRENCH KARSTOLOGY OF THE 20th CENTURY

conducted by IVO LUČIĆ

Interview with Professor Jean Nicod is the shortest in the series of interviews published in Acta Carsologica. His answers are short and precise, as if they were. He is stingy with words, professor Nicod is devoted to the traditional means of communication: he does not use internet and does not pay particular attention to photos. However, he sent us a map of Mediterranean karst, which is published here as an illustration of his work and his approach to karst studies. The interview as is, was completed two weeks before prof. Nicod's ninetieth birthday. Throughout his life he has demonstrated freshness, viability, good memory and dedication to karst research. This interview is a homage to Jean Nicod and his invaluable contributions to karstology.

Professor Nicod, would you tell us how did you become an karstologist?

I was born in 1923 at Vesoul, Haut- Saône, near Jura plateau. In a secondary school I visited caves in the surrounding of Vesoul. As a geography student at the University at Nancy, I described karst features of Haute-Saône plateaus in my graduate thesis. In 1947 I started to work as a secondary school teacher at "Lycée de Marseille" and preparing the doctoral thesis on Limestone morpholog in Basse Provence. In 1967 I defended the thesis at Aix-en-Provence, where I strongly supported the idea that there are different types of karst in the region, from Calanques to the Grand Canyon de Verdon. I introduced the use of hydro-chemical data to determine denudation rates in karst.

As an assistant of geography at the Faculty of Arts of Aix-en-Provence and at Nice, and from 1949 as a Professor at Aix, I presented problems of karst in SE of France at university courses, and during many field trips.

At Aix-en-Provence, the CNRS foundation "Evolution of karst in the Mediterranean and Alpine regions" enabled research of several doctoral students involved in numerous karst regions. Within Groupe "Procope" (Aix-Tübingen 1987–1990) we started the research on erosion and weathering of dolomites, together with Prof. K.-H. Pfeffer from Tübingen.

Which are the most important phases and milestone in karst research, according to your opinion? (the answer is related to the karst research in France)

Until 1960s research had been dispersed among:

- speleologists (E.A. Martel and his followers),
- geologists (work of B. Gèze),
- geomorphologists (successive editions of Emmanuel de Martonne works, chapter "*The Limestone Relief*", strongly influenced by J. Cvijić),
- hydrogeologists.

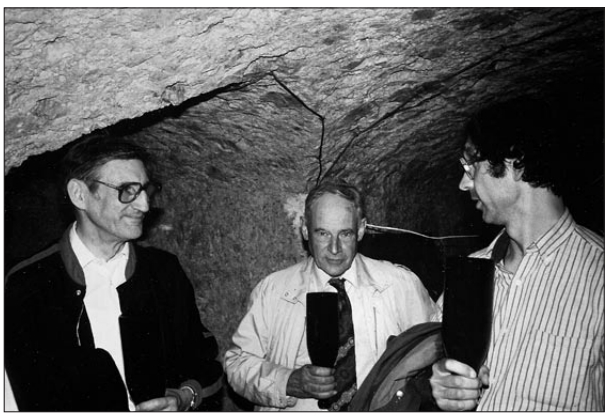

Fig. 1: With Hubert Trimmel and in Richard Maire during »Journées internationales de karstologie en souvenir de Jean Corbel, Metz 1985« in a champagne cellar excavated in chalk (Photo: courtesy J. Nicod).

Commission on Karst Phenomena, founded by the National Committee of Geography, had evolved into the "Association Française de Karstologie " (AFK), founded in 1977, which linked the French karst researchers. It became even more efficient with the journal *Karstologia,* which has been published since 1983. Unfortunately, the commission has not operated since 2000. Recently, howeve, Dr. Nathalie Vanara has been re-establishing the connection between geomorphologists and geographers.

The journal *Karstologia* was initiated in 1983 by Richard Maire and is now published by the EDYTEM of the University of Savoie at Chambéry (2 issues per year). This publication is connected with the "Fédération Française de Spéléologie" (FFS) and its journal *Spelunca.* The FFS assures the distribution of *Karstologia,* its financing and subscription. AFK also publishes

Fig. 2: One of the numerous field trip guided by Prof. Nicod (Photo: courtesy J. Nicod).

"*Karstologia Mémoire*", which mainly comprises thesis and is partially financed by the universities and research centers.

Two researchers initiated the relations between speleological research and geomorphological studies:

- Jean Corbel – doctoral thesis Lyon 1957 – *Les Karsts du Nord-Ouest de l'Europe et des quelques regions de comparison: etude sur le role du climat dan l'erosion des calcaires* (Karsts of NW Europe and other regions: the role of climate on erosion rates in limestone),

- Richard Maire – doctoral thesis Nice 1990 – *La Haute Montagne Calcaire* (Limestone of High Mountain).

J. Corbel was the first to use water analyses to evaluate recent dissolution rate (Karst denudation). R. Maire was the first in France who used isotopic datations to determine evolution phases of a karst system (measurements of speleothems of the Galerie Arandzadi of Pierre-Saint-Martin in the Western Pyrenees, datations made by Y. Quinif at Mons).

What are the most important things in recent karstology: trends, studies and publications?

Beside interdisciplinary work of geologists, hydrogeologists, and bio-speleologists, I have to stress two points:

- The recent importance of paleo-environmental research based on cave sediments (especially speleothems), and the carbonate tufa on the slopes or in the valleys of karst massifs.

- Relations with archaeologists, either in connection with the study of caverns used by man through Prehistory and History, or through the co-operation at datations and study of paleo-environmental conditions.

Numerous French karstologists are working on karst hydrogeology, on the problems of aquifer structure and spring flow, such as the Mediterranean submarine springs. Several speleologists are working with archaeologists. Fine examples are the work of Jean-Jacques Delannoy and colleagues from Chambery in the Chauvet cave (Ardèche) and the work Laurent Bruxelles in the old prehistoric sites in Southern Africa. Historical human presence in numerous caves were also recognized by Christophe Gauchon (1997). The karstologists and speleologists play an important role in the definition of the geomorphosites and the protection of the karst heritage and show caves. Most french karstologists have great interest in environmental problems in kars areas of France and other countries, particularly in Morocco and also in tropical areas (Salomon & Pulina 2005).

Some new trends in karst research in France are given in "*Grottes et karsts de France*", edited by Philippe Audra in 2010:

- the structure of the endokarst related tothe tectonics and paleoclimatic evolution, particularly in the Alpine Karsts: Philippe Audra (1994), Fabien Hobléa (1999) in the Alps, Nathalie Vanara (2000) in the western Pyrenean range,

- relation of karst evolution to the sea-level changes, particularly to the Messinian salinity crisis: research in the karst networks of Languedoc by Hubert Camus (1997) and in Saint-Marcel cave in Ardèche canyon by Ludovic Mocochain (2006),

- the relation between the karst structure and hydrological functioning (base-level control, phreatic or epiphreatic conditions, hypogene caves …),

- dating of karst evolution and paleoclimatic phases by radiometric analyses of speleothems, initiated by Richard Maire (1990) in the Aranzadi gallery of the Pierre-Saint-Martin in western Pyrenean range,

- the studies of the paleokarst and paleoforms, such a giant karrens, megadolines, old caves ghost rock weathering (examples in Southern Causses by Laurent Bruxelles 2001) and their deposits (bauxites, ferricrusts, *terra rossa* etc, recent inventory of the ferricrusts in the Parisian Basin by Jean-Paul Fizaine (2012),

- studies of the geomorphological evolution of the poljes and valleys with fine examples in chalk-karst in Normandy by Joël Rodet (2003), the cover-karst of Barrois by Stéphane Jaillet (2005), the role of karst network in the famous piracy of the upper Moselle by Benoît Losson (2004) and also dating of the stages of deepening by travertines deposits in Quercy-Périgord by Frédéric Hoffmann (2005).

Fig. 3: On a field trip in Chalk karst of Normandy in 2003 (Photo: Nadja Zupan Hajna).

A selection of important recent studies by French karst reserchers:

Audra Ph., 1994: *Karsts alpins, genèse des grands réseaux souterrains*.- Karstologia Mémoire n°5, 279 p.

Bruxelles L., 2001: *Dépôts et altérites des plateaux du Larzac central: Causses de l'Hospitalet et de Campestre (Aveyron, Gard, Hérault). Evolution géomorphologique, conséquences géologiques et implications pour l'aménagement*.- Document BRGM n°304, 266 p.

Camus H., 1997: Formation des réseaux karstiques et creusement des vallées (Larzac-Hérault).- Karstologia, 29, 23–40.

Delannoy J.J., 1997: *Recherches géomorphologiques sur les massifs karstiques du Vercors et de la Transversale de Ronda (Andalousie). Les apports morphogéniques du karst*.- Ed. du Septentrion, Lille, 677 p.

Fizaine J.P., 2012: *Les paléokarsts et les formations ferrugineuses associées dans le Bassin Parisien et ses bordures: caractérisations et évolutions géomorphologiques*.- Thesis Nancy 2, 2 vol., 671 p.

Gauchon Ch., 1997: *Des cavernes et des hommes. Géographie souterraine des montagnes françaises*.- Karstologia Mémoire n°7.

Audra, Ph. (editor), 2010: *Grottes et karsts de France 2010*.- Karstologia Mémoire n°19, 358 p.

Hoblea F., 1999: *Contribution à la connaissance et à la gestion environnementale des géosystèmes karstiques montagnards*.- Thesis. Lyon 2, 995 p.

Hoffmann F., 2005*: Les tufs et travertins en Périgord-Quercy*.- Karstologia Mémoire n°13, 260 p.

Jaillet S., 2005: *Le Barrois et son karst couvert*.- Karstologia Mémoire n°12, 235 p.

Losson B., 2004: *Karstification et capture de la Moselle (Lorraine, F): vers une identification des interactions*.- *Mosella (Metz) XXIX n°1–2, 491 p.*

Maire R.,1990: *La haute montagne calcaire*.- *Karstologia Mémoire* n° 3, 729 p.

Mocochain L., Bigot J.Y., Clauzon G. 2006: La grotte de Saint-Marcel (Ardèche), un référentiel pour l'évolution des endokarsts méditerranéens depuis 6 Ma.- Karstologia,48, 33–50.

Rodet J., 2003: Karst et Craie en Normandie: une approche géographique.- Actes Journées AFK Rouen 2003, p.17–31.

Salomon J.N.et Pulina M., 2005 – Les karsts des régions extrêmes.- *Karstologia Mémoire n°14*, 220 p.

Vanara N. 2000: *Le karst des Arbailles*.- Karstologia Mémoire n°8, 320 p..

How you see Dinaric Karst? With which centers and colleague from Dinaric karst did you have productive cooperation?

The scientific research od Dinaric karst is very important due to multiple reasons: its extent, interdependence between hydrogeology and karst units, the variety of geomorphological types, relations with man's works (double meaning of the term *polje*), and classical landscape.

I gained a lot from Josip Roglić whom I met for the first time in Languedoc in 1968 and with whom I made a field tour through Croatia and Bosnia in 1975. I gained from the International Speleological Congress at Ljubljana 1965, and by visiting Montenegro. Many relations with my Slovene colleagues were of great benefit: Ivan Gams, Peter Habič, Andrej Kranjc. I have attended many meetings, colloquiums, congresses and field trips organized by the Karst Research Institute in Postojna. Thanks to C. Milić I visited the karst of Eastern Serbia in 1980

and the area around lake of Ohrid in Macedonia with D. Manaković (1982).

These numerous meetings and excursions enabled me to write different papers and works: "*Les karsts dinariques, paysages et problems*", co-edited by SAZU (Ljubljana 2003) and l'Association Française de Karstologie.

Which world karst areas you would particularly emphasized and why?

From the most classical and studied I should mention:

- Les Grands Causses (due to E.-A. Martel from the end of the 19th century).
- Jura (in France and Switzerland).
- Schwäbische Alb.
- Different Pre-Alpine massifs of Germany, Austria (especially Dachstein), France (Vercors, Chartreuse, Bauges, Dévoluy, etc.), Italy (Dolomites, Lessini, etc.), Slovenia (Triglav), Switzerland (Hölloch Karst, Siebenhengste, etc.).
- Attached map shows the typology of the Mediterranean Karst.
- Question of springs of Garonne and later the famous Pierre-Saint-Martin attracted international focus upon the karst of Pyrenees.
- In France the karst research intensified recently especially on the plateaus of Ardèche, in Quercy-Périgord, and on the "chalk" karsts of Normandy and Champagne.
- And in Spain (Andalusia) ridges of "Betiques", in Italy Abruzzes, Nizke Tatry in Slovakia, highland karst of Krakow-Czenstochowa in Poland, plateaus of the Middle Atlas in Marocco, Taurus in Turkey, Mt. Lebanon, etc.
- The works of Jakucs on the caves of Transdanubian Mts. in Hungary are reference works on the functioning of hydrothermal karst.
- It was possible to define the evolution types of tropical karst by the karsts of Cuba, Porto-Rico, Jamaica, and Indonesia. But the most extensive and variable are karsts of Southern China (see the studies of R. Maire in collaboration with the institute of Guilin).
- According to the works of G. Rossi and J.-N. Salomon I think that the karst of Madagascar is of great variety and the karst of Yucatan is interesting especially regarding the difficulties of finding water during the ancient civilisation of Maya.

How you see problems of the diffusion of the karst knowledge?

In France, the manual of J.-N. Salomon "*Précis de Karstologie*" (two editions already, 2000 & 2006) is used at the moment. The journals, such as *Acta carsologica* (Ljubljana) or *Spelunca* and *Karstologia* (France) are widely distributed. These journals are read and discussed by scientists as well as by "sport and explorer" speleologists.

Tourist visit of famous sites such as National Park of Plitvice or Grand Canyon of Verdon and caves as Postojna, Aggtelek or Padirac, can be an introduction to many different aspects of karstology for the great public as well as for pupils. It is supported by numerous guide-books and didactical works.

Biography of Prof. Jean Nicod

Born on March 25, 1923 at Vesoul (Haute-Saône Department).

University career:

- Geography "Professor agrégé" (1947).
- Grammar school professor at Nancy, later at Marseille (1947–53 and 1955–57).

Fig. 4: At Doux de Coly in 1992 with Prof. Gams (left) and Michel Chardon (right) (Photo: Fabien Hobléa).

- Researcher probation at CNRS (1953–55).
- Director of the Regional Centre of pedagogical documentation of Marseille (1957–60).
- Assistant and "Maître Assistant" at the Geographical Institute of Aix-en-Provence (1959–65).
- "Maître Assistant" at the Faculty of Arts of Nice (Geographical Section) (1965–68).
- Assistant-Professor (Maître de Conferénces), later Professor at the Geographical Institute of Aix-en-Provence, University of Aix – Marseille II (1968–89).
- Professor Emeritus of the Geographical Institute of Aix-en-Provence (1989–93).

Scientific activities and awards

- The founder of the ERA 282 of the CNRS, at Aix-en-Provence: "*Evolution karstique dans les milieu méditerranéens et alpins*" (Evolution of karst in the Mediterranean and Alpine environments), which later became URA 903 of CNRS (1971–83).
- The president of the Commission of Karst Phenomena and of the National Committee of Geography and of the Karstological Association of France (A.F.K.) (1977–86).

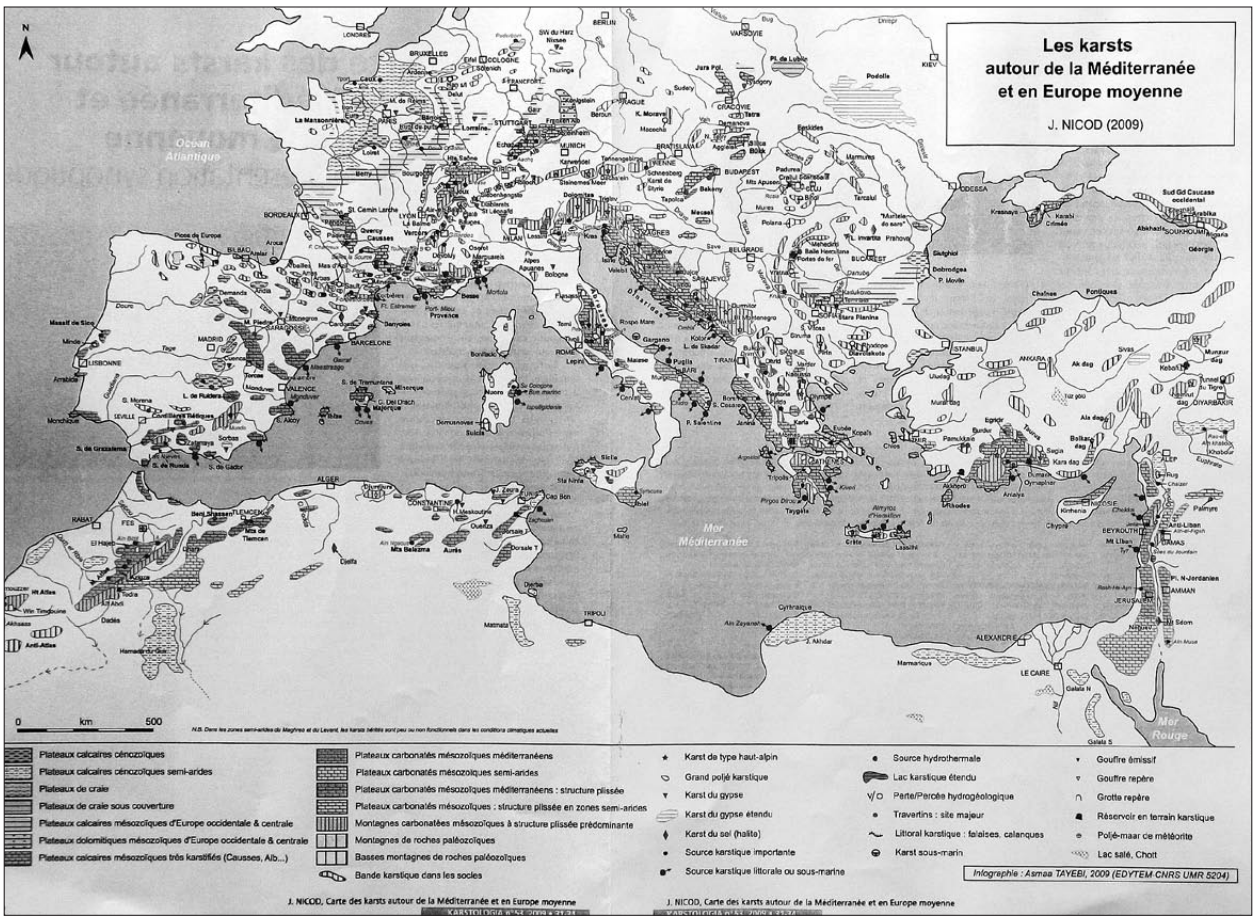

Fig. 5: The map of Mediterranean karst compiled by J. Nicod.

- The co-leader of the Group *Procope* Aix-en-Provence- Tübingen *"Erosion et alteration des Dolomies"* (Erosion and weathering of dolomite) (1987–90), together with Prof. K.-H. Pfeffer.

- Doctor *honoris causa* of the Silesian University (Katowice – Sosnowiec) (1994).

- Corresponding member of the Slovenian Academy of Sciences and Arts (Ljubljana) from 2002.

- Honorary President of the journal *Karstologia.*

N.B. The work *"Karsts et evolutions climatiques – Hommage à Jean Nicod",* (Karst and climate dedicated to Jean Nicod) edited by J.-N. Salomon and R. Maire, Presses Universitaires de Bordeaux (1992), 520 pp.

Thesis* and works on karstology by J. Nicod:

- *Morphological research of limestone Basse-Provence (Thesis Aix-en-Provence 1967) (Louis-Jean, Gap, 1967) 557 pp. + 7 maps in annex.

- Limestone Lands and Landscapes, collection "Le Géographe" SUP (Presses Universitaires de France), Paris, 1972, 244 pp.

- The Dinaric Karsts, paysages and problems, Co-edition Inštitut za raziskovanje krasa, *Carsologica,* ZRC SAZU – Ljubljana 2003 – AFK *Karstologia Mem.,* No. 10, 183 pp., a map in annex.

- Many papers on karst geomorphology and hydrology, on covered karst, paleokarst, gypsum karst, karst springs and use of its water, tufa and travertines, and on different karst sites …, mainly from South-eastern France, Jura, Dinaric lands, and Morocco.

Most recent important contribution:

- Les Gorges de Trévans dans le front subalpin – un site exceptionnel des Alpes de Haute-Provence. *Etudes de Géographie Physique* (Nice) n° XXXVIII, 2011, p. 23–42.

- My last book: Sources et sites des eaux karstiques (Sources and sites of karst water**s**), *Méditerranée,* Special issue, Aix-en-Provence 2012, 277 p.

COBISS: 1.01

THE PROBABLE KARST ORIGIN AND EVOLUTION OF THE VENDICARI COASTAL LAKE SYSTEM (SE SICILY, ITALY)

VERJETNI KRAŠKI IZVOR IN RAZVOJ OBALNEGA JESERSKEGA SISTEMA VENDICARI (JV SICILIJA, ITALIJA)

F. Javier GRACIA[1], Francesco GEREMIA[2], Sandro PRIVITERA[3] & Concetto AMORE[3]

Abstract UDC 551.435.83(450.82)

F. Javier Gracia, Francesco Geremia, Sandro Privitera & Concetto Amore: The probable karst origin and evolution of the Vendicari coastal lake system (SE Sicily, Italy)

The Vendicari coastal lake system (SE Sicily) presents several geomorphic characteristics, which suggest it was originated as a part of a 6 km long karst polje during the Late Pleistocene sea level lowstand. Exhumed cryptokarst karren and terraced concentric surfaces point to this working hypothesis. The generation of this depression could have been favoured by the low to moderate neotectonic activity in the zone, which consisted in slight uplifting and subsequent fracturing. Open joints in the Vendicari Pleistocene carbonates show a radial outline with the prevalence of NNW-SSE discontinuities. Once formed, polje evolution would have consisted in a progressive compartmentalisation and splitting into several polje bottoms, some of which form a part of the present Vendicari lake system and are surrounded by stepped corrosion surfaces. The postglacial sea level rise had drowned most part of the original polje, which can be still recognized in the inner continental shelf. Sea level stabilization after the Holocene eustatic maximum favoured the development of a beach barrier, which generated additional coastal lakes of lagoonal type.

Keywords: Coastal lake, Karst, Polje, Sea level changes, Sicily.

Izvleček UDK 551.435.83(450.82)

Francisco Javier Gracia Prieto, Francesco Geremia, Sandro Privitera & Concetto Amore: Verjetni kraški izvor in razvoj obalnega jezerskega sistema Vendicari (JV Sicilija, Italija)

Obalni jezerski sistem Vendicari (JV Sicilija) predstavlja več geomorfoloških značilnosti, ki kažejo, da je sistem nastal kot del 6 km dolgega kraškega polja med znižanjem gladine morja v poznem Pleistocenu. Razkrite škraplje pokritega krasa in uravnana koncentrična površja kažejo na to delovno hipotezo. Razvoj te depresije bi bil lahko povezan z nizko do zmerno neotektonsko aktivnostjo, ki je zajemala manjša dviganja in posledične razpoke. Odprte razpoke v Pleistocenskih karbonatih področja Vendicari kažejo radialen načrt s prevladujočimi prekinitvami v smeri SSZ-JJV. Ko je polje nastalo, je njegov razvoj zajemal postopno ločevanje in delitev v več polj. Nekatera polja tvorijo današnji obalni sistem Vendicari in so obkrožena s stopničastimi korozijskimi površinami. Dvig morja po glacialnem obdobju je potopil večji del prvotnega polja, ki ga še lahko zasledimo v notranjem kontinentalnem grebenu. Stabilizacija nivoja morja po maksimalnem dvigu vode je bila ugodna za razvoj obalne pregrade, ki je povzročila nastanek dodatnih obalnih jezer lagunskega tipa.

Ključne besede: obalno jezero, kras, polje, spreminjanje nivoja morja, Sicilija.

[1] Dpt. Earth Sciences, Faculty of Marine and Environmental Sciences, University of Cádiz, 11510 Puerto Real, Spain, e-mail: javier.gracia@uca.es

[2] Società Italiana di Geologia Ambientale, Vía Livenza, 6, 00198 Roma, Italia

[3] CUTGANA – Centro Universitario per la Gestione e la Tutela degli Ambienti Naturali e degli Agroecosistemi, Università degli Studi di Catania, Via Terzora 8, 95027 San Gregorio di Catania (CT), Italia.

Received/Prejeto: 04.07.2014

INTRODUCTION

Investigations relating coastal and non-coastal karst evolution are increasing in the last decade, especially in Mediterranean coastal environments (Nicod 1986; Bruno *et al.* 2008; De Waele *et al.* 2011; Canora *et al.* 2012). One of the most important difficulties when studying karst forms in coastal environments lies in the fluctuating location of their base level, represented by the sea level. During the Quaternary, 70 % of the time the sea level was between −30 and −120 m with respect to the present sea level (Purdy & Winter 2001), which means that many forms presently submerged in the inner continental shelf were originally generated under subaerial conditions (Surić 2002; Van Hengstum *et al.* 2011). In karst environments typical submerged forms are marine caves, quite common in Mediterranean coasts, or valleys whose bottoms lie below the present sea level (Gams 2005). The analysis of all these submerged forms supply valuable information on the palaeogeographic evolution of coasts, extent of the area affected by karst processes and by sea level fluctuations, and duration of the lowstand episodes during Quaternary times, and is also useful for evaluating the submerged geological heritage (Taviani *et al.* 2012). In Sicily these outcrops are present throughout the coastal zone and occupy much of the NW and SE sides of the island (Di Maggio *et al.* 2012). However, no descriptions have been made on the interactions between the littoral karst and marine processes and coastal evolution, except in NW Sicily (Ruggieri & De Waele 2014).

The Vendicari area, situated in SE Sicily (36°47'N – 15°05'E), represents a suitable area to study the interaction of karst and marine processes. The site area is in a microtidal, wave-dominated and bedrock-confined coastal environment, where there are evidences of karst processes in Quaternary carbonate shore-platforms and eolianites. It is also characterized by the presence of a sandy dune-beach system *(Bay of Vendicari)* and a coastal lacustrine-palustrine system (Vendicari coastal lakes, locally called "Pantani di Vendicari") with three presently flooded coastal lakes and four ancient coastal wetlands (Fig. 1). In 1984 the Vendicari area was declared "Oriented Natural Reserve" by the Regional Government of Sicily, with the objective of safeguarding migratory and native wildfowl. The "Oasi faunistica di Vendicari" Regional Natural Reserve encompasses 1512 ha, from which 575 are included in an Integral Reserve extended about 8 km along the coast and between 200 and 1300 m inland. The site is also designated as a Special Protection Area under the EC Birds Directive (79/409/EEC) and on 1989 it was included in the Ramsar List of wetlands of international importance.

The aim of this research is to investigate the origin and evolution of the Vendicari area, using historical maps, aerial photos and field observations. The possible origin of the depressions is related to karst processes. Bathymetric information is also used to evaluate the submarine extent of the karst landforms in the area. The

Fig. 1: Location of Vendicari coastal wetlands and lakes. Elaborated from Google Earth (2013).

evolution of the lake/karst system is established in relation to Late Quaternary sea level changes. This contribution presents a working hypothesis by which different indirect evidences point to the generation of a polje during the Late Quaternary, controlled by sea level changes and presently drowned in its most part.

GEOLOGICAL AND GEOMORPHOLOGICAL SETTING

Detailed geological and geomorphological maps of the zone (Figs. 2 and 3) were elaborated through aerial photointerpretation and field work. Two sets of aerial photographs were used for this purpose, one from the Società Aerofotogrammetrica Siciliana, taken in 1977 at 1:4000 scale, and the other from the Società Riprese Aeree di Parma, taken in 1987 at 1:10,600 scale. Data were represented upon an original topographic base at a 1:4000 scale. Bathymetric data were obtained from the nautic chart no. 21 (Da Capo Passero a Capo S. Croce, scale 1:100,000), elaborated by the Italian Istituto Idrografico della Marina.

The Vendicari area is located in the northern border of the Ispica-Capo Passero depression at the South East part of the Hyblean Plateau, a carbonate platform constituted by Late Triassic to Early Pleistocene sediments with some interbedded volcanic levels. It forms part of the northern margin of Africa plate, which is to the North bounded by the thrust front of the allochthonous units. To the East, it is cut off by the Malta escarpment, a large fault system separating the continental shelf from the thinned crust underlying the Ionian Sea (Grasso *et al*. 1992). The Hyblean Plateau includes a wide variety of karst forms (Di Maggio *et al.* 2012), mostly studied by local speleological groups (Ruggieri *et al.* 2009; Ruggieri & Carbone 2010; among others).

The detailed stratigraphy of the Vendicari area is described in Ruggieri (1959) and Lentini *et al*. (1984). Although during the Early Pliocene the Hyblean Plateau was largely emerged, pelagic chalks (Trubi formation) were deposited all around the Vendicari area (Fig. 2). This unit was subsequently folded into gentle anticlines with axial planes oriented around 60°N and normal faults trending 150°N, perpendicularly to the local fold axes (Grasso *et al*. 1992). During Early Pleistocene times biocalcarenites were deposited in shallow marine basins, being afterwards raised up to 150 m along the margins of the depression (Grasso *et al*. 1992). The Quaternary sediments were formed during two main sedimentary cycles. The first one took place in the Lower-Middle Pleistocene and is represented by homogeneously lithified calcarenites mainly composed of fine and medium carbonate particles. The second cycle, covering the Late Pleistocene, is represented by yellow calcarenites composed of medium carbonate particles with typical aeolian oblique and cross-bedded laminae, sometimes disturbed by collapse structures. These are separated from the precedent cycle by lacustrine deposits capped by a palaeosoil at about 1–2 m above the sea. The top of this second sedimentary cycle appears at + 16 m, a height fairly similar to those related to Tyrrhenian deposits recognized along the SE coast of Sicily (Antonioli *et al*. 2006).

The Quaternary tectonic evolution of the Southeast Hyblean Plateau, as well as its fault geometry, were analysed by Adam *et al.* (2000) and Monaco & Tortorici (2000). Since Pliocene times the Hyblean Plateau has suffered brittle deformation in the form of a certain vertical tectonic motion and limited uplift, mainly associated with the activity of some transpressional faults (Antonioli *et al.* 2006). Middle Pleistocene calcarenites onlap the Trubi, and are softly folded (Grasso *et al.* 1992). Deformational processes between Early Pliocene and Late Pleistocene (Tyrrhenian) times in the area were dominated by a well developed trending fault system (Grasso *et al*. 1992): NNE–SSW normal faults control the Ionian coast of Eastern Sicily and continental shelf, while NNW–SSE faults characterize the regional Malta escarpment, among others.

The landscape of the outermost sector of South East Sicily is flat and slowly inclined in direction to the sea, with several fluvial terraces along the Roveto and Saia Scirbia river valleys (Figs. 1 and 2). Their hydrographic basins are 7 km^2 and 35 km^2, respectively. These streams are often dry in the summer months and occasionally communicate with the sea through the coastal lacustrine-palustrine system. Holocene to recent deposits in the area are represented by palustrine and lacustrine deposits in the Pantani sites and mainly a sandy barrier beach with an extensive coastal dune system. In the study area, there are also evidences of erosional forms cut into carbonate units such as cliffs, caves and shore platforms and mainly karst depressions incised in carbonate-cemented marine and aeolian sandstones.

The climate is typically Mediterranean (semi-arid and steppe type) and controlled by seasonal weather patterns: temperate-arid with concentrated rainfall from October to March and insufficient rainfall from April to

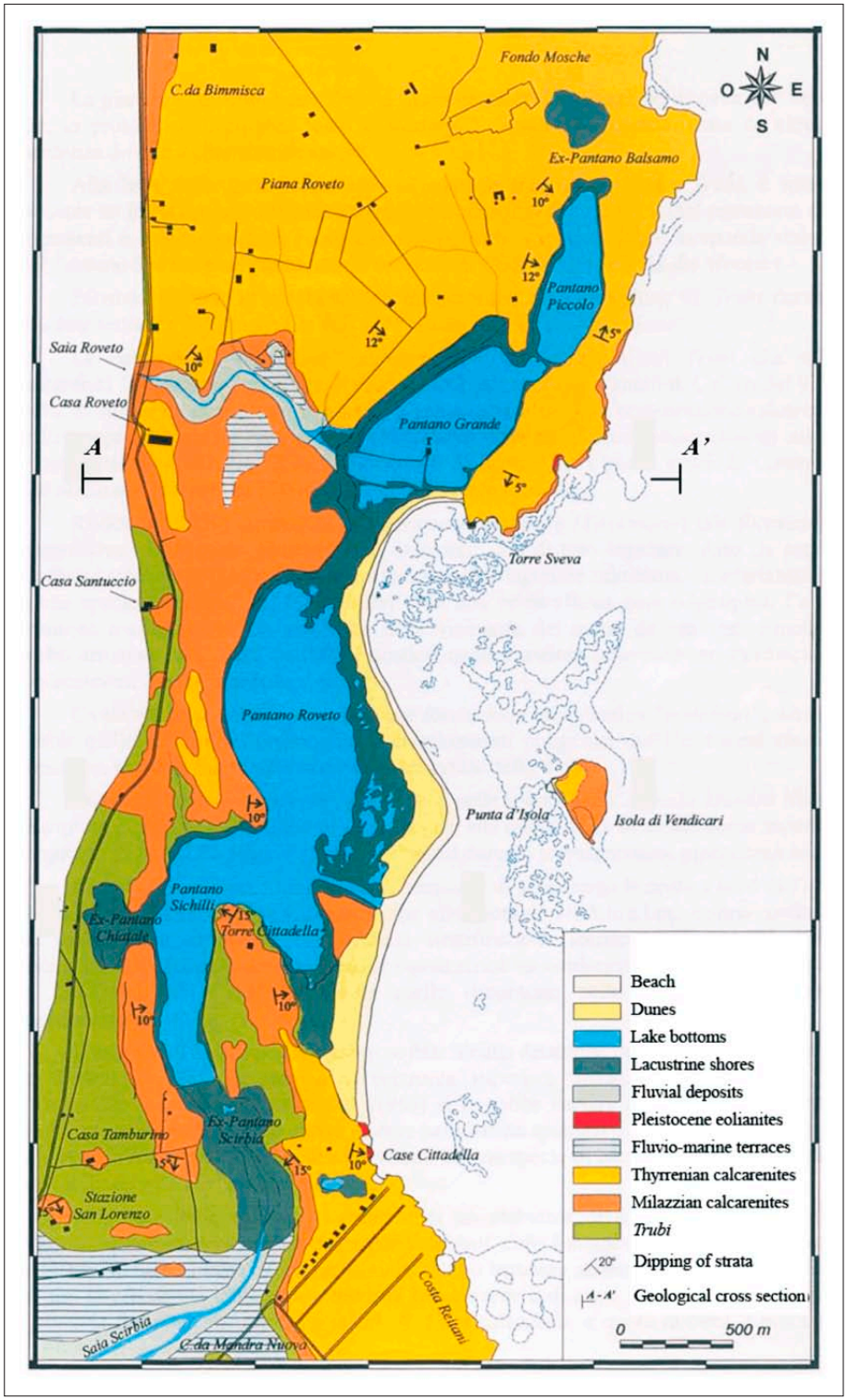

Fig. 2: Geological map of Vendicari area.

September. At the meteorological station of Cozzo Spadaro (Regione Siciliana 1998), located 10 km South of Vendicari, mean annual temperature and precipitation are 18 °C and 400 mm respectively. The Tellàro river is the main source of sediments to the coastal system. It is one of the most important rivers in South Sicily, more than 40 km long, and its mouth is located just 2 km to the north of Vendicari. It forms part of a set of long and deep fluviokarst canyons that strike along the main regional gradients (Di Maggio *et al.* 2012).

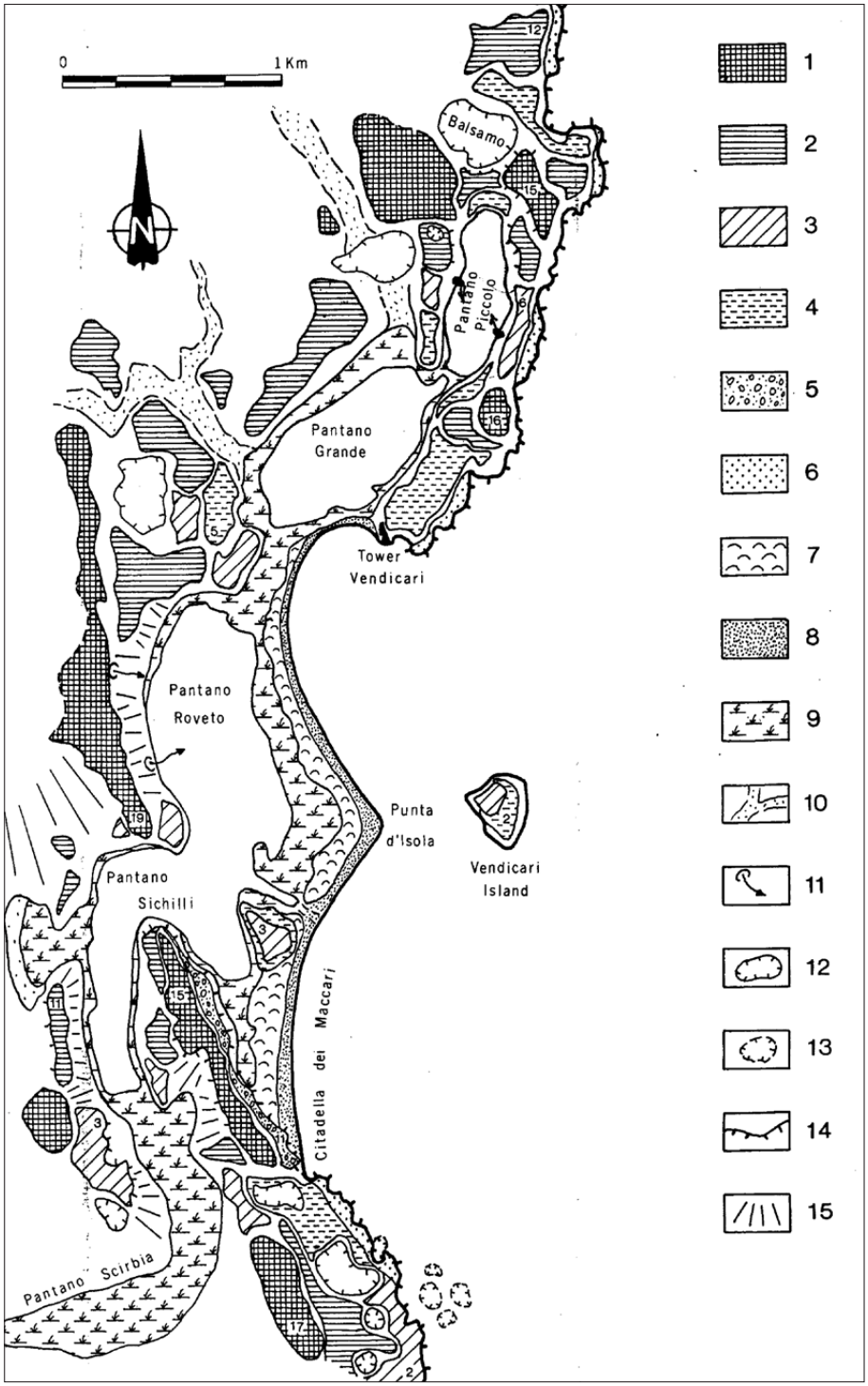

Fig. 3: Geomorphological map of Vendicari coast. Legend: 1-Karst corrosion surface C1; 2- Surface C2; 3-Surface C3; 4-Surface C4; 5-Thyrrenian eolianites; 6-Hanging shore platform (Flandrian?); 7-Dune ridges; 8-Beach; 9-Marshes; 10-Flat bottomed valleys; 11-Spring; 12-Doline; 13-Submerged doline; 14-Escarpment; 15-Gentle slope. Numbers refer to meters above the sea.

The Vendicari coastal lacustrine-palustrine system is composed by seven, ancient and present coastal wetlands and lakes segmented and distributed parallel to the coastline (Fig. 3), with shallow and very flat bottoms. Three of them are permanently flooded although seasonally fluctuating wetlands locally used as salt extraction areas since Greek-Roman times. The northern coastal lagoons (Pantano Piccolo and Pantano Grande) and other ancient lakes and ponds (like Balsamo lake, North of Pantano Piccolo) are restricted from the sea by rocky carbonate ridges about 15–16 m high (Fig. 4), rich of karst meso and microforms (karren, grikes, dolines, etc.). Pantano Scirbia, Sichilli and Roveto form an estuarine depression related to Saia Scirbia River, partly seg-

Tab. 1: Main morphometric characteristics of the Vendicari coastal lakes.

Coastal Lakes	*Balsamo*	*Piccolo*	*Grande*	*Roveto Sichilli*	*Scirbia*	*Chiatale*	*Cittadella*
Surface Area (ha)	4.4	15.6	34	103.5	14	4.4	0.4
Altitude (m)	4.2	0.0	0.0	0.0	0.70	0.70	1.10
Lake shape	Subcircular	Elliptical	Elliptical	Elliptical–Dendritic	Dendritic	Elliptical	Subcircular
Max length (m)	288	775	725	1750	646	375	99
Max width (m)	250	265	427	650	198	162	51
Max depth (m)	0	1	0.5	1	0.5	0	0

Fig. 4: A view of Pantano Piccolo lake to the North from Tower Vendicari area. Note the planated surface developed on carbonates between the lake and the sea.

mented by calcareous ridges. It is a blind estuary, separated from the sea by a cuspate sand barrier. The main morphometric characteristics of these transitional areas are synthesized in Tab. 1.

Most lakes in the Vendicari wetland system are interconnected. Lakes Grande and Piccolo are connected though a narrow pass developed upon the calcareous substratum. Lakes Grande and Roveto are separated by calcareous hills and by marshes. Roverto, Sichilli and Scirbia form part of a single lacustrine depression, partly segmented by low calcareous ridges. Completely dry lakes appear both to the North of Piccolo Lake (Balsamo Lake) and to the South of Sichilli wetland. Their bottoms

Fig. 5: The trace of a littoral freshwater spring can be seen on the western coast of Pantano Roveto lake. Vertical aerial photography taken in 1987, scale 1:10,600 (Società Aerofotogrammetrica Siciliana 1988).

hang some meters above sea level and are separated from the present lakes by calcareous planated ridges.

Water supply to the lakes comes from runoff and from underground fluxes. Pantano Grande lake receives fresh water incomes through several springs located in its western side, both at the rocky slope and on the lacustrine shore (Fig. 5). Lake water levels are linked to the present sea level: there is direct hydrogeological connection between lakes Grande-Roveto-Sichilli and the sea through the Vendicari sandy barrier, while between Pantano Piccolo Lake and the sea water connection is made through fissures and fractures in the intervening rocky ridges.

At present Vendicari lake levels do not fluctuate significantly and their depth is always lesser than 1 m. Sedimentology of the lacustrine sediments of the lakes and recent environmental evolution were previously studied by Amore *et al.* (1994), Amore & Geremia (2001) and Geremia (2000).

RESULTS

The geomorphological map reveals the presence of four stepped planation surfaces with a rough concentric distribution about the bottoms of Sichilli, Grande and Piccolo lakes (Fig. 3). The surfaces horizontally cut all the folded Quaternary units, producing flat surfaces typical of karst environments, where corrosion processes act beneath an alluvial cover (corrosion planation), controlled by the position of the water table (Fabre & Nicod 1982; Ford & Williams 2007). In Vendicari all these corrosion surfaces are inset in relation to a group of surrounding hills developed on Pliocene chalks. The slopes between different stepped corrosion surfaces show convex-concave longitudinal profiles. Lakes Pantano Grande and Pantano Piccolo are separated from the sea by calcareous ridges on which the four planation surfaces are also present.

Surface C1 develops between +15–19 m above the sea, forming a very continuous ridge in a structurally controlled NNW-SSE direction, only interrupted by the Pantano Sichilli estuarine lake. Remains of this surface can be also recognized SW of Sichilli lake and surrounding Pantano Piccolo lake, in the northern sector. This can be considered as the highest corrosion surface in the zone and also the less preserved one.

Surface C2 develops between +10–12 m above the sea, almost completely surrounding Balsamo, Piccolo and Sichilli lakes. It forms the northern and NW limits of Grande and Roveto lakes. This surface can be also recognized to the south of Cittadella as a coastal planated rim which continues some distances to the south of the studied zone.

Surface C3 develops between +3–6 m above the sea and appears discontinuosly surrounding Piccolo, Roveto and Sichilli lakes and also to the South of Cittadella.

Surface C4 develops between +1–2 m above the sea surrounding Balsamo, Piccolo and Grande lakes. It also appears in Vendicari Island (Fig. 6) and to the south of Cittadella.

The planation levels display a considerable degree of karstification, with pan-shaped dolines and extensive karren development. Most karren morphologies can be identified on the surfaces, like hohlkarren, kluftkarren, small grikes and kamenitzas, as well as ruiniform micromorphologies (Fig. 7), that were generated beneath a soil cover. Although soil is still present covering some portions of the surfaces, most of them are presently bare and hence the existing karren can be considered as mostly exhumed, a common characteristic of karst corrosion

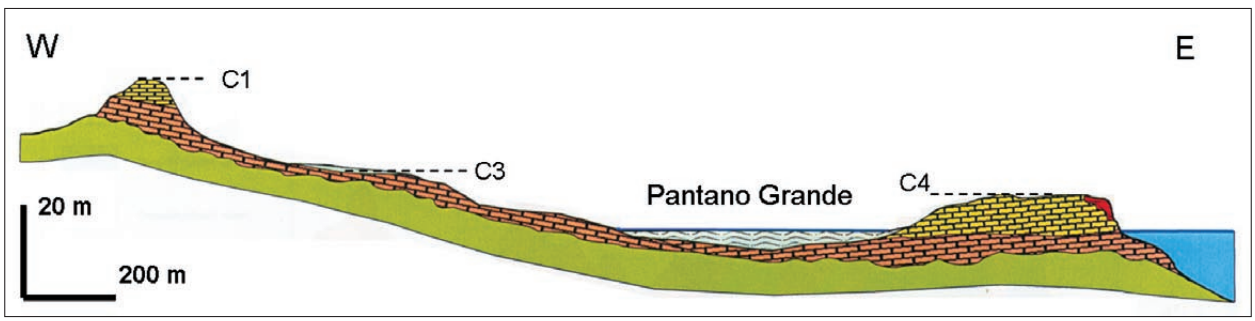

Fig. 6: Geological/Geomorphological cross section A-A' of the Vendicari lake system. See location of the cross-section A-A' and legend in Fig. 2.

Fig. 7: Exhumed karren developed upon corrosion surface C1, north of Pantano Piccolo lake.

surfaces in the Mediterranean region (Gracia *et al.* 2003). It is worth to note that these types of karren are very different from those developed on the present rocky shore platforms of the zone, represented by typical pits, small pinnacles and roughly irregular surfaces.

Kluftkarren and grikes are controlled by the fracture pattern affecting the Pleistocene carbonates. All of them are vertical open joints (up to 30 cm) filled with lateral carbonate crusts, red clays (terra rossa) and small clasts. Systematic measurement of discontinuities all along the zone shows a radial distribution with a significant concentration of joints at NNW-SSE (Fig. 8). A very minor secondary family of discontinuities appears in a normal, NE-SW direction.

Other karst forms present in the zone are dolines, usually of low depth and not well defined margins. There

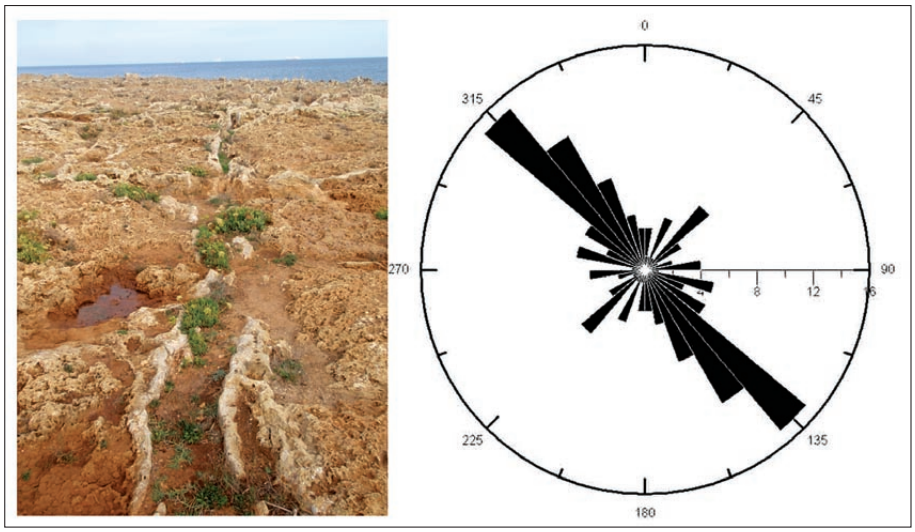

Fig. 8: Left, open vertical joint affecting Late Pleistocene carbonates and filled with calcareous crusts and terra rossa. Right, rose diagram of fractures affecting Quaternary units in Vendicari coastal zone (87 data; radial length represents percentage of data in each direction).

Fig. 9: Aerial photography showing several submerged dolines and a coastal captured doline to the south of Cittadella. Photo taken in 1987, scale 1:10,600 (Società Aerofotogrammetrica Siciliana 1987).

is a special concentration of dolines to the south of Cittadella, where coastal retreat has produced the capture of a coastal doline, which presently forms a small semicircular microbay with vertical walls. In the same sector, at least four submerged dolines can be recognized close to the shore, developed on submerged carbonates, at about 2 m depth, which could be considered as possible drowned dolines (Fig. 9). Morphological control of coastal sinkholes in the development of coastal inlets and bays has been also reported in other Italian regions (Bruno *et al.* 2008; Basso *et al.* 2013).

Available bathymetric and textural data of surface sediments from nautical charts show different rocky outcrops in the sublittoral zone and inner continental shelf together with other submerged shallow depressions covered by loose sands. The rocky outcrops form two very continuous strips NNW-SSE oriented and levelled at a broadly constant depth (Fig. 10). The first one, 1 km far from the coastline, is levelled at about 8 m depth, while the second one, 2 km far from the shoreline, develops at –14–17 m. The intervening area between the first strip and the coast, as well as that existing between both submerged outcrops, form flat-bottomed closed or semi-closed depressions, at –11 m and –25–28 m depth respectively. Out from this rocky sublittoral zone, the continental shelf shows a progressively deeper sandy bottom with no rocky outcrops.

DISCUSSION ABOUT THE EVOLUTION OF THE KARSTIC DEPRESSION

The submerged morphology of the sublittoral and inner shelf zones draws a complex closed depression with a flat bottom limited by carbonate outcrops, levelled at roughly constant depths. These characteristics are quite similar to those of karst poljes, depressions commonly developed along the Mediterranean karst regions (Gospodarič & Habič 1979; Julian & Nicod 1989; Gracia *et al.* 2002, 2003; Parise 2006). The almost closed nature of the submerged depression, its connection to a coastal area with stepped planation surfaces and the presence of other submerged closed depressions on carbonates suggest a karst origin linked to the generation and development of a polje, which at present is mostly drowned. The genesis of poljes is related to the corrosional lowering of the land surface, commonly beneath a loose, permeable and non-karst cover, usually alluvial or soil cover (crypto corrosion; Fabre & Nicod 1982). The genesis of a cryptocorrosion surface requires the exhumation of the soil-bedrock contact by erosion processes of any kind (like water erosion by runoff, glacial erosion, or marine erosion in coastal areas like in the Vendicari case). Dismantling of the soil cover may be produced by vegetation cover decrease due to climatic aridification, or to relative base level lowering and rejuvenation of the fluvial-runoff erosion, or a combination of them. The deepening of the polje bottom progresses until the topography reaches the level of frequent inundation and then the corrosion processes tend to expand the polje bottom by retreat of the marginal slopes (Ford & Williams 2007). The sequence of four-stepped levels of corrosion surfaces represents alternating periods, some of them dominated by deepening and others by planation and expansion of the polje bottom, always controlled by the position of the water table. In coastal environments poljes can develop seasonal or permanent lakes, according to sea level (Bonacci 1987; Nicod 2003).

The N-S succession of interconnected closed depressions excavated on carbonates could be interpreted as an uvala. In reality it is not easy to differentiate uvalas and poljes. Cvijić (1893) considered that uvalas were genetically an intermediate stage between dolines and poljes and concluded that it is difficult to clearly differ between uvalas and poljes. In the description and classification of poljes made by Gams (1978) intermediate terms can be found, like uvala-like-polje, polygenetic polje or compound polje. Nicod (2003) indicates that some poljes may proceed from connection of previous uvalas. Diagnostic indicators of poljes with respect to uvalas are: flat bottom (uvalas usually have uneven bottom), karst inflow and outflow, terraced corrosion levels, steep slopes surrounding the bottom, tectonic origin or control and relationship with water table, among others. A discussion about this topic can be found in Frelih (2003). An additional diagnostic indicator in favour of the polje hypothesis is the recognition of cryptocorrosion markers, since cryptocorrosion is a genetic process typical of poljes (Fabre & Nicod 1982; Nicod 2003): hohlkarren, kluftkarren, etc., are very different from the typical coastal phytokarst micromorphologies (Ford & Williams 2007). The absence of these cryptokarren morphologies does not discard the polje hypothesis, but their presence is an argument in favour of the latter. These morphologies are present in all the surfaces surrounding Vendicari lakes, and the depressions also fulfill all the other requirements to be considered as a polje.

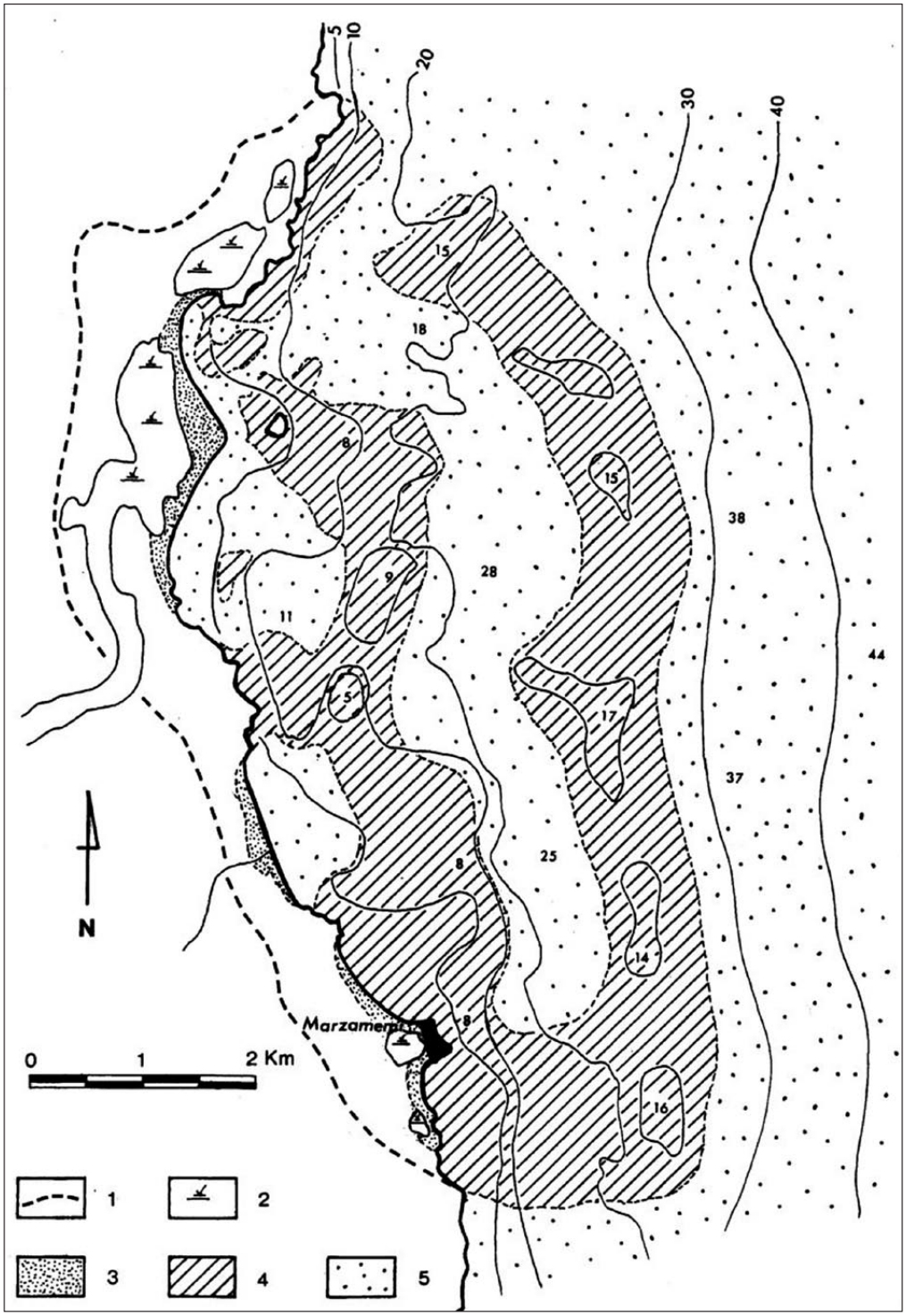

Fig. 10: Bathymetric and morphological map of the submerged bottoms in the vicinity of Vendicari coast, elaborated from data included in the Italian nautic chart no. 21, at 1:100,000 scale (Istituto Idrografico della Marina 1999). 1-emerged limit of the corrosion surfaces; 2-wetlands; 3-beaches; 4-rocky outcrops of submerged carbonates; 5-submerged sand sheets. Numbers refer to meters below sea level.

The enveloping line enclosing the corrosion surfaces and the submerged depression draws an approximate figure of the original karst depression, which could have reached about 6 km long in a N-S direction, and width of over 5 km (Fig. 10). Height difference between the highest emerged corrosion surface and the deepest submerged bottom is slightly higher than 40 m. These dimensions are relatively modest if compared with other typical Mediterranean poljes (Gracia *et al.* 1996; Gams 2005). Some poljes identified in the Venetian Prealps are smaller (usually less than 5 km long) and typically deep, with more than 200 m of vertical difference between the

surrounding summits and the polje bottoms (Lehman 1959). Instead, the Canale di Pirro polje, in Apulia (SE Italy) is located on a wide planated zone and has an overall length of some 30 km (Parise 2006). Several poljes have been identified in the North and NW zones of Sicily (Trapani, Palermo and Madonie mountains), all of them exhibiting dimensions lesser than 8 km^2 and controlled by faults (Di Maggio *et al.* 2012).

Although drowned karst features are widely cited in the literature (Paskoff & Sanlaville 1978; Ford & Williams 2007) and some coastal poljes have been referred in the Mediterranean context (Peña-Monné *et al.* 2008), not many examples exist regarding submerged poljes. Gavazzi (1904) describes in Croatia the coastal freshwater lakes of Vransko Jezero (South East of Zadar) and Vransko Jezero (Cres Island) as polje floors, deepened when sea level was lower and transformed into lakes when sea level raised their bottoms. Some deep submarine depressions south of Florida have been interpreted as karst features (Jordan 1954). Jennings (1985) describes large karst depressions beneath the sea in Šibenik harbour (Croatia) and the Bay of Kotor (Montenegro), while the Novigrad Bay (Istria, Croatia) is regarded by this author as a polje invaded by the sea. Other examples of coastal or drowned karstic depressions are cited by Gams (2005) in the Dalmatian coast, or by Taviani *et al.* (2012) in the Italian Adriatic coast and continental shelf. It is very likely that in karst coasts where many originally subaerial morphologies (dolines, caves) are at present submerged in the sublittoral zone due to sea level rise, poljes can also be found below present sea level. The scarcity of previous cites referring drowned poljes probably is due to their shape and dimensions (wide, flat depressions) and their natural tendency to be filled with marine sediments, which would obliterate their original aspect. Only in the case of poljes recently drowned by the last eustatic cycle and located in coasts with little sediment supplies they would still maintain at present great part of their original morphology below sea level. This seems to be the case of Vendicari, where the subhorizontal disposition of the carbonate series surely favoured the development of a wide depression with low depth.

Many poljes have a tectonic origin or at least a strong structural control (Gams 1978; Julian & Nicod 1989; Gracia *et al.* 2003; Di Maggio 2012). The longitudinal development of these depressions following active or neotectonic faults is a common indicator of this relationship. Eastern Sicily is considered as a region submitted to tectonic movements during the Late Pleistocene. Antonioli *et al.* (2006) concluded that the Hyblean Plateau is experiencing a mean uplift rate of 85 mm/ka, according to the elevations of MIS 5.5 deposits, probably because of the effects of the near offshore Malta Escarpment, a NNW-SSE active fault of regional importance. Open joints measured in Vendicari indicate that prevailing directions of fracturing are parallel to the Malta Fault, which would confirm the hypothesis of Antonioli *et al.* (2006). The slight rate of uplift would also be justified by the radial distribution of minor fractures and joints (Fig. 8). Furthermore, the general outline of the Vendicari submerged polje presents a clear control of the NNW-SSE structural trend, which also conditions the orientation of the Marzamemi rocky coast, south of Vendicari (Fig. 10). Hence, it could be assumed that a slight uplift during the Late Pleistocene, especially supported by Malta Fault-parallel fractures, would have been the responsible for the primary generation of a gentle tectonic depression NNW-SSE oriented. As a consequence, the high density of open fractures would have enhanced karst dissolution, which led to the initiation of corrosion planation processes and subsequently to the formation of a polje.

In contrast with continental poljes, where the stepping of corrosion surfaces is typically linked to falling episodes in the karst base level, in Vendicari the hydrological base level is represented by the sea level. In Vendicari coastal area, carbonate-rock aquifers have been probably karstified during the Late Pleistocene sea-level lowstand.

The subaerial corrosion surfaces at Vendicari are indicative of the height reached by the relative sea level in different moments along the Late Quaternary. In this sense, the regional highest altitude reached by the Thyrrenian marine terraces is + 15 m above the sea (Antonioli *et al.* 2006). Small sea level oscillations around that level as well as the later sea level fall during the last glaciation should have brought about the stepping of karst surfaces and the subsequent compartmentalisation and splitting of the original depression into other minor ones – the present Grande, Piccolo and Balsamo lakes, and maybe the depression encompassing Roveto and Sichilli lakes. The topographic lowering associated with the polje bottom deepening would have also favoured the incision of the Saia Scirbia river (Figs. 1 and 3), which probably continued to the NNE crossing the northern margin of the polje (Fig. 10). Subsequently, postglacial sea level/base level rise produced sedimentary deposition in the lakes, as well as the transformation of the lower Saia Scirbia river valley into a progressively infilling estuary. The estuary was closed by the post-glacial growth of a confining sand barrier, where a cuspate sandy foreland formed in the Punta d'Isola has intermittently functioned as a tombolo in historical times.

CONCLUSIONS

The formation, variability and configuration of Vendicari coastal lakes are strongly influenced by inherited geological factors at long-term temporal scale like relative sea-level fluctuations, regional tectonic setting and mainly karst processes. This is an unusual case of coastal lakes produced by karst processes, especially if we consider the broad context where the lakes were generated: a probable Late Pleistocene polje presently drowned in the inner shelf, still recognizable through nautical charts. Its development and the generation of up to four stepped corrosion surfaces give an idea about the velocity at which poljes and other similar karst depressions can be formed under favourable conditions like those converging in coastal environments: enhanced carbonate dissolution and rapid base level (e.g. sea level) fluctuations. Slow to moderate tectonic uplifting during the Late Pleistocene very probably favoured the stepping of the surfaces, by progressive water table lowering. Prevailing orientation of joints, as well as of the drowned polje itself, suggest that regional stress field, controlled by the Malta Fault, were the responsible for the genesis of the depression, which subsequently evolved by karst corrosion processes during the last sea level lowstand.

Theoretically submerged poljes may present a very low preservation potential, linked to their tendency to be filled with marine sediments in the medium-long term. Only poljes recently drowned during the last eustatic cycle and located in coasts with little sediment supplies would still maintain at present great part of their original morphology below sea level. This seems to be the case of Vendicari, which gives it an additional interest.

Once the polje was drowned after the last sea level rise, during Holocene and recent times the sea level stabilization on a height roughly similar to the present one favoured the prevalence of coastal transport and deposition processes. As a consequence, a beach barrier developed closing the pre-existing karst-originated coastal embayment.

ACKNOWLEDGEMENTS

The authors are very grateful to the Ispettorato Ripartimentale delle Foreste di Siracusa, Administrator of Vendicari Natural Reserve, for logistic field support. This work is a contribution to Research Group RNM-328 of the Plan Andaluz de Investigación.

REFERENCES

Adam, J., Reuther, CD, Grasso, M. & L. Torelli, 2000: Active fault kinematics and crustal stresses along the Ionian margin of southeastern Sicily.- Tectonophysics, 326, 217–239.

Amore, C., Costa, B., Di Geronimo, S., Giuffrida, E., Randazzo, G. & A. Zanini, 1994: Temporal evolution, sediments and fauna of the Vendicari lagoons (Siracusa).- Bolletino della Società Paleontologica Italiana, 2, 1–15.

Amore, C. & F. Geremia, 2001: Evolutionary Model of a microtidal and wave-dominated coastal wetland system in Sicily (Italy). In: Mascle, J. (ed.) *Marine Geosciences, Proceeding of the 36° CIESM Congress*, 24th–28th September 2001, Monaco, Rapp. Comm. Int. Mer Médit., 349, Monaco,

Antonioli, F., Kershaw, S., Renda, P., Rust, D., Belluomini, G., Radtke, U. & S. Silenzi, 2006: Elevation of the last interglacial highstand in Sicily (Italy): A benchmark of coastal tectonics.- Quaternary International, 145–146, 3–18.

Basso, A., Bruno, E., Parise, M. & M. Pepe, 2013: Morphometric analysis of sinkholes in a karst coastal area of southern Apulia (Italy).- Environmental Earth Sciences, 70(6), 2545–2559.

Bonacci, O., 1987: *Karst Hydrology: with Special Reference to the Dinaric Karst*.- Springer-Verlag, pp. 184, Berlin.

Bruno, E., Calcaterra, D. & M. Parise, 2008: Development and morphometry of sinkholes in coastal plains of Apulia, southern Italy. Preliminary sinkhole susceptibility assessment.- Engineering Geology, 99, 198–209.

Canora, F., Fidelibus, M.D. & G. Spilotro, 2012: Coastal and inland karst morphologies driven by sea level stands: a GIS based method for their evaluation.- Earth Surface Processes and Landforms, 37, 1376–1386.

Cvijić, J., 1893: *Das Karstphänomen*.- Versuch einer morphologischen Monographie. Geographische Abhandlungen, B.5, H.3, pp. 113, Wien.

De Waele, J., Lauritzen, S.E. & M. Parise, 2011: On the formation of dissolution pipes in Quaternary coastal calcareous arenites in Mediterranean settings.- Earth Surface Processes and Landforms, 36, 143–157.

Di Maggio, C., Madonia, G., Parise, M. & M. Vattano, 2012: Karst of Sicily and its conservation.- Journal of Cave and Karst Studies, 74, 2, 157–172.

Fabre, G. & J. Nicod, 1982: Modalités et role de la corrosion cryptokarstique dans les karst méditerranéens et tropicaux.- Zeitschrift für Geomorphologie, N.F. 22, 209–224.

Ford, D. & P. Williams, 2007: *Karst Hydrogeology and Geomorphology*.- John Wiley & Sons, pp. 562, Chichester.

Frelih, M., 2003: Geomorphology of karst depressions: Polje or uvala – A case study of Lučki Dol.- Acta Carsologica, 32, 2, 105–119.

Gams, I., 1978: The polje: the problem of definition.- Zeitschrift für Geomorphologie, 22, 170–181.

Gams, I., 2005: Tectonics impact on poljes and minor basins (case Studies of Dinaric karst).- Acta Carsologica, 34, 1, 25–41.

Gavazzi, A., 1904: *Die seen des karstes*.- I.Th. Morpholog. Material. Abhandl. Geogr. Gesel., 5, 2, Wien.

Geremia, F., 2000: *Evoluzione morfologica e dinamica sedimentaria dei "Pantani di Vendicari" (Sicilia sud-orientale).*- Doctoral Thesis, University of Messina, pp. 195.

Google Earth, 2013: Satellite imagery ellaborated from DigitalGlobe and TerraMetrics. Tele Atlas North America, Inc.- [Online] Available from: https://earth.google.com/ [Accessed 15th November 2013].

Gospodarič, R. & P. Habič, 1979: Karst phenomena of Cerknisko polje.- Acta Carsologica, 8, 150–162.

Gracia, F.J., Gutiérrez, F. & M. Gutiérrez, 1996: Los poljes de la región de Layna (Cordillera Ibérica noroccidental).- Cuaternario y Geomorfología, 19, 3–4, 33–45.

Gracia, F.J., Gutiérrez, F. & M. Gutiérrez, 2002: Origin and evolution of the Gallocanta polje (Iberian Range, NE Spain).- Zeitschrift für Geomorphologie, 46, 245–262.

Gracia, F.J., Gutiérrez, F. & M. Gutiérrez, 2003: The Jiloca karst polje-tectonic graben (Iberian Range, NE Spain).- Geomorphology, 52, 3–4, 215–231.

Grasso, M., Reuther, C.D. & L. Tortorici, 1992: Neotectonic deformations in SE Sicily: the Ispica Fault, evidence of Late Miocene-Pleistocene decoupled wrenching within the central Mediterranean stress regime.- Journal of Geodynamics, 16, 1–2, 135–146.

Istituto Idrografico della Marina, 1999: *Da Capo Passero a Capo S. Croce, 21. 1:100 000*.- Genova.

Jennings, J.N., 1985: *Karst Geomorphology*.- Basil Blackwell, pp. 293, Oxford.

Jordan, G.F., 1954: Large sink holes in Straits of Florida.- American Association of Petroleum Geologists Bulletin, 38, 1810–1817.

Julian, M. & J. Nicod, 1989: Les karsts des Alpes du Sud et de Provence.- Zeitschrift für Geomorphologie, Suppl. Bd. 75, 1–48.

Lehmann, H., 1959: *Studien über Poljen in den Venezianischen Voralpen und im Hochappennin*. Erdkunde 13.

Lentini, F., Di Geronimo, I., Grasso, M., Carbone, S., Sciuto, F., Scamarda, G., Cugno, G., Iozzia, S. & M. Romeo, 1984: Carta geologica della Sicilia sud-orientale, 1:100,000. Ed. S.EL.CA., Firenze.

Monaco, C. & L. Tortorici, 2000: Active faulting in the Calabrian Arc and eastern Sicily.- Journal of Geodynamics, 29, 407–424.

Nicod, J., 1986: Les karsts littoraux, directions et methodes d'étude.- Travaux U.A. 903 C.N.R.S. 15, 13–19.

Nicod, J., 2003: A little contribution to the karst terminology: Special or aberrant cases of poljes?- Acta Carsologica, 32, 2, 29–39.

Parise, M., 2006: Geomorphology of the Canale di Pirro Karst Polje (Apulia, Southern Italy).- Z. Geomorph. N.F., Suppl. 147, 143–158.

Paskoff, R. & P. Sanlaville, 1978: Observations geomorphologiques sur les cotes del'archipel Maltais.- Zeitschrift für Geomorphologie, 22, 310–328.

Peña-Monné, J.L., De Dapper, M., Constante, A., De Vliegher, B. & K. Pavlopoulos, 2008: El sistema de poljes de la región de Dystos-Almyropotamos (Isla de Eubea, Grecia): Cartografía y evolución geomorfológica.- Geographicalia, 53, 143–161.

Purdy, E.G. & E.L. Winter, 2001: Origin of atoll lagoons.- Geological Society of America Bulletin, 113, 7, 837–85.

Regione Siciliana, 1998: *Climatologia della Sicilia*.- Assessorato Agricoltura e Foreste Gruppo IV – unità di Agrometeorologia. Vol. 2, pp. 239, Palermo.

Ruggieri, G., 1959: Geologia della zona costiera di Torre Vendicari (Sicilia sudorientale).- Rivista Mineraria Siciliana, 55, 10, 12–14. Palermo.

Ruggieri, R., Carbone, S. & I. Galletti, 2009: Un géomorphosite: les Monts hybléens (sud-est de la Sicile).- Karstologia, 54, 11–20.

Ruggieri, R. & S. Carbone, 2010: Tectonic and karstic morphogenetic evolution of the Northeastern sector of the Hyblean Plateau (Southeast Sicily).- Speleologia Iblea 14, 229–255.

Ruggieri, R. & J. De Waele, 2014: Lower-to Middle Pleistocene flank margin caves at Custonaci (Trapani, NW Sicily) and their relation with past sea levels.- Acta carsologica, 43, 1, 11–22.

Societá Aerofotogrammetrica Siciliana, 1988: *1987 Aerial photographs of Sicily, 1:10,600*.- Palermo.

Surić, M., 2002: Submarine karst of Croatia – Evidence of former lower sea levels.- Acta Carsologica, 31, 3, 89–98.

Taviani, M., Angeletti, L., Campiani, E., Ceregato, A., Foglini, F., Maseli, V., Morsilli, M., Parise, M. & F. Trincardi, 2012: Drowned karst landscape offshore the Apulian Margin (Southern Adriatic Sea, Italy).- Journal of Cave and Karst Studies, 74, 2, 197–212.

Van Hengstum, P.J., Scott, D.B., Gröcke, D.R. & M.A. Charette, 2011: Sea level controls sedimentation and environments in coastal caves and sinkholes.- Marine Geology, 286, 35–50.

COBISS: 1.01

MORPHOLOGICAL STUDY OF RED LAKE IN DINARIC KARST BASED ON TERRESTRIAL LASER SCANNING AND SONAR SYSTEMS

MORFOLOŠKA ŠTUDIJA CRVENEGA JEZERA V DINARSKEM KRASU NA PODLAGI TERESTIČNEGA LASERSKEGA SKENIRANJA IN SONARNEGA SISTEMA

Ivo ANDRIĆ[1] & Ognjen BONACCI[1]

Abstract UDC 556.55:528.8(497.5)
551.435.8:528.8(497.5)

Ivo Andrić & Ognjen Bonacci: Morphological study of Red lake in Dinaric karst based on terrestrial laser scaning and sonar system

Red Lake (Dinaric karst, Croatia) is an exceptional karst phenomenon, worldwide known for its beauty and extreme depth. Even so, through the history of Red Lake's research there were many controversies in the conclusions and the theories concerning its genesis, geomorphology and hydrology. The aim of this work is to give an overview of existing findings about Red Lake as well as to present the newest research results gained with the help of emerging technologies based on terrestrial laser scanning and hydro acoustics. The measuring was conducted during September 2013. A new generation of equipment developed to advance the geoscientific research was deployed during the field work. The gathered data enabled a thorough analysis which led to new important findings on Red Lake. Deployment of Remotely operated underwater vehicle (ROV) equipped with imaging sonar resulted in the first hydro acoustic survey of the lake. Some of the results confirmed the already known and well documented characteristics of Red Lake whereas others disputed the widely accepted assumptions in the scientific community and the general public. The presented research generated, for the first time, a DEM for Red Lake which allowed a good estimate on the lake's volume. For the recorded maximum water level at 311 m a.s.l. the volume of water stored is 8.24 x 10^6 m^3. A temperature profile of the lake was recorded during the field work and it offered an insight on possible water mixing through karst conduits near the surface of the water. The application of TLS and ROV sonar systems considerably improved the understanding of Red Lake's morphology.

Keywords Lidar, Sonar, Red Lake (Croatia), Dinaric karst.

Izvleček UDK 556.55:528.8(497.5)
551.435.8:528.8(497.5)

Ivo Andrić & Ognjen Bonacci: Morfološka študija Crvenega jezera v Dinarskem krasu na podlagi terestičnega laserskega skeniranja in sonarnega sistema

Crveno jezero (Dinarski kras, Hrvaška) je izjemen kraški pojav, po vsem svetu poznan po svoji lepoti in skrajnih globinah. Kljub temu je bilo v zgodovini raziskav Crvenega jezera veliko polemik v sklepih in teorijah o njegovem nastanku, geomorfologiji in hidrologiji. Namen tega dela je podati pregled obstoječih spoznanj o jezeru, kakor tudi predstaviti najnovejše rezultate raziskav, pridobljenih s pomočjo novih tehnologij, ki temeljijo na terestičnega laserskega skeniranja in hidroakustike. Raziskave so potekale septembra 2013. Nova generacija opreme, razvite za napredovanje geoznanstvenih raziskav, je bila uporabljena med delom na terenu. Zbrani podatki so omogočili temeljito analizo, ki je privedlo do novih pomembnih ugotovitev o Crvenem jezeru. Uporabili smo podvodno vozilo na daljinsko upravljanje (ROV), opremljeno z imaging sonarjem, ki je prineslo prve hidroakustične raziskave jezera. Nekateri rezultati so potrdili že znane in dobro dokumentirane značilnosti jezera, medtem ko so drugi izpodbijali splošno sprejete predpostavke znanstvene skupnosti in širše javnosti. V raziskavi prvič predstavljamo DEM za Crveno jezero, kar je omogočilo oceno o njegovem obsegu. Za najvišji zabeleženi nivo vode na 311 m nadmorske višine je ocenjena količina shranjene vode 8,24 x 10^6 m^3.Temperaturni profil jezera je bil posnet med delom na terenu in je ponudil vpogled v možno mešanje vode s kraških kanalov, blizu površini vode. Uporaba TLS in ROV sonarnega sistema je precej izboljšal razumevanje morfologije jezera.

Ključne besede: Lidar, sonar, Crveno jezero (Hrvaška), Dinarski kras.

[1] Faculty of Civil Engineering, Architecture and Geodesy, Split University, 21000 Split, Matice hrvatske str. 15, Croatia
E-mail addresses: ivo.andric@gradst.hr (I. Andrić); obonacci@gradst.hr (O. Bonacci)

Received/Prejeto: 29.01.2014

INTRODUCTION

Red Lake (local name "Crveno jezero") near the town of Imotski (Croatia) represents an impressive surface karst feature in the Dinaric karst with extreme dimensions. The first mention of Red and Blue Lake in literature is over a century old (Cvijić 1893), but since then there have been a few scientific researches. There is a general disagreement in the literature over defining Red and Blue Lake as sinkholes, caves, cenotes, lakes or other karst features. Some of the older researchers argue that both lakes are collapsed dolines. Younger authors argue that Red Lake is a cave, and their conclusions are based on the classification of Union International de Spéléologie (UIS). From a hydrological point of view, Blue Lake Blue Lake has been investigated more, and recent results were published in the paper (Bonacci *et al.* 2014).

Although the lakes exhibit extreme karst topography, the lack of related scientific work and especially scientific papers published in international journals is evident. The insufficiency in scientific research of Red Lake lies primarily in the difficulties that arise during hydrological and geomorphologic measurements. Because of the inaccessible nature of the local terrain and the extremely steep slopes above the lake shores, measurements are very difficult to obtain, expensive and even dangerous (Bonacci *et al.* 2014).

The application of Terrestrial Laser Scanning (TLS) for precise modelling of land relief and quantitative and qualitative estimations of spatial and temporal alterations can contribute to better understanding of the processes shaping the area (Abellán 2006; Oppikofer *et al.* 2008). This particular remote sensing tool was used to acquire topographic datasets with high accuracy and spatial resolution of Red Lake's geometry model above the water table.

The modern robotic technology, such as ROVs, is used successfully for scientific research, mostly in deep-sea exploration (Bachmayer *et al.* 1998; Yoerger *et al.* 2007). Industrial work-class ROVs are designed to support a great variety of oceanographic instrumentation, navigate precisely, and provide comprehensive multimodal data-collection ((Bachmayer *et al.* 1998). This work represents the results of ROV deployment for the purposes of morphological investigation of Red Lake's submerged part. Because of Red lake's great depth over 260 m (Petrik 1960; Garašić 2001), the deployment of ROV was necessary to evaluate lake's geometry at its bottom.

This was the first instance of using emerging technologies in order to obtain the morphometry of this exceptional karst phenomenon. The performed morphological measurements during September 2013, should significantly contribute to the clarification of some unknown attributes of Red Lake. The measures revealed numerous new facts that differ to a great extent from those specified in the existing literature. This work will give an overview of existing facts and summarized conclusions from the publications which deal with the nature of Red Lake.

STUDY AREA

Red Lake presents one of the world's deepest submerged karst features (Garašić 2001) and some authors believe that Red Lake is one of the most spectacular collapsed dolines in the world (Sauro 2005). It is located in the central part of the bare Dinaric karst region. Located in its immediate vicinity, only approximately 500 m to the east, is Blue Lake (local name "Modro jezero"). Fig. 1 is a location map showing the area around Red and Blue Lake as well as the hydrological features such as surface stream flows, significant natural karst water phenomenon (Prološko Blato natural retention, Red Lake and Blue Lake) and the locations of three reservoirs.

Fig. 2 shows on the satellite image of both lakes. Red Lake is permanently filled with water, whereas Blue Lake dries up periodically (Bonacci 2006; Bonacci *et al.* 2014).

The study area is located at the periphery of the Mediterranean climate belt, with a strong influence of continental climate. It is located only 20 km from the Adriatic Sea, but it is separated from the sea by the Biokovo Mountain chain, which has a maximum altitude of 1762 m a.s.l. The average annual air temperature in the catchment varies from 12 °C (northern higher part) to 14 °C (southern lower part) with a minimum daily temperature in January below 0 °C, and a maximum daily temperature in July and August higher than 35 °C. The annual rainfall ranges from 750 to 2,350 mm with an average of about 1,500 mm. The maximum rainfall occurs in October and November, and the minimum in July and August. In spite of relatively numerous geological, hydrogeological (especially groundwater tracing) and hydrological investigations

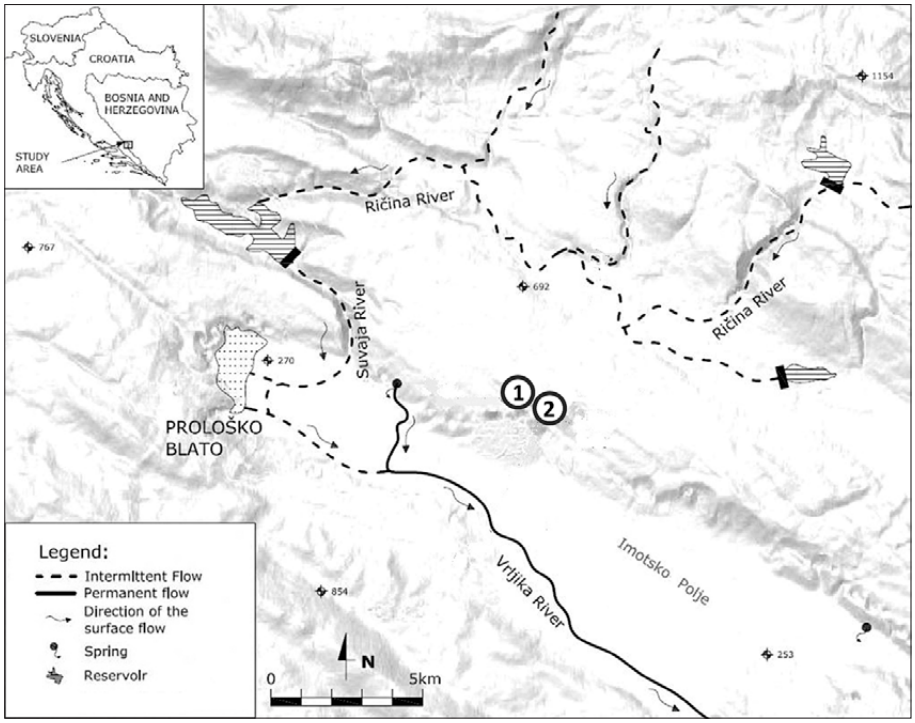

Fig. 1: Location map of the study area with the locations of Red (1) and Blue Lake (2) (Bonacci et al. 2014).

in study area, it has not been possible to define either the catchment boundaries or the directions of groundwater circulation in different hydrological situations during different regional groundwater levels (Bonacci 2006). The reason for this is the extremely complex surface and underground karst morphology.

Fig. 3 represents the geological sketch of the area around Red and Blue Lake, which is a part of the Outer or karstic Dinaric Alps (Herak 1986).

The carbonate rocks of the area are predominantly limestones, and only partly dolomites of Tertiary and Cretaceous formations. The dolomites do not consider-

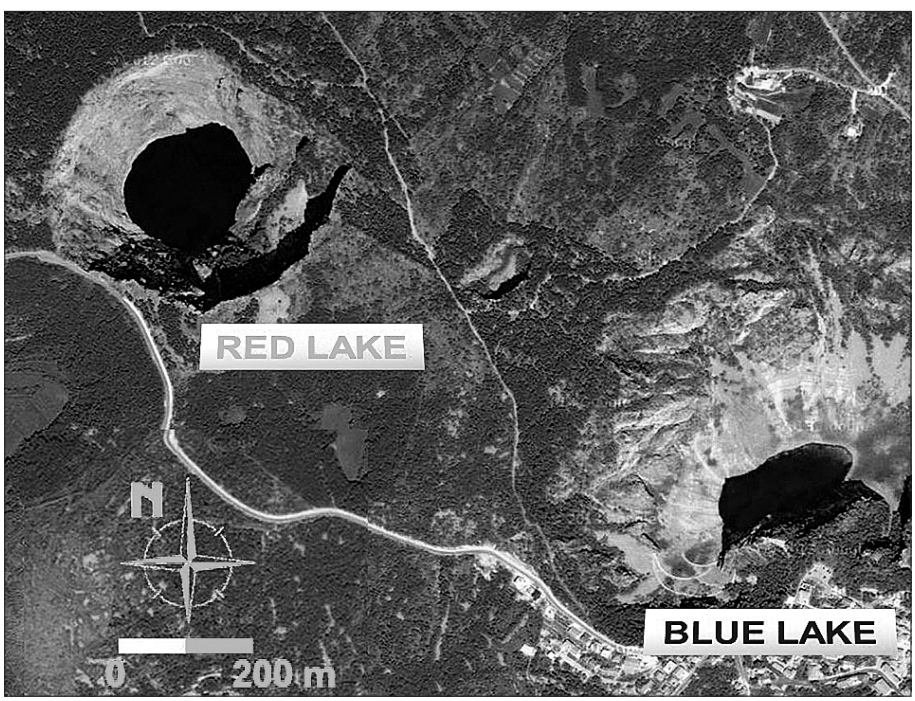

Fig. 2: Satellite photograph of Blue and Red Lakes (Google Maps 2010).

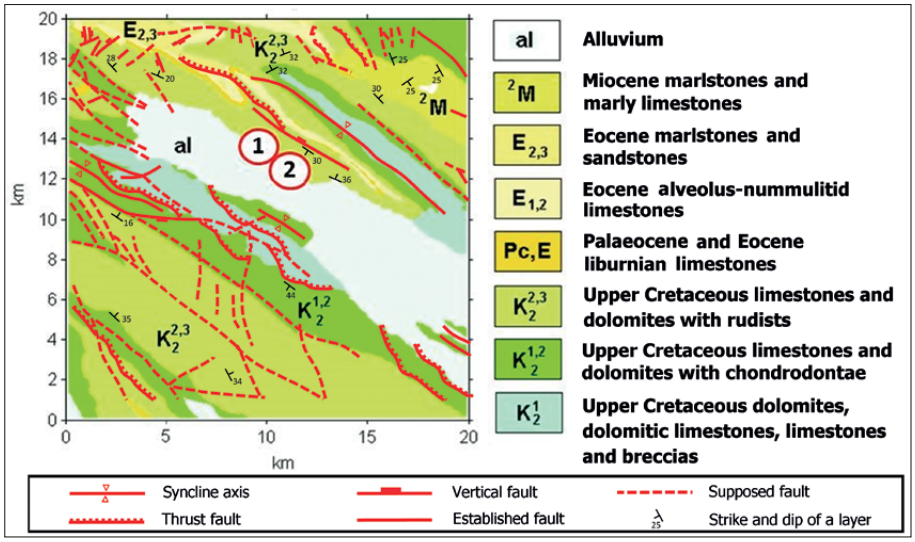

Fig. 3: Geological sketch of the area around Red (1) and Blue (2) Lake (partly after Basic Geological Map of SFRY 1:1,000,000, sheet: Imotski).

ably obstruct groundwater flows. Lower Cretaceous dolomites and thin bedded limestones make underground barriers to groundwater flow. Only after extremely intensively precipitations, water table in the limestone, as well as in the broader study area rises up to the surface (Bonacci 2006).

OVERVIEWS OF THE EXISTING LITERATURE

At the end of the nineteenth and the beginning of the twentieth century Cvijić (1896), Grund (1903), Gavazzi (1903/04) and Daneš (1905) published the first scientific papers about Red and Blue Lake.

Cvijić (1896) established a hypothesis that both depressions were formed by collapsing of the "cave ceiling".

Roglić (1938) suggests that both phenomena are cylindrical shaped dolines, at the same time he excludes the possibility that both lakes functioned as a sinkhole in the past. According to Roglić (1974) a doline is defined as a simple, solitary funnel-shaped and closed karst depression, which is drained at the bottom. It is always wider than deeper and it is formed by corrosion processes and the mechanical activity of surface water and groundwater in areas of karst fissures crossings, resulting in intense water sinking and limestone solution.

Petrik (1960) believes that Red Lake is the youngest doline of all ten significant dolines around the town of Imotski. In the period between April 1955 and June 1956, Petrik was undertaking numerous hydrographic measurements in this region. He measured the highest and the lowest point on Red Lake's rim at 522.9 m a.s.l. and 425.4 m a.s.l. respectively. An estimation was given that Red Lake bottom altitude is 4.1 m a.s.l. At the water level of 254.6 m a.s.l., Petrik (1960) calculated the surface area of the lake of 32,900 m^2.

During the period of measurements, the highest and lowest water levels were recorded at 274.45 m a.s.l. and 252.78 m a.s.l. respectively. The amplitude of water level oscillations of Red Lake measured by Petrik (1960) was 21.67 m. He calculated that at the water level of 254 m a.s.l. water loss from the lake is 89 l/s.

Petrik (1960) also estimated that at water level of 268 m a.s.l. the volume of water in Red Lake is at least 6 x 10^6 m^3. Hydrological regime of Red and Blue Lake is considered different and it is assumed that they have no significant relationship with the hydrological regime of Imotski Polje and surrounding area.

Milanović (1981) sees Blue and Red Lake as dolines, by formation the type that usually occurs as a result of the chemical action of water on limestone.

Bahun (1991) analyzes the genesis of Red and Blue Lake in his work. For him, whether Red Lake is a doline or cave is not a problem of terminology problem, rather, it is important from the point of forming of the karst phenomena. Bahun (1991) believes that both lakes are in the carbonate environment and that either lithological or tectonic characteristics did not give a predisposition for the development of these features. His conclusions are substantially different from all previously presented and therefore they

will be fully quoted: "The results of analysis of the sequence of geological events and of the present hydrogeological relations and the development of the morphology of the wider area of Red and Blue Lake, allow the reconstruction of surroundings in the late Miocene. Northeast of today's Imotski Polje existed a vast lake at elevation of 400–500 m. Back then, there was an elevated region between the lake and the sea. Water from the lake flowed through sinkholes to a lower surface level. Neotectonic caused the differential disturbance of terrain and the area of the former lake got dissected so that some parts were relatively elevated to the present level at 900 m a.s.l., and some parts were relatively lowered, such as Imotsko Polje, to the current elevation of 260 m a.s.l. Such movements caused the lake to dry up, sinkholes were left without water so by their exogenous influenced destruction and side collapsing they were turned into a huge sinkhole (Blue Lake) or deep pits (Red Lake). Permanent water and its oscillations in Red Lake as well as the occasional flooding of Blue Lake are the results of the dynamics of underground karst water. It flows through the karst underground of the area from the upper parts in the north and northeast to the erosion base – Neretva River in the east and to the Adriatic Sea in the south."

Garašić (2001, 2012) reports the results of the international cave diving expedition in Red Lake, which took place during September and October 1998. According to him, Red Lake is a water reservoir with a minimum of 16×10^6 m^3 of water. He does not specify whether it is a volume of stored water in the lake or the maximum volume defined by the geometry of the lake. He claims that at the bottom of Red Lake there is a strong flow, in other words an underground river. Garašić (2001, 2012) lists the following important results of this expedition: (1) a cave inlet was found east of the lake at the depth of 175 m, measuring 30 x 30 m; (2) new species of cave fish and shrimp as well as frogs and insects in the lake and its immediate environment have been found and specified; (3) the deepest point on the bottom of the lake at an elevation of 6 m below sea level has been measured which established a new maximum depth of Red Lake of 528.9 m; (4) at depths below 50 m, a constant water temperature of 7.9 °C was measured; and (5) the westward movement of groundwater in the bottom of the lake was registered.

Kovačević (1999) suggests that water from Red Lake will leak when the level rises up to a cave on the west side, and that the leak stops when the water level drops. Local residents claimed that the water from these caves overflows in the spring Jažva. Gavazzi (1903/04) documents the existence of this cave and Cvijić (1960) also writes about it. Roglić (1938, 1954) and Petrik (1960 did not register the cave's position) during their field research, although its existence was previously documented. The international cave diving expeditions in 1998 recorded more than 300 m of channels of this cave. On November 29th, 2011 the cavers from Imotski Caving Club had the chance to explore the very same dried up cave. At that point, the historically lowest water level of the Red Lake was recorded at 228 m a.s.l. The cave's influence on the hydrological regime of the lake can partly explain why the maximum water level in Red Lake is lower than the maximum water level in Blue Lake.

Williams (2004) provides the following information about Red Lake: "The deepest known case of collapse doline containing a lake is the Crveno Jezero (Red Lake) in Croatia, which is 528 m deep from its lowest rim, the bottom of the collapse extending 281 m below the modern level of the nearby Adriatic Sea. The collapse diameter at the surface is about 350 m and at lake level is about 200 m. Recent diving has found an active subterranean river that crosses the doline near its floor. The whole feature is thought to have been formed by progressive upwards collapse of cave roof, much of the collapse debris having been transported away by underground river."

Gams (2005) found the reasons for the deep lowering of the bottom of Red Lake in the regional seismic activity that is still present. He notes that seismic station near Imotski registered in the period 1946–1989 the strongest earthquake of 7 degree of MCS. Gams (2005) mentioned that the earthquake that occurred in 1942 reduced the depth of Blue Lake and caused a massive rock fall event in Red Lake. He assumes that the bottom of Red Lake is covered with a thick layer of collapsed rock material.

Bonacci *et al.* (2013) mention Red and Blue Lake as two exceptional karst phenomena in the complex system of sinking, losing and underground transboundary karst rivers, lakes and aquifers in the central part of the deep and bare Dinaric karst in Croatia and Bosnia and Herzegovina.

METHODS

In order to obtain an accurate computer model of Red Lake's geometry above the water table the Terrestrial 3D Laser Scanner (TLS) was used. This instrument is also known as a Ground based LIDAR (Light Detection and

Ranging system). TLS is one of the most promising remote sensing techniques for slope monitoring because of its capability to accurately acquire dense three-dimensional (3-D) coordinates of the terrain (Bauer *et al.* 2005; Biasion *et al.* 2005; Oppikofer *et al.* 2008). A TLS point cloud data set of the slopes above Red Lake's shores was acquired using a ILRIS 3D Optech™ laser scanner (Intelligent Laser Ranging and Imaging System). Operation of the TLS is based on stationary distance and its data sampling rate is up to 2,500 pt/s. The laser pulse has a wavelength of 1,500 nm and a maximum measurable distance of 1,250 m at 80 % reflectivity. Range measurement can be undertaken using the first or the last pulse of the return signal; the last pulse is the optimal choice to obtain the return signal of the rock face (vegetation filter). Since TLS ILRIS-3-D is constrained by a 40×40° field-of view, five scan positions were necessary to cover all the slopes at a given distance. The final dataset consisted of five point clouds and over one million measurement points. Some of the measurement points were overlapped due to the repeated scanning from a different angle. The point clouds from each scan position were incorporated into a unique model using the PolyWorks® software. The process consisted of unifying all the obtained point clouds from each scan position within 3D space. Geo-referencing was carried out by surveying each scanning position using the total station and GPS receiver. The point cloud data set was filtered with respect to outliers and noise using manual point removal. Generation of a solid surface from a point cloud dataset was carried out through the nearest neighbor gridding interpolation method.

For the purpose of underwater investigations of the lake the remotely operated underwater vehicle, commonly referred to as an ROV, was deployed. The ROV was equipped with a HD camera, precision compass with gyro and sound and navigation and ranging (sonar) systems for hydro acoustics survey. ROVs are used extensively by the offshore drilling industry to support deep water activities (Jones 2009), and are now being increasingly used by the international scientific community for enhanced deep-sea observation, fine scale mapping and sampling (Bachmayer *et al.* 1998; Yoerger *et al.* 2007). ROV can accurately measure the depth of the dive and the geometry of the horizontal sections in spherical coordinates. Underwater survey and photographic observations of Red Lake were made with a ROV Seaeye Falcon with maximum operating depth of 300 m. The vehicle control unit and power supply were set on the built floating platform, connected with the ROV through umbilical cable of 450 m length. Using the equipped digital multi-frequency imaging sonar IMAGENEX 881A, the horizontal sections of the lake were obtained with five m step. With operating frequency automatically adjusted to 310 kHz and the power of transmitted signal of 23 dB, the range of the sonar goes up to 200 m. The surface that represents the shape of submerged part of Red Lake was generated using the rotary sonar scans and nearest neighbor gridding interpolation of data in 3D space.

The coupling of two geometry models obtained with sonar and lidar technology was made using the PolyWorks® software. Due to the gridding of scattered geometry data it was easy to calculate the volume of the lake at any given depth by numerically evaluating triple integral over a given three dimensional rectangular region using MATLAB® applications.

All the water temperature measurements of Red Lake were carried out using CTD diver DI 273 SWC with accuracy of ±0.1 °C and resolution of 0.01 °C.

RESULTS OF THE MEASUREMENTS PERFORMED IN SEPTEMBER 2013

The most recent hydrological and geomorphologic field research of Red Lake near Imotski resulted with an accurate computer model of Red Lake's geometry.

Fig. 4 presents a computer model of Red Lake geometry, generated using the lidar and sonar data.

It provides a complete picture of the shape of the lake at the very bottom. It shows that at the level of –4 m a.s.l., the bottom of the lake has an elliptical shape with dimensions of 20 x 10 m. Abundance of registered echo return suggests the narrowing of the bottom due to the collapsed material which is confirmed on the recorded images taken with the camera installed on the ROV. The camera also reveals the presence of collapsed material of anthropogenic origin, confirming the rumors that Red Lake has been used for years as an illegal dump for solid waste. Fig. 5 shows two photographs taken at the bottom of the Red Lake.

Because of the risk of damaging the ROV by the sharp metal objects on the bottom, further descent was not possible, although the bottom of the lake goes below the reached depth, expected up to –6 m a.s.l. Video recording reveals the presence of suspended particles on the bottom that are steady and only moving due to propulsion activity of the ROV. It proves that earlier assumptions about the active flow through karst conduits on the bottom are not accurate.

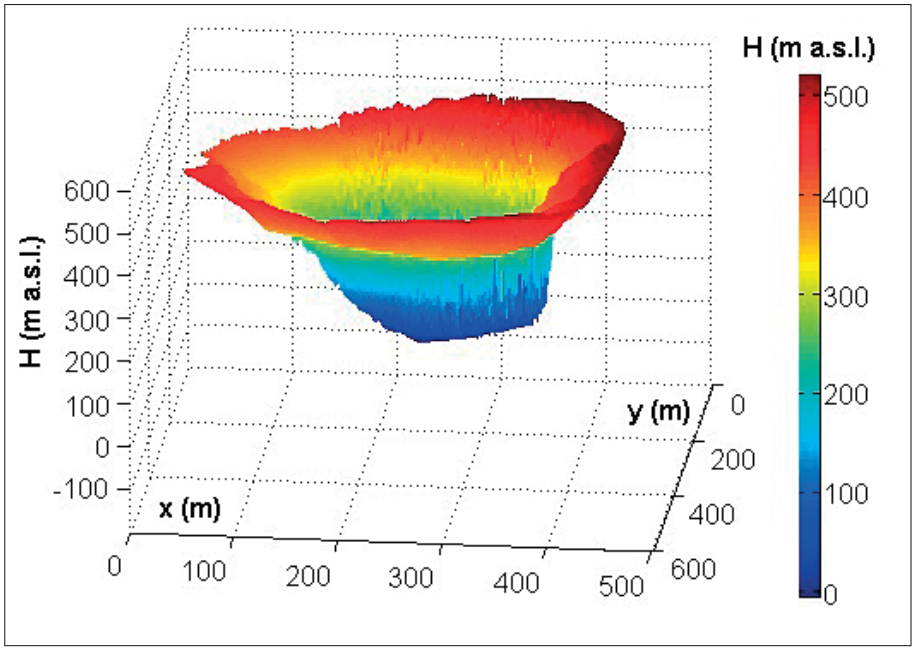

Fig. 4: Mesh/bathymetry model of Red Lake generated using LiDAR and sonar data.

The historical minimum and the maximum water levels of Red Lake were recorded in November 2011 and in April 2013 at 228 m a.s.l. and 311 m a.s.l. respectively. This means that the maximum amplitude of water level oscillations in Red Lake is over 83 m. The water level on the day of the survey was recorded at the elevation of 251 m a.s.l.

Fig. 6 shows four separate sonar images recorded at the following four depths: (1) 5 m (246 m a.s.l.); (2) 100 m (151 m a.s.l.); (3) 200 m (51 m a.s.l.); (4) 255 m (–4 m a.s.l.).

The strength of the return echo is shown in a range of colors from red to violet, where red shows the strongest signal, and purple the weakest. The received signal can be affected by various factors such as water temperature, density, suspended particles, distance from the transmitter to the registered object, angle of incidence and the density of the registered solid material. Referring to the examples in Fig. 6, it can be seen that at the elevation of 151 m a.s.l (diving depth of 100 m) echo return was registered over the entire horizontal section with a relatively weak signal. It can be explained with the large operating radius, irregular surface of the lake shore and varying density of the material from which the shore is made. Recorded echo return at elevation of 151 m a.s.l. registered the lack of feedback signal on the north side of the lake. This can be interpreted in several ways. One explanation may be the location of karst conduit or a vast underwater cave. However, the conclusions should be drawn carefully, because the lack of feedback signal may lie in the refraction and scatter of sound waves due to the geometry and characteristics of the observed material.

Fig. 7 presents the relationship between the elevation of water level *H* and volume of water *V* for Red Lake. According to this data, when the water level in the lake reached its historical maximum at the elevation of

Fig. 5: Underwater photographs taken at depth (elevation) of 255 m (–4 m a.s.l.); heading: a) 268° and b) 328°.

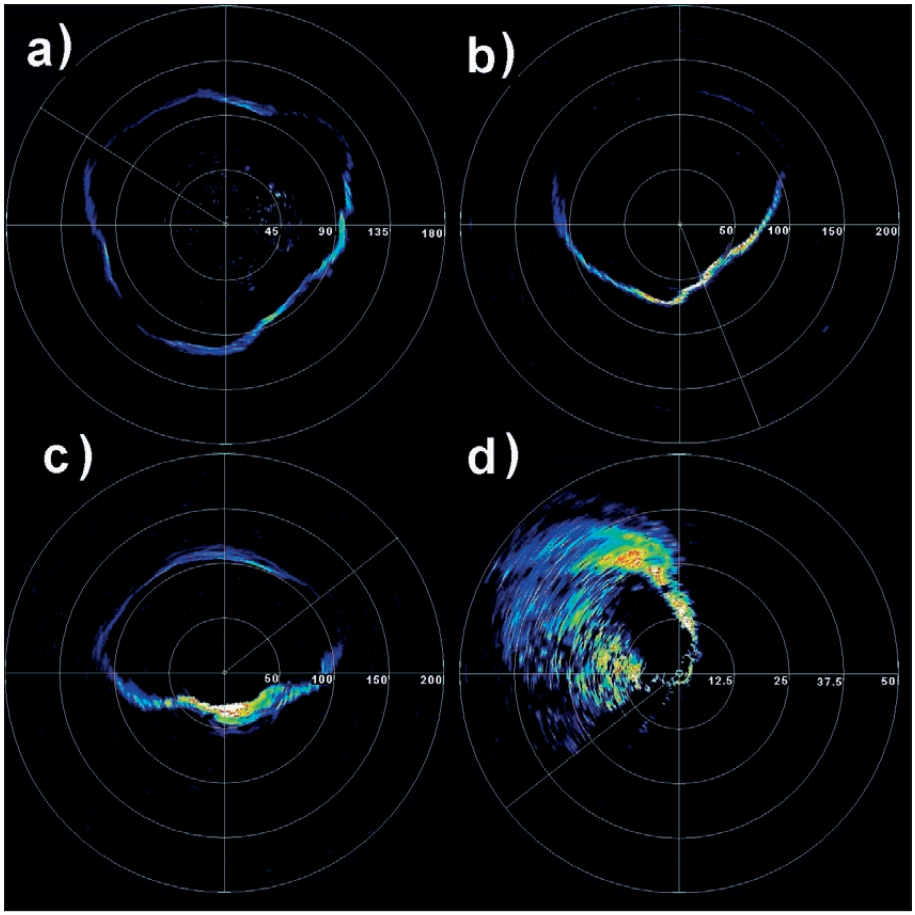

Fig. 6: Sonar recorded horizontal cross sections of Red Lake at depths (elevations) of: a – 5 m (246 m a.s.l.); b – 100 m (151 m a.s.l.); c – 200 m (51 m a.s.l.); d – 255 m (–4 m a.s.l.)

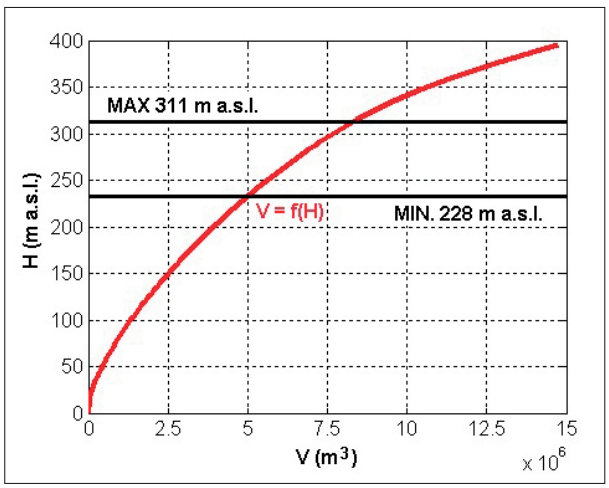

Fig. 7: Relationship between water level, H, and the volume of water, V.

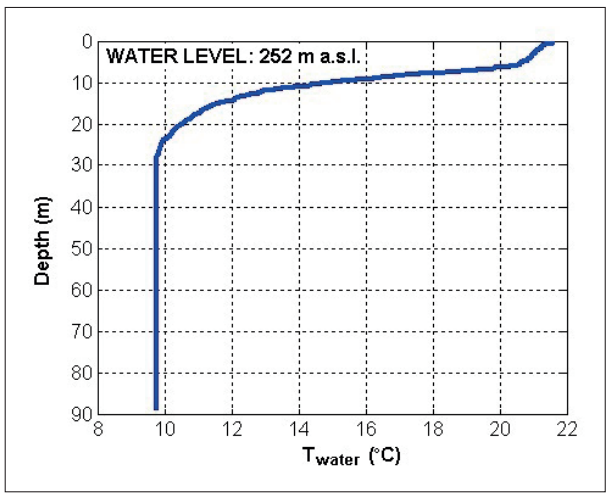

Fig. 9: Water temperature profiles of Red Lake measured 8 Sep. 2013.

311 m a.s.l., the volume of water stored in it is approximately 8.24 x 10^6 m^3.

Fig. 8 shows two typical cross-sections of Red Lake. By creating the characteristic cross sections of the lake, the position and dimensions of the cave on the west side

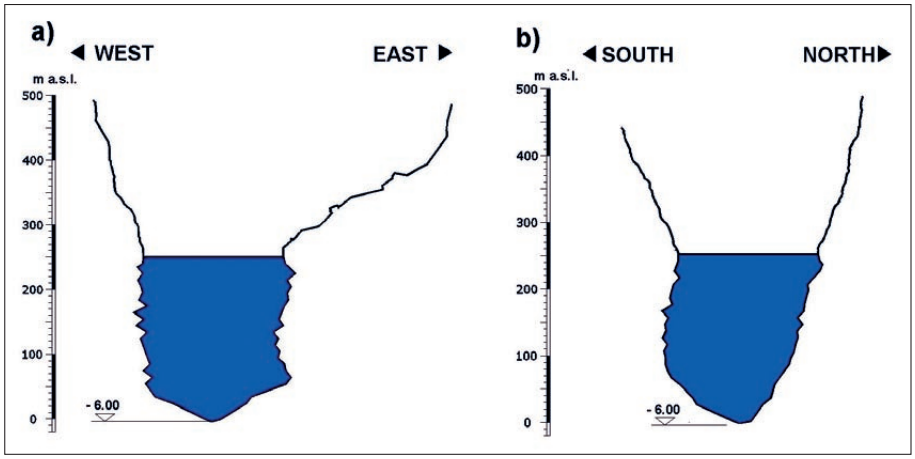

Fig. 8: Two characteristic vertical cross sections of Red Lake.

were ignored as well as the areas without recorded echo return.

The temperature profile at the middle of the lake up to the depth of 90 m was measured using the CTD Diver. Fig. 9 represents the temperature profile, which shows that the temperature from 30 to 90 m below the water surface was constant at 10 °C. The water temperature near the surface was recorded at 22 °C. The isotherm at depths below 30 m also suggests the absence of flow through the great karst conduits thus the low transmission of temperature signal due to the mixing of water.

CONCLUSIONS AND DIRECTIONS FOR FURTHER WORK

Although the recent research of Red Lake did leave behind some unknowns concerning its geomorphology, more important are the results which indisputably give the answers regarding the lake's basic features such as volume and bathymetry. It is an important turning point in the study of Red Lake because, for the first time, there is a solid base for further hydrological research and modelling in the form of its precisely defined geometry.

The measurements conducted showed the usefulness of TLS in the analysis of the morphology of karst features such as Red Lake. The high-resolution DEM obtained from a point cloud permits spatial analysis with accuracy adjusted to the scale of the phenomena and processes such as lakeshore erosion and material collapse which will be conducted in future research.

This work has also shown that it is possible to use an industrial work-class ROV for morphological study of submerged karst features in deep water. A model of the submerged part of Red Lake was derived from plots of the ROV's track and sonar rotary scans.

The survey integrating TLS and sonar scans provided a complete picture of Red Lake's bathymetry and close landscapes. Data acquired by both sensors was successfully organized into a point cloud representing the mesh/bathymetry model from which the water level/volume relationship was determined.

During the conducted fieldwork a CTD diver was installed at a depth of 40 m which continuously records the hourly data of water level, temperature and electrical conductivity. This data will provide insight into the future inflow and outflow of the water from the lake (hydrological and hydrogeological behavior) with regard to the specific geometry defined by the latest measurements. With the water level monitoring which is already in progress, it will be possible for the first time to determine the hydrological budget of the lake.

Further research on Red Lake involves the regular lidar scanning of the lake's shores above the surface of the water to provide an insight into ongoing geological processes of lakeshores on spatial and temporal scale. The research will also consist of periodical temperature and dissolved oxygen records and continuous monitoring of water turbidity. It is of crucial importance to expand the scope of future measurements and to simultaneously measure the hydrological parameters in Red and Blue Lake with the option to monitor other karstic water bodies in the vicinity. An insight into the regional direction of circulation of groundwater would be possible

with adequate spatial distribution of deep piezometers in the study area.

Further geomorphologic research priorities of Red Lake should concentrate on the exploration of the north side to examine the areas with no signal recordings.

ACKNOWLEDGEMENTS

This work was created as part of a joint international project of the Croatian Ministry of Science, Education and Sports and the Japanese Cooperation Agency JICA entitled "Risk identification and land use planning for disaster mitigation in landslides and floods in Croatia." Special thanks goes to the company Neptun-SUB Ltd. (Šibenik, Croatia) for the transfer of equipment and professionals who offered their services free of charge for academic purposes. The authors are especially grateful to ROV pilots Ivan Selak and Dorijano Mohorović as well to the cavers from Caving Club Imotski for their technical support. Without their help, the field research would not be possible. The authors are grateful for the financial support provided by the town of Imotski Tourist Board.

REFERENCES

Abellán, A., Vilaplana, J.M. & J. Martínez, 2006: Application of a long-range Terrestrial Laser Scanner to a detailed rockfall study at Vall de Núria (Eastern Pyrenees, Spain).- Eng. Geol., 88, 136–148.

Bachmayer, R., Humphris, S., Fornari, D., Dover, C.V., Howland, J., Bowen, A., Elder, R., Crook, T., Gleason, D., Sellers, W. & S. Lerner, 1998: Oceanographic research using remotely operated underwater robotic vehicles: exploration of hydrothermal vent sites on the Mid-Atlantic Ridge at 37°North 32°West.- Mar. Technol. Soc. J., 32, 37–47.

Bahun, S., 1991: O postanku Crvenog i Modrog jezera kod Imotskog (Genesis of Red and Blue Lakes near Imotski). Geološki Vjesnik, 44, 275–280.

Bauer, A., Paar, G., & A. Kaltenböck, 2005: Mass movement monitoring using terrestrial laser scanner for rock fall management.- In: von Oosterom, P.; Zlatanova, S.&. Fendel E. M. (eds) *Geo- Information for Disaster Management, Proceedings of the First International Symposium*, March 2005, Delft, Springer, 393–406, Berlin.

Biasion, A., Bornaz, L., & F. Rinaudo, 2005: Laser Scanning Applications on Disaster Management.- In: von Oosterom, P.; Zlatanova, S.&. Fendel E. M. (eds) *Geo- Information for Disaster Management, Proceedings of the First International Symposium*, March 2005, Delft, Springer, 19–33, Berlin.

Bonacci, O., 2006: Crveno i Modro jezero kod Imotskog (Red and Blue Lakes near Imotski). Hrvatske Vode, 14(54), 45–54.

Bonacci, O., Andrić, I. & Y. Yamashiki, 2014: Hydrology of Blue Lake in the Dinaric karst. Hydrological Processes, 28(4), 1890–1898, DOI:10.1002/hyp.9736.

Bonacci, O., Željković, I. & A. Galić, 2013: Karst rivers' particularity: an example from Dinaric karst (Croatia/Bosnia and Herzegovina). Environmental Earth Sciences, 70(2), 963–974, DOI:10.1007/s12665-012-2187-9.

Cvijić, J., 1893: *Das Karstphänomen (Karst phenomena). Versuch einer morphologischen Monographie*. Geographischen Abhandlung Wien V(3), pp 218–329, Vienna

Cvijić, J., 1926: *Geomorfologija 2 (Geomorpholgy 2)*.- Srpska Akademija Nauka i Umetnosti, pp. 587, Belgrade.

Cvijić, J., 1960: *La géographie des terrains calcaires (Geography of carbonate terraines)*. Naučno Delo, pp. 164, Belgrade.

Daneš, J. V., 1905: *Úvodi Dolni Neretvy (The Neretva River Valley)*. Geomorphologická Studie 8, pp. 108, Prague.

Ford, D. & P. Williams, 2007: *Karst Hydrogeology and Geomorphology*.- Wiley, pp. 576, Chichester.

Gams, I., 2005: Tectonics impact on poljes and minor basins (case studies of Dinaric karst).- Acta Carsologica, 34(1), 25–41.

Garašić, M., 2001: New speleohydrogeological research of Crveno Jezero (Red Lake) near Imotski in Dinaric karst area (Croatia, Europe): International Speleodiving expedition "Crveno Jezero 98".- In: *13th International Congress of Speleology*, 15th–22nd. July 2001, Brasilia Speleo Brazil, 168–171, Brasilia.

Garašić, M., 2012: Crveno jezero – the biggest sinkhole in Dinaric Karst (Croatia).- In: *EGU General Assembly 2012*, 22th–27th April 2012, Vienna, COPERNICUS, 7132, Vienna.

Gavazzi, A., 1903/04: *Die Seen des Karstes (Karst Lakes)*.- Abhandlungen der K. K. Geographischen Gesellschaft 5(2). Lechner, pp. 136, Vienna.

Grund, A., 1903: *Die Karsthydrographie. Studien aus Westbosnien (Karst Hydrographic studies in Western Bosnia)*. Geographischen Abhandlungen 7(3), pp. 200, Leipzig.

Herak, M., 1986: A new concept of geotectonics of the dinarides.- Acta Geologica, 16, 1–17.

Jones, D.O.B., 2009: Using existing industrial remotely operated vehicles for deep-sea science. Zool. Scr. 38, 41–47.

Milanović, P. T., 1981: *Karst Hydrogeology*.- Water Resources Publications. pp. 434, Littleton.

Oppikofer, T., Jaboyedoff, M., & H.-R. Keusen 2008: Collapse of the eastern Eiger flank in the Swiss Alps, Nat. Geosci., 1(8), 531– 535.

Optech: ILRIS-3D, 2009: Intelligent Laser Ranging and Imaging System. – [Online] Available from: http://www.optech.ca/i3dprodline-ilris3d.htm [Accessed 3rd June 2009].

Petrik, M., 1960: Hidrografska mjerenja u okolici Imotskog (Hydrographic measurements near Imotski).- Ljetopis JAZU, 64, 266–286.

Roglić, J., 1938: *Imotsko Polje – Fizičko-Geografske Osobine. (Physical-Geographic Characteristics of Imotski Polje)*.- Posebno Izdanje Geografskog Društva 21, pp. 125, Belgrade.

Roglić, J., 1954. Polja zapadne Bosne i Hercegovine (Karst poljas of Western Bosnia and Herzegovina).- In: *III Kongres geografa Jugoslavije,* 1953, Sarajevo, Geografsko društvo NR BiH, Sarajevo.

Roglić, J., 1974: Prilog Hrvatskoj Krškoj Terminologiji (Contribution to Croatian Karst Terminology).- Carsus Iugoslaviae 9/1, 72.

Roglić, J., 1974: Odnos između površja i podzemlja Dinarskog krša (Relationship between surface and underground of Dinaric karst).- Acta Carsologica, 6, 11–19.

Sauro, U., 2005: Closed depressions.- In: Culver, D. C. & White, W. B. (eds.) *Encyclopedia of caves*. Elsevier, pp. 108–122, Amsterdam.

Williams, P., 2004: Dolines.- In: Gunn, J. (ed.) *Encyclopedia of caves and karst science*. Fitzroy Dearborn, pp. 304–310, New York, London.

Yoerger, D.R., Bradley, A.M., Jakuba, M., German, C.R., Shank, T. & M. Tivey, 2007: Autonomous and remotely operated vehicle technology for hydrothermal vent discovery, exploration, and sampling.- Oceanography, 20, 152–161.

COBISS: 1.01

THE CREATION OF COLLAPSE DOLINES: A 3D MODELING APPROACH

TRIDIMENZIONALNI NUMERIČNI MODEL NASTANKA UDORNIC

Thomas HILLER[1,2], Douchko ROMANOV[1], Franci GABROVŠEK[3] & Georg KAUFMANN[1]

Abstract UDC 551.435.8

Thomas Hiller, Douchko Romanov, Franci Gabrovšek & Georg Kaufmann: The creation of collapse dolines: A 3D modeling approach

We present a 3D numerical karst evolution model describing mechanisms governing the evolution of collapse dolines. The results confirm the current state of the art of the knowledge about the conditions necessary for a collapse doline to grow. We demonstrate that these geological features develop in karst aquifers, above subsurface rivers flowing through active cave systems or mechanically unstable zones. The mechanisms of growth of single/isolated collapse dolines are generally two dimensional and can be modeled with very dense numerical models. On the other hand, our results demonstrate that there can be more than one location, within a karst system, where the conditions allow the development of a collapse doline. For such complex scenarios a 3D modeling approach and a detailed knowledge of the hydro-geological situation is required in order to correctly predict and describe the development of collapse dolines.

Keywords: Three-dimensional, Karst, Modeling, Doline, Limestone.

Izvleček UDK 551.435.8

Thomas Hiller, Douchko Romanov, Franci Gabrovšek, Georg Kaufmann: Tridimenzionalni numerični model nastanka udornic

V članku predstavimo tridimenzionalni numerični model razvoja kraških udornic. Rezultati potrjujejo dosedanja spoznanja o pogojih, potrebnih za rast udornic. Pokažemo, da udornice nastajajo kot del razvoja kraškega vodonosnika nad podzemnimi rekami, ki tečejo skozi aktivne jamske sisteme oz. mehansko nestabilna območja. Mehanizem nastanka ene same izolirane udornice lahko pojasnimo z dvodimenzionalnim numeričnim modelom z dovolj gosto mrežo. Za študij prostorskega razvoja in porazdelitve sistema udornic potrebujemo 3D numerični model, ki ga lahko ob podrobnem poznavanju hidrogeoloških razmer uporabimo tudi za napovedovanje in interpretacijo pojavljanja udornic na nekem kraškem območju.

Ključne besede: Tridimenzionalni model, kras, udornice, apnenec.

1. INTRODUCTION

Karst rocks such as limestone, dolomite, anhydrite, and gypsum can be dissolved by water, either by dissolution of the rock, or in the case of the first two rock types by chemical dissolution in water enriched with carbon dioxide. The removal of rock in fissures and bedding partings creates larger voids and cavities, which results in an

[1] Institute of Geological Sciences, Geophysics Section, Freie Universität Berlin, Malteserstr. 74-100, Haus D, 12249 Berlin, Germany, e-mail: georg.kaufmann@fu-berlin.de

[2] Max Planck Institute for Dynamics and Selforganization, Am Fassberg 17, 37077 Göttingen, Germany

[3] Karst Research Institute ZRC SAZU, Titov trg 2, 6230 Postojna, Slovenia

Received/Prejeto: 15.05.2014

efficient drainage of water through the karst rock. Once the cavities grow to a certain size, the void can become unstable and detachment of slabs at the roof of the cavity initiates mechanical breakdown. The breakdown can propagate towards the surface and finally results in a typical karst surface structure such as a collapse doline.

Dolines are closed depressions on the surface, which drain part of the karst landscape; they are, along with poljes and uvalas, typical karst surface features (e.g. Kranjc 2006). The term doline is derived from the Slavic word for valley, *dolina*, and is used mainly in Europe. In North America the term sinkhole has a similar meaning. Sizes and shapes of dolines are manifold and range from a few meters to hundreds of meters both in diameter and depth (see Fig. 1).

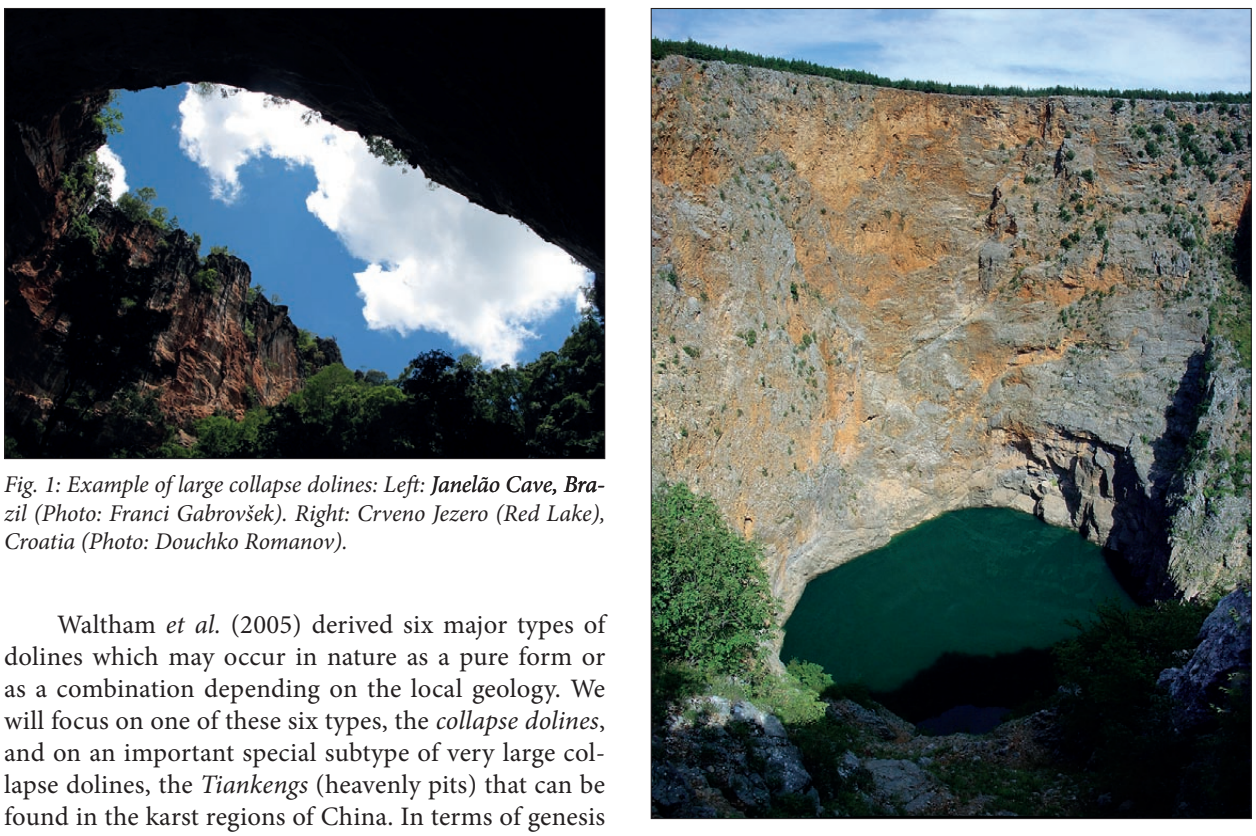

Fig. 1: Example of large collapse dolines: Left: ***Janelão Cave, Brazil*** *(Photo: Franci Gabrovšek). Right: Crveno Jezero (Red Lake), Croatia (Photo: Douchko Romanov).*

Waltham *et al.* (2005) derived six major types of dolines which may occur in nature as a pure form or as a combination depending on the local geology. We will focus on one of these six types, the *collapse dolines*, and on an important special subtype of very large collapse dolines, the *Tiankengs* (heavenly pits) that can be found in the karst regions of China. In terms of genesis a Tiankeng is similar to a collapse doline but has become its own characteristic term in karst science (Zhu & Waltham 2006). However, the major distinction is made by its size as a Tiankeng has to be at least 100 m deep and wide.

A general overview on dolines can be found in Waltham *et al.* (2005), also with a focus on practical implications close to collapse features in karst. Kranjc (2006) gives an overview on large collapse dolines in the Dinaric karst, whereas Waltham (2006) concentrates on large collapse dolines and/or Tiankengs throughout the world. Zhu and Chen (2006) and Zhu and Waltham (2006) focus on Tiankengs especially in China.

Summarizing the given references, there are a few characteristics typical for large collapse dolines:

1. Dolines are generally a few tens to a few hundreds of meters wide and deep.

2. Doline walls are very steep or close to vertical and the floor can be covered with breakdown debris.

3. A large river is either flowing on the floor of the doline or below the ground but not too deep (tens of meters).

4. Dolines can appear in groups all belonging to the same active subsurface cave system (e.g the Dashiwei group or the dolines of the Slovenian Škocjanska jama).

5. Some Dinaric collapse dolines are assumed to be in the range of millions of years old (Gabrovšek 2011 – personal communication), whereas Tiankengs can be as young as 200 000 years (Zhu & Chen 2006; Zhu & Waltham 2006).

Although some dolines, especially smaller ones, can be created by subsidence events or collapse of a cave ceiling, the dolines that are sometimes two orders of magnitude bigger than the largest known cave chambers (Gabrovšek & Stepišnik 2011) cannot be explained by these processes alone. Thus the collapse of a sub-surface void alone is often not capable to explain the size of the doline.

A possible explanation on the creation of large collapse dolines has been given by Palmer and Palmer (2006):

- A sub-surface cavity grows to a certain size, and depending on the mechanical stability of the host rock, breakdown of the cavity roof starts.
- The collapsed material accumulates along the floor of the cavity, partially blocking water flow and thus increasing the hydraulic pressure head in the cavity.
- Here, the blocks can be removed by mechanical erosion, and more efficiently by chemical dissolution.
- The void propagates upwards into the overburden.
- If the overburden is entirely made up of soluble rock, the material can be removed completely and after the final collapse of the remaining rock ledge, a deep doline remains. If the overburden comprises insoluble rocks, part of the debris accumulates at the bottom of the doline.

This concept was modeled by Gabrovšek and Stepišnik (2011) with a 2D karst evolution model to estimate the material removal in such a crushed zone. In terms of material removal rates their model is in quantitatively good agreement when compared to the size and evolution time of known dolines.

The goal of our paper is to develop the numerical approach of Gabrovšek and Stepišnik (2011) further and extend it into the third dimension. We use the KARSTAQUIFER tool (e.g. Kaufmann *et al.* 2010) to simulate the evolution of a karst aquifer, and we define several steps for our analysis: (i) In a first step we rebuild the crushed zone from the 2D model of Gabrovšek and Stepišnik (2011) with our KARSTAQUIFER code and compare the evolution of both models to find a common basis for the further simulations. (ii) As large collapse dolines often appear in groups we extend the model and embed several crushed zones into a single 3D domain. Because so far erosional processes are not directly implemented in our model, the creation of collapse dolines by means of surface lowering due to the crushed zones is simulated with a distinct collapse mechanism. (iii) By activating more than one crushed zone in a single domain, we then study the evolution of several collapse dolines and their interaction.

2. THEORY

The term karstification generally describes the alteration of soluble bedrock such as limestone or gypsum by means of dissolution. Water penetrates into the karst bedrock through fissures and bedding partings, removes material and the voids are widened to cavities and caves. In general, modeling karstification can be partitioned into two major sub-steps: The first is calculating flow of water depending on the hydraulic conductivity of the host rock and the hydrological boundary conditions. The second is to calculate the dissolutional widening determined by flow and calcium concentration and the transport of the dissolved calcium.

The flow of water through a fissured and fractured aquifer can be described by a transient continuity equation:

$$\frac{\partial}{\partial x}\left(K(t)\frac{\partial h}{\partial x}\right)+\frac{\partial}{\partial y}\left(K(t)\frac{\partial h}{\partial y}\right)+\frac{\partial}{\partial z}\left(K(t)\frac{\partial h}{\partial z}\right)=S\frac{\partial h}{\partial t}, \quad (1)$$

where $K(t)$ [ms^{-1}] is the time-dependent hydraulic conductivity, S [m^{-1}] the specific storage and h [m] the hydraulic head as a sum of elevation head z [m] and pressure head p [m]. Furthermore, x [m], y [m] and z [m] denote the spatial coordinates, and t [s] is time. We solve (1) by means of the finite-element method (e.g. Istok 1989), using three-dimensional parallelepiped finite elements for the rock matrix and linear bar elements for fissures and bedding partings to assemble the modeling domain.

The hydraulic conductivity of the rock matrix $K = K_m$ (see Tab. 1) is fixed to a constant value for all calculations. Therefore, the increase of hydraulic conductivity over time is controlled only by the dissolutional widening of the conduits. For laminar flow the hydraulic conductivity K_c^l of such a conduit is given by

$$K_c^l=\frac{gd^2}{32\nu}, \quad (2)$$

where g [ms^{-2}] is the gravitational acceleration, d [m] the conduit diameter and ν [m^2s^{-1}] the kinematic viscosity of the solution. If the flow inside the conduit becomes turbulent the non–linear Darcy–Weissbach flow law is applied. The hydraulic conductivity K_c^t of a conduit is then given by

$$K_c^t=\frac{2gd}{f}, \quad (3)$$

where f is the friction factor, which has to be calculated in dependence of the Reynolds number (see e.g. Kaufmann 2009). Each conduit can be assigned with an individual in-

itial diameter d_0 to account for any kind of heterogeneous (e.g. statistical) distribution of the hydraulic conductivity.

Tab. 1: Standard model parameters.

Model Parameters	*Symbol*	*Unit*	*Value(s)*
Model domain:			
Length	X	m	≤ 500
Width	Y	m	≤ 500
Height	Z	m	≤ 50
Horizontal resolution	dx, dy	m	5–25
Vertical resolution	dz	m	1–5
Nodes	N_n	[–]	42135
Elements	N_ϵ	[–]	37856
Conduits	N_c	[–]	116494
Matrix conductivity	K_m	$m \cdot s^{-1}$	1×10^{-5}
Limestone chemisty			
Linear kinetic exponent	n_1	[–]	1
High-order kinetic exponent	n_2	[–]	4
Linear rate constant	k_1	$mol \cdot m^{-2} \cdot s^{-1}$	4×10^{-7}
Calcium concentration	c	$mol \cdot m^{-3}$	$c_{in} < c < c_{eq}$
Initial calcium concentration	c_{in}	$mol \cdot m^{-3}$	0
Calcium switch concentration	c_s	$mol \cdot m^{-3}$	9.9 c_{eq}
Temperature	T		10
Partial pressure of carbon dioxide	pCO_2	atm	0.05

The enlargement of the conduit diameter by chemical dissolution is described by the relation

$$d(t_i) = d(t_{i-1}) + F \frac{m_{MIN}}{\rho_{MIN}} (t_i - t_{i-1}), \tag{4}$$

Here, t_{i-1} and t_i are two consecutive time steps, F [$mol\ m^{-2}\ s^{-1}$] is the calcium flux rate which describes the removal of bedrock per unit area and time, m_{MIN} [$kg\ mol^{-1}$] is the molar mass and ρ_{MIN} [$kg\ m^{-3}$] the density of the soluble mineral (calcite in this case), respectively.

The flux rate F as a function of calcium concentration has been intensively studied (e.g. Buhmann & Dreybrodt 1985a,b; Dreybrodt 1988; Eisenlohr *et al.* 1999; Kaufmann & Dreybrodt 2007; Plummer *et al.* 1978; Svensson & Dreybrodt 1992) and can be described by the rate law

$$F = k_i \left(1 - \frac{c}{c_{eq}}\right)^n, i = 1, n \tag{5}$$

with k_i [$mol\ m^{-2}\ s^{-1}$] a rate coefficient, c [$mol\ m^{-3}$] the actual concentration of Ca^{2+} in the water, c_{eq} [$mol\ m^{-3}$] the equilibrium concentration with respect to calcite and n_i [–] a power–law exponent. The coefficient k_i and the exponent n_i are characteristic parameters for the bedrock mineral, and depend on the amount of undersaturation with respect to calcite in the subsurface water. For $c \le c_s$ the system exhibits linear kinetics, $i = 1$ with in eq. 5. This leads to coefficients and. For $c > c_s$ the system exhibits higher–order kinetics where the rate becomes non–linear and the coefficients k_2, and n_2 are used (see Tab. 1 for details). The switch concentration in our model is $c_s = 0.9\ c_{eq}$.

The calcium equilibrium concentration depends on temperature T [°C] and carbon-dioxide pressure p [atm]. Using a simplified charge balance valid for karst water, an analytical expression can be used (e.g. Dreybrodt 1988):

$$c_{eq}(T, p) = \sqrt[3]{\frac{K_1(T) K_C(T) K_H(T)}{4 K_2(T) \gamma_{Ca^{2+}} \gamma^2_{HCO_3^-}}}\, p. \tag{6}$$

With $K_H\ (T)$ the equilibrium constant for the dissolution of atmospheric carbon dioxide into water (Henri constant), $K_0\ (T)$ the equilibrium constant for the reaction of water and carbon dioxide to carbonic acid, $K_1\ (T)$ and $K_2\ (T)$ the equilibrium constants for the dissociation of carbonic acid into bicarbonate, carbonate, and hydrogen (e.g. Usdowski 1982), $K_C\ (T)$ the equilibrium constant for dissolved calcite, $\gamma_{Ca^{2+}}$ and $\gamma^2_{HCO_3^-}$ the activity coefficients for calcium and bicarbonate (e.g. Harned & Hamer 1933). The carbon-dioxide pressure remains constant in the open-system case, as carbon dioxide can be replenished from the atmosphere, but decreases, once the solution becomes decoupled from the atmosphere in the closed-system case:

$$p = \begin{cases} p_{atm} & open \\ p_{atm} - \dfrac{c_{eq}(T, p)}{K_H(T)\left(1 + \dfrac{1}{K_0}(T)\right)} & closed, \end{cases} \tag{7}$$

with p_{atm} [atm] the initial carbon-dioxide partial pressure.

For more details on the implementation of the KARSTAQUIFER model, see Kaufmann *et al.* (2010) and Hiller *et al.* (2011). See Tab. 1 for the values we have used within this study.

3. MODEL

The conceptual model for the evolution of a collapse doline is shown in Fig. 2. Here, **A** is the karst rock in which the collapse doline **B** is going to evolve. Following Palmer and Palmer (2006), one of the necessities to create collapse dolines are fault zones inside the rock. These fault zones mark the *boundaries* of a mechanically unstable crushed zone. The fault planes are indicated by the dashed lines in Fig. 2. Another necessity in the presented concept is a subsurface passage for water to enter (**D1**) and leave (**D2**) the cavity present at the bottom of the crushed zone. As this passage crosses the highly fractured bedrock, breakdown of parts of the cavity roof block the passage and material accumulates in the crushed zone **C**, which resembles a highly fissured part of the domain. The hydraulic gradient increases and incoming aggressive water enlarges passages between the blocks in the crushed zone by chemical dissolution. The dissolved material is leaving the crushed zone through the output passage. Because the crushed zone is mechanically unstable, the removal of the crushed blocks induces further collapse of the cavity roof, with upward propagation of the void space, and finally the creation of a collapse doline. This breakdown is indicated by the thin circle lines below the doline *cylinder* in Fig. 2. Note again, that the bedrock is only removed by dissolution, and the model does not account for the real mechanical properties of the bedrock and/or erosional processes that might as well remove collapsed material from the bottom of the crushed zone.

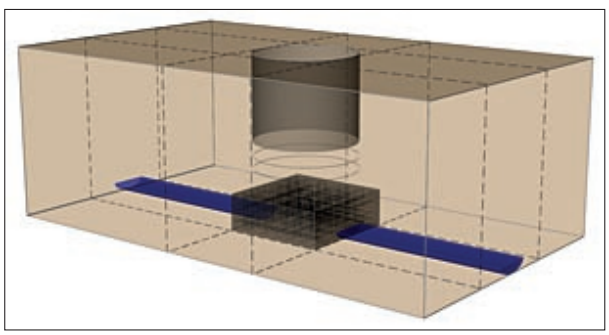

Fig. 2: Conceptual model of the doline model: A karst bedrock; B collapse doline; C crushed zone; D1 subsurface passage/stream (input); D2 subsurface passage/stream (output); the dashed lines represent fault planes inside the bedrock; modified after Gabrovšek & Stepišnik (2011).

3.1. 3D MODEL DOMAIN AND BOUNDARY CONDITIONS

The model domain used in this work for simulating the doline evolution is shown in Fig. 3. The relevant modeling parameters are summarized in tables 1 and 2.

The model domain for the final 3D doline models is a 500 × 500 × 50 m^3 limestone block. The grid discretization varies between $dx = dy = 5\ m$ inside and $dx = dy = 25\ m$ outside of the crushed zones. The vertical grid discretization varies between $dz = 1\ m$ and $dz = 5\ m$, respectively. Due to the use of a rectangular network and a constant amount of grid nodes in each spatial direction, the crushed zones are not implemented as pure local grid refinements (see Fig. 3). In other words, the smaller distance between the nodes in the crushed zones results in small distance between the conduits entering and exiting these areas also outside of them. The effect can be seen within the green square and Fig. 3b for example. We need small distance between the nodes in crushed zone 2 (CZ2). For this reason all conduits that enter and leave this zone (coordinates X (100 to 200) and Y (100 to 200) are closer to each other in comparison to the conduits not crossing CZ2 (coordinates X (0 to 100), Y (0 to 100)). This leads to domain regions with a higher spatial resolution than necessary (e.g. between the crushed zones) and has to be considered in the interpretation of the results. The hydraulic conductivity of the matrix is $1 \times 10^{-5}\ ms^{-1}$. In contrast to this uniform conductivity, which is defined for each block inside the modeling domain, the conduit network is represented by a rectangular network with a log-normal statistical distribution of initial conduit diameters. The parameters describing this distribution for the whole domain are $\hat{d}_0 = 0.05\ mm$ and $\sigma = 0.75$, which represents an intact (or immature) and only slightly fissured karst bedrock. The blue face in Fig. 3a marks the region where a constant head boundary condition (BC) ($H = 10\ m$) is applied to the grid nodes. On the opposite domain boundary (not visible in Fig. 3a) a constant head BC of $H = 0\ m$ is applied to induce flow through the domain in positive x–direction.

The domain is intersected by two active subsurface cave passages (black lines in Fig. 3a) passing through the model in x–direction at $z = 0\ m$. The passages have an initial conduit diameter of $d_0 = 0.13\ m$ to obtain flow rates between 1 m^3s^{-1} and 5 m^3s^{-1}, depending on the chosen setup and applied boundary conditions. These flow rates are in agreement with values used in previous studies or reported from the field (e.g. Gabrovšek & Stepišnik 2011; Palmer & Palmer 2006). The denser parts of the rectangular conduit network on Fig. 2 visualize the areas which we can model as crushed zones. We use/alter three of these four zones depicted in the figure for creating the different models calculated for this work. The areas are marked by CZ (see Fig. 3). The initial diameters of the conduits in the zone are assigned according to the statistical distribution, which is chosen for the whole

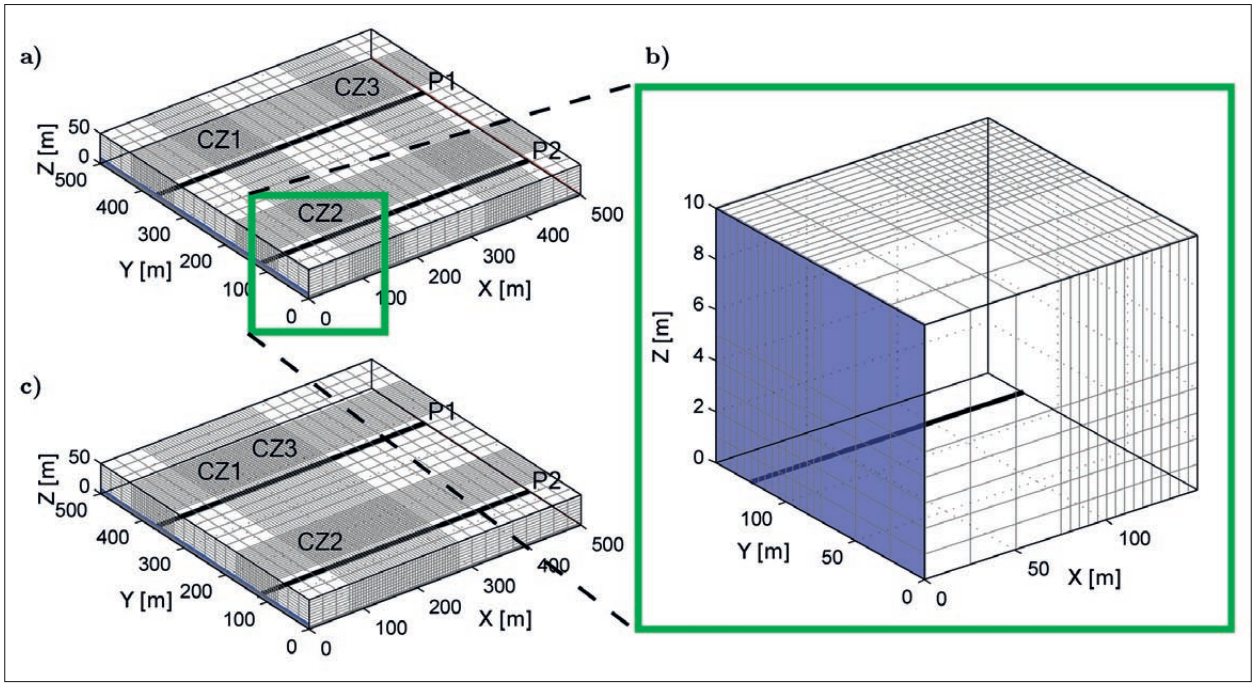

Fig. 3: 3D doline model setup: a) Setup for model 1 and model 3; four zones with increased resolution due to the regular grid, but only one to three active crushed zones (CZ), two subsurface passages (black lines), see also Tab. 2. Blue face marks const. head boundary condition of H = 10 m and red face const. head boundary condition of. b) Green frame marks enlarged part from a, note that here the grid is out of scale; c) setup for model 2.

modeling domain. If one of the zones is activated and modeled as a crushed zone, its hydraulic conductivity is modified by assigning new initial conduit diameters to the conduits inside this zone. With this approach, the mechanical weakening (enlarged fissures and fractures are already present) of the crushed zone is simulated. The parameters for these conduits are $\hat{d}_0$ = 0.05 *mm* and σ = 0.75 and are chosen following the calibration presented in 4.1.

3.2. CRUSHED ZONE – COLLAPSING MECHANISM

Gabrovšek and Stepišnik (2011) used two mechanisms to mimic the material removal processes inside a crushed zone. The first one they called *continuous infilling* and is similar to the limited widening scheme presented by Romanov *et al.* (2010). If a fracture reaches a critical aperture width A_{lim} then its enlargement is stopped but the dissolution is still active. Therefore, material is removed in every time step but the fracture aperture is always reset to A_{lim}. With this approach, a continuous collapse of the crushed blocks is assumed, with voids between the blocks keeping their size, and a more or less constant flux rate (removal rate) is established. The second mechanism they called *discontinuous collapsing* which resets the fracture apertures to the initial or smaller value, if a critical aperture width is reached. After this resetting, the growth of the fracture starts again. This second approach mimics the periodically collapsing breakdown area.

In this work we use a variant of the *discontinuous collapsing* mechanism from Gabrovšek and Stepišnik (2011): The general implementation is shown in Fig. 4 (note that the dimensions are not to scale). Fig. 4a shows a fraction of the model domain. The initially small passages inside the crushed zone mark passages between collapsed blocks. These passages are enlarged over time by dissolution (Fig. 4b), and the breakdown area becomes mechanically instable once the passages reach a critical size d_{crit}, then they collapse again, reducing the passages between the blocks. Thus a periodic behavior of the breakdown area is simulated. The smaller diameter of the passages is derived by the same statistical parameters $\hat{d}_0$ and σ that are initially used for the conduits in the corresponding crushed zone. The difference between the critical and the small diameter after collapsing $\Delta d = d_{crit} - d_{imit}$ is used as the maximal possible value for surface lowering (Fig. 4c).

In our model we represent the intersection of bedding partings and fractures of the bedrock by cylindrical conduits. We assume that a limestone block can collapse (move virtually downward) only if all four bordering fractures (conduits) have reached a critical size. Here, by limestone block we mean each cuboid whose edges are conduits. The lengths of these conduits are *dx*, *dy* and *dz*.

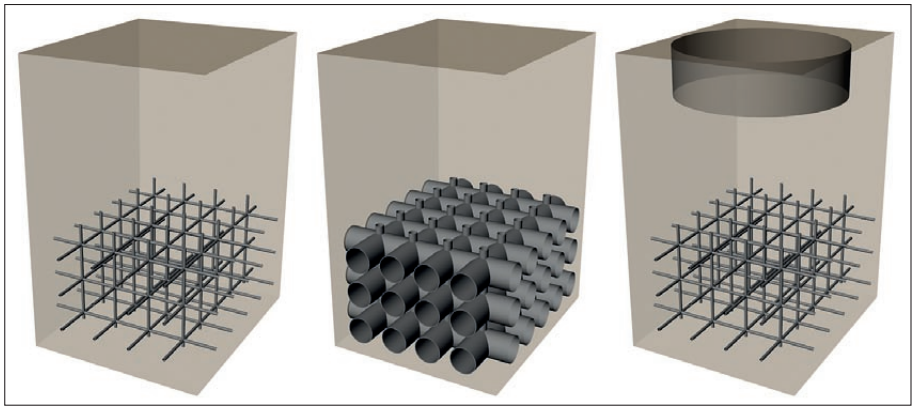

Fig. 4: Simulated mechanical collapse of the doline above the crushed zone: a) initial situation of the conduit network inside the crushed zone; b) horizontal conduits have reached a certain critical diameter; c) the horizontal conduits have collapsed and the topography is lowered accordingly.

We further constrain this collapse procedure and only allow the collapse of one depth layer inside the crushed zone if at least 75 % of all conduits in this layer have reached the critical diameter . If in a single time step this criterion is fulfilled, then all conduits in this layer are reset and the surface collapses.

4. RESULTS

4.1 2D MODEL CALIBRATION

As this doline model is inspired by the 2D model of Gabrovšek and Stepišnik (2011) and is consequently a 3D extension of their 2D approach, the first objective is to compare 2D results of Gabrovšek and Stepišnik (2011) with the results from the 3D KARSTAQUIFER code used here. Therefore, we first consider only the crushed zone and use the determined values from the calibration when embedding the crushed zones into the 3D domain as it is shown in Fig. 3. For the calibration runs we use the same grid layout as Gabrovšek and Stepišnik (2011), which means one layer of a 200 × 200 m^2 conduit network with a horizontal spacing of $dx = dy = 2\ m$. Furthermore, we use the same boundary conditions in our setup as in the original 2D model. To find a comparable initial conduit diameter distribution that simulates the evolution of their dual–fracture network, we test many different non–uniform conduit networks with varying distribution parameters. To pick the most suitable initial conduit diameter distribution out of the tested set, we consider only the breakthrough time TB of the resulting flow curve. This is done because we are mainly interested in a similar temporal evolution of the model as the amount of flow (the pure amplitude) through the domain will of course differ due to the different fracture network geometries (fractures in the 2D model – conduits in the 3D model).

Fig. 5a shows a set of the tested conduit diameter distributions. All distributions have a mode of $\hat{d}_0$ = 0.3–0.6 *mm* and a varying within larger boundaries standard deviation σ. The wider the distribution gets the more non–uniform the conduit network will be. For σ = 0.35 (black curve) the distribution of the conduit diameters spans about one order of magnitude, whereas for σ = 1 (green curve) it spans about four orders of magnitude, respectively. In Fig. 5b the corresponding flow curves are plotted for 3000 years of evolution together with the 2D flow curve (dashed black curve) from Gabrovšek and Stepišnik (2011). All curves are characterized by an initially low flow rate, which increases due to the enlargement of fractures by dissolution. Within a short time period, flow rates increase by several orders of magnitude, an event called breakthrough and the corresponding time breakthrough time. After breakthrough, the flow rate increases with a much slower rate. When comparing flow rates for the 2D and 3D models, we find that the breakthrough times of the red curve with σ = 0.75 and the 2D curve are almost identical. Although the amount of flow before and after breakthrough of these two curves differs, it is within one order of magnitude and we will regard this as acceptable. Once again, we regard this as acceptable because our initial calibration criterion was the evolution/breakthrough time and not the absolute flow rate. The flow rates between both models, the one suggested by Gabrovšek and Stepišnik cannot be the same for similar evolution times, because in KARSTAQUIFER we use conduits and not fractures.

Because in the end we want to study the interaction of several crushed zones (dolines), it is not feasible to stick to the grid discretization for the whole domain. This would lead to model sizes in the range of 400 × 400 × 25

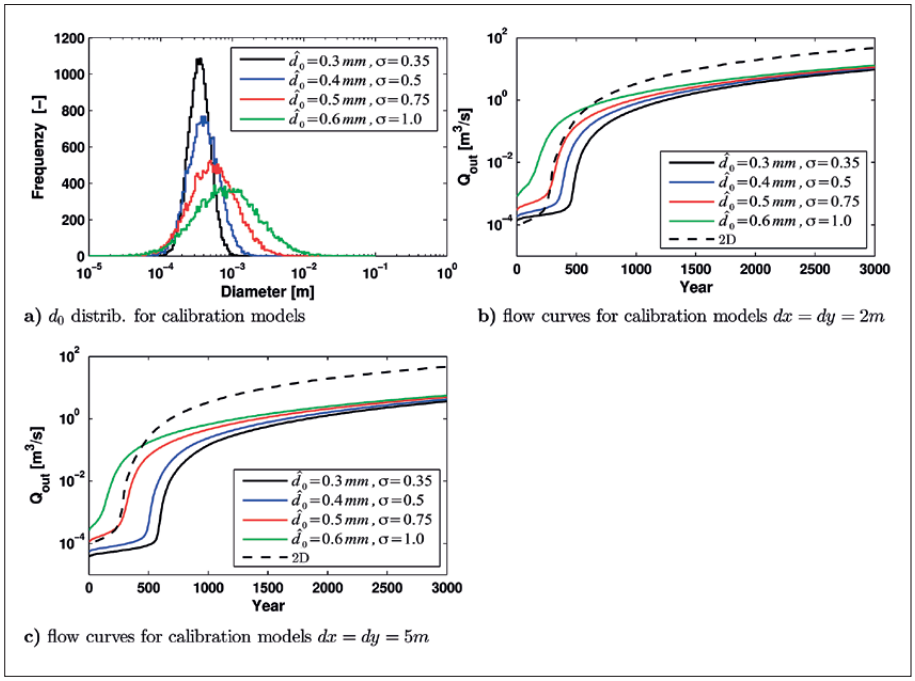

Fig. 5: Doline model calibration: a) initial diameter distributions for different 3D models to calibrate the 3D code to the 2D model; b) corresponding flow curves to a plus the 2D flow curve; c) flow curves for calibration models with a coarser network.

nodes and therefore exceed the available computational power. To cope with this limitation the crushed zone resolution is decreased to $dx = dy = 5\ m$. To check if this coarsening has an effect on the breakthrough time of the crushed zone, we simulate the evolution with the same conduit diameter distributions and boundary conditions as the model with the $dx = dy = 2\ m$ discretization from before. The coarser network for the model with σ = 0.75 (red curve in Fig. 5c) fits the 2D curve comparably well as for the dense network so that these are the final distribution parameters that will be chosen for the 3D model (see also Tab. 2).

We thus have determined the initial conduit diameter distribution yielding comparable results to the 2D model and proceed discussing 3D scenarios.

4.2. 3D EVOLUTION MODELS

4.2.1. MODEL 1 – ONE ACTIVE CRUSHED ZONE

The first 3D doline model that is presented has the following setup: Two subsurface passages cross the domain as shown in Fig. 3 and the head difference between entrance and exit is. So far only one crushed zone (CZ1) is

Tab. 2: Doline model parameters.

Name	*x-extent (dx)*	*y-extent (dy)*	*z-extent (dz)*	*network*
Domain size	500 m	500 m		$\hat{d}_0$ = 0,05 *mm*, $\acute{o}$ = 0.75
	(5 – 25 m)	(5 – 25 m)		
Crushed zones (CZ):				
CZ1	75 – 175 m	325 – 425 m	0 – 5	$\hat{d}_0$ = 0,05 *mm*, $\acute{o}$ = 0.75
CZ2	75 – 175 m	75 – 175 m	0 – 5	$\hat{d}_0$ = 0,05 *mm*, $\acute{o}$ = 0.75
CZ3, model 1&3	325 – 425 m	325 – 425 m	0 – 5	$\hat{d}_0$ = 0,05 *mm*, $\acute{o}$ = 0.75
CZ3, model 2	175 – 275 m	325 – 425 m	0 – 5	$\hat{d}_0$ = 0,05 *mm*, $\acute{o}$ = 0.75
	(5 m)	(5 m)	(1 m)	
Passages				
P1	0 – 500 m	375 m	0 m	d_0 = 0.13 *m*
P2	0 – 500 m	125 m	0 m	d_0 = 0.13 *m*

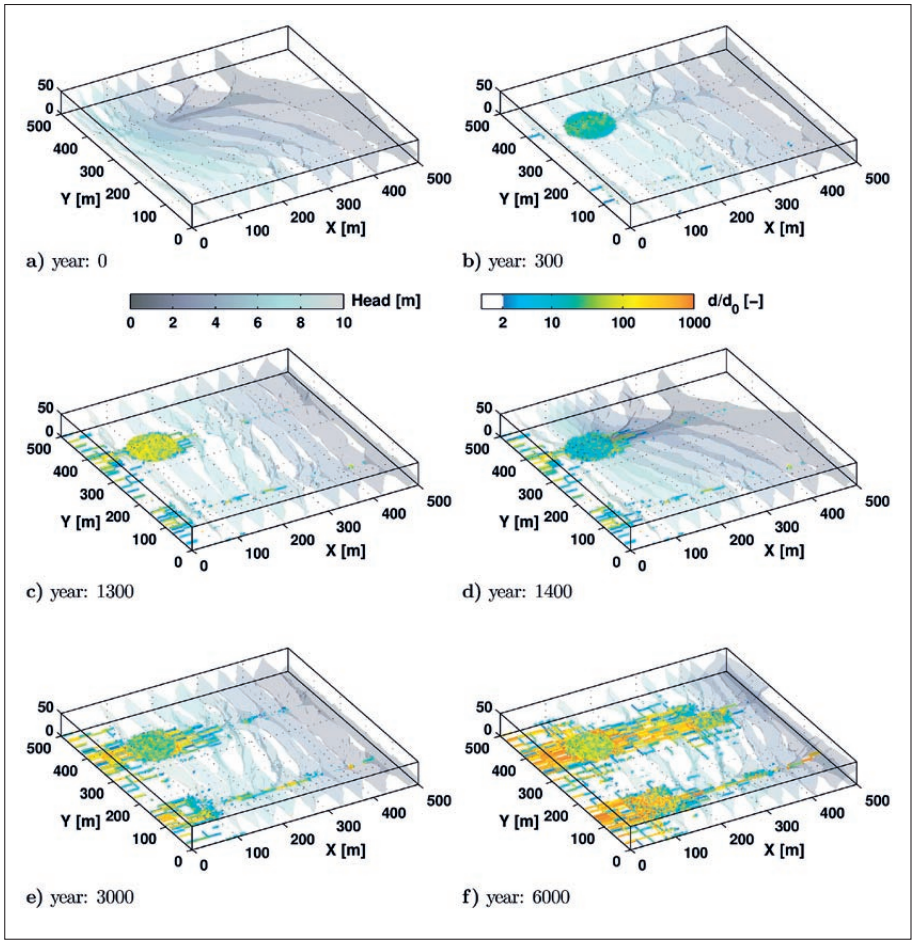

Fig. 6: Conduit diameter evolution of the 3D doline model 1 (one active crushed zone) for different snapshots in time. Below each subplot the year is given; plotted are the isosurfaces of constant head from low (dark grey) to high (light grey) values and the relative increase of the conduit diameter compared to the initial diameter on a log–scale from 2 (blue) to ≥ 1000 (orange).

activated to study the evolution of a single crushed zone inside our model domain. The domain and crushed zone parameters are summarized in Tab. 2. Because crushed zones CZ2 and CZ3 are not activated their initial network parameters are the same as the global network parameters. The evolution of model 1 is shown in Fig. 6 (evolution of model with six snapshots in time) and in Fig. 9a+b (relevant system parameters as a function of time).

Fig. 6 shows the evolution of the conduit diameters in model 1 for six snapshots in time over 6000 years. Shown are the isosurfaces of constant head from low (dark gray) to high (light gray) values and the relative increase of the conduit diameter compared to the initial diameter on a log–scale from a factor of 2 (blue) to a factor of ≥ 1000 (orange). For enhanced visibility only the conduits that have grown at least by a factor of $d/d_0 > 2$, are shown.

Fig. 6a shows the initial head distribution inside the domain. We have assumed that the roof of the cavity started to collapse, creating a breakdown area (crushed zone), which inhibits flow through the cave passage P1. This is clearly seen from the isosurfaces of constant head that show an increase of the hydraulic gradient close to the crushed zone (the closer the isosurfaces are the higher is the gradient and vice versa).

After 300 years of evolution (Fig. 6b), the crushed zone has significantly evolved, when compared to the rest of the domain. The conduit diameters are generally increased by a factor of $d/d_0 \approx 10$ (cyan)whereas in the central part of the domain also larger conduits are visible (increased by a factor of $d/d_0 \approx 100$ (yellow)). The reason for this enlargement is twofold: First, passage P1 feeds the crushed zone directly with undersaturated water which locally decreases the calcium concentration of the water and thereby increases the dissolutional strength. Secondly, due to the larger conduits, the crushed zone is more conductive and thus focusing flow and hence the calcium aggressive water is more likely to be transported into the crushed zone than flowing around it.

After 1300 years of evolution (Fig. 6c), the conduits inside the crushed zone are significantly enlarged by more than a factor of $d/d_0 \approx 100$. The collapsing is soon to happen as most of the conduits inside one layer of the crushed zone have already reached their critical diameter. But also along the second passage (without an ac-

tivated crushed zone) a few conduits have increased in size because the passage allows for aggressive water to be transported through the whole domain and dissolve material along its extent.

Fig. 6d shows the domain after 1400 years of evolution and effectively right after the collapse has happened. The crushed zone is now blocked again (see the increase of the hydraulic heads in the crushed zone) and the conduit diameters are reset to a value similar to their initial value (blueish colors). This cycle continues for the remaining time steps until the simulation is stopped after 6000 years.

Figs. 6e+f show the domain after 3000 and 6000 years, respectively. After 3000 years, few hundred years after the second collapsing event, the zone of enlarged conduits downstream of the crushed zone has reached half of the domain. Because the crushed zone acts like a natural divergence, aggressive water is released along the whole width of the crushed zone. In contrast to this, along the second passage, without an active crushed zone, only the conduits close to the passage have enlarged deep into the domain. After 6000 years the wide enlarged zone downstream of the crushed zone has almost reached the boundary of the domain. Also conduits along the second passage have enlarged especially inside the non activated crushed zone. The reader may notice that it looks like as if there is a stronger evolution inside the non activated crushed zones. This is a side effect of the domain layout and the increased grid resolution there.

In Fig. 9a the temporal evolution of the flow through passage 1 is shown. The local breakthrough event, or in other words the fast increase of flow through the passage, happens within the first 150 years. The parts of the passage that were blocked by the crushed zone get enlarged very quickly and the flow increases by roughly two orders of magnitude. After this first steep increase the enlargement process slows down significantly and continues until ≈ 1400 years. At that time the first collapse of crushed zone CZ1 occurs, passage 1 is blocked again and consequently the flow rates drop by two orders of magnitude (compare Fig. 6d). After the collapse the high flow rates are quickly reestablished due to the consecutive breakthrough event, comparable with the beginning of the simulation. The flow curve shows three more collapse events at ≈ 2700, ≈ 4000 and ≈ 5200 years, respectively. Fig. 9b shows the estimated cumulative loss of surface volume above the crushed zone (black line and axis). The corresponding topographical height above the crushed zone is shown in red. In the presented model always the maximal possible amplitude of a collapse event is chosen, so that the volume v_{CZ} that is removed from the surface directly above a crushed zone is given by

$$V_{CZ} = A_{CZ}\, max\left(d^i_{crit} - d^i_{new}\right). \quad (8)$$

Here A_{CZ}, is the total area of the crushed zone and the new reset diameter of a single conduit i inside the crushed zone. In our approach, the total volume loss at a certain time is given by the surface area A_{CZ} and the largest difference between pre– and post–collapsing diameter d_{new}. As explained in 3.2, this procedure accounts for the representation of fractures by conduits in our model and allows a surface lowering of Δd $[m]$. Within the model, the locations of the nodes inside the crushed zone are not changed and the volume loss/height difference is directly applied to the surface nodes (as if the whole column of bedrock has moved downwards). Fig. 9b shows that one collapse event removes ≈ 2200 m^3 of material leading to a surface lowering of ≈ 0.25 m. The visible periodicity of the model is determined by the critical diameter d_{crit} which is, from a mechanical point of view, rather small within our model but chosen for practical reasons. We always apply a critical diameter of $d_{crit} = 0.05\ m$ to allow at least four big collapse events within 6000 years of evolution. If a larger value for d_{crit} would have been chosen the simulation times would have been increased significantly. Furthermore, a larger d_{crit} would allow for larger conduits to develop before a collapse event. We assume that in such cases a model has to consider not only the dissolution processes (as done by KARSTAQUIFER) but also to account for the mechanical erosion and the mechanical stability within the bedrock. Such scenarios are outside of the scope of this paper and will not be considered. Fig. 9b shows that after 6000 years of evolution the surface has been lowered by ≈ 1.25 m. Choosing this value to estimate the surface lowering of a typical collapse doline in nature, leads to a ≈ 100 m deep doline after ≈ 450000 years. This is an acceptable time frame for the creation of a large collapse doline. Note that collapse dolines in the Dinaric karst of southern Europe are assumed to have developed during millions of years, whereas the Tiankengs in China may be as young as 200000 years (Zhu & Chen 2006, Zhu & Waltham 2006).

4.2.2. MODEL 2 & 3 − THREE ACTIVE CRUSHED ZONES

Now that we have presented a model for the creation of one single collapse doline we want to focus on the interplay of three dolines within one model. Therefore, not only the CZ2 along passage 2 is activated but also two different scenarios for the position of CZ3 are tested. In the first case (model 2) CZ3 is placed close to CZ1 whereas in the second case (model 3) CZ3 is placed further downstream (for the layout see Fig. 3 and Tab. 2).

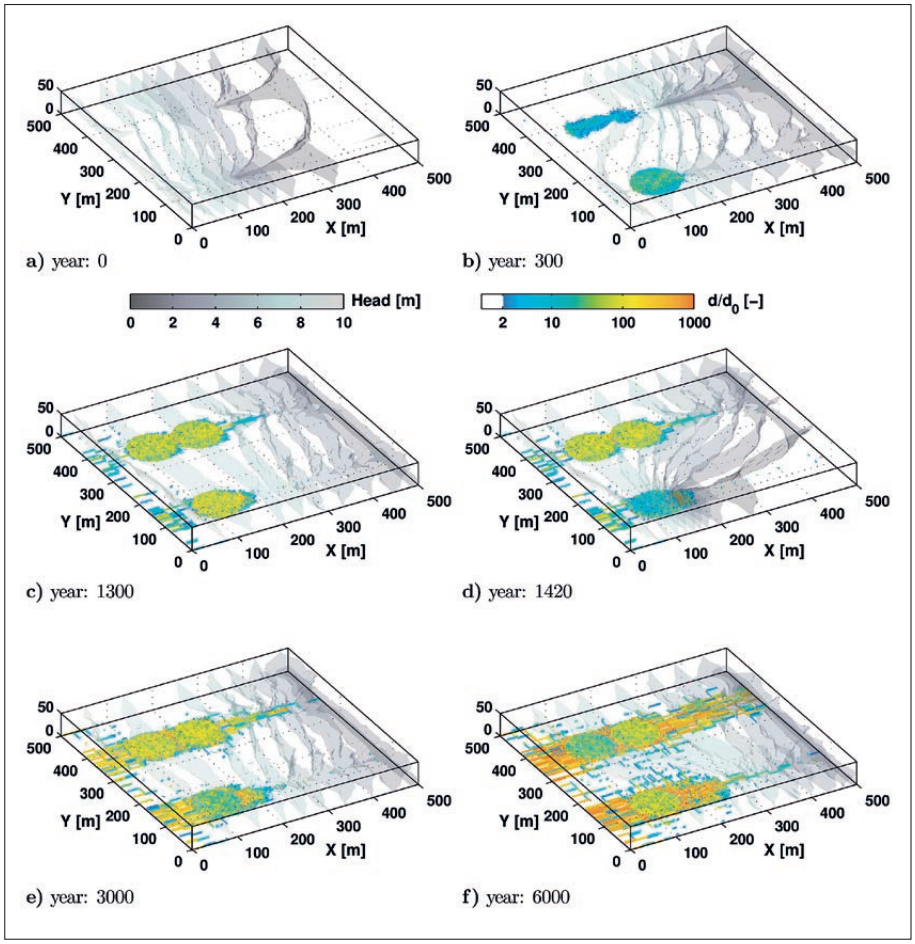

Fig. 7: Conduit diameter evolution of the 3D doline model 2 (three active crushed zones) for different snapshots in time. Below each subplot the year is given; plotted are the isosurfaces of constant head from low (dark grey) to high (light grey) values and the relative increase of the conduit diameter compared to the initial diameter on a log–scale from 2 (blue) to ≥ 1000 (orange).

In this section we will simultaneously describe the evolution of model 2 & 3 and highlight only the differences in their evolution. The evolution snapshots for model 2 & 3 can be found in Fig. 7 and Fig. 8, respectively. The color codes for the head distribution and the conduit diameter increase are the same as for model 1 (Fig. 6).

The initial head distribution (subfigures a) already reveals that the effect of more than one active crushed zone within the model domain is recognizable. When the two active crushed zones along passage 1 are closer together (model 2) then the evolution of the downstream crushed zone allows for higher flow rates and hence more effective development than for the single crushed zone case (model 1). This effect is less pronounced in model 3 which looks initially more like model 1, due to the greater distance between CZ1 and CZ3. After 300 years of evolution two major differences, in comparison to model 1, are visible. In both cases (model 2 & 3) the crushed zones have evolved slower than the single crushed zone and also the general flow field inside the domain is different. Both observations are directly linked to the decreased hydraulic gradients along passage 1. The first effect follows consequently from the reduced flow along passage 1 and is therefore the cause for the weaker evolution. The distortion of the flow field in models 2 & 3 potentially also allows flow from passage 1 towards the single crushed zone and passage 2 which was not the case for model 1. There, the head isosurfaces are almost parallel along the not activated passage 2. But comparing the evolution of the single crushed zone in all three models, the evolution in model 2 & 3 seems to be not much effected by the other two crushed zones or the effect is just not resolvable with our simulation.

As for model 1, also for model 2 & 3 the first collapse event happens for the single crushed zone after ≈ 1400 years of evolution. However, one difference can be recognized when comparing the evolution of the volume loss over time for the single crushed zone in model 2 & 3 with model 1 (Fig. 9b,d,f). As for model 1 also in model 2 the initial collapse of all layers happens within one time step at ≈ 1400 (curves start at ≈ 2000 m^3). For model 3 the curve for CZ2 starts at ≈ 400 m^3, indicating that only one layer collapsed at that time with the other layers following shortly after. This effect is again visible after ≈5000 years of evolution when the jump of vol-

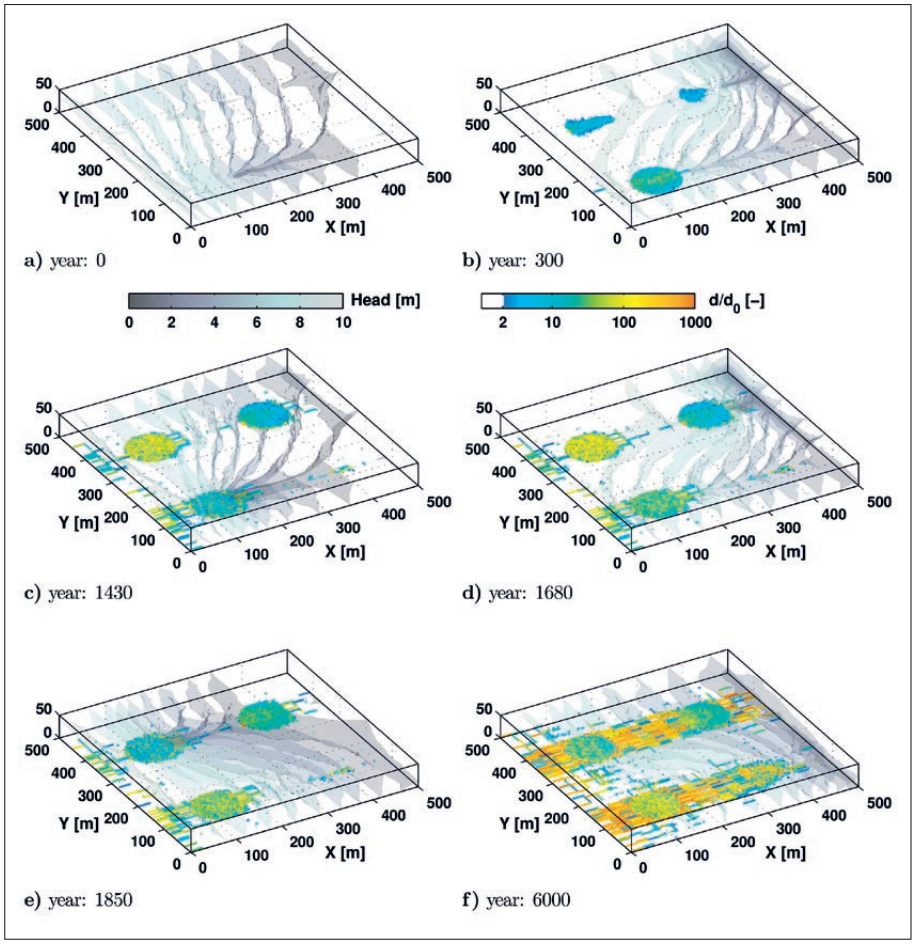

Fig. 8: Conduit diameter evolution of the 3D doline model 3 (three active crushed zones) for different snapshots in time. Below each subplot the year is given; plotted are the isosurfaces of constant head from low (dark grey) to high (light grey) values and the relative increase of the conduit diameter compared to the initial diameter on a log–scale from 2 (blue) to ≥ 1000 (orange).

ume loss for CZ2 in model 2 occurs from ≈6000 m^3 to ≈8000 m^3 within a single time step whereas for model 3 this jump shows again a small kink indicating consecutive collapse events. As already stated above, these effects are rather minor and may be addressed in more detail in a future study. Here we focus on the interplay of two crushed zones along one subsurface passage.

After ≈1700 years of evolution the first collapse event happens in both models 2 & 3 in CZ3, but with different magnitude. In model 2 four layers inside CZ3 collapse shortly after each other, in model 3 only 2 layers collapse. This is due to the different head values within the crushed zones, which causes several layers of the crushed zone to be above the water table and therefore not affected by dissolution. In model 3 where CZ3 is further downstream of CZ1 this effect is stronger. The first collapse of CZ1 in both models 2 & 3 happens shortly after CZ3 but with a stronger amplitude indicating that all active layers within the crushed zone have been collapsed.

From Fig. 9c-f we see that the periodicity of collapse events for CZ1 follows the one of the single crushed zone CZ2 with a time–lag of ≈450 years. Initially this also counts for CZ3 in model 2. The second collapse event happens at the same time as for CZ1 at ≈3000 years but with fewer layers. The remaining collapse of the other layers happens several hundred years later. The third collapse of CZ3 in model 2 is now completely shifted ≈ 500 years after the collapse of CZ1. The whole evolution of CZ3 is slowed down. In model 3 the second collapse of CZ3 is no longer a single event but a series of individual events between 3300–3500 years. The shift in the periodicity of collapse events between CZ1 and CZ3 is even stronger in model 3 than in model 2. This can be explained by the fact that the evolution of the higher layers in CZ3 stops completely every time CZ1 collapses. Then, only the lowermost layer(s) in CZ3 are below the water-table and supplied by fresh aggressive water. Individually, all three dolines show the periodicity in their evolution, only the onset and the amplitude of the individual collapse events differ due to the effect the dolines have on each other. The slowing down of the evolution of CZ3 persists throughout the whole simulation of model 2 & 3 and leads to a difference in topographic height between CZ1 and CZ3 of ≈0.3 m (model 2) and ≈0.6 m (model 3) after 6000 years of evolution.

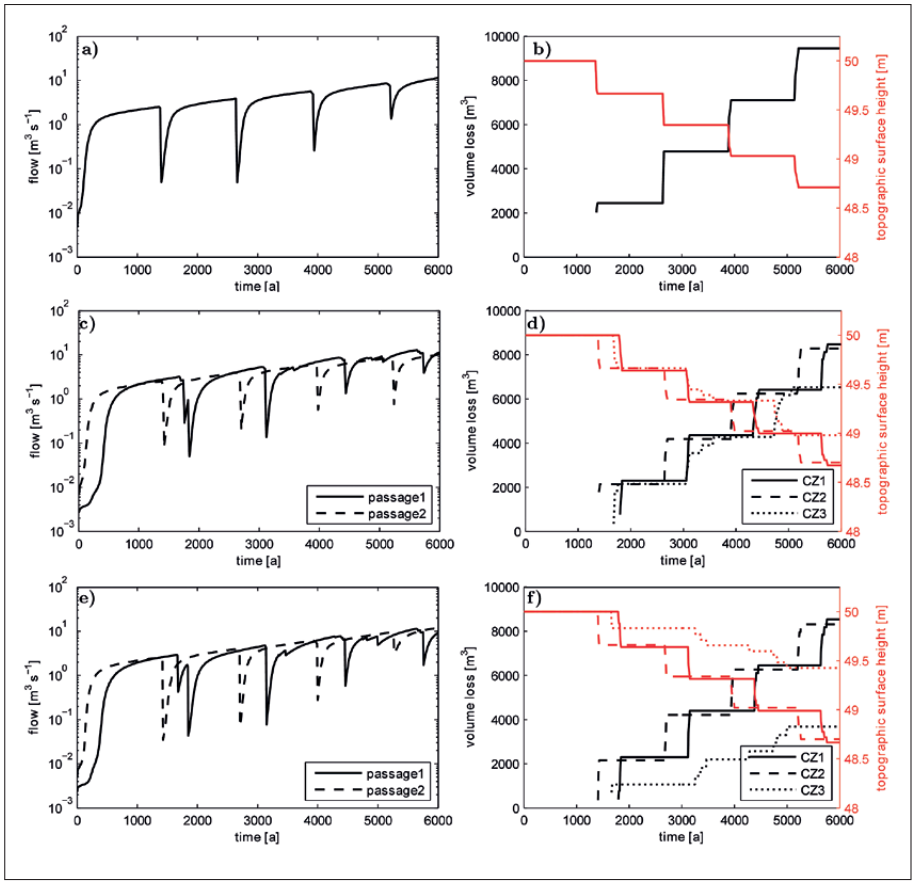

Fig. 9: Flow curves and surface data for the three models. a, c, e) flow rates at the exit of passage 1 (all models) and 2 (only model 2 & 3); b, d, f) cumulative surface volume loss (black) and topographical height (red) above the crushed zone(s) for b) model 1, d) model 2 and f) model 3.

For the three–doline–models shown here, two major observations can be made in Fig. 9c-f: First, if two potential dolines are connected via a subsurface passage, the downstream doline slows down the evolution of the upstream doline compared to the single doline case by ≈400 years in our model. Considering the fact that this model is highly simplified, one can easily imagine how this effect is even stronger when multiple dolines are connected via a common karst system involving also a branched network of passages. Our model shows that a single large collapse doline can evolve quite fast if not disturbed by a group of dolines and that the surface lowering (material removal) is in accordance with values reported in the literature. Secondly, the further away a doline out of a connected group is located downstream, the more its evolution is slowed down, or eventually even stopped. The slow–down for CZ3 is approx. a factor of 3 in the lowering of the surface (model 3).

5. CONCLUSION

There are several conditions that have to be fulfilled for a large collapse doline to evolve (see Waltham *et al.* 2005; Kranjc 2006; Waltham 2006; Zhu & Chen 2006; Zhu & Waltham 2006). A doline with tens to hundreds of meters width and depth, with very steep walls and a floor full of debris, can develop above an active cave system, or above a highly permeable, mechanically unstable zone within a karst aquifer. Furthermore, a necessary condition is that a large amount of water (a subsurface river for example) flows through this system and guarantees the effective dissolution of the soluble host rock.

Following the hypothesis of Palmer and Palmer (2006), Gabrovšek and Stepišnik (2011) developed a 2D numerical karst evolution model to simulate the initiation and evolution of a collapse doline. The outcome of this numerical simulation supports the hypothesis of Palmer and Palmer (2006), and concludes that within a reasonable time frame a collapse doline can develop.

A first goal of our work was to verify the above mentioned conditions with the help of a 3D numerical karst evolution model. In this way we address the main shortcoming of the model presented by Gabrovšek and Stepišnik (2011), namely that all the water was pushed through a single layer of an active crushed zone, which possibly can lead to an overestimation of the rate of material removal/surface lowering and an underestimation of the time required for a doline development. Our results confirm the conclusions suggested by Palmer and Palmer (2006) and Gabrovšek and Stepišnik (2011) and demonstrate that for simple geological settings (a single crushed zone with a large subsurface river flowing at its bottom) the above mentioned conditions are sufficient to predict and explain the development of a large collapse doline. Furthermore, we show that a 2D karst evolution model can describe the evolution of an isolated doline sufficiently well, allowing the development of models describing real location with very high spatial resolution.

The second goal of our study was to extend the 3D karst evolution model in space and to simulate the evolution of complex systems of collapse dolines. The results show that also for these complex geological settings, the main processes governing the growth of large dolines remain valid. We demonstrate that the interactions between the growing dolines are very complex and that the distance between the dolines and the hydro-geological local conditions around them can influence the location of maximum rock dissolution, the frequency of the collapsing events and the time scale of the doline development. This means that for areas above long active cave passages, one would need a detailed knowledge and a dense network of geophysical investigations in order to be able to point the zones of possible sinkhole or dolines development. This result is especially important for locations in the vicinity of large hydraulic structures or large infrastructure projects.

Finally, we would like once again to underline that the goal of the paper is to verify the hypothesis for development of collapse dolines presented by Palmer and Palmer (2006) and to extend the earlier verification of this hypothesis presented by Gabrovšek and Stepišnik (2011). What we present is a synthetic model based on these publications. All results presented here are valid within this synthetic model. A direct application of these results to real collapse dolines as part specific case studies has to be done with care. This is especially valid for locations, for example very large collapses, where an account for the mechanical erosion and the rock mechanics is required. Our model has to be further developed in order to be able to describe such places. This will be the topic of further publications.

ACKNOWLEDGEMENTS

We would like to thank the German Research Society (Deutsche Forschungsgemeinschaft - DFG) for funding the Project KA1723/6 within this work was prepared. Furthermore, the constructive and very helpful reviews provided by two anonymous reviewers were of a great help when preparing this manuscript.

REFERENCES

Buhmann, D. & W. Dreybrodt, 1985a: The kinetics of calcite dissolution and precipitation in geologically relevant situations of karst areas: 1. Open system.- Chemical Geology, 48, (1–4), 189–211.

Buhmann, D. & W. Dreybrodt, 1985b: The kinetics of calcite dissolution and precipitation in geologically relevant situations of karst areas: 2. Closed system.- Chemical Geology, 53, (1–2), 109–124.

Dreybrodt, W., 1988: *Processes in Karst Systems – Physics, Chemistry and Geology*.- Springer Series in Physical Environments 4, Springer Berlin, New York.

Eisenlohr, L., Meteva, K., Gabrovšek, F. & W. Dreybrodt, 1999: The inhibiting action of intrinsic impurities in natural calcium carbonate minerals to their dissolution kinetics in aqueous $H_2O - CO_2$ solutions.- Geochimica et Cosmochimica Acta, 63, (7–8), 989–1001.

Gabrovšek, F. & U. Stepišnik, 2011: On the formation of collapse dolines: A modelling perspective.- Geomorphology, 134, 23–31.

Harned, H. S. W. J. & Hamer, 1933: The ionization constant of water.- J. Am. Chem. Soc., 55, 693–695.

Hiller, T., Kaufmann, G. & D. Romanov, 2011: Karstification beneath dam–sites: From conceptual models to realistic scenarios.- Journal of Hydrology, 398, 202–211.

Istok, J. D., 1989: *Groundwater Modeling by the Finite Element Method* – American Geophysical Union, pp 495, Washington.

Kaufmann, G., 2009: Modelling karst geomorphology on different time scales.- Geomorphology, 106 (1–2), 62–77.

Kaufmann, G. & W. Dreybrodt, 2007: Calcite dissolution kinetics in the system $CaCO_3 – H_2O – CO_2$ at high undersaturation.- Geochimica et Cosmochimica Acta, 71 (6), 1398–1410.

Kaufmann, G., Romanov, D. & T. Hiller, 2010: Modeling three-dimensional karst aquifer evolution using different matrix-flow contributions.- Journal of Hydrology, 388 (3–4), 241–250.

Kranjc, A., 2006: Some large dolines in the Dinaric karst.- Speleogenesis and Evolution of Karst Aquifers, 4 (9), 1– 4.

Palmer, A. N. & M. V. Palmer, 2006: Hydraulic processes in the origin of tiankengs.- Speleogenesis and Evolution of Karst Aquifers, 4 (9), 1–8.

Plummer, L. N., Wigley, T. M. L. & D. L. Parkhurst, 1978: The kinetics of calcite dissolution in CO_2 – water systems at 5 °C to 60 °C and 0.0 to 1.0 atm CO_2.- American Journal of Science, 278, 179–216.

Raines, T. W., 1967: Sótano de las Golondrinas.- Bulletin of the Association for Mexican Cave Studies, 2, 1–37.

Romanov, D., Kaufmann, G. & T. Hiller, 2010: Karstification of aquifers interspersed with non-soluble rocks: Fom basic principles towards case studies.- Engineering Geology, 116 (3–4), 261–273.

Svensson, U. & W. Dreybrodt, 1992: Dissolution kinetics of natural calcite minerals in CO_2 – water systems approaching calcite equilibrium.- Chemical Geology 100 (1–2), 129–145.

Usdowski, E., 1982: Reactions and equilibria in the systems $CO_2 –H_2O$ and $CaCO_3 – CO_2 –H_2O$ (0 °–50 °C).- N. Jb. Miner. Abh., 144 (2), 148–171.

Waltham, T., 2006: Tiankengs of the world, outside China.- Speleogenesis and Evolution of Karst Aquifers 4 (9), p. 1.12.

Waltham, T., Bell, F. G. & M. G. Culshaw, 2005: *Sinkholes and Subsidence*.- Springer Berlin, Heidelberg, pp 282, New York.

Zhu, X. & W. Chen, 2006: Tiankengs in the karst of China.- Speleogenesis and Evolution of Karst Aquifers, 4 (9), 1–18.

Zhu, X. & T. Waltham, 2006: Tiankeng: definition and description.- Speleogenesis and Evolution of Karst Aquifers, 4 (9), 1–8.

COBISS: 1.01

CAVE ROCK SURFACE TEMPERATURE EVALUATION USING NON-CONTACT MEASUREMENT METHODS

MERITVE TEMPERATUR JAMSKIH STEN Z BREZSTIČNIMI METODANI

Hana STŘEDOVÁ[1,2*], Tomáš STŘEDA[1,2] & Miroslav VYSOUDIL[3]

Abstract UDC 551.584.6:772.96(437.3)

Hana Středová, Tomáš Středa & Miroslav Vysoudil: Cave rock surface temperature evaluation using non-contact measurement methods

The aim of this study was to evaluate the rock surface temperature (RST) regime in Kateřinská Cave in the Moravian Karst (Czech Republic, South Moravia) using nondestructive infrared methods. Air temperature monitoring was also included to quantify the dominant factors affecting the RST. Measurements were taken during the period covering January, 2010 to March, 2012. HOBO air temperature sensors with data loggers were placed in front of the cave entrance, in the entrance corridor and on selected sites in the cave interior. An infrared (IR) thermometer was used to measure the surface temperature of the solid rock. The RST in the cave interior during each season was also recorded by IR camera. The average temperature of the rock surface over the two year period was 6.95 °C. The long-term average of the RST was always 0.01 to 0.79 °C lower than the air temperature. The dynamics of the RST are most obvious at the entrance corridor to the cave, with temperature variability up to 17.34 °C. The dynamism of both the RST and air temperature decrease as the distance from the entrance increases. The lowest RST variability (1.19 °C) was detected at a distance of 271–280 meters from the entrance. The differences in the maximum RST in the monitored profile were relative small, ranging from 7.30 to 8.70 °C. Minimum temperatures in the cold season showed a significant difference among themselves. Changes in rock surface and air temperatures are dominantly influenced by air exchange with the external environment, although the RST may be locally influenced on a short-term basis by other factors, such as attendance and biota. Temperature heterogeneous zones over space in Kateřinská Cave with no air flow were located by thermal imaging. It is therefore an area where unknown spaces or exterior access can be expected.

Key words: cave microclimate, infrared thermometer, infrared camera, rock temperature; Kateřinská Cave, the Czech Republick.

Izvleček UDK 551.584.6:772.96(437.3)

Hana Středová, Tomáš Středa & Miroslav Vysoudil: Meritve temperatur jamskih sten z brezstičnimi metodani

Z meritvami infrardečega sevanja smo raziskovali temperaturne značilnosti površine jamskih sten v Kateřinski jami na Moravskem krasu v Republiki Češki. Sočasno smo med januarjem in marcem 2010 merili tudi temperaturo zraka. Pri tem smo temperaturna tipala z zapisovalniki podatkov (HOBO) namestili pred vhod v jamo, v vhodni del jame in na več izbranih mest v jami. Temperaturo površine jamskih sten smo merili z infrardečim termometrom in z infrardečo kamero. Povprečna temperatura površine jamskih sten v dvoletnem obdobju meritev je bila 6,95 °C. Dolgo-časovno povprečje površine jamskih sten je med 0,01 °C in 0,8 °C nižje od povprečja temperature zraka. Temperatura stene se preko leta najbolj spreminja v vhodnem delu jame, za več kot 17 °C in pada z oddaljenostjo od vhoda. Najnižja spremenljivost (1,19 °C) temperature kamnite površine smo zabeležili na oddaljenosti med 271 m in 280 m od vhoda. Najvišja temperatura površine se na izmerjenem profilu gibljejo v območju med 7,3 °C in 8,7 °C, medtem ko je minimalnih temperatur vzdolž profila v hladnem obdobju precej večja. Spremembe temperature zraka in površine sten so pretežno posledica izmenjave zraka z zunanjo atmosfero. Na temperaturo sten lahko pomembno vplivajo tudi drugi faktorji, kot so prisotnost skupin obiskovalcev in živali (netopirjev). V jami smo odkrili temperaturno heterogena območja na mestih, kjer ni zaznavnega toka zraka,kar kaže na morebitno prisotnost neznanih jamskih prostorov oz. bližino neznanih vhodov.

Ključne besede: jamska mikroklima, infrardeči termometer, infrardeča kamera, temperatura kamnite površine, Republika Češka.

[1] Mendel University in Brno, Zemědělská 1, 613 00 Brno, Czech Republic, e-mail: hana.stredova@mendelu.cz

[2] Czech Hydrometeorological Institute, Kroftova 43, 616 67 Brno, Czech Republic, e-mail: tomas.streda@chmi.cz

[3] Palacký University Olomouc, 17. listopadu 12, 771 46 Olomouc, Czech Republic, e-mail: vysoudil@pfnw.upol.cz

[*] corresponding author

Received/Prejeto: 08.10.2013

INTRODUCTION

The transport of heat into the cave system and the influence of airflow are usually critical for the temperature regime in a cave (de Freitas & Littlejohn 1987). The air temperature in the cave is characterized by significantly smaller daily and seasonal amplitudes than the external air temperature (e.g. Šebela & Turk 2011 and others) and is in equilibrium with the internal temperature of its solid rock and water (Badino 2010). In particular, the rock acts as the regulator and stabilizer of air temperature in the cave (Hebelka *et al.* 2011). The homeostasis of the internal environment of accessible caves is also influenced by the energy input of electrical equipment and visitors, and there is a risk that the capacity of these external inputs will exceed the cave's capacity to absorb them, causing irreversible damage to this unique environment.

Cave rock surface temperature (RST) regimes have been investigated primarily in connection with the creation of ice and its persistence in ice caves (Turri *et al.* 2005), with bat hibernation (e.g. Clawson *et al.* 1980 and others), with the effects of visitors (Carrasco *et al.* 2002) and with the condensation corrosion of limestone (de Freitas & Schmekal 2005). Potential climate changes can be identified and quantified according to the long-term trend of cave rock temperature after the elimination of the effects of various radiation shield designs, land cover near meteorological stations, etc.

RST is normally monitored by temperature sensors placed in holes in the rock and connected to a data logger. The depth of the sensor location (for monitoring within the rock) plays an important role in measuring the temperature of the rock massif. Luetscher *et al.* (2008) quantified the energy balance of the Monlesi Cave system by sensors placed in 0.80 m long boreholes drilled into the cave rock (with a diameter of 0.04 m). Martin *et al.* (2006) used an external probe placed object in a 0.01 m hole drilled into the rock substrate. Turri *et al.* (2005) measured rock temperature in an ice cave by two thermocouples inserted into the rock at depths of 0.10 m and 0.40 m.

The aim of the study was to evaluate the RST regime in Kateřinská Cave using nondestructive IR methods. The outputs of monitoring contribute to better understanding of the karst formation and to more efficient protection and management of accessible caves, as well as to describe the influence of external climate on cave microclimates, etc. as stated for example by Gabrovšek *et al.* (2011).

For primary thermal surveying and for identifying sites with different temperature conditions, methods of infrared (IR) camera or IR thermometer temperature measurement are ideal because they do not involve contact and are environmentally friendly with no interior cave destruction. IR camera and IR thermometer were used in the research of cave thermal regimes by Marwin and Thompson (2005), Wynne *et al.* (2008) and Curtis and Kyle (2011). Clawson *et al.* (1980) used IR thermometers for monitoring ceiling rock and bat cluster temperatures in a cave environment. Boyles *et al.* (2007), Boyles *et al.* (2008), Sun-Sook *et al.* (2009) used IR cameras and thermometers for the interior monitoring of caves with hibernating bats. In karst areas outside the cave environment, airborne thermography was used to locate submerged springs, caves, crevasses, sinkholes, etc. (e.g. Campbell *et al.* 1996; Rinker 1975 and others).

Although IR thermometry is currently used in a wide range of mostly technical activities (building energy audits, medical applications, fire detection, night vision optics, etc.), its use in monitoring cave temperatures is relatively rare. Recently, the infrared thermography to studying cave interior microclimate used for instance Berenguer-Sempere *et al.* (2014) or Pflitsch *et al.* (2012). In particular, continuous monitoring of the surface temperature of the rock surface in a cave environment is unique.

DATA AND METHODS

STUDY AREA

The cave environment temperature regime was monitored in the Moravian Karst in Kateřinská Cave (the Czech Republic, South Moravia). According to the climate assessment of the Moravian Karst by Rožnovský *et al.* (2010a), the long-term average air temperature during the period 1961–2008 was 8.4 °C and the annual precipitation total was 600 mm. The warmest month is July, with an average temperature of 18.3 °C, and the coldest is January, with an average temperature of –2.2 °C.

The cave system consists of corridors and three spacious halls with horizontal orientation trending SW – NE. "Hlavní dóm" hall, with dimensions measuring 96 × 45 × 20 m, is the largest underground space acces-

sible to the public in the Czech Republic. "Dóm chaosu" and "Dóm Bambusového lesíku" halls were discovered in 1909, after the discovery of the so-called "Nová Kateřinská" Cave. In the cave, there is no water course or reservoir exerting a strong effect on the microclimate. "Dóm chaosu" hall is vertically connected with an upper floor of the cave "Dantovo peklo". Individual segments of the cave are shown and described in Fig 1. The total length of all known passages reaches 950 m with denivelation of more than 50 m. The spacious cave entrance is located approximately 10 m above the bottom of the "Pustý žleb" gorge, which is approximately 100 m deep. The cave entrance is closed by a door with a hole for migrating bats. Annual attendance in Kateřinská Cave varies between 30 to 50 thousand visitors (up to 900 visitors in one day, maximum of 60 persons per group). The cave is closed to visitors from December to the end of February.

Three main climate zones occur in the cave. The dynamic climate zone extends from the cave entrance to the entrance of the "Hlavní dóm" hall. The transitional climate zone includes the remaining cave spaces, except for the blind side corridors. The corridors lying away from the chimney-effect influence are included in the climatically static zone (Hebelka *et al.* 2007). Air movement in Kateřinská Cave depends on external temperature changes. External temperatures above approximately 5 °C causes a reversal of air-flow direction, which is typical for a climatically dynamic cave (Piasecki & Sawiński 2007).

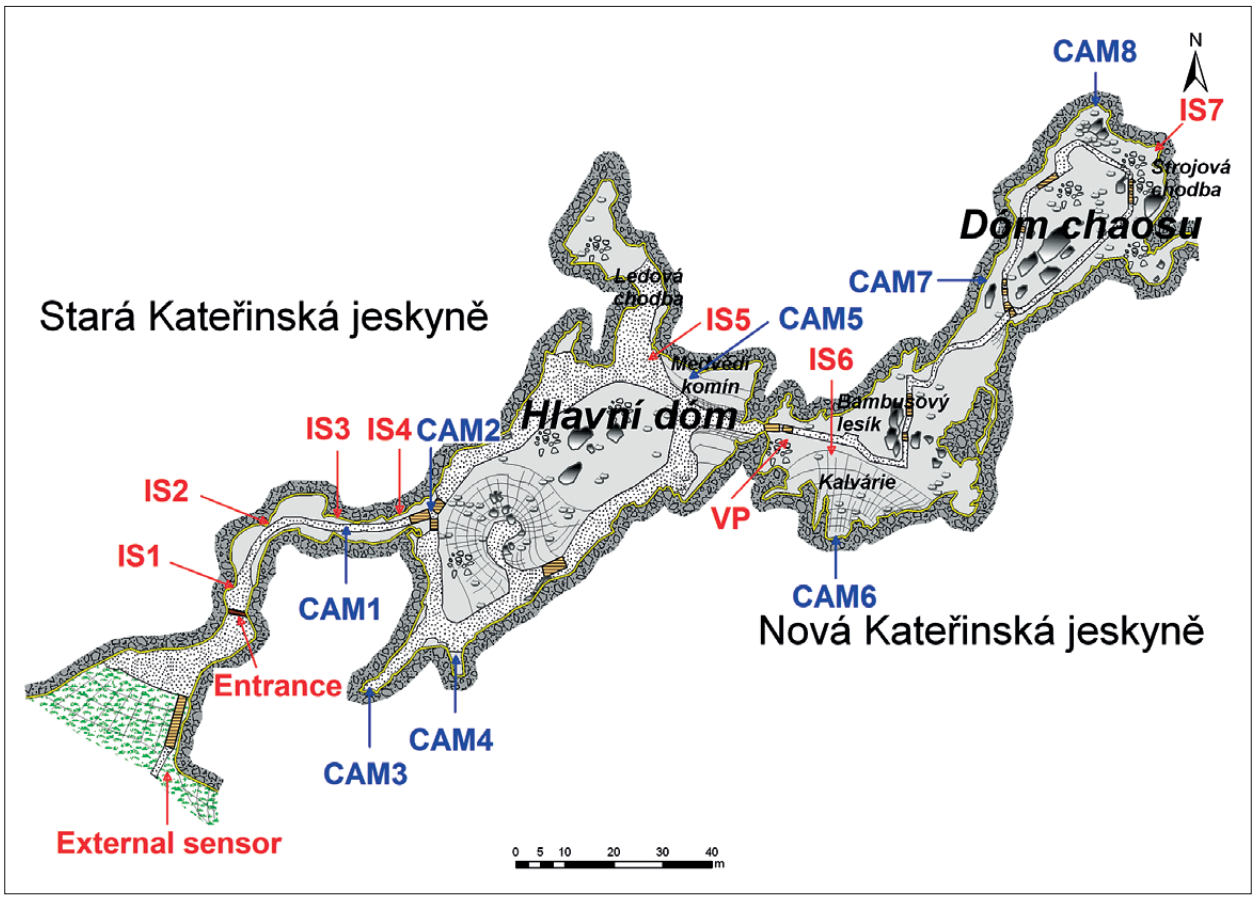

Fig. 1: Location of air temperature sensors (red dots IS1 – IS7 and VP) and the position of the thermal capture records (blue points CAM1 – CAM8).

AIR TEMPERATURE MEASUREMENT

Air temperature at a height of 1 m was measured in representative areas, i.e., the entrance corridor (IS1 – IS4 sensors) and the deep main cave parts (sensors IS5 – IS7 and vertical profile VP) – Fig. 1. Those areas and the external environment (measured with an external sensor in front of the cave entrance) were monitored by the U23 HOBO Pro V2 with a data logger, an accurate air temperature sensor. The accuracy of the HOBO U23 V2 is ±0.21 °C, with a resolution of 0.02 °C. It took one minute

for the interior sensor to capture air temperature differences caused by human attendance and other visitors. External sensors and interior control sensors measured at 15 minute intervals, and the fifteen minute averages were used for the air temperature evaluation.

RST MEASUREMENT (IR THERMOMETER)

The surface temperature of the rock was measured with the Raytek MX4 Raynger® MX4™ IR thermometer. The sensor measures the amount of long wave radiation emitted from the monitored surface based on the Stefan – Boltzmann law and shows the surface temperature of the monitored subject. The amount of emitted radiation varies according to the physical and chemical properties of the surface. The recommended value for limestone emissivity, ε = 0.98 (Thermemether's manual – Raytek® 1999), was used. The sensor measures the surface temperature with a resolution of 0.1 °C and an accuracy of 1.0 °C. Monitoring was conducted at semi-monthly to monthly intervals. The interval is fully sufficient because of the limited annual dynamism of the RST. The RST was measured along the tour route and blind corridor in the southwest part of the cave at 0.03 sec intervals at a height of 1.50 m above the ground. The constant speed of the sensor movement was controlled by the BOSS DB-60 digital metronome.

RST MEASUREMENT (IR CAMERA)

In addition to point measurements, the cave surface temperature for each season was also monitored by the Fluke Ti55 IR fusion technology IR camera with a thermal sensitivity ≤ 0.05 °C. The size of the images taken was 320 × 240 pixels. The actual size of the monitored area and the spatial resolution depends on the distance from the target. In our case, the target distance did not exceed 20 m, indicating that the size of the monitored area is 8 × 6 m. Other technical parameters of the device are given in Fluke® (2007). The Technology IR – Fusion allows simultaneous recording of both the IR and the visible spectrum.

The position of monitored points (CAM1–CAM8) is given in Fig. 1. Point CAM1 is located in the northern wall of the entrance corridor at a height of 0–2 m. CAM2 shows the RST of "Hlavní dóm" hall ceiling at a height of 20 m. CAM3 was placed in a vertical chimney in a blind corridor in "Hlavní dóm" hall. CAM4 is located in the horizontal projection and depressions in the southeastern part of "Hlavní dóm" hall. CAM5 shows the RST of the "Medvědí komín" chimney in the northeastern part of "Hlavní dóm" hall. CAM6 is located in "Dóm Bambusového lesíku" hall and above the debris field called "Kalvárie". CAM7 shows the RST in a vertical chimney leading to the upper levels of the cave in the southwestern part of "Dóm chaosu" hall. CAM8 is located the north vertical walls in "Dóm chaosu" hall at a height of 8 m.

DATA EVALUATION

The results that we evaluated represent the period from January 2010 to March 2012, i.e., three cold and two hot seasons. The evaluation and statistical expression of the data were generated by the STATISTICA software (StatSoft, ver. 7) – Fig 2. This software was also applied to evaluate the dependence of internal temperature on the external temperature and its delay for a specific location in a cave (cross correlation method). The data from the IR thermometer measurement was interpolated by the kriging method in SURFER software (Golden Software, ver. 8.03) – Fig. 3 and 4. The course of the RST during different seasons is dependent on the distance from the entrance and was subsequently expressed in 2D projection. Thermal images from the IR camera were processed by the SmartView® 3.1.89.0 software, Fluke Thermography – Fig. 5 to 11.

RESULTS AND DISCUSSION

IR THERMOMETER MEASUREMENT

The results of RST monitoring are presented in Fig. 2. The RST along the return (southeastern) route of the guided tour was evaluated. The average statistical indicators of rock temperature in 10 m sections were processed for the entire period, and the two-year rock temperature average was 6.95 °C. Significant dynamics of surface temperature presented in the entrance area, with temperature variability up to 17.34 °C; this dynamism decreases with increasing distance from the entrance. Stronger temperature variability in the cave rear caused by lower minimum temperatures occurred only at the interface of "Stará Kateřinská jeskyně" and "Nová Kateřinská jeskyně" and in the "Kalvárie" area, 161–190 m from the entrance.

Average RST increased significantly 110 m from the entrance. Differences in the maximum RSTs (7.30–8.70 °C) in the monitored profile are relatively small. Significant differences in minimum temperatures for the monitored temperature profile were gener-

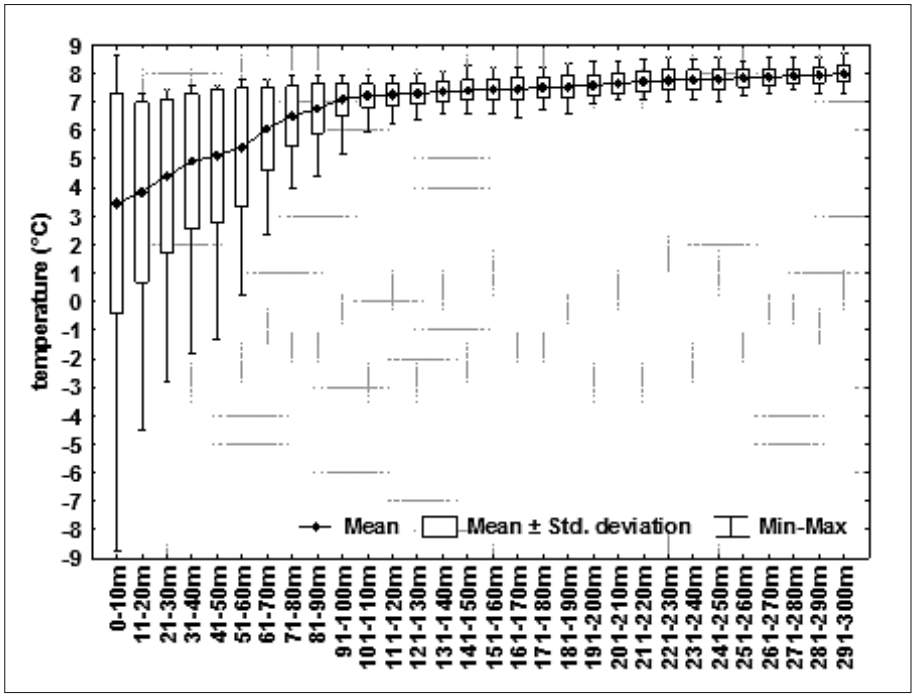

Fig. 2: Basic statistical characteristics of RST in 10 m section from the cave entrance.

ated during the cold months. During the winter, cold air flows through the cave; the cave undergoes changes in temperature and relative humidity as a result of the heat transferred to and from the cave walls (Luetscher *et al.* 2008).

The lowest measured RST in Kateřinská Cave during this period was –8.75 °C, and the highest was 8.70 °C. The smallest variability of RSTs (1.19 °C) was found 271–280 m from the entrance. For neighboring "Punkevní jeskyně" during the period from 2007 to 2011, Hebelka *et al.* (2011) reported an average rock temperature of 8.21 °C, a maximum temperature of 8.49 °C and a minimum temperature of 7.90 °C (sensors located 0.20 m in rock massif). Turri *et al.* (2005) reported seasonal rock temperature fluctuation of up to 2 °C; during "cold" events, the rock was affected by the air temperature minimally, at least in the first 0.40 m. Badino (2010) reported daily limestone temperature fluctuations in thicknesses of 0.2 m and annual fluctuations in thicknesses of 3–4 m. Luetscher *et al.* (2008) present a temperature gradient in Monlesi Cave between 0.44 and 0.70 °C.m^{-1}.

The monitoring in Kateřinská Cave showed that changes of air and RST are dominantly influenced by exterior conditions. Rožnovský *et al.* (2010b) arrived at the identical conclusion while evaluating air temperatures, with possible connection to rock temperatures, in Kateřinská Cave. Air temperatures vary up to 2 °C in the central part of Kateřinská Cave. Hebelka *et al.* (2011) employed a method of cross correlation which is generally used when measuring information between two different time series. Is it a standard method of estimating the degree to which two series are correlated. An analysis of the closeness of the relationship with the outside temperature using a cross-correlation method was processed using the IS7 air temperature sensor. The most significant statistical correlation between internal and external temperatures was when the outer line was shifted approximately 22 days backwards (R = 0.822). This indicates that Kateřinská Cave has an inertia of internal air temperature of approximately 3 to 5 weeks, and the correlation coefficients ranging from 21 to 35 days are almost identical.

Semi-monthly to monthly measurements of rock temperature by IR thermometers were interpolated and expressed in a 2D graph (Fig. 3). The RST was stable in the summer months, with a lower value in the entrance area. It is probably caused by the fact the heat conduction from exterior as well as weak outflow of relatively warm air do not outweigh the consequence of winter temperature decline. The RST has a dynamic character in the front part of the cave during the rest of the year. The effects of an energy exchange between the rock massif and the cave atmosphere is clear here. Obleitner & Spötl (2011) described the seasonal influences on rock temperature at the cave entrance identically in similar climatic condition within the Eisriesenwelt Cave, Austria. Towards the interior of Kateřinská Cave, the influence of external conditions weakens and a delay as to the temperature in cave rear is fairly stable throughout the whole period (see Fig. 3).

The differences between air temperature and RST (rock temperature substracted from air temperature)

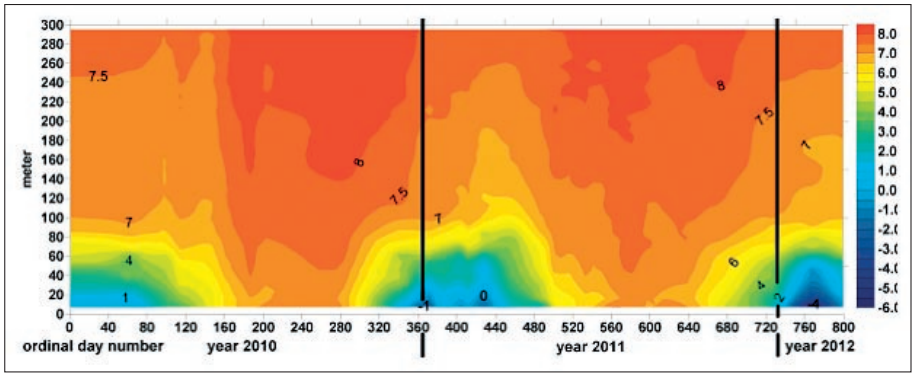

Fig. 3: RST (°C) in Kateřinská Cave from January 2010 to March 2012.

were calculated, using the time and position in the cave. More significant temperature differences were recorded in winter. Positive temperature differences occur in the winter immediately behind the entrance into the cave. This phenomenon is mainly caused by the freezing of the rock massif by heat conduction and increased by the sudden supply of cold air from the external environment (see Fig. 4 – for instance: 30th to 40th day, 280th to 300th day and 680 to 700th day). The cold air flows into the cave and cools the host rock. The temperature regime of the entrance hall is also affected by the temperature gradient of interior and exterior temperatures, which influences the direction of airflow in the cave. When changing the direction of air flow, the difference between the temperature of incoming autochthonous air and rock temperature shoots up briefly to 6 °C. In summer, warm air flows through the chimneys into the entrance corridor hall, bringing heat to the rock. Air temperature and RST in the summer are identical most of the time.

Behind the dynamic section of the entrance corridor, there is an area that is made up of part of the entrance corridor connected to the "Hlavní dóm" hall and the southeastern part of the "Hlavní dóm" hall; in this area, the air temperature in winter is up to 3 °C lower over the short-term than the temperatures of the rock surface. Winter subcooling of this section is caused by the inflow of cold air from the entrance corridor. Allochtonous air flows around the cave from the southern side (Hebelka *et al.* 2011). Stratification of air temperature and RST in the "Hlavní dóm" hall is significantly influenced by its topography. The influence of the cold air intake from the area near CAM4 (Fig. 11) and its accumulation in the southern part is possible, below "Hlavní dóm" hall. Air temperature and RST in the remaining parts of the cave are basically identical.

The monitoring results of air temperature and the RST differences at sensors IS1 – IS7 are listed in Tab. 1. Long-term averages do not present higher temperatures for the rock surface. Average long-term RST was always lower than the air temperature, with a range of difference from 0.01 to 0.79 °C. These results correspond with the findings of Carrasco *et al.* (2002) that rock temperature is approximately 1.0 °C to 2.0 °C lower than air temperature; they also correspond to the findings of Jeannin (1991) and Luetscher and Jeannin (2004) that rock temperature is close but slightly lower than air temperature (approximately 0.15 °C). The RST variability decreases with increasing distance from the entrance. The air flowing and temperature regime of RST and air temperature is also influenced by number of other factors. In individual cases in the differences between air and rock temperature depends for example on whether it is upper or lower entrance, or convection cell. Milanolo a Gabrovsek (2009) described an effect of gravity on seasonal temperature regime of Srednja Bijambarska Cave, Bosnia and Herzegovina. An influence of atmospheric

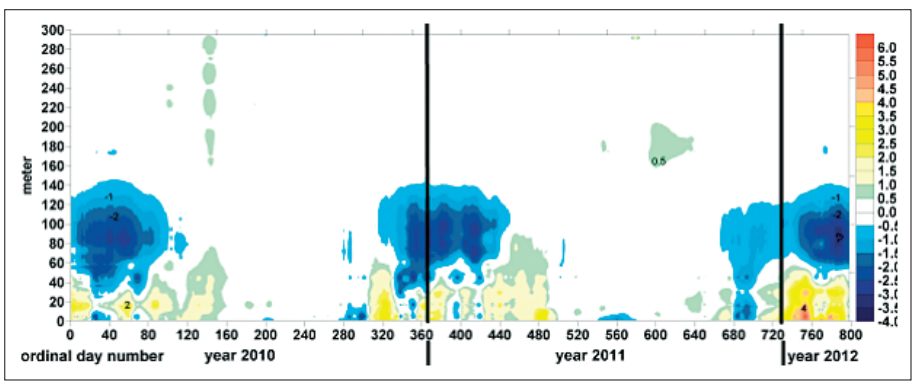

Fig. 4: Difference of air temperature and RST (°C) from January 2010 to March 2012.

Tab. 1: Comparison of air temperature and rock surface temperature at measurement points (entire period).

Measurement point	*Place*	*Average*	*Std. deviation*	*Minimum*	*Maximum*	*Variability*
IS1	Air	4.03	3.13	–6.34	7.69	14.03
	Rock	3.32	3.67	–7.08	8.54	15.62
IS2	Air	4.61	2.57	–4.55	8.23	12.78
	Rock	3.82	2.92	–3.88	7.30	11.18
IS3	Air	5.21	1.96	–0.50	8.07	8.57
	Rock	4.54	2.39	–1.54	7.39	8.93
IS4	Air	5.13	2.41	–2.51	8.23	10.74
	Rock	5.06	2.15	–0.94	7.60	5.54
IS5	Air	7.43	0.36	6.60	8.12	1.52
	Rock	7.42	0.33	6.75	8.17	1.42
IS6	Air	7.62	0.52	6.08	8.57	2.49
	Rock	7.51	0.37	6.80	8.20	1.40
IS7	Air	8.05	0.22	7.53	8.81	1.28
	Rock	8.02	0.27	7.54	8.70	1.16

pressure gradient is described by Fernandez-Cortes A. *et al.* (2009).

Anomaly IS4 (lower minimum air temperature than IS3 when temperature tends to decrease with increasing distance from the entrance) results from the leveling of the bottom of the cave and from inverse temperature stratification. The IS4 sensor was affected by the inflow of cold air from outside in winter. Cold air accumulates at the end of the entrance corridor in front of the stairs to the "Hlavní dóm" hall. Lower minimums and higher maximums of air temperature near IS6 (area "Kalvárie") show the influence of the external environment on air temperature. Under the dome ceiling, air flows through the rubble of the unknown parts of the cave system. Air temperature is influenced here by rock thermals and access to the exterior. In the summer, the partial effects of visitors on the maximum air temperature (IS6) remain in place for a long time.

IR CAMERA MEASUREMENT

During our study, parts of the cave were monitored by IR camera. Monitoring also focused on areas in which the influence of external conditions on the temperature regime was expected. Kermode (1979) attributed 3.6 % of temperature changes to visitors and lighting effects in Waitomo Cave. For this reason, areas with direct and indirect influence of visitors were also monitored (Fig. 5 and 6). The possible influence of factors such as visitors or biota on the RST may be considered to be short–term and significant for local measurements. The large volume of air and its flow in Kateřinská Cave takes away and disperses transferred heat energy radiated by visitors. Carrasco *et al.* (2002) present the maximum daily fluctuations of rock temperature caused by the influence of visitors at 0.15 °C. Zelinka (2002) recorded and correlated the influence of visitors to the changes in rock and aragonite temperature, with a quick return to average

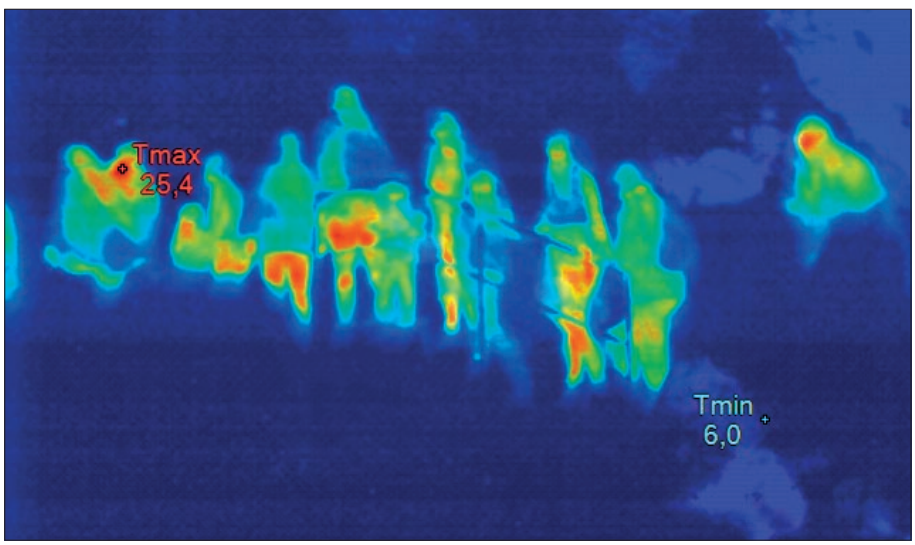

Fig. 5: Anthropogenic input of heat into the cave environment by visitors.

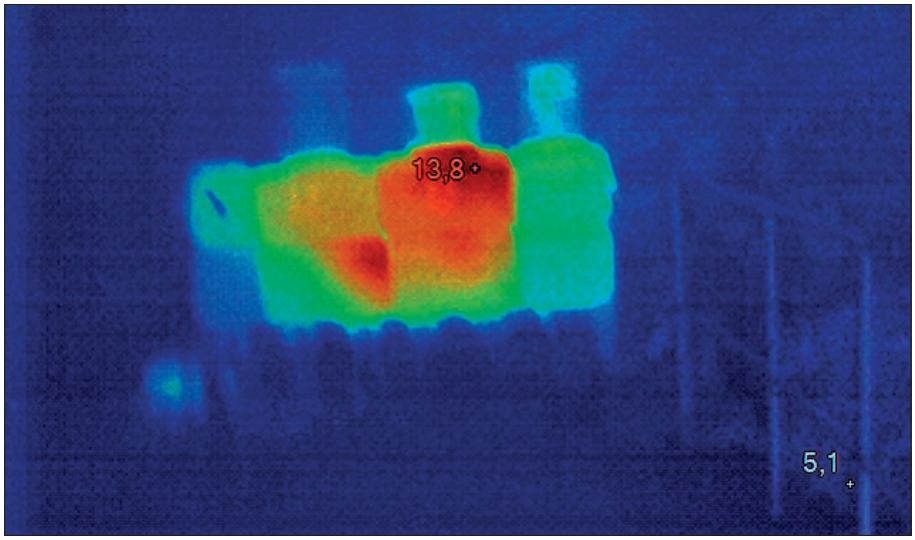

Fig. 6: Anthropogenic input of heat into the cave environment by electrical device.

values. Calaforra *et al*. (2003) presented a temperature memory effect for visitors of 5–6 hours for cave air. The memory effect on rock temperature in this case is negligible. In caves with bats, the rock temperature is influenced (locally) by bat roosting. Boyles *et al*. (2008) discovered temperature differences between rock and cluster temperatures of 0.30 °C, using thermal analysis and a cluster of hibernating bats. Lundberg and McFarlane (2009) used the Raytek ST60 IR thermometer to determine that the temperature of "bell holes" with bats is approximately 1.1 °C higher than those without bats. Rock temperature returns to normal during bat foraging periods after approximately 5 hours.

Temperature minimums and maximums for the individual measuring points during the year are given in Tab. 2. CAM4 monitoring was performed only in February 2011; therefore, it is not evaluated in Tab. 2. Absolute values of RST are approximately 1–2 °C lower than the values measured by the IR thermometer. The differences are caused by divergent measuring principles, such as point measurement of several square meters versus surface measurement. IR cameras monitor the scene with a size of tens of square meters and a scattering of values that are associated with it. It is also affected by the accuracy of the instruments (IR thermometer 1.0 °C, IR camera ±2 °C or 2 %). In addition to this the IR camera required to set a background temperature. In our case was set identically for all measuring points as 7 °C. To assess the development of the RST in time and to compare temperatures of various places during one measurement, the relative expression of temperatures (their difference) is sufficient. In accordance with previous results, the largest RST differences in frame of seasonal imagines were found in the entrance corridor (CAM1) 12.4 °C, in a blind corridor in the southwest part of the cave (CAM3) 5.4 °C and in the locality "Kalvárie" (CAM6) 9.5 °C (see Tab. 2). By contrast, the results of CAM2 are influenced by the localization of monitoring (the RST of the ceiling

Tab. 2: Thermal characteristics of the rock surface in each season based on the evaluation of thermal images.

		Measurement point						
	Date	CAM1	CAM2	CAM3	CAM5	CAM6	CAM7	CAM8
Minimum temperature (°C)	28.2.11	–2.5	4.2	3.8	4.2	1.0	5.4	6.6
	3.5.11	2.4	4.2	4.1	4.8	5.1	5.8	6.0
	2.8.11	4.5	5.5	5.4	4.2	6.8	5.1	5.8
	29.9.11	5.1	4.8	7.3	5.9	5.9	7.1	7.5
	8.2.12	–5.9	4.3	4.2	4.3	–1.5	5.0	5.0
Range		11.0	1.3	3.5	1.7	8.3	2.1	2.5
Maximum temperature (°C)	28.2.11	–1.5	5.6	5.4	6.0	5.6	6.5	7.9
	3.5.11	4.1	5.6	5.8	6.4	6.6	7.0	7.6
	2.8.11	6.0	7.0	7.4	6.9	8.0	6.5	7.4
	29.9.11	6.5	6.6	9.2	7.5	7.0	8.4	7.5
	8.2.12	–2.6	5.6	5.5	5.1	5.3	6.3	5.3
Range		8.0	1.4	3.8	2.4	2.7	2.1	2.6

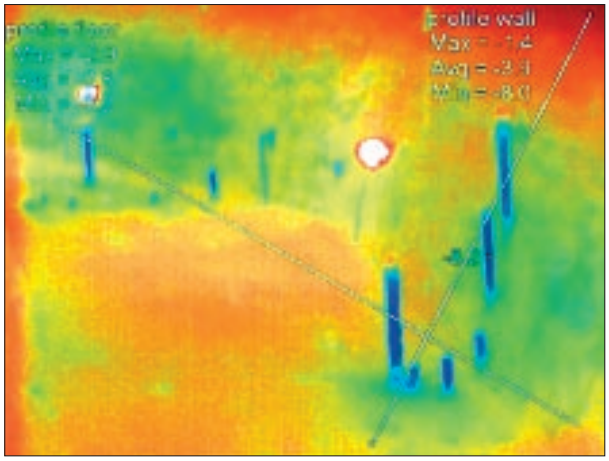

Fig. 7: Thermal image of entrance corridor (CAM1 February 8 2012).

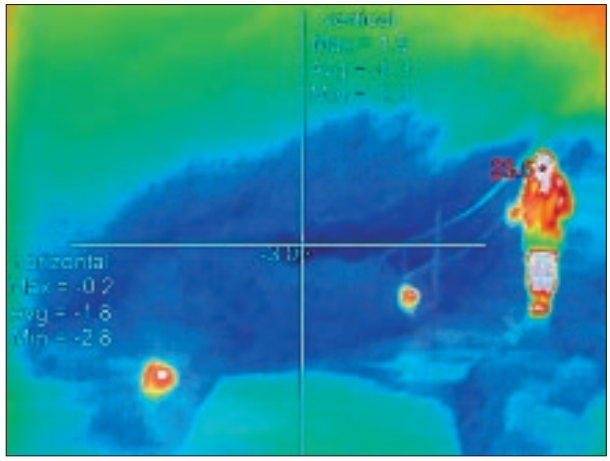

Fig. 8: Penetration of cold air from the entrance corridor to "Hlavní dóm" hall (February 8 2012).

of the cave at a height of 20 m). At this height, near the ceiling of "Hlavní dóm" hall, airflow is eliminated due to rugged ceiling morphology and higher temperature compared to floor. The area is also thermally stable.

Chosen thermal images were analyzed in detail and their analyses are shown in Fig. 7 to 11.

RST inversion (i.e. lower temperature above the floor than under the ceiling) is demonstrated by the IR camera image from the entrance corridor (February 2012) in Fig. 7. Ice stalagmites have been generated in the front part of entrance corridor. They are not formed on a higher level than approximately 1.20 m. In combination with an absence of ice stalactites it proves an assumption of warmer air layer in upper part of the corridor. Warm internal air from remote parts of the cave flows above cool air layer (Hebelka *et al.* 2011). A layer of warmer air occurs under the cave roof and the cooling of the rock is thus less intense and slower. Additionally, Smithson (1993) recorded significant vertical temperature stratification over the winter. Bourges *et al.* (2006) found the highest temperature in the central part of the vertical profile of the spacious cave l'Aven d'Orgnac.

The thermal image in Fig. 8 shows the area near sensor IS4 and CAM2 in the winter. At the boundary between the entrance corridor and "Hlavní dóm" hall, cold air and warm air mix. A significantly heterogeneous temperature zone is generated there. In winter rock

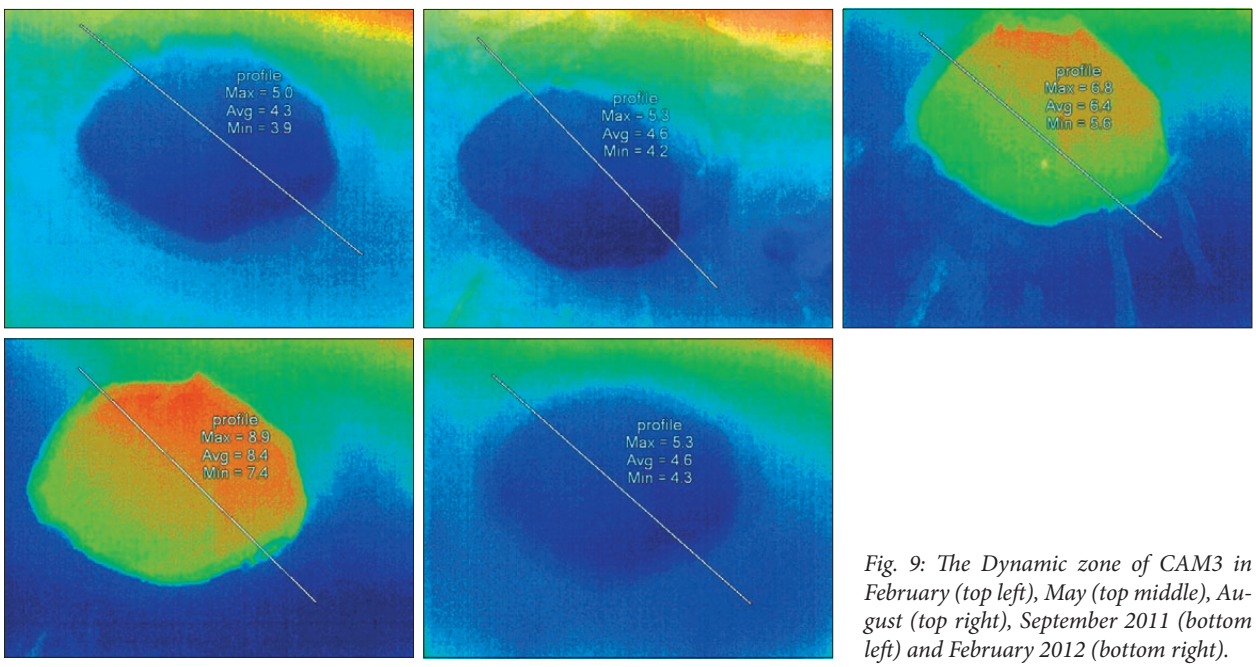

Fig. 9: The Dynamic zone of CAM3 in February (top left), May (top middle), August (top right), September 2011 (bottom left) and February 2012 (bottom right).

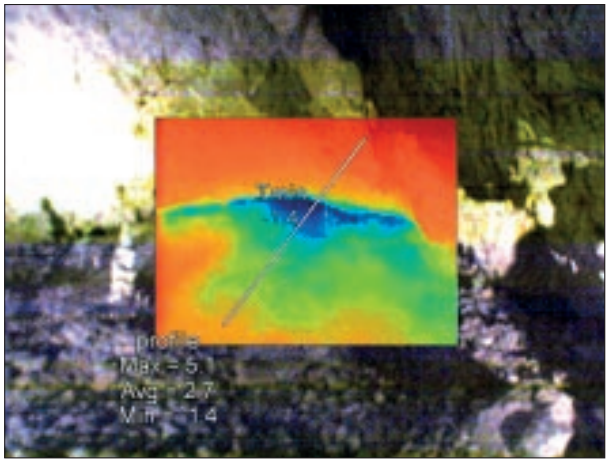

Fig. 10: Thermal recording of CAM6 dynamic zone in February 2012 – thermal image integrated into a visible image.

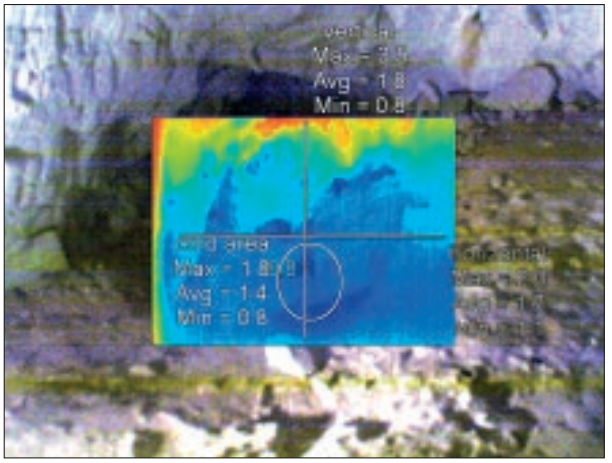

Fig. 11: Example of CAM4 dynamic zone detection in February 2012 – thermal image integrated into a visible image.

above the floor of the cave entrance corridor is colder than the rock under the ceiling and therefore absorbs more heat and energy from the relative warm air. The RST at ground level is significantly cooler than the air and the rock near the ceiling. Cold air entering from the entrance corridor greatly affects the temperature regime across the southern part of "Hlavní dóm" hall (see measurement by IR thermometer).

The morphology of "Suchý žleb" gorge and the thickness of overburden significantly reduces the effect of solar radiation on the cave interior. The active surface above the cave consists of mixed forest and therefore the insolation is significantly reduced. The exception is a zone of CAM3. The CAM3 area (Fig. 9) has a seasonal variability of maximum and temperature of 3.8 °C and 3.5 °C respectively (Tab. 2) due to heat conduction from the surface which is beeing insolated. Furthermore, presence of tree roots in this part of the cave indicates thinner overburden layer and contact with the nearby cave environment.

The effect of the debris cone on the external environment by the debris cone in the area of "Kalvárie" and above "Bambusový lesík" (CAM6) was demonstrated by using a thermal IR camera for monitoring – Fig. 10. In this area, the seasonal variability of minimum surface temperature is up to 8.3 °C.

Temperature heterogeneous zones probably indicating unknown cave spaces and contacts with the exterior was also detected by point CAM4 (Fig. 11). For example, during a cold episode in February 2012, the RST was 3–4 °C lower than in the immediate vicinity (i.e., a few meters away) in this part of the cave. In this area, cold air also accumulates, which is demonstrated in Fig. 4.

CONCLUSIONS

The results are important for the karst formation research and are useful for efficient protection of the cave environment and biota. Proper management of accessible caves requires quantification of the external climate influence on it.

IR Sensors enable useful descriptions of the spatial and temporal temperature variability of the observed surfaces. With use of the planar information of an IR camera the approximate RST was obtained. An IR thermometer provides standard point outputs. A series of detailed IR thermometer points measuring along the entire length of the cave was transferred to the spatial output. Interpolation methods enabled an expression of the RST as a daily step.

Through thermal imaging, heterogeneous zones in Kateřinská Cave in which we expect new and unknown spaces and/or communication with the exterior were located. Using IR camera monitoring, the effect of the exterior was clearly demonstrated in the "Kalvárie" above "Bambusový lesík" and apparently also in a small area in the southeast of "Hlavní dóm" hall. The effects of attenuated overburden and the effect of heat exchange by conduction were found in the blind corridor in the southern part of the "Hlavní dóm" hall. Significant influence of the

exterior through the upper floors of the cave ("Dantovo peklo") across the chimney "Strojová chodba" (IS7) was not demonstrated. If the outside air flows to the "Dantovo peklo", it is most likely thermally transformed in vast areas and the climate of Kateřinská Cave is not significantly affected.

The most dynamic part of the cave temperature is at the entrance corridor, which has several-fold higher dynamics than the rest of the cave. With increasing distance from the entrance, the temperature variability of the rock surface decreases, with the exception of those sites with a specific regime.

ACKNOWLEDGEMENTS

The work was supported by project ME No. SP/2D5/5/07 "Determination of cave microclimate depending on external weather conditions in CR show caves".

REFERENCES

Badino, G., 2010: Underground meteorology – „What's the weather underground?".- Acta Carsologica, 39, 427–448.

Berenguer-Sempere, F., Gómez-Lende, M., Serrano, E. & J.J. de Sanjosé-Blasco, 2014: Orthothermographies and 3D modeling as potential tools in ice cave studies: the Peña Castil Ice Cave (Picos de Europa, Northern Spain).- International Journal of Speleology, 43, 35–43.

Bourges, F., Genthon, P., Mangin, A. & D. D'Hulst, 2006: Microclimates of L'Aven d'Orgnac and other French limestones caves (Chauvet, Esparros, Marsoulas).- International Journal of Climatology, 26, 1651–1670.

Boyles, J.G., Dunbar, M.B., Storm, J.J. & V. Brack, 2007: Energy availability influences microclimate selection of hibernating bats.- The Journal of Experimental Biology, 210, 4345–4350.

Boyles, J.G., Storm, J.J. & V. Brack, 2008: Thermal benefits of clustering during hibernation: a field test of competing hypotheses on Myotis sodalis.- Functional Ecology, 22, 632–636.

Calaforra, J.M., Fernández-Cortés, A., Sánchez-Martos, F., Gisbert, J. & A. Pulido-Bosch, 2003: Environmental control for determining human impact and permanent visitor capacity in a potential show cave before tourist use.- Environmental Conservation, 30, 160–167.

Campbell, C.W., Abd, E.L.M. & J.W. Foster, 1996: Application of thermography to karst hydrology.- Journal of Cave and Karst Studies, 58, 163–167.

Carrasco, F., Vadillo, I., Liñán, C., Andreo, B. & J.J. Durán, 2002: Control of environmental parameters for management and conservation of Nerja Cave (Malaga, Spain).- Acta Carsologica, 31, 105–122.

Clawson, R.L., LaVal, R.K., LaVal, M.L. & W. Caire, 1980: Clustering behavior of hibernating Myotis sodalis in Missouri.- Journal of Mammalogy, 61, 245–253.

Curtis, A. & P. Kyle, 2011: Geothermal point sources identified in a fumarolic ice cave on Erebus volcano, Antarctica using fiber optic distributed temperature sensing.- Geophysical Research Letters, 38, 7 p.

De Freitas, C.R. & R.N. Littlejohn, 1987: Cave climate: assessment of heat and moisture exchange.- Journal of Climatology, 7, 553–569.

De Freitas, C.R. & A. Schmekal, 2005: Prediction of condensation in caves.- Speleogenesis and Evolution of Karst Aquifers, 3, 9 p.

Fernandez-Cortes, A., Sanchez-Moral, S., Cuezva, S., Cañaveras, J.C. & R. Abella, 2009: Annual and transient signatures of gas exchange and transport in the Castañar de Ibor cave (Spain).- International Journal of Speleology, 38, 153–162.

Fluke®, 2007: *Fluke TiR2, TiR3, TiR4, Ti40, Ti45, Ti50, Ti55 IR FlexCam Thermal Imagers. Users manual.* Rev. 2, 5/09.- Fluke Corporation, pp. 132, Everett, WA, USA.

Gabrovšek, F., Knez, M., Kogovšek, J., Mihevc, A., Mulec, J., Perne, M., Petrič, M., Pipan, T., Prelovšek, M., Slabe, T., Šebela, S. & N. Ravbar, 2011: Development challenges in karst regions: Sustainable land use planning in the karst of Slovenia.- Carbonates and Evaporites, 26, 365–380.

Hebelka, J., Piasecki, J. & T. Sawiński, 2007: Air exchange in the Kateřinská Cave. First contribution.- Aragonit, 12, 136.

Hebelka, J., Korzystka, M., Piasecki, J., Sawiński, T., Rožnovský, J., Středová, H., Fukalová, P., Středa, T., Lejska, S. & T. Litschmann, 2012: *Stanovení závislosti jeskynního mikroklimatu na vnějších podmínkách ve zpřístupněných jeskyních České republiky* [in Czech].- Acta Speleologica, 3, 243 pp.

Jeannin, P.Y., 1991: Températures dans la zone vadose du karst.- In: *Actes du 9e Congrès national de la SSS*, Société Suisse de Spéléologie, 71–76, Charmey.

Luetscher, M. & P.Y. Jeannin, 2004: Temperature distribution in karst systems: the role of air and water fluxes.- Terra Nova, 16, 344–350.

Luetscher, M., Lismonde, B. & P.Y. Jeannin, 2008: Heat exchanges in the heterothermic zone of a karst system: Monlesi Cave, Swiss Jura Mountains.- Journal of Geophysical Research, 113, 13 p.

Lundberg, J. & D.A. McFarlane, 2009: Bats and bell holes: The microclimatic impact of bat roosting, using a case study from Runaway Bay Caves, Jamaica.- Geomorphology, 106, 78–85.

Martin, K.W., Leslie, D.M., Patron, M.E., Puckette, W.L. & S.L. Hensley, 2006: Impacts of passage manipulation on cave climate: Conservation Implications for Cave-Dwelling Bats.- Wildlife Society Bulletin, 34, 137–143.

Milanolo, S. & F. Gabrovšek, 2009: Analysis of carbon dioxide variations in the atmosphere of Srednja Bijambarska Cave, Bosnia and Herzegovina.- Boundary – Layer Meteorology, 131, 479–493.

Obleitner, F. & C. Spötl, 2011: The mass and energy balance of ice within the Eisriesenwelt cave, Austria.- The Cryosphere, 5, 245–257.

Piasecki, J. & T. Sawiński, 2007: Acoustic measurements of airflow in speleo-climatological studies.- Karst and Cryokarst, Studies of the Faculty of Earth Science, University of Silesia, Sosnowiec – Wrocław, 45, 237–256.

Pflitsch, A., Grebe, Ch. & M. Grudzielanek, 2012: About the use of thermal imaging in cave micrometeorological studies.- In: *Akten des 13. Nationalen Kongresses für Höhlenforschung*, 29th September–1st October 2012, Muotathal, Schweiz: Schweizerische Gesellschaft für Höhlenforschung. Kommission für Wissenschaftliche Speläologie, Arbeitsgemeinschaft für Speläologie Regensdorf, Arbeitsgemeinschaft Höllochforschung, Höhlengruppe Muotathal, 141–144, Muotathal.

Raytek®, 1999: *Raynger® MX4™ High performance infrared thermometer. Rev. D, 01/1999.*- Raytek Corporation, pp. 111, Santa Cruz, California, USA.

Rinker, J.N., 1975: Airborne infrared thermal detection of caves and crevasses.- Photogrammetric Engineering and Remote Sensing, 41, 1391–1400.

Rožnovský, J., Středa, T., Litschmann, T., Pokladníková, H. & P. Fukalová, 2010a: Mesoclimate as a part of recreation potential of the landscape on the example of the Moravian Karst.- In: *Recreation and Environmental Protection*, 5th–6th May 2010, Krtiny, Mendel University in Brno, 60–64, Brno.

Rožnovský, J., Fukalová, P., Pokladníková, H. & T. Středa, 2010b: The impact of visitors on microclimate of Katerinska cave assessed on the base of ambulatory measurement in 2008 and 2009.- In: *Recreation and Environmental Protection*, 5th–6th May 2010, Krtiny, Mendel University in Brno, 167–171, Brno.

Smithson, P.A., 1993: Vertical temperature structure in a cave environment.- Geoarcheology, 3, 229–240.

Sun-Sook, K., Yu-Seong, Ch., Bong-Hyeon, K. & Y. Neony-Chil, 2009: The current distribution and habitat preferences of hibernating Myotis formosus in Korea.- Journal of Ecology and Field Biology, 32, 191–195.

Šebela, S. & J. Turk, 2011: Local characteristics of Postojna Cave climate, air temperature, and pressure monitoring.- Theoretical and Applied Climatology, 105, 371–386.

Thompson, J. & M. Marvin, 2005: Experimental research using Thermography to locate heat signatures from caves.- In: *Congress proceedings 14th International Congress of Speleology*, 21st–28th August 2005, 70–74, Kalamos, Greece..

Turri, S., Citterio, M., Bini, A., Maggi, V., Favaron, M., Fraternali, D., Alberici, A., Borghi, S., Colombo, M., Gottardi, R. & D. Zappalà, 2005: Preliminary data recorded by a monitoring station to study the hypogean climate in a ice cave: the LO LC 1650 Ice Cave "Abisso sul margine dell'Alto Bregai" (Grigna Settentrionale, Lecco – Italy).- In: *Congress proceedings 14th International Congress of Speleology*, 21st–28th August 2005, 74–79, Kalamos, Greece.

Wynne, J.J., Titus, T.N. & G.Ch. Diaz, 2008: On developing thermal cave detection techniques for Earth, the Moon and Mars.- Earth and Planetary Science Letters, 272, 240–250.

Zelinka, J., 2002: Microclimatic research in the Slovakian show caves.- Acta Carsologica, 31, 151–163.

COBISS: 1.01

MULTI-ROTOR UNMANNED AERIAL VEHICLES (UAVS) AND HIGH-RESOLUTION COMPACT DIGITAL CAMERAS: A PROMISING NEW METHOD FOR MONITORING CHANGES TO SURFACE KARST RESOURCES

MULTIROTORSKA ZRAČNA PLOVILA BREZ POSADKE (UAV) IN KOMPAKTNE DIGITALNE KAMERE VISOKE LOČLJIVOSTI: OBETAVNA NOVA METODA ZA SPREMLJANJE SPREMEMB POVRŠINSKIH KRAŠKIH POJAVOV

Carolyn L. RAMSEY[1], Paul A. GRIFFITHS[2] & Timothy R. STOKES[3]

Abstract UDC 528.715:629.735(711)
551.435.8:528.715(711)

Carolyn L. Ramsey, Paul A. Griffiths & Timothy R. Stokes: Multi-rotor unmanned aerial vehicles (UVAs) and high-resolution compact digital cameras: a promising new method for monitoring changes to surface karst resources

In the course of doctoral research, the authors required a quick and accurate means of documenting the real-time state of surface karst features at a variety of scales in remote and challenging field conditions. The main difficulty was finding an aerial platform that was 1) consistently effective; 2) versatile; and 3) relatively inexpensive. High resolution vertical images obtained during recreational use of a small multi-rotor unmanned aerial vehicle (UAV) seemed to have the potential to answer this need. Using five case studies, the authors examine the potential of these images for mapping, documenting, and monitoring changes to surface karst resources following forestry-related activities in the coastal temperate rainforest of British Columbia (B.C.). Possible applications, strengths and limitations of this technology are discussed. The authors conclude that mini quadcopter UAVs equipped with high-resolution compact digital cameras are a promising and cost-effective new tool for karst scientists and karst managers.

Key words: Unmanned aerial vehicle (UAV), quadcopter, vertical aerial photography, monitoring, karst, British Columbia.

Povzetek UDK 528.715:629.735(711)
551.435.8:528.715(711)

Carolyn L. Ramsey, Paul A. Griffiths & Timothy R. Stokes: Multirotorska zračna plovila brez posadke (UAV) in kompaktne digitalne kamere visoke ločljivosti: obetavna nova metoda za spremljanje sprememb površinskih kraških pojavov

V okviru doktorskih raziskav, avtorji zahtevajo hiter in točen način dokumentiranja stanja površinskih kraških pojavov različnih velikosti v realnem času ter v oddaljenih in zahtevnih terenskih pogojih. Glavna težava je bila v iskanju letalne naprave, ki bi bila 1) konsistentno učinkovita; 2) vsestranska; in 3) relativno poceni. Ugotovili so, da imajo vertikalne slike visoke ločljivosti pridobljene med prostočasnimi aktivnostmi z multirotorjem brez posadke (UAV) potencial, ki bi odgovarjale zahtevanim potrebam. Z uporabo petih študijskih primerov so avtorji preučili potencial pridobljenih posnetkov za kartiranje, dokumentiranje in spremljanje sprememb kraških površinskih pojavov povezanih z gozdarskimi dejavnostmi v predelih obalnega deževnega gozda zmernih širin v Britanski Kolumbiji (B.C.). Razpravljali so o možnih aplikacijah, prednostih ter omejitvah te tehnologije. Avtorji ugotavljajo, da je mini Quadkopter UAV opremljen s kompaktno kamero visoke ločljivosti stroškovno obetaven in da je to učinkovito novo orodje za krasoslovce in upravljavce krasa.

Ključne besede: letalna naprava brez posadke (UAV), quadkopter, vertikalna zračna fotografija, monitoring, kras, Britanska Kolumbija.

[1] Carolyn L. Ramsey: PhD student, University of Nova Gorica; Honorary Research Associate, Vancouver Island University, 900 Fifth Street, Nanaimo, British Columbia, Canada V9R 5S5, e-mail: clramsey@shaw.ca
[2] Paul A. Griffiths, 544 Springbok Road, Campbell River, B.C. Canada V9W 8A2, e-mail: pgriff@shaw.ca
[3] Timothy R. Stokes, PGeo, PhD, Earth Science Department, Vancouver Island University, 900 Fifth Street, Nanaimo, B.C. Canada V9R 5S5, e-mail: tim.stokes@viu.ca

Received/Prejeto: 14.08.2013

INTRODUCTION

Adequate protection and management of karst resource features has been a major concern in the coastal temperate rainforests of British Columbia (B.C.) (Griffiths 2013). Research and monitoring of karst resources in this region are often hampered by terrain conditions, the distances involved in getting to and from field sites, and a scarcity of funding. Long hours of painstaking ground-based surveys in rugged and remote locations are often required to adequately document baseline conditions or the nature and scale of disturbance events. Affordable new technologies which optimize the use of field time while lowering the cost of study are therefore of great interest.

Fig. 1: Mini multi-rotor UAVs equipped with compact high-resolution cameras are inexpensive and have the potential to increase data collection and monitoring capacity for karst researchers and managers (Photo: C.L. Ramsey).

Multi-rotor unmanned aerial vehicles (UAVs) equipped with high-resolution compact digital cameras have the potential to revolutionize the monitoring of surface karst resources in coastal B.C. because they permit rapid, accurate and inexpensive collection of high-resolution aerial images at different scales. The resulting images provide permanent records of the condition of a karst site or feature at a given point in time. These images can be used to derive scale-appropriate measurements of the surface elements of karst resource features at time intervals defined by the karst researcher or manager.

The authors flew an inexpensive UAV quadcopter at a number of northern Vancouver Island karst sites, obtaining low-altitude aerial photography in typical field conditions. The karst sites were located on land managed by the Provincial Government on behalf of the public. Primary access to all of the karst sites was by road. Images thus obtained are presented in the case studies, below.

The legal requirements for use of UAVs differ from country to country. Recreational flying of commercially available quadcopter UAVs in Canada does not require any special licence or training if the vehicle weighs less that 35 kg. Nevertheless, established safe model aircraft flying rules and standards must be respected at all times and in all locations in Canada, including those most remote.[1]

STUDY AREA DESCRIPTION

Vancouver Island is situated on Canada's west coast. The island is 450 km long and has a total area of about 32,000 km^2. The general climate regime is temperate oceanic mesothermal with some regional and local variations related to physiography (Moore *et al.* 2010). Vancouver Island falls within the northern temperate coastal rainforest biome. The dominant vegetation is evergreen conifers.

[1] Flying any quadcopter in Canada for commercial purposes, profit or reward requires a Special Flight Operation Certificate from Transport Canada. The federal agency has been proactively addressing the rapidly evolving use of UAVs in Canada, attempting to ensure the highest standards of safety while enabling commercial UAV use through a formal approval process.

About 4 % of Vancouver Island is underlain by bedrock that has the potential to form karst. This encompasses a geographic area of about 1,200 km^2. Quatsino Formation limestone represents the most important bedrock unit for hosting karst as well as the most extensive of three limestone units on Vancouver Island (Fischl 1992).

The primary land use activity affecting karst in coastal B.C. and on Vancouver Island is industrial forestry. Most of the timber harvesting carried out on the karst has been first-pass logging of old-growth forest stands using the clearcut harvest method (Griffiths & Ramsey 2006). Clearcutting with 10 % of the total cutblock area timber left standing as reserve patches is the most common silvicultural system used in B.C. at present (Vyse *et al*. 2010). Other land use activities on Vancouver Island on or near karst include mining, quarrying and hydroelectric development.

PROBLEM STATEMENT

The natural conditions of coastal B.C. impose certain limitations on karst research and monitoring activities. Most of the karst on Vancouver Island is located in remote areas. Distances between karst sites of research or management interest can be great. The sites themselves are often rugged and difficult to move about in, especially when covered with logging debris, tree windthrow or dense vegetation.

Stereoscopic aerial photos and satellite images for many areas of interest are commercially available or can be obtained online from Google Earth, but image resolution is often insufficient for the detection of smaller karst features or for use in site evaluation to assist research or management objectives. Additionally, the high-altitude imagery is sometimes compromised by cloud or snow cover. The maximum resolution provided by commercial satellites is commonly 60 cm per pixel (Murray *et al*. 2012).

Helicopters make it possible to reduce travel time to and between remote karst sites, and to obtain lower-altitude aerial images, but they remain expensive to charter.[2] Even with sufficient budgeting capacity, helicopters are not always ideal for some research and monitoring applications in B.C.'s coastal temperate rainforest karst. Low ceilings can limit accessibility to some karst sites or altogether obscure features on the ground from aerial views. Forest vegetation, rugged topography and weather conditions can also limit where and when helicopters can manoeuvre or land safely. Few helicopters are equipped with external camera mounts for accurate vertical photography, and cameras cannot penetrate dense forest canopy even if these mounts are present.

Ground-based travel to karst sites is more affordable than helicopters, but the slower traveling time limits the number of sites that can be visited in a given day. Finally, ground-based fieldwork is also limited by line of sight and cannot always provide overviews of site conditions unless high promontories or photopoints with unobstructed views are available.

Though remote sensing methods such as LiDAR (Light Detection and Ranging) may allow for some characterization of karst sites under dense canopy cover, the ranging data are either publicly unavailable at present or unavailable at the resolutions required by some of the inspection tasks. Moreover, remote sensing imagery or aerial photography may be dated and may not, therefore, accurately represent the current state of karst sites.

UAVs have the potential to circumvent many of the preceding issues. With a small camera mounted on an aerial platform, it is possible to obtain high-resolution images of a site on any particular day inexpensively and to rapidly examine an area greater than can be walked in a day. In many cases, a vertical view of a site is preferred over an angled terrestrial view, which may not accurately depict the overall site conditions (e.g., areal distribution of logging debris). While such images cannot replace walking on the ground and site verification, they do serve as a useful tool to assist and enhance field work.

[2] Hourly rates can range from $1,250 to $1,750 USD for a Bell 206 Jet Ranger and Eurocopter AStar B Model, respectively.

METHODS AND EQUIPMENT

THE QUADCOPTER

The multi-rotor UAV aerial platform used by the authors is classified as a radio-controlled mini quadcopter equipped with a compact digital camera. The quadcopter can be defined as a four-rotor helicopter (Bošnak *et al*. 2012). It uses four brushless and gearless electrical mo-

tors, has no mechanical components, and is therefore virtually maintenance-free (Roßmann 2009).

The model of quadcopter under study was a DJI Phantom Quadcopter. This quadcopter is powered by a 2200 mA LiPo rechargeable battery pack providing up to 15 minutes of flight time without the camera payload and 8–10 minutes with the camera. Extra battery packs and a charging regimen using a vehicle 12 volt battery and a power inverter were available for use as needed. The radio controller is based on a 2.4 GHz frequency and capable of a range of at least 300 m. When flown in GPS mode, this quadcopter has autonomous landing and return-to-home capability in case of a low battery or loss of radio signals.

Tab. 1: Key technical specifications of DJI Phantom Quadcopter.

Hovering accuracy in GPS mode	Vertical: ± 0.8 m; horizontal: ± 2.5m
Max tilt angle	45°
Maximum ascent/descent speed	±6 m/s
Max flight velocity	10 m/s
Battery type, rechargeable	2200 mAh LiPo
Transmitter frequency	2.4GHz ISM
Minimum communication distance	300 m
Diagonal distance (motor center to motor center)	35 cm
Take-off weight	<1000 g

THE CAMERA

For image acquisition, the quadcopter was equipped with a GoPro HD Hero2 high-resolution camera in a polycarbonate waterproof housing. At 230 g, this compact digital camera, including battery and protective housing, is well within the payload capacity of the DJI Phantom Quadcopter. The quadcopter frame is purposely designed with a mount for use with this camera. The camera can record high-definition (HD) video at a maximum of 1920 × 1080 screen resolution, or still imagery at 11, 8 or 5 megapixels.[3] The camera was used in time-lapse photo mode for our field trials, but it can also be operated in continuous HD video mode at a variety of resolutions, although video cannot be recorded during still image capture.

FLIGHT PARAMETERS

The onboard GPS navigation system is used to maintain a hover position, and allows the quadcopter to return 'home' if the radio signal is lost. The quadcopter was flown manually in GPS mode to capture the particular scenes or elements of interest at the sites. Although the radio control range is potentially greater than 300 m, for safety reasons the quadcopter was not flown higher than 120 m above the ground and was kept within sight at all times.[4]

Tab. 2: Key technical specifications of the GoPro Hero2 camera.

Optical sensor type	CMOS
Effective maximum photo resolution	11 MP
Photo recording format	JPEG
Maximum view angle	170°
Lens aperture	F/2.8
Supported memory cards	SD, SDHC
Battery type, rechargeable	1100 mAh Li-ion
Dimensions without protective housing	58.4 x 44.5 x 31.8 mm
Camera and battery	100 g
Camera, battery and protective housing	230 g

All of the aerial images were captured with the camera pointed downward at the nadir, and were collected in time lapse photo mode with an interval setting of one image every 2 seconds at the maximum resolution of 11 megapixels. The memory card has a 16 GB capacity, allowing for the storage of up to 1600 still images at the maximum resolution. Saved images from the installed SD card were downloaded periodically to a laptop in the field to verify image quality and the area of the karst site covered. If the recorded images or photo alignments were unsatisfactory, the route was reflown. The camera operation by itself was limited to approximately 2.5 hours between battery charges using a laptop USB port.

In some cases, a 50 cm diameter white plastic disk with a black cardinal cross and indication of true north position was used as a control point to measure the camera height above the ground at a target. The disk, used previously in ground surveys, facilitated the setting of camera height above the ground as well as the orientation of the acquired image with respect to true north in any subsequent image processing.

[3] The recording of HD video can be used to optimize spatial coverage of a karst site.

[4] A first-person viewing (FPV) system can be used with a quadcopter UAV to facilitate flights beyond the visible range. The cost of FPV can add 350–400 USD to overall costs of the aerial platform.

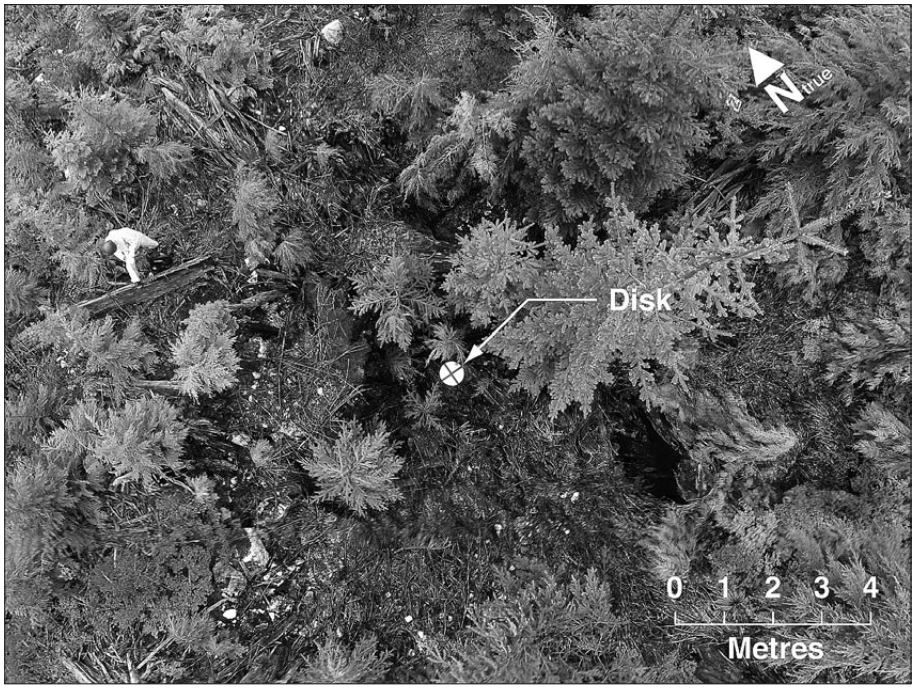

Fig. 2: A white 50 cm diameter disk with a black cross indicating the cardinal directions can be used to measure the camera height above the ground at a target. The disk, used in ground-based field work, is easily visible in the images acquired with the UAV.

FIVE CASE STUDIES: FIELD TRIALS USING THE QUADCOPTER AERIAL PLATFORM

The following case studies illustrate how UAV-assisted low-altitude aerial photography has the potential to overcome some of the barriers to karst monitoring, research and management initiatives.

CASE STUDY 1: RETENTION PATCH

The Retention Patch is a karst site with a small karst window at its core. The old-growth forest around the feature was logged *ca*. 2010. A retention patch 20–30 m wide comprised of 100 % standing timber was established around the karst window as a management measure. In the intervening years, the standing timber 'reserve' began to blow down, the upturned root masses of the windthrown trees exposing well-developed epikarst. The authors spent two person-days surveying and mapping the karst window and the distribution of windthrown trees on 06 October 2011. The results are shown in Fig. 3. The authors returned to the Retention Patch site on with the quadcopter aerial platform and sent it aloft for approximately 3–5 minutes to acquire aerial images. A representative aerial photo is shown in Fig. 4A, with superimposition of the results of the two person-day survey.

One can rapidly delineate the downed trees and many of the areas of exposed epikarst using the high-resolution aerial images acquired with the quadcopter UAV. These data were equivalent to, or more accurate than, those acquired by the ground-based survey methods, and the images were collected in a fraction of the time. Ground-truthing would have been required to ascertain the decay classes of the downed wood. It was also noted that not all of the exposed epikarst is visible from the air based on the altitudes and routes flown. Nevertheless, this case study illustrates how a mini multi-rotor UAV flown at low altitudes is able to quickly capture accurate data related to disturbance events at karst sites in relatively inaccessible and remote areas.

CASE STUDY 2: Q1 DOLINE AND THE DOLINE GROUP

The Q1 doline measures 9.87 m long, 8.47 m wide, and 2.89 m deep. It is nested along with eight other topographical lows within a larger elongate karst depression. During an initial field visit, a forest road had been built against the east rim of the doline and some mature second-growth timber on that side of the feature had been felled in the process. Full-scale timber harvesting operations had not yet begun. The doline rim, adjacent road and sideslope profiles were surveyed on the ground during the initial field visit. Standing trees and downed trees in and around the doline were also

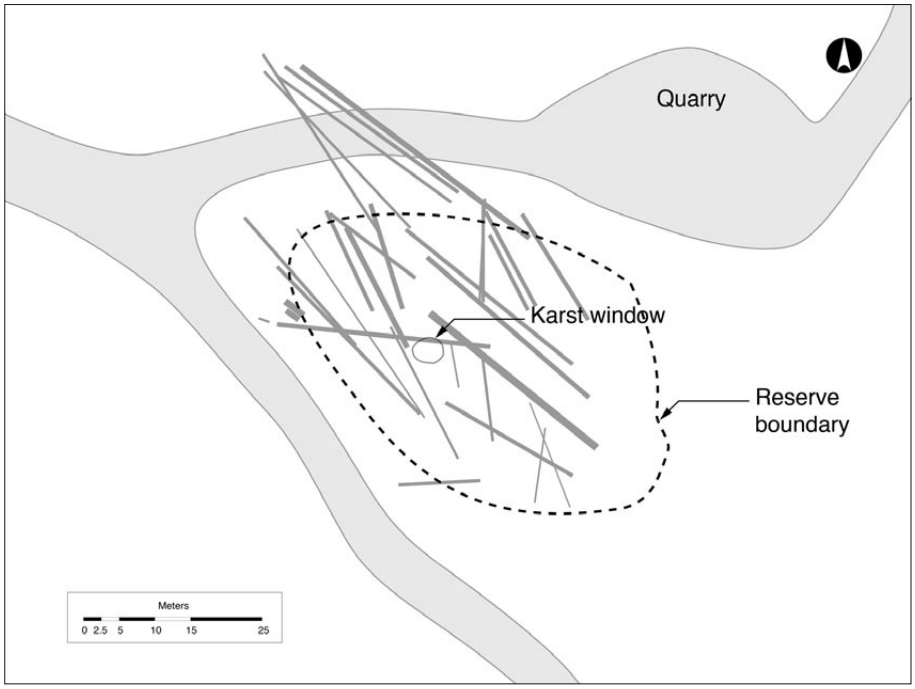

Fig. 3: Planimetric map of the windthrown trees at the Retention Patch, produced from data collected over 2 person-days in the field in October 2011. The dashed black line shows the approximate boundary of the tree retention area.

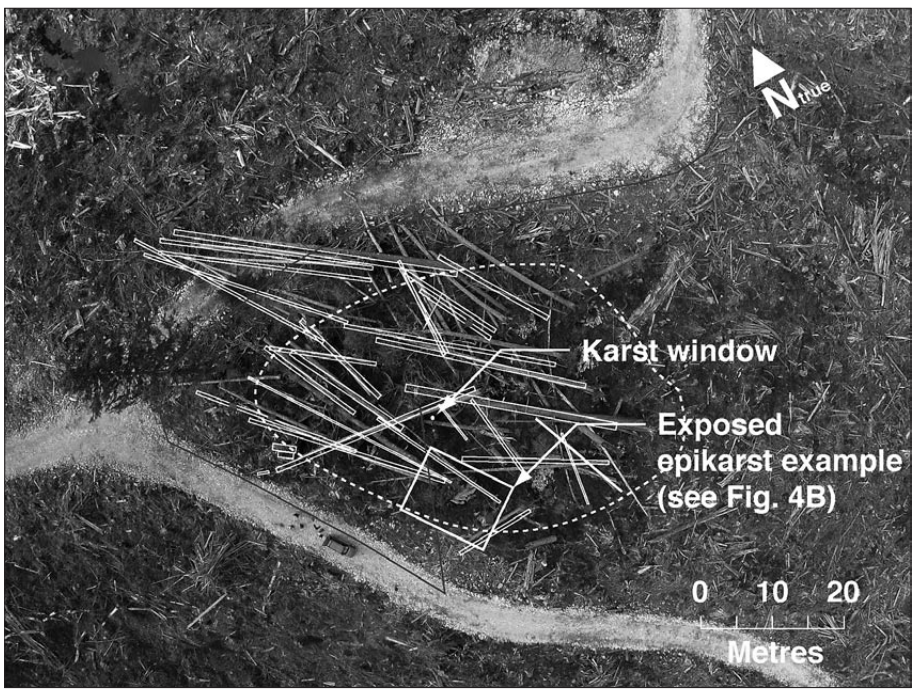

Fig. 4A: UAV image of the Retention Patch with the October 2011 survey of the windthrown trees superimposed. The dashed white line indicates the approximate boundary of the tree retention area.

surveyed and rough estimates of percent coverage of surface substrates were noted. Additionally, disturbance indicators used by B.C.'s Forest and Range Evaluation Program (FREP) for this karst feature type, were evaluated and recorded.

Fourteen other dolines in a cluster were located in a stand of mature second-growth timber about 500 m from the Q1 doline. This second set of dolines, referred to here as the 'Doline Group' (Fig. 7), and some other minor karst features, were tied into known points on the ground using overland survey techniques on 10 June 2012 and then plotted on a 1:1000 scale planimetric map. It took approximately one person-day to survey these karst features to establish their geographical locations and spatial distribution, and to document their pre-harvest condition using ground-based oblique photography.

Fig. 4B: Low-altitude UAV image of the epikarst in the tree retention area exposed by the tree windthrow.

The authors returned to the two karst sites with the camera-equipped quadcopter after timber harvesting operations had been completed. The aerial platform was sent aloft to acquire images of the Q1 doline followed by the Doline Group at the second site.

Case study #2 illustrates how low-altitude aerial imagery acquired by a quadcopter UAV can be used to document accurately and rapidly any post-harvest changes such as ground disturbance, logging debris, machine trails, retained understory vegetation and replanting at karst sites.

Field trials at the Q1 Doline and Doline Group sites also show the potential for the multi-rotor UAVs to be used within B.C.'s Forest and Range Evaluation

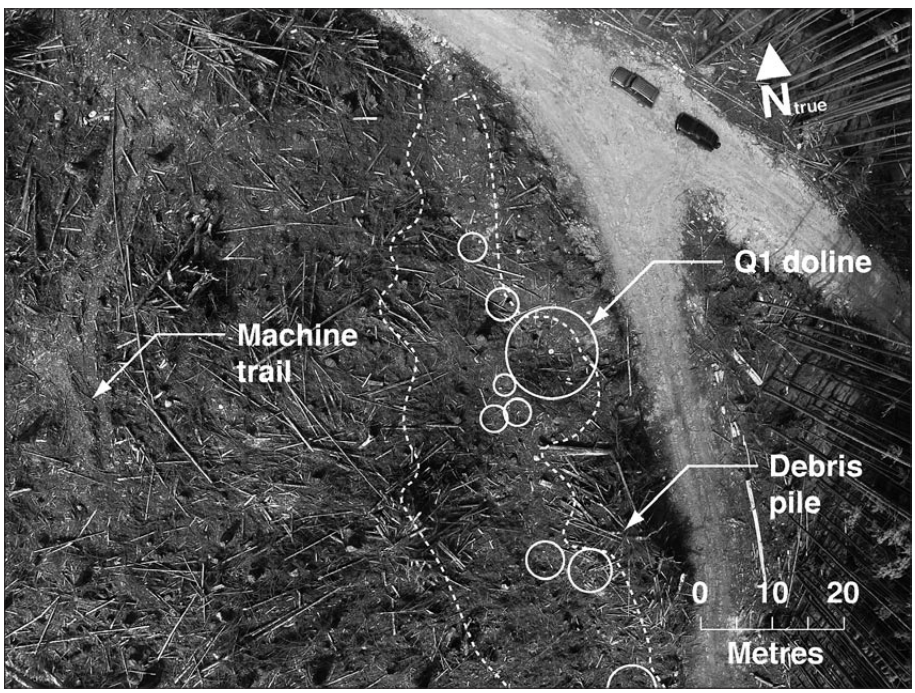

Fig. 5: UAV image of the Q1 doline and the associated depression complex. The dashed white line indicates the larger enclosing karst depression. The solid white lines show the nested depressions, including the Q1 doline, surveyed on the ground in one person-day on June 2012 prior to timber harvesting.

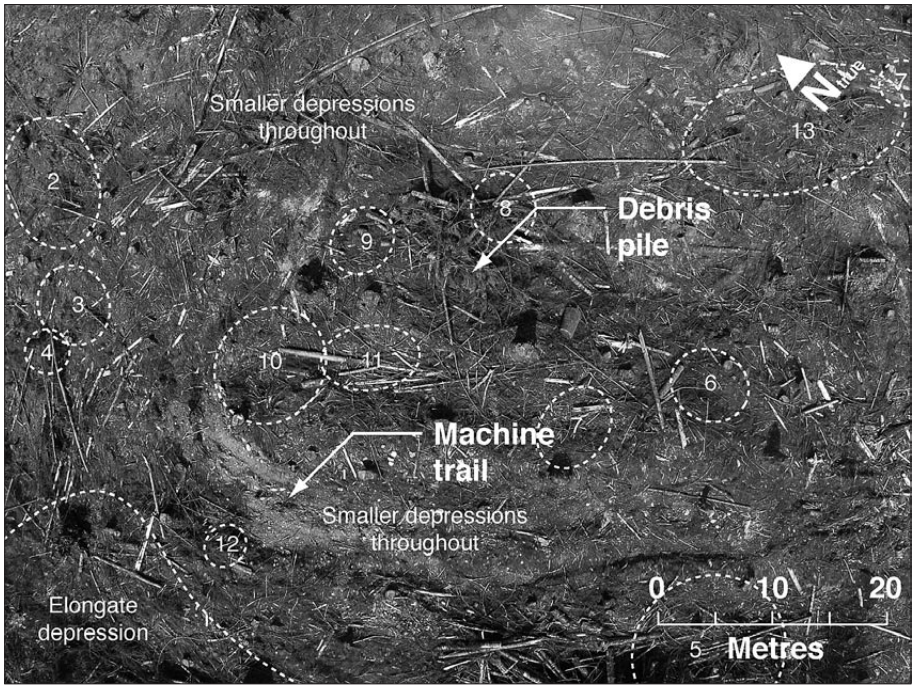

Fig. 6: UAV image of a group of dolines with superimposition of dashed white line outlines of the numbered dolines surveyed on the ground in June 2012.

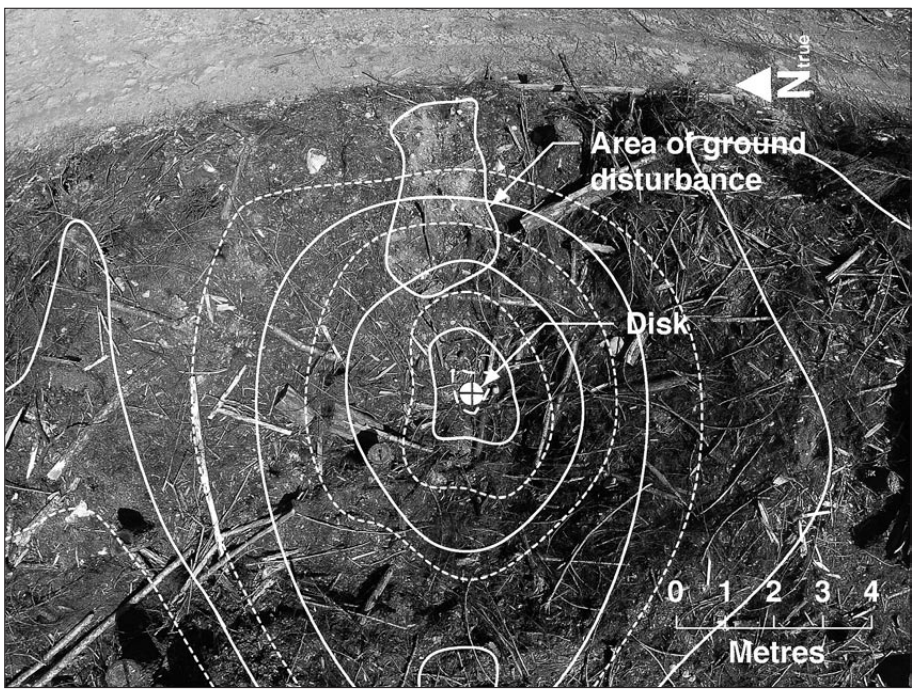

Fig. 7: Low-altitude UAV image of an area of ground disturbance on the inner slopes of the Q1 doline. Aerial images obtained using the mini quadcopter UAV allow for the rapid estimation of harvest-related ground disturbance. The solid white lines are 1 m contours and the dashed white lines represent 0.5 m contours.

(FREP) program. The high-resolution aerial images acquired by the quadcopter can easily detect many of the disturbance indicators that are assessed using the FREP procedure. The rapid acquisition of low-altitude high-resolution aerial imagery of karst sites and features offers an opportunity to reduce the costs of conducting effectiveness evaluations for karst using the FREP indicators. For example, the number of mature trees removed from within the Q1 doline can easily be established by counting the number of freshly cut tree stumps showing in the doline on the low-altitude aerial images. Similarly, the aerial images obtained by the quadcopter enable estimation of any harvest-related ground disturbance.

CASE STUDY 3: BURN AREA

The Burn Area is a well-developed karst site on which the old-growth forest stands were clearcut in 2000–2001. In August 2009, the site and surrounding karst areas burned as a result of a fire caused by lightning strike. The 200 ha (2 km^2) fire incinerated residual tree stumps and organic soil in the clearcut karst areas. Fig. 8 is a ground-based oblique photograph showing the karst site a few months following the fire. This site presents an excellent opportunity to document the effects of intense fire on thinly covered epikarst in a clearcut area, as well as the subsequent regeneration of vegetation over time.

Much of the Burn Area consists of exposed and well-developed epikarst. The many solutionally-enlarged openings and the "fire-cracking" of bedrock projections hamper walking on the karst and present a sig-

Fig. 8: March 2010 ground-based photo showing part of the Burn Area. The fire occurred in August 2009.

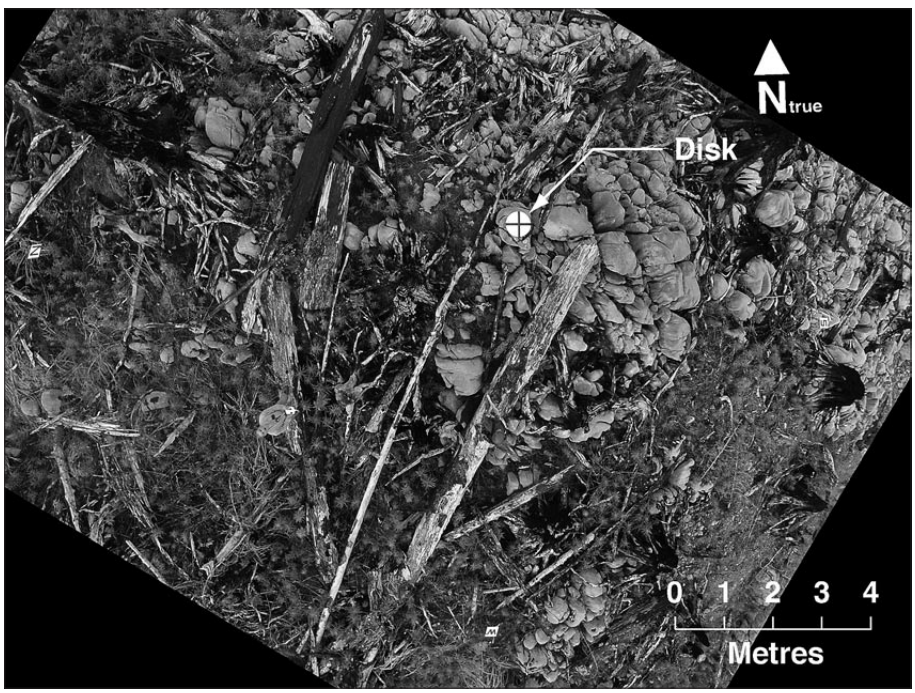

Fig. 9: High-resolution UAV image of part of the Burn Area. UAV-assisted photography makes it possible to conduct cost-effective mapping and ongoing monitoring of disturbed karst sites.

nificant risk of human injury from falling or tripping. The authors visited the site with the camera-equipped quadcopter UAV, established spatial ground controls, and sent the aerial platform aloft. The results are shown in Fig. 9.

The Burn Area is an example of a case where there is a limited amount of time to document baseline conditions after a severe disturbance at a karst site. Ideally, monitoring should have begun immediately after the fire, but the area is remote and funding for a detailed post-fire impact assessment project was not available. By using the UAV and low-altitude flights over the Burn Area, it was possible to acquire high-resolution, real-time imagery and documentation of site conditions for a modest cost. These images could be used for future study and enable ongoing monitoring. The field trial at this site showed that images suitable for fine-scale mapping of forest vegetation and other groundcover on karst sites could be acquired easily when the quadcopter UAV is flown at a very low altitude. The use of the quadcopter UAV in this application also minimized the need for personnel to move about on a hazardous karst area (Fig. 10).

CASE STUDY 4: PARADISE LOST

Paradise Lost is a cave system with an underground stream that was discovered and mapped in 1986. The known, normally dry entrances are located at the base of the 70 m long, 50 m wide, and 25–30 m deep entrance doline.

Much of the old-growth forest of the Upper Tahsish Valley karst was clearcut between 1982 and 1986. B.C. lacked specific karst management guidelines and legislation at that time, and little heed was paid to the well-known ability of karst to evacuate sediments from the surface, resulting in soil erosion/loss during and after harvest operations. Portions of the karst in this valley bottom, including Paradise Lost, are covered by significantly thick unconsolidated glacial sediments.

Roads were put in on three sides of the Paradise Lost entrance doline in 1986. The old-growth forest within the doline and its surroundings was clearcut. In the early 1990s, a depression in the cover material (regolith) began to form on the upper northern slope of the doline (Figs. 11A and 11B). This new feature eventually breached the ceiling of the largest chamber within the upstream part of the cave system. It is now possible to view the Paradise Lost entrance doline (Latitude 50°17'16.40"N and Longitude 127°7'30.28"W) using Google Earth and other available satellite coverage. This imagery, however, lacks detail and the 'real-time' information needed to monitor the ongoing breakdown and loss of cover material to the subsurface. Also, the karst feature is currently unstable and obtaining such measurements on the ground or inside the unroofed cave chamber would be extremely hazardous.

When the authors visited the Paradise Lost entrance doline site, the roads leading to the site were found to be unmaintained and heavily overgrown. Subsidence of these roads had occurred and in some places small holes

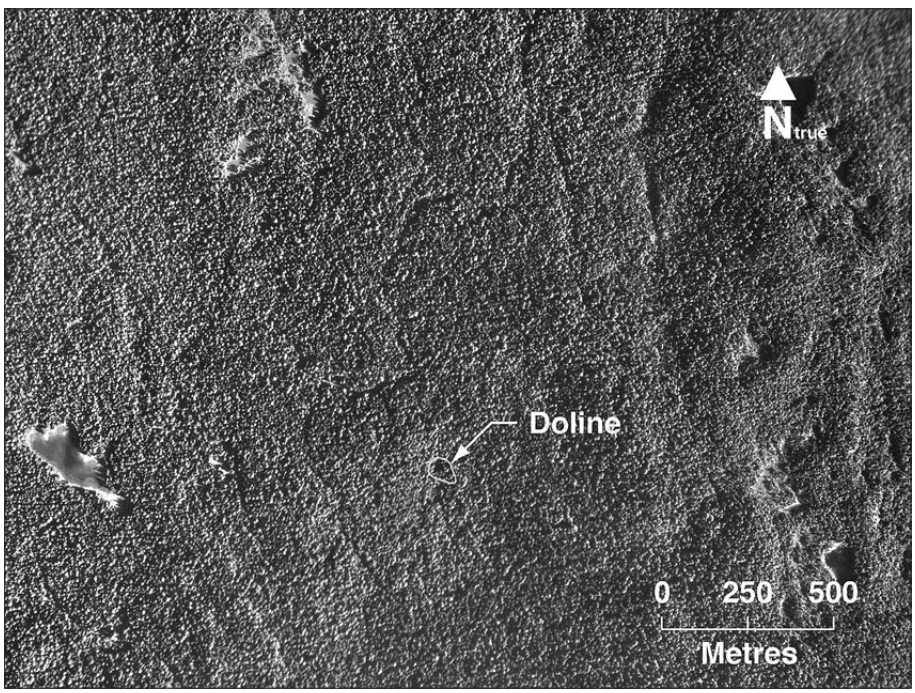

Fig. 10: This high-altitude Province of British Columbia aerial photo shows the Paradise Lost entrance doline area in 1980. Harvesting of the doline and the area immediately surrounding it began in 1986.

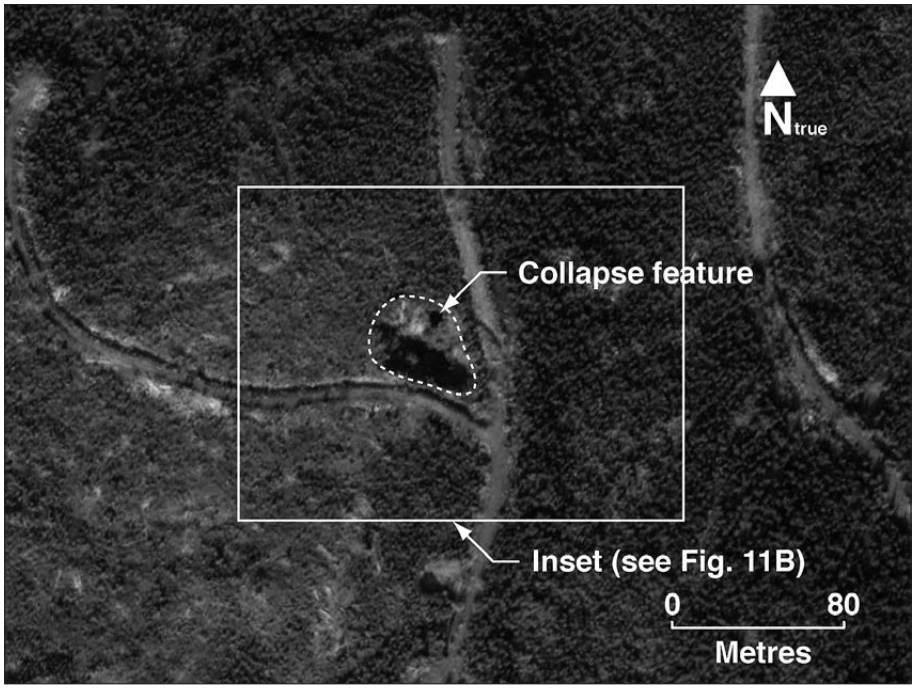

Fig. 11A: The most current Google Earth satellite imagery (dated 2002) shows the Paradise Lost entrance doline and the collapse feature on the sidewall. The dashed white line indicates the doline rim.

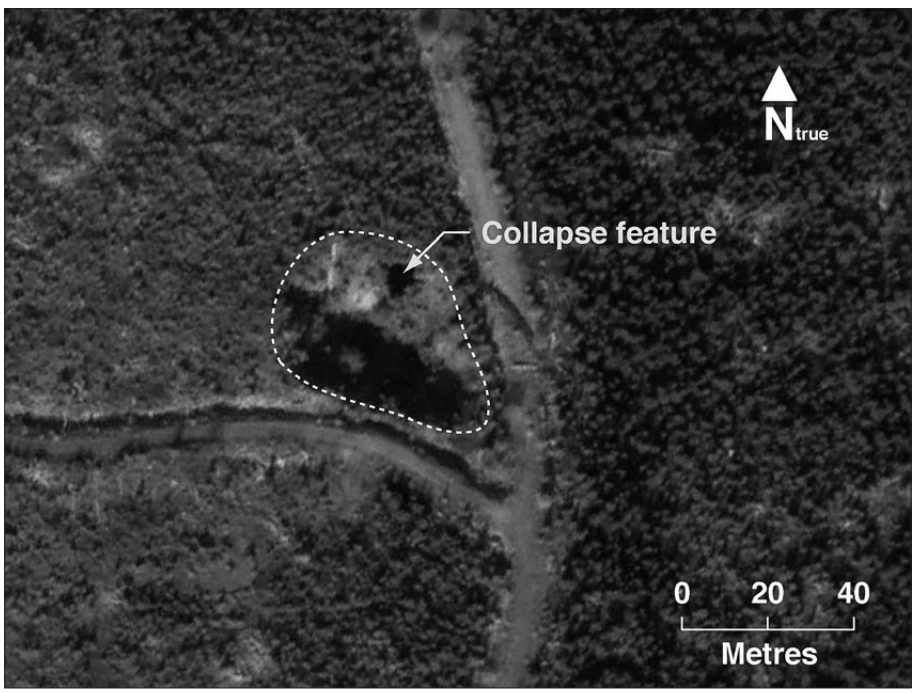

Fig. 11B: Inset area of Fig. 11A with the dashed white line outlining the doline rim.

had opened up in the roadbed. It was therefore decided to walk along the road for the remaining half kilometre to the site, carrying the camera and housing, the quadcopter, radio controller and spare batteries in a small backpack. The aerial platform was flown over and into the collapse feature repeatedly for approximately 5 minutes. The results are shown in following Fig. 12A, 12B, 12C and 12D.

This case study illustrates how low-altitude, high-resolution aerial imagery captured with a quadcopter UAV makes it possible to inspect and document hazardous or unstable karst sites or features with minimal risk of human injury. The negligible weight and size of the aerial platform allow for easy storing in a small backpack for remote-area expeditions. Also, the images acquired

are of higher resolution and more recent than the available air and satellite imagery.

CASE STUDY 5: DEVIL'S BATH

The Devil's Bath is a vertical- and steep-walled collapse feature containing a 110 m by 120 m lake. The doline lake is in hydrological continuity with, and connected to, multiple inflow and outflow cave passages and conduits occurring to the northeast and west of the Devil's Bath. Bath Cave, situated on the west side, receives flow from, and recirculates flow to, the doline lake. The main water-filled passage extension from Bath Cave to the northwest is also connected to the Gorge Caves. This underwater connection has been explored and mapped by diving for a distance of 375 m.

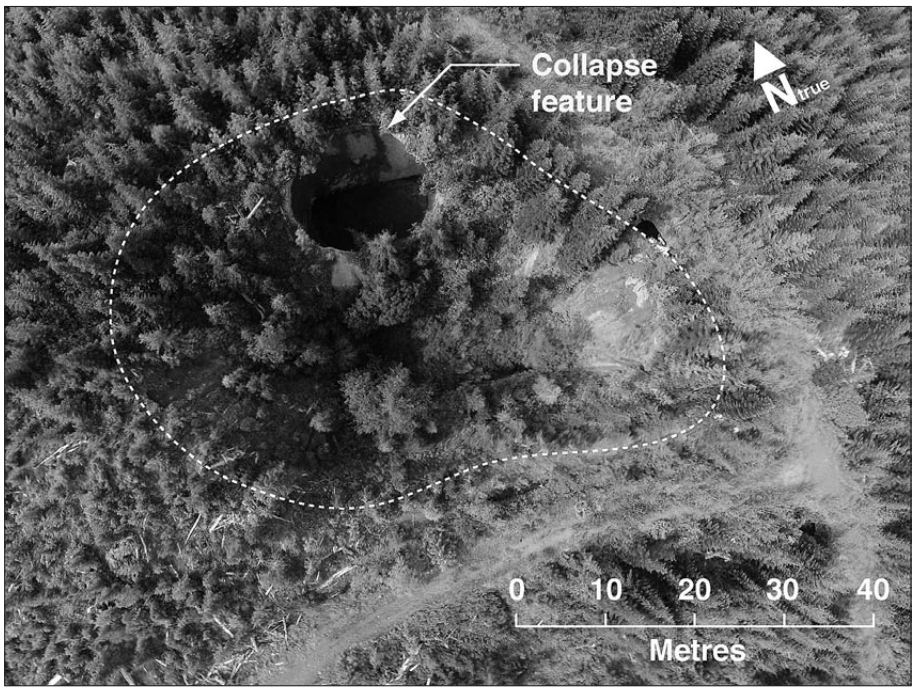

Fig. 12A: UAV image of the Paradise Lost entrance doline with the dashed white line outlining the doline rim.

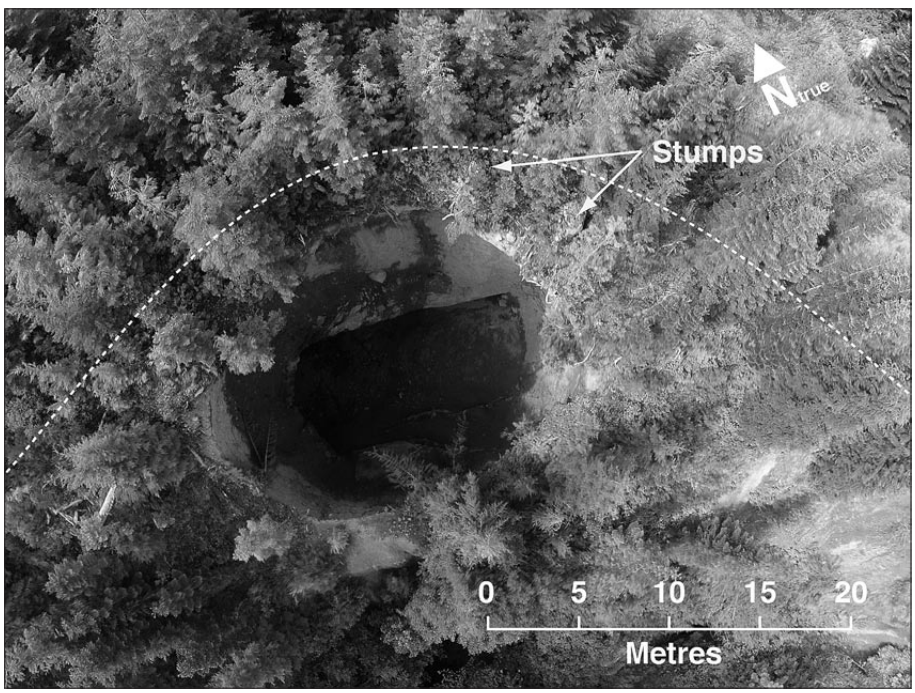

Fig. 12B: UAV image focusing on the collapse feature. The dashed white line outlines the doline rim.

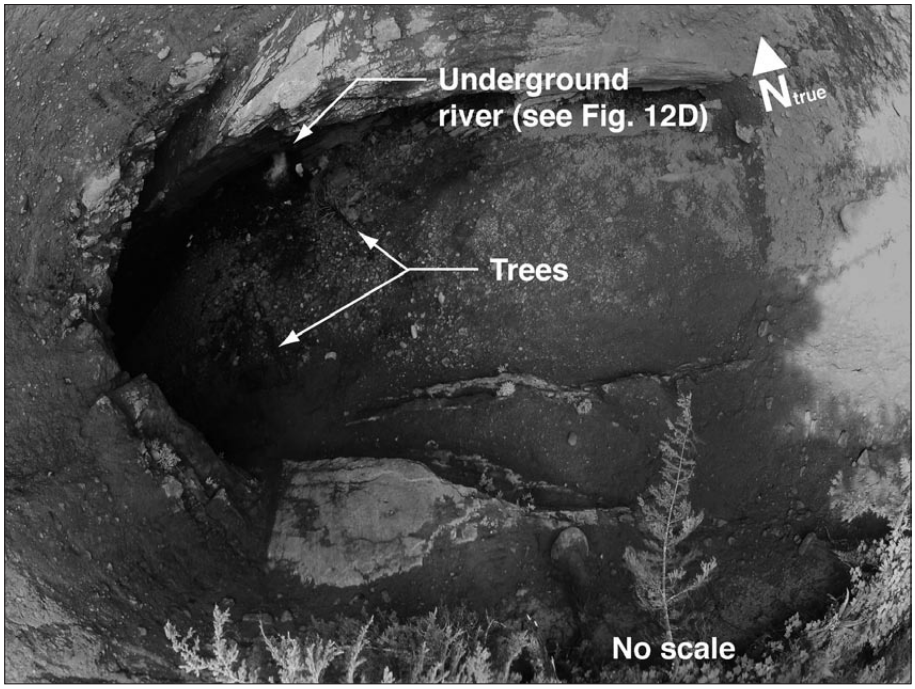

Fig. 12C: UAV image of the collapse feature from the elevation of the rim. These figures show the possible uses of the mini quadcopter UAV to investigate hazardous collapse features and to measure them over time.

Fig. 12D: Ground-based photo of the cave stream viewed from the bottom of the collapse feature.

On the surface, the Devil's Bath feature closely resembles a cenote similar to those found in Mexico's Yucatán Peninsula.[5] It is a unique and significant karst feature on Vancouver Island, as well as at the regional and possibly provincial or national level.[6] The consider-

[5] Cenote is the Spanish language term coined after the Mayan *tzonet* or *dzonot*. One of the most famous Mexican cenotes, Chichen Itza, measures 60 m across with 30 m high vertical walls.

[6] The Vermillion Creek collapse doline in the NWT measures 120 m long, 60 m wide and 40 m deep to the waterline (Ford 1997), and is described as the finest example of a doline of this type anywhere in Canada and the United States (Ford 2009).

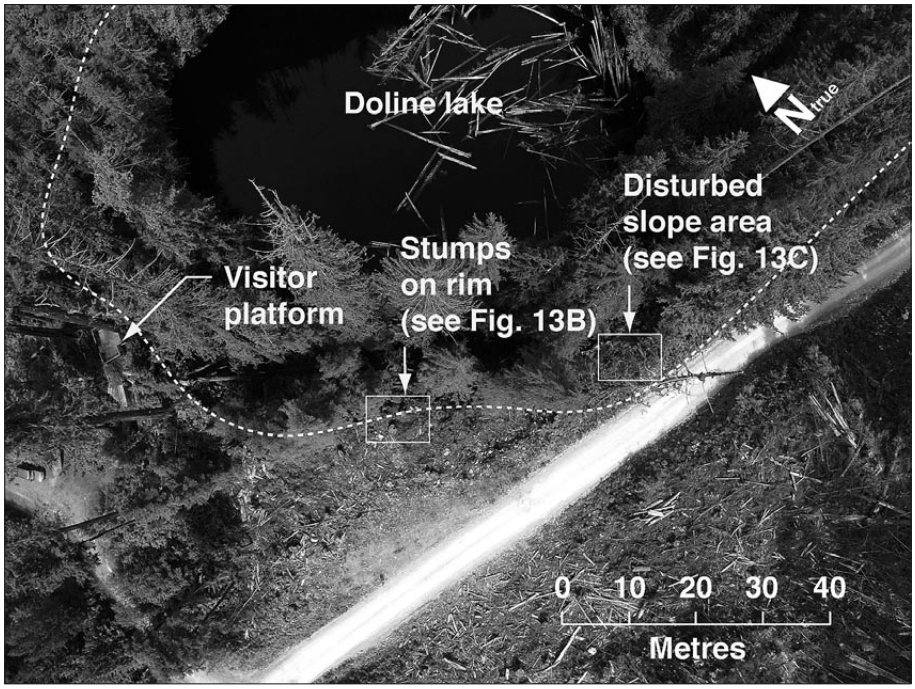

Fig. 13A: UAV image showing part of the area of the 2012 harvesting next to the Devil's Bath doline lake. The dashed white line indicates the approximate doline rim location based on the lowermost continuous slope break. Establishing the post-harvest condition of surface karst resource features is now possible with rapid assessments using a mini quadcopter UAV and large-scale aerial photography.

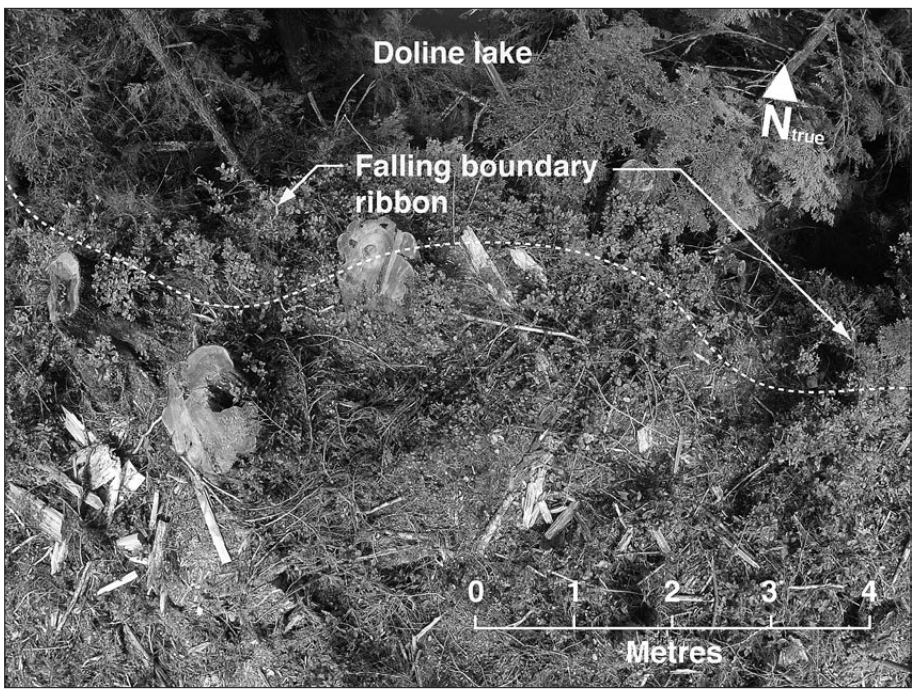

Fig. 13B: UAV image showing the tree stumps on the doline rim. The dashed white line indicates the approximate doline rim location based on the lowermost continuous slope break.

able size and scenic nature of the doline, its origin and evolution, and its relationship to the greater Devil's Bath hydro-geological karst system are of significant interest to both scientists and the public. A trail and platform to view the doline lake were provided initially in 1997 and renewed in 2009.

Large-scale forestry operations within the contributing karst catchment adjacent to the site began in earnest in the 1960s, while lesser amounts of cutting for mining exploration and timber production purposes trace back to the early 1900s. Harvest operations within the greater Devil's Bath site were carried out in *ca*. 1972, 1981, 1984, 1985, 1999–2000 and 2012.

Built in the 1960s, Alice Lake Main is an active hauling road that passes along one side of the doline. In one area, this road sits directly above cave passages

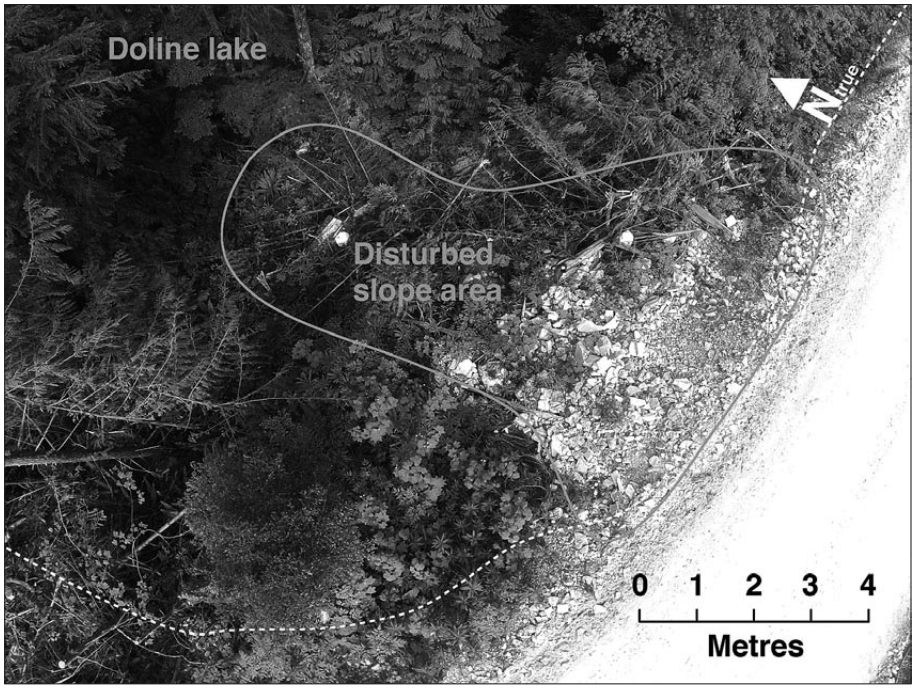

Fig. 13C: UAV image showing a disturbed slope area (raveling road fill and vegetation damage due to snag falling activity). The dashed white line indicates the approximate doline rim location based on the lowermost continuous slope break.

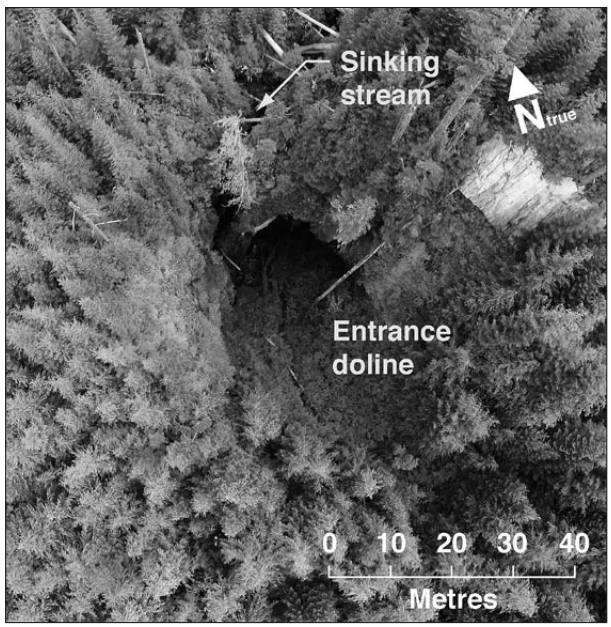

Fig. 14: UAV image of the Glory 'Ole entrance doline. The very short focal length and wide-angle viewing of the GoPro Hero2 camera lens provide a very large coverage area for image capture. This offers the advantage that multiple UAV images are not required to cover the same site.

and chambers that form part of the Devil's Bath hydrogeological system and provide subterranean habitat for three or more fish species.

Harvest operations in 2012 removed about 2 ha of the old-growth forest on the south side of the Devil's Bath doline. The logging on the site and in the upland karst south of the road is clearly visible from the doline lake viewing platform and from numerous other vantage points within and surrounding the doline (Figs. 13A and 13B).

The aerial images of the Devil's Bath in the context of its immediate suroundings can be used to show how different karst elements at complex sites are related and linked hydrologically. Such images can assist in the interpretation of complex karst sites in order to educate the public or inform forestry planning and management. The imagery can also be used to capture, document, and illustrate the cumulative impacts to this and other important karst sites.

IMAGERY PROCESSING AND STORAGE

The spatial data obtained from vertical aerial photography acquired with a quadcopter UAV can be validated using accurately surveyed ground control points (GCPs). Images can be geo-referenced or orthorectified to enable proper scaling. Inexpensive software is readily available to transform and correct images for photogrammetric analyses and measurements. Use of the camera with a narrower viewing field may provide better results for photogrammetric analyses and measurements.

STEREO REQUIREMENTS

The individual high-resolution images acquired by the quadcopter can be stitched together manually using common graphics software to create a larger image of the karst site even if no GCPs are established. The image-stitching software typically identifies and calculates con-

trol points within areas of neighboring images and uses these points to match the images together and produce a tiled image area.

The very short focal length and wide field of view of the camera lens provides a very large coverage area for each image. This offers the advantage that the quadcopter can be flown below the safe height of 120 m above the ground and multiple mosaic images are not required to cover the same site. Due to the wide field of view setting used for these test flights, the images are increasingly distorted away from the center of the photograph and are not, therefore, uniform in scale. This can be compensated through cropping and correcting for the lens effects, or use of a camera with a narrower field of view setting. The quadcopter operator can trade on the efficiency of the wide field of view and area per image (see Fig. 14) with orthogonal accuracy of the degree necessary for use in precision mapping within a GIS environment.

Typically large file sizes require significant storage space for images as well as capabilities to reduce image size for future transfer. Many images can be taken during a flight and time is required to sort and select the best images. Therefore, it is best to check images in the field, particularly if in remote areas, so as to secure appropriate image capture.

DISCUSSION

The previous five case studies demonstrate that the quadcopter UAV-assisted aerial imagery is a valuable new tool for the evaluation and assessment of karst resources, particularly following timber harvesting activities. While the uses and applications of this technology require further exploration the following strengths are apparent:

- Versatility in terms of scale: Multi-rotor UAV-assisted aerial photography allows karst researchers or managers to acquire high-resolution imagery at a variety of scales – from broad 'overviews' to lower elevation photography at finer scales for such uses as detailed mapping of individual dolines or exposed epikarst areas.
- Ability to capture scaled vertical imagery at high resolutions: The quadcopter UAV enables imagery at high resolution providing that spatial ground control points or scales are present in the photographs and that the images acquired with the quadcopter are of sufficient resolution to make detailed measurements of biophysical elements of the karst site (e.g., plants and substrates, surface openings, etc.).

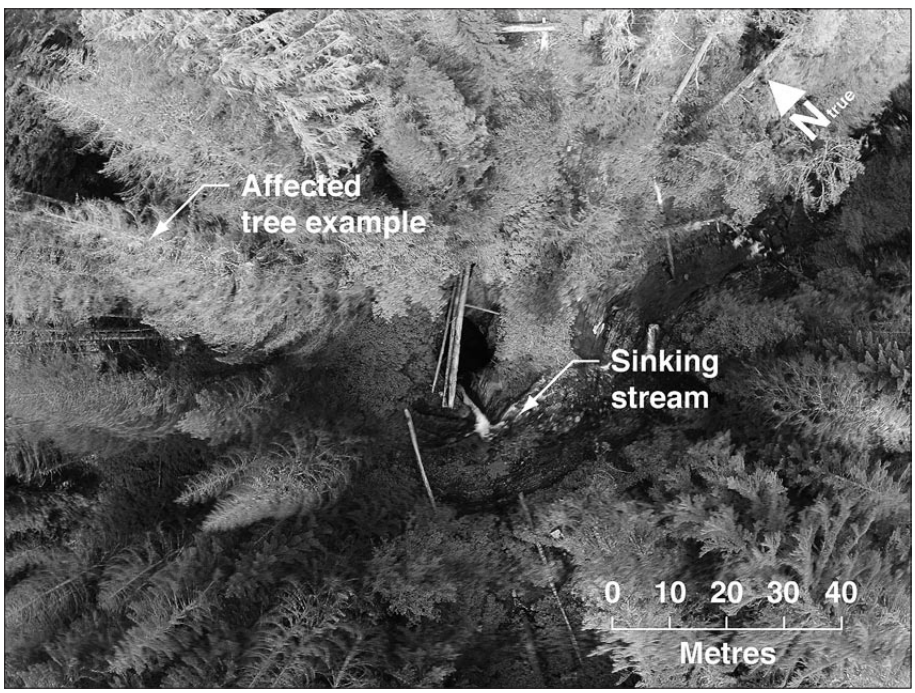

Fig. 15: UAV image shows the developing tree mortality at the Vanishing River site.

- Ability to capture real-time imagery: The quadcopter UAV can provide karst scientists and management authorities with real-time updates on site conditions during or after natural disturbance events or land use activities (e.g., see Fig. 15).
- Optimal visibility: Lower elevation flights allow the quadcopter to acquire overhead imagery of karst sites that might otherwise be masked by cloud cover or vegetation in the available satellite imagery.
- Speed and cost-effectiveness: The ease and speed with which UAV-supported aerial images are acquired make it possible to monitor many types of karst sites and features with less expense and effort than other methods.
- Inexpensive: Multi-rotor UAV aerial platforms are economical (i.e., about $1200 USD for the quadcopter UAV and a high-resolution compact digital camera). One hobbyist UAV aerial platform can be purchased for a price equivalent to that of a single hour of helicopter time at current charter rates.
- Ease of use: Multi-rotor UAVs are relatively easy to learn to fly. It took the authors only a few evening practice sessions to gain sufficient proficiency to take the aerial images used in the case studies. Excellent free web tutorials are available for novice pilots.
- Portable: The compact size of the complete aerial platform makes it easily transportable to remote areas.
- Increased safety margin for field workers: UAV-assisted imagery gives karst scientists and managers the ability to obtain detailed observations of karst features or sites that are unstable, hazardous, confined or operationally active, without risk of resource damage or human injury.
- Highly manoeuvrable: An open area of 100 cm wide or less is needed to launch and retrieve the aerial platform. Within-canopy and cave entrance flights are possible with some practice. The authors have made some limited successful attempts to fly the quadcopter inside larger cave entrances under manual control.
- The authors were easily able to hand-launch and land the vehicle with complete control.
- Low impacts on karst resources and karst environments: UAV-assisted imagery can be used to inspect or document some very sensitive karst sites or features where ground-based access might constitute an unacceptable level of disturbance, either to the features themselves or their surrounding environment. The quadcopter generates less noise and rotor wash than a manned helicopter in low-altitude flying or hovering positions, thus minimizing the potential for wildlife and/or vegetation disturbances. The battery operation of the quadcopter reduces the risk of accidental ignition of vegetation and other potential fuels at dry sites.

LIMITATIONS OF THIS QUADCOPTER UAV AERIAL IMAGERY TECHNIQUE INCLUDE:

- GPS signal reception: The built-in GPS may not work in closed karst features such as deep, steep-sided dolines, owing to an inadequate number of available satellite signals. With practice it is possible to fly the UAV without GPS navigation capability, but the ability of the unit to hover in a stationary position is compromised.
- Forest canopy and shrub layer obstacles: Forest canopy does not interfere with the GPS controls as sometimes happens with older, less sensitive GPS receivers, but low branches or a high shrub layer may cause the UAV to crash.
- The "Jello" effect: A problem often reported by recreational users of UAV-assisted photography is the so-called "jello" effect, or image distortion resulting from vibration in flight during video recording. Using a gimbal mount and/or vibration isolation accessories can reduce the vibration effects of the vehicle in flight.
- Image distortion: In the case studies above, the high-resolution compact digital camera was used in still-image capture mode with the 170° field-of-view setting, resulting in some distortion toward the edges of the photograph. Inexpensive software such as PTLens [http://epaperpress.com/ptlens/] is available to correct for the distortion, but it requires research, downloading and some skill acquisition for use with the proper settings.
- Weather factors: The quadcopter UAV performed reasonably well in moderate wind speeds. It has also been tested successfully in drizzle for short test flights. Nevertheless, very high winds or rain can make it more difficult or impossible to acquire images over a karst site.
- Depth perception: Depth perception can be hampered as the quadcopter gets further away, and it could become difficult to determine whether the UAV is actually over the target. This problem may be corrected using a first-person viewing (FPV) system.
- Battery time: Batteries can be recharged using an inverter plugged into a vehicle cigarette lighter, but recharging LiPo batteries must be monitored and recharging batteries may not be possible in situations where the work is carried out far from a vehicle.

CONCLUSIONS

Field trials have shown that a relatively inexpensive radio-controlled, mini quadcopter UAV mounted with a high-resolution compact digital camera can be used to rapidly gather detailed low-altitude aerial images of surface karst resources. Future experimentation using the quadcopter UAV for photogrammetric analyses of sensitive karst sites and features of high conservation value to produce accurate digital elevation models for these sites has already been planned. In future, acquired imagery could be incorporated into the range data provided by terrestrial laser scanning. It is concluded that UVA-assisted high-resolution digital photography is a promising new tool for karst researchers and managers.

ACKNOWLEDGEMENTS

This article was written in the course of doctoral study, which was partly co-financed by the European Union through the European Social Fund within the framework of the Operational Programme for Human Resources Development for 2007–2013 (development priorities promoting entrepreneurship and adaptability; directions priority, 1. 3: Scholarship Scheme). The authors gratefully acknowledge this support.

The authors also wish to thank Nadja Zupan-Hajna, Pavel Bosák, Bill I'Anson and James Reddicopp for reviewing the manuscript. Their thoughtful feedback and helpful comments are much appreciated.

REFERENCES

Bošnak, M., Matko, D., & S. Blažič, 2012: Quadrocopter control using an on-board video system with off-board processing.- Robotics and Autonomous Systems, 60, 657–667.

Fischl, P., 1992: *Limestone and Dolomite Resources in British Columbia*.- B.C. Geological Survey Branch, Open file number: 1992–18.

Ford, D.C., 1997: Principal features of evaporite karst in Canada.- Carbonates and Evaporites. 12(1), 15–23.

Ford, D.C., 2009: *Mapping Known and Potential Karst Areas in the Northwest Territories, Canada*.- Environment and Natural Resources, Government of the Northwest Territories.

Griffiths, P. A., 2013: Managing and remediating forested karst landscapes in B.C.: an ounce of prevention is worth more than a pound of cure.- B.C. Forest Professional, 20(2), 18.

Griffiths, P.A., & C. Ramsey, 2006: *The Digital Karst Status Map for Coastal British Columbia*.- Unpublished report.

Moore, R.D., Spittlehouse, D.L., Whitfield, P.H., & K. Stahl, 2010: Weather and climate.- In: Redding, T. (ed.) *Compendium of Forest Hydrology and Geomorphology in British Columbia*. Forum for Research and Extension in Natural Resources (FORREX), pp. 47–84, Kamloops.

Murray, J.C., Neal, M.J. & F. Labrosse, 2012: Development and deployment of an intelligent kite aerial photography platform (iKAPP) for site surveying and image acquisition.- Journal of Field Robotics, 30(2), 288–307.

Roßmann, J., 2009: High-detail local aerial imaging using autonomous drones.- Presented at the *12th AGILE International Conference on Geographic Information Science*. 2–5 June 2009, Leibniz University, Hannover, Germany. [Online] Available from: http://www.agile-online.org/Conference_Paper/CDs/agile_2009/AGILE_CD/pdfs/113.pdf [Accessed 11th June 2014]

Vyse, A., Bendickson, D., Hannam, K., Cuzner, D. & K.D. Bladon, 2010: Forest practices.- In: Redding, T. (ed.) *Compendium of Forest Hydrology and Geomorphology in British Columbia*. Forum for Research and Extension in Natural Resources (FORREX), pp. 111–131, Kamloops.

COBISS: 1.01

ADSORPTIVE BEHAVIOUR OF ARSENIC IN A KARST SUBTERRANEAN STREAM AND PRINCIPAL COMPONENTS ANALYSIS OF ITS INFLUENCING VARIABLES: A CASE STUDY AT THE LIHU SUBTERRANEAN STREAM, GUANGXI PROVINCE, CHINA

ADSORPCIJSKO OBNAŠANJE ARZENA V KRAŠKIH PODZEMNIH TOKOVIH IN ANALIZA GLAVNIH KOMPONENT SPREMENLJIVK, KI VPLIVAJO NANJ: PRIMER PODZEMNEGA TOKA LIHU, PROVINCA GUANGXI, KITAJSKA

Yang HUI[1] & Zhang LIANKAI[1,2,*]

Abstract UDC 551.444:546.19(510)

Yang Hui & Zhang Liankai: Adsorptive behaviour of arsenic in a karst subterranean stream and principal components analysis of its influencing variables: A case study at the Lihu subterranean stream, Guangxi province, China

Arsenic (As) pollutants are serious threat to water ecological security and human health, especially in karst areas because of their unique hydrogeological characteristics. Physical-chemical analyses of karst water and its sediments at the Lihu subterranean stream, southwest China, were conducted by ICP-MS and XRF to elucidate the reaction mechanisms of arsenic in karst subterranean streams. The results show that inorganic arsenic comprise most of the total arsenic, while organic arsenic including monomethylated arsenic (MMA) and dimethyl arsenic (DMA) are not detected or infinitesimal. The reducing environment in the subterranean stream makes As(III) dominant and accounts for 53 % of the inorganic species. Adsorptive behaviour of arsenic occurred and the removal rates of As, As(III) and As(V) in the Lihu subterranean stream are 51 %, 36 % and 59 % respectively after a 25.6 km underground distance. To find out the main influencing factors on arsenic adsorptive process in this underground river, principal component analysis in SPSS and Minitab were applied. Seven main factors, i.e. sediment Fe (Fe_{sed}), sediment Al (Al_{sed}), sediment Ca (Ca_{sed}), particulate organic matter (POM), sediment Mn (Mn_{sed}), water Ca^{2+} (Ca^{2+}) and water HCO_3^- (HCO_3^-) are extracted from thirteen indicators. The rank of those factors for total arsenic and As(III) is $Ca_{sed} > Fe_{sed} > Ca^{2+} > POM > Mn_{sed} > Al_{sed} > HCO_3^-$, while it is $Fe_{sed} > Ca_{sed} > Ca^{2+} > Mn_{sed} > POM > Al_{sed} > HCO_3^-$ for As(V). Of these seven factors, Fe_{sed}, Al_{sed}, Ca_{sed}, POM, Mn_{sed} and

Izvleček UDK 551.444:546.19(510)

Yang Hui & Zhang Liankai: Adsorpcijsko obnašanje arzena v kraških podzemnih tokovih in analiza glavnih komponent spremenljivk, ki vplivajo nanj: primer podzemnega toka Lihu, provinca Guangxi, Kitajska

Arzen (As) je nevaren onesnaževalec, ki ogroža ekološko stanje voda in zdravje ljudi; še posebej v krasu zaradi njegovih edinstvenih hidrogeoloških značilnosti. Z namenom pojasnitve reakcijskih mehanizmov arzena v kraških podzemnih tokovih so bile z uporabo ICP-MS in XRF opravljene fizikalno-kemijske analize kraške vode in sedimentov v podzemnem toku Lihu na jugozahodu Kitajske. Rezultati kažejo, da večino skupnega arzena predstavlja anorganski arzen, organski arzen, vključno z monometil arzenovo kislino (MMA) in dimetil arzenovo kislino (DMA), pa ni bil zaznan. Zaradi redukcijskega okolja v podzemnem toku prevladuje As(III), ki predstavlja 53 % anorganskega tipa. Pojavilo se je adsorpcijsko obnašanje arzena in deleži As, As(III) in As(V) so se zmanjšali za 51 %, 36 % in 59 % na 25,6 km dolgem podzemnem toku Lihu. Z namenom določitve najpomembnejših faktorjev, ki vplivajo na procese adsorpcije arzena v tej podzemni reki, je bila uporabljena anliza glavnih komponent v SPSS in Minitab. Sedem glavnih faktorjev, to so Fe v sedimentu (Fe_{sed}), Al v sedimente (Al_{sed}), Ca v sedimentu (Ca_{sed}), suspendirana organska snov (POM), Mn v sedimentu (Mn_{sed}), Ca^{2+} v vodi (Ca^{2+}) in HCO_3^- v vodi (HCO_3^-), je bilo povzeto iz trinajstih indikatorjev. Zaporedje teh faktorjev za skupni arzen in As(III) je $Ca_{sed} > Fe_{sed} > Ca^{2+} > POM > Mn_{sed} > Al_{sed} > HCO_3^-$, za AS(V) pa $Fe_{sed} > Ca_{sed} > Ca^{2+} > Mn_{sed} > POM > Al_{sed} > HCO_3^-$. Od teh sedmih faktorjev Fe_{sed}, Al_{sed}, Ca_{sed}, POM, Mn_{sed} in Ca^{2+} spodbujajo adsorpcijo, HCO_3^- pa

[1] Yang H, Institute of Karst Geology, Chinese Academy of Geological Sciences, 50 Qixing Road, Guilin 541004, China, Karst Dynamics Laboratory, Ministry of Land and Resources & Guangxi Zhuang Autonomous Region, 50 Qixing Road, Guilin 541004, China, E-mail: yanghui-kdl@karst.ac.cn

[2] Zhang L (Corresponding author), Institute of Karst Geology, Chinese Academy of Geological Sciences, 50 Qixing Road, Guilin 541004, China, Institute of Geochemistry, Chinese Academy of Sciences, 46 Guanshui Road, Guiyang 550002, China, Karst Dynamics Laboratory, Ministry of Land and Resources & Guangxi Zhuang Autonomous Region, 50 Qixing Road, Guilin 541004, China, E-mail: zhangliankai@karst.ac.cn

Received/Prejeto: 10.12.2013

Ca^{2+} are promoting factors for arsenic adsorption while HCO_3^- is an inhibiting factor. Calcium and bicarbonate turn out to be the main influencing factors for water arsenic adsorption in the study area, largely because the high calcium and alkaline values in karst water. This finding is an obvious distinction compared with the research findings at a non-karst area.
Keywords: karst subterranean stream, sediment, arsenic, influencing factors, principal component analysis.

jo zavira. V vodah proučevanega območja sta kalcij in hidrogenkarbonat glavna faktorja, ki vplivata na adsorpcijo arzena, predvsem zaradi visoke vsebnosti kalcija in alkalnosti v kraških vodah. Ta ugotovitev je značilna razlika v primerjavi z raziskovalnimi rezultati za nekraško območje.
Ključne besede: kraški podzemni tok, sediment, arzen, faktorji vpliva, analiza glavnih komponent.

INTRODUCTION

As an ubiquitous element in the environment, arsenic (As) is a carcinogen to both humans and animals. The arsenic contamination for water, air and soil is a significant environment health concern because of its toxicity (Ng *et al.* 2003). Arsenic mine drainage, a common type of pollution that forms at non-ferrous metal mining districts, is one of the most important anthropogenic arsenic sources. Gross arsenic discharged by mining activity has reached up to 72.6 % of man-made sources in the world (Han *et al.* 2003).

The arsenic storage in China is rich and it accounts for about 70 % of the world's total storage (Xiao *et al.* 2008). Guangxi province, located in southern China, reserves 41.5 % of China's total arsenic (Wei & Zhou 1992). Arsenic pollutants produced by mining, mineral processing and metal chemical process in this area have polluted the soil, vegetation, surface water and groundwater through runoff, leaching and wind transportation (Segura *et al.* 2006, Li & Su 2001, Li *et al.* 2010, Zhai *et al.* 2008). Jian *et al.* 2012 has reported that the arsenic concentration in sediments of the Diao River in northern Guangxi hit 1000 mg/kg (67 times more than the background level).

The total area of the karst globally is about 22 million km^2 and covers 15 % of the Earth's land surface (Nguyet & Goldscheider 2006). Guangxi province is just located in the world's largest karst contiguous distribution area (Li & Luo 1983). Karst aquifers are becoming an increasingly important resource in many countries and currently contribute one quarter of world-wide drinking water supply (Nguyet & Goldscheider 2006), predicted to rise to almost 50 % in the near future (Kollarits *et al.* 2006). Karst systems are more complicated than sand and gravel aquifers, because of the strong karst development, slow soil forming process, substantial uplift in Cenozoic (in China), and the duplex structure in surface and underground (Yuan & Cai 1988). Karst problems such as rock desertification, soil erosion, and soil degeneration cause loss of natural protective and filtration layer and therefore, the groundwater is vulnerable to being polluted (Ford & Williams 1989). Many studies on the geochemical behavior of arsenic in closed basin groundwater or surface water have been conducted by scholars (Ahmed *et al.* 2004, Bissen & Frimmel 2003, Guo *et al.* 2003, Guo *et al.* 2008, Guo *et al.* 2011, Jay *et al.* 2005, Redman *et al.* 2001, Savage *et al.* 2000, Segura *et al.* 2006, Smedley & Kinniburgh 2002, Smedley *et al.* 2002, Wang *et al.* 2010). Compared with those homogeneous aquifer systems, karst subterranean streams have special geological background, spatial structure, hydrodynamic conditions and water chemical characteristics, i.e. the carbonate rock geological background, uneven distribution of underground spatial structure, the strong karst dynamic process and unique hydrochemical characteristics. These features would affect the migration of arsenic in groundwater. Unfortunately, few studies have been done in this field. In-depth research is needed and it is also conducive to reveal the arsenic environmental geochemical behavior in this well-known fragile environment.

STUDY AREA AND METHODS

SITE DESCRIPTION

The Lihu subterranean stream catchment, with the karstification of 31.67 %, is located in NW Guangxi province, southwest China (Fig.1). This river originates from Layi village and Guanxi village, wherein the peak cluster, peak forest and uvala are the main physiographic

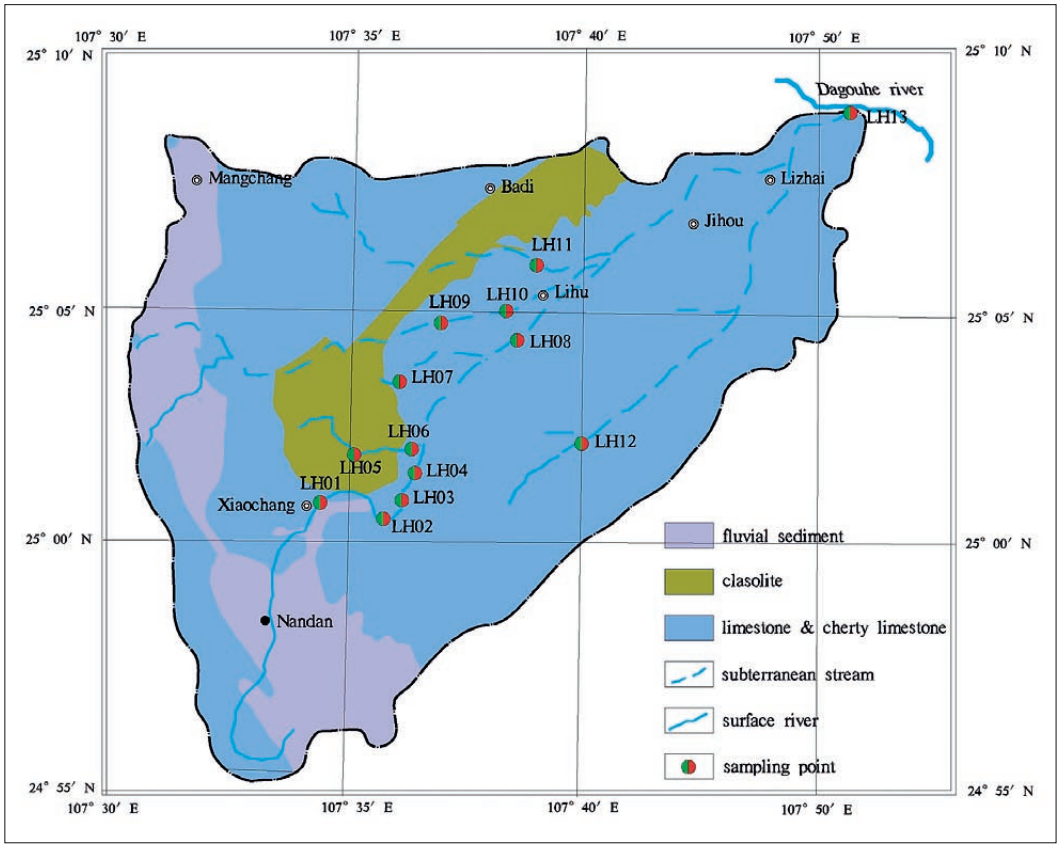

Fig.1: Location of study sites and the geological background of Lihu subterranean stream catchment.

types. It discharges at a steep cliff of the Dagouhe River after flowing through 25.6 km of limestone hills and depressions. The basin area is 517.4 km^2, and the average water flow is 4594 L/s in rainy season (June to August), while 3340 L/s in dry season (December to February). There are three tributaries in this underground river, i.e. Lizhai, Jihou and Badi subterranean streams. The mean annual precipitation in study area ranges from 1261 mm to 1628 mm. Geologically, The Lihu subterranean stream basin consists of various rocks from Carboniferous, Permian, Triassic, to Quaternary fluvial sediments. Cherty limestone is widely distributed in this basin. Geography and geological background of the study area are shown in Fig. 1.

SAMPLES AND EXPERIMENT

The river surface sediments (0 to 5 cm) and water samples were collected in June 2012. Three to five equally spaced distributed samples were obtained on each sampling point. Branches, leaves, roots and other debris were picked out. Collected sediment was put into polyethylene bags that were rinsed with HNO_3 (5 %) and preserved in a refrigerator (at approximately 4 °C) instantly, then freeze dried in laboratory and sieved with 2 mm nylon mesh after being triturated in agate mortar. Concentrations and speciation of arsenic were measured by inductively coupled plasma mass spectrometer (ICP-MS) and inductively coupled plasma-atomic emission spectrometer (ICP-AES) at National Research Center for Geoanalysis, Beijing, China. The contents of major elements (Fe, Mn, Ca, Mg and Al) in sediment samples were determined by X-ray fluorescence spectrometer (XRF, Axios X). Water anions and cations were monitored by plasma spectrometer (IRIS Intrepid II XSP) at the karst geology resources environment supervision and inspection center, Ministry of Land and Resources, PRC. In situ measurement of pH, redox potential (Eh), temperature and electrical conductivity were performed by portable probes (Multi 3420 Set, Water Test Meters). All apparatus and beakers utilized throughout the study were cleaned using acid reagents and deionized water and chemicals in the analysis were of analytical grade.

DATA PROCESSING

Principal component analysis and correlation analysis were performed by SPSS 13.0 software. Maps were generated by ArcGIS 9.0, and Patero diagram was drawn by Minitab 15 software.

MULTIVARIATE STATISTICAL ANALYSIS

There are many influential factors such as sediment physical-chemical properties, coexisting ions, etc., that could affect the migration and transformation of arsenic in groundwater (Singh *et al.* 1999, Su *et al.* 2009). In order to clarify the reaction mechanisms of arsenic in karst underground river, water chemical characteristics and sediment physical-chemical properties were measured in this study. Multivariate statistical analysis methods were also applied to the correlation analysis and principal component analysis (PCA). The aim was to identify the main hydrogeological factors on arsenic adsorption in karst subterranean stream.

PRINCIPAL COMPONENT ANALYSIS

Impact factors, i.e. sediment iron (Fe_{sed}), sediment aluminum (Al_{sed}), sediment magnesium (Mg_{sed}), sediment calcium (Ca_{sed}), particulate organic matter (POM), sediment manganese (Mn_{sed}), water potassium (K^+), water sodium (Na^+), water calcium (Ca^{2+}), water magnesium (Mg^{2+}), water chloride (Cl^-), water sulfate ion (SO_4^{2-}), water bicarbonate ion (HCO_3^-) and sediment arsenic (As_{sed}, $As(III)_{sed}$, $As(V)_{sed}$) were selected in this research for PCA. The contents of those indicators were listed in Tab. 1. To ensure their comparability among these different dimensions of data, dimensionless normalization was used in data processing before PCA. Through normalization processing, a new 16 × 17 matrix were attained. The weight in each column of the new matrix is the same, with a mean value of 0 and standardized deviation of 1. SPSS 13.0 software was then used for correlation analysis. The results are listed in Tab. 2. Most indexes have high Pearson correlation coefficient ($r > 0.3$, $p < 0.05$), indicating a suitable factor analysis and extractable common factors from the matrix.

In PCA, rotated eigenvalues that are higher than 1 were chosen as explanatory variables according to the total variance interpretation instead of without varimax rotation. Accumulative variance contribution of the first four principal components (PC1-PC4) that were extracted from the PCA was 76.4 % (Tab. 3). Namely, most of the information of the total variance of the original variables has been explained by the top four common factors. Correlation of common factors and the original variables before rotation are shown in Tab. 4. The correlations of the first four common factors are not statistically significant. In order to distinguish the relationship between various factors clearly, initial factor loading matrix was rotated in SPSS software. After rotation, the original variables variances were redistributed with the accumulative variance invariably. The changing of variance contribution makes common factors clear and easy to explain.

As can be seen from Tab. 4, seven variables i.e. As_{sed}, $As(III)_{sed}$, $As(V)_{sed}$, Fe_{sed}, Al_{sed}, Ca_{sed}, POM, Mn_{sed}, Ca^{2+} and HCO_3^- have high load on the first common factor PC before and after rotating, illustrating the high intercorrelation between those seven variables. Those seven main influencing variables that impact arsenic contents and its speciation in karst groundwater were drawn from thirteen indicators.

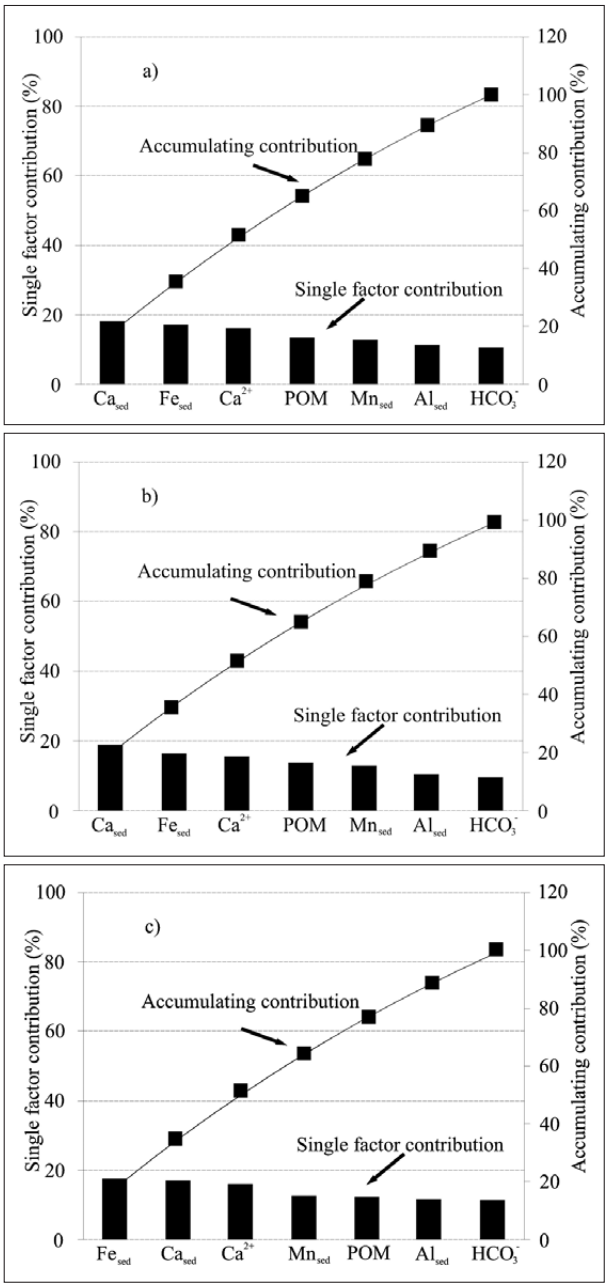

Fig. 2: Pareto sorts of influencing variables on a) total As; b) As(III); c) As(V).

Tab. 1: Sediments physical-chemical properties and water hydro-chemical characteristics in Lihu and Longzhai subterranean stream.

Sampling points	No.	Sediments									Water (mg/L)						
		Fe (%)	Al (%)	Mg (%)	Ca (%)	POM (%)	Mn (μg/g)	As (μg/g)	As(III) (μg/g)	As(V) (μg/g)	K^+	Na^+	Ca^{2+}	Mg^{2+}	Cl^-	SO_4^{2-}	HCO_3^-
Xiaochang	LH01	10.39	5.25	0.56	5.33	5.05	363.00	98.40	39.73	58.67	0.10	1.46	41.57	6.34	3.22	22.16	132.20
Layi cave	LH02	13.00	4.87	0.51	6.89	7.35	518.00	113.40	67.08	46.32	1.44	1.28	65.68	6.74	1.25	30.75	147.76
Layi Karst window	LH03	8.73	5.09	0.53	0.95	1.49	356.00	23.72	9.82	13.90	1.58	0.14	10.02	3.32	2.33	49.62	152.43
Liangfeng Cave	LH04	9.21	5.12	0.52	1.72	3.97	277.00	48.26	19.71	28.55	1.49	0.60	34.40	5.85	3.11	25.33	150.88
Qiaocun	LH05	10.97	5.85	1.25	2.33	1.09	378.00	49.70	12.92	36.78	1.06	1.52	48.60	1.41	1.89	35.21	122.88
Ganhe spring	LH06	9.91	9.14	0.51	3.85	5.33	419.00	38.66	15.86	22.80	0.74	1.51	31.90	5.70	4.35	53.62	158.65
Bachuanhe	LH07	7.89	8.33	0.23	2.64	2.64	330.00	38.20	22.30	15.90	2.64	1.74	38.80	6.09	6.47	60.78	125.99
Gantianba	LH08	8.47	5.52	0.39	4.53	1.72	304.00	45.80	29.10	16.70	1.73	1.22	33.70	6.40	5.67	37.22	152.43
Jihou	LH09	6.58	5.29	0.91	3.31	3.31	444.00	43.50	16.80	26.70	1.56	1.15	46.70	6.69	1.65	40.22	155.21
Hongxinghe	LH10	6.03	4.82	0.29	3.16	3.16	249.00	14.94	4.34	10.60	1.44	1.01	45.80	6.27	3.88	29.88	208.42
Badi	LH11	11.30	8.14	0.39	8.56	4.53	494.00	121.60	63.20	58.40	0.72	0.69	62.30	3.81	1.29	17.26	149.32
Lizhai	LH12	4.95	2.67	0.22	1.69	1.69	223.00	9.64	3.65	5.99	0.58	1.28	36.10	8.82	2.53	22.87	213.42
Xiaolongdong	LH13	6.91	3.46	0.38	3.88	2.30	281.00	9.33	5.12	4.21	0.19	1.24	13.94	1.57	1.34	39.87	236.42
Xiaolongdong	LH13	6.91	3.46	0.38	3.88	2.30	281.00	9.33	5.12	4.21	0.19	1.24	13.94	1.57	1.34	39.87	236.42

Tab. 2: Correlation analysis among influencing factors.

	Fe_{sed}	Al_{sed}	Mg_{sed}	Ca_{sed}	POM	Mn_{sed}	As_{sed}	$As(III)_{sed}$	$As(V)_{sed}$	K^+	Na^+	Ca^{2+}	Mg^{2+}	Cl^-	SO_4^{2-}	HCO_3^-
Fe_{sed}	1															
Al_{sed}	0.655(**)	1														
Mg_{sed}	0.520(*)	0.272	1													
Ca_{sed}	0.696(**)	0.565(*)	0.124	1												
POM	0.471(*)	0.290	−0.045	0.581(**)	1											
Mn_{sed}	0.670(**)	0.463(*)	0.409	0.516(*)	0.472(*)	1										
As_{sed}	0.820(**)	0.546(*)	0.296	0.871(**)	0.640(**)	0.622(**)	1									
$As(III)_{sed}$	0.778(**)	0.506(*)	0.136	0.890(**)	0.657(**)	0.618(**)	0.967(**)	1								
$As(V)_{sed}$	0.802(**)	0.548(*)	0.450	0.783(**)	0.573(*)	0.580(**)	0.960(**)	0.856(**)	1							
K^+	0.114	0.302	0.053	−0.132	−0.127	0.106	−0.033	0.064	−0.137	1						
Na^+	0.125	0.235	0.155	0.228	0.133	−0.072	0.132	0.120	0.135	0.029	1					
Ca^{2+}	0.639(**)	0.492(*)	0.363	0.747(**)	0.501(*)	0.420	0.770(**)	0.744(**)	0.738(**)	0.156	0.358	1				
Mg^{2+}	0.314	0.400	0.004	0.411	0.326	0.035	0.366	0.380	0.323	0.245	0.260	0.564(*)	1			
Cl^-	−0.059	0.262	−0.224	−0.222	−0.076	−0.076	−0.237	−0.197	−0.262	0.475(*)	0.142	−0.171	0.230	1		
SO_4^{2-}	−0.026	0.406	0.032	−0.177	−0.175	−0.055	−0.256	−0.219	−0.277	0.363	0.215	−0.206	0.024	0.237	1	
HCO_3^-	−0.629(**)	−0.498(*)	−0.481(*)	−0.302	−0.161	−0.316	−0.510(*)	−0.457(*)	−0.529(*)	−0.376	−0.257	−0.549(*)	−0.255	−0.047	−0.210	1

** Correlation is significant at the 0.01 level (2-tailed). * Correlation is significant at the 0.05 level (2-tailed). *n=13*

Tab. 3: Eigenvalues, variances and cumulative contribution rate of principal components before and after rotation.

Principal components	Before rotating			After rotating		
	Eigenvalues	Variance contribution (%)	Accumulating contribution (%)	Eigenvalues	Variance contribution (%)	Accumulating contribution (%)
PC1	7.07	44.16	44.16	6.34	39.65	39.65
PC2	2.43	15.20	59.36	2.26	14.14	53.79
PC3	1.54	9.62	68.99	2.13	13.29	67.08
PC4	1.18	7.37	76.35	1.48	9.27	76.35

Tab. 4: Factors loading matrix before and after rotation.

Variables	Common factors before rotating				Common factors after rotating			
	PC1	PC2	PC3	PC4	PC1	PC2	PC3	PC4
Fe_{sed}	0.89	0.09	–0.22	0.11	0.78	0.15	0.47	–0.02
Al_{sed}	0.67	0.51	0.00	0.13	0.57	0.56	0.28	0.14
Mg_{sed}	0.41	0.12	–0.74	–0.28	0.13	–0.05	0.89	0.03
Ca_{sed}	0.87	–0.19	0.23	–0.03	0.89	–0.12	0.05	0.20
POM	0.64	–0.23	0.38	0.16	0.76	–0.08	–0.22	0.05
Mn_{sed}	0.68	–0.05	–0.30	0.44	0.67	0.12	0.34	–0.41
As_{sed}	0.96	–0.19	0.04	0.06	0.95	–0.10	0.22	0.06
$As(III)_{sed}$	0.92	–0.16	0.16	0.14	0.95	–0.03	0.09	0.04
$As(V)_{sed}$	0.92	–0.21	–0.10	–0.04	0.87	–0.17	0.36	0.08
K^+	0.08	0.76	0.00	0.29	0.01	0.81	0.09	–0.02
Na^+	0.24	0.34	0.21	–0.72	0.06	0.08	0.17	0.84
Ca^{2+}	0.85	0.03	0.12	–0.27	0.75	–0.01	0.25	0.42
Mg^{2+}	0.46	0.32	0.55	–0.19	0.46	0.31	–0.21	0.55
Cl^-	–0.14	0.67	0.36	0.29	–0.10	0.76	–0.31	0.07
SO_4^{2-}	–0.12	0.72	–0.14	0.00	–0.27	0.64	0.23	0.13
HCO_3^-	–0.39	–0.35	–0.62	–0.21	–0.61	–0.44	0.33	0.15

SORTING ANALYSIS

Pareto diagram is a queuing method in some scientific statistical work. Minitab 15 software was applied to sort the seven variables mentioned at "Principal component analysis" section. The results were shown in Fig. 2. The influence degree of each factor on the arsenic shows a gradient descent. This suggests none of the factors occupy a dominant position. Arsenic in the sediment was affected by the coactions of those seven variables. The impact on As(III) and total As decreased in the order Ca_{sed} > Fe_{sed} > Ca^{2+} > POM > Mn_{sed} > Al_{sed} > HCO_3^-; for As(V), the order is Fe_{sed} > Ca_{sed} > Ca^{2+} > Mn_{sed} > POM > Al_{sed} > HCO_3^-. What should be noted about these seven variables is that HCO_3^- has negative relationships with total As, As(III) and As(V). The correlation coefficient of HCO_3^- with total As, As(III) and As(V) are –0.51, –0.46 and –0.53, respectively as shown in Tab. 2.

ARSENIC ADSORPTIVE PROCESS IN KARST SUBTERRANEAN STREAM

The concentrations of total arsenic, As(III) and As(V) in the Lihu subterranean stream are listed in Tab. 5. Most of the sampling points' arsenic content were rich and exceed 10 μg/L (the guideline concentration for drinking water set by the World Health Organization) (Ahmed *et al.* 2004). The average value is 35.76 μg/L, slightly above the value 20.71–27.05μg/L in the Diaojiang river sediment detected by Jian *et al.* (2010) near study area. Mining and metallurgy processes upstream are the main causes of arsenic pollutants. Field investigation completed by our group found that there is a small quarry and a coal mine running into the Layi and Badi cave inlet, respectively, which make the arsenic content of these two points higher than that of other's (Tab. 5). So the arsenic content in the underground river is closely related to human activities. Due to high dissolved oxygen and high Eh in surface rivers, As(V) is dominant in inorganic arsenic at surface points. The average is 76.3 %. At karst under-

Tab. 5: The concentration of total As, As(III) and As(V) in Lihu subterranean stream.

Sampling points	No.	Total As /μg·L^{-1}	As(III) /μg·L^{-1}	As(V) /μg·L^{-1}
Xiaochang	LH01	42.32	15.10	27.22
Layi cave	LH02	86.30	25.89	60.41
Layi Karst window	LH03	35.15	19.28	15.87
Liangfeng Cave	LH04	15.93	7.50	8.43
Qiaocun	LH05	33.60	6.32	27.28
Ganhe spring	LH06	12.50	6.00	6.50
Bachuanhe	LH07	17.22	11.05	6.17
Gantianba	LH08	25.26	15.25	10.01
Jihou	LH09	32.51	12.60	19.91
Hongxinghe	LH10	16.45	5.68	10.77
Badi	LH11	126.19	1.76	124.43
Lizhai	LH12	22.06	3.80	18.26
Xiaolongdong	LH13	15.60	7.33	8.27

Tab. 6: Average content of elements in parent material and soil (Cao & Yuan 2005, Chen et al. 1999) (Wb /10^{-6}).

Elements	Mean value in Earth's crust	Limestone parent material (Qingxudong Fm)	Dolomite parent material (Aoxi Fm)	Yellow soil (basalt)	Red soil (basalt)	Calcareous soil
Al	84100	700	3600	121700	140100	88500
Fe	70700	670	2100	170500	170200	59900
Mn	1400	160	300	1400	600	700
Ca	52900	390400	234600	700	700	16600
Mg	32000	3300	102100	2700	100	8900

ground rivers, Eh may decrease and thus the reducing environments formed, so As(V) is reduced to As(III). The average percentage of As(III) in whole underground river system reaches up to 53 %.

The line chart shown in Fig. 3 represents the changes of arsenic along the main streams of Lihu subterranean stream. Arsenic concentrations from upstream to downstream manifested a declining trend, except for LH02 point, which is influenced by quarry waste residue. The decline of arsenic contents in the subterranean stream implies a water self-purification process in karst groundwater.

For example, the concentration of total As, As(III) and As(V) in sample point LH01 are 42.32 μg/L,

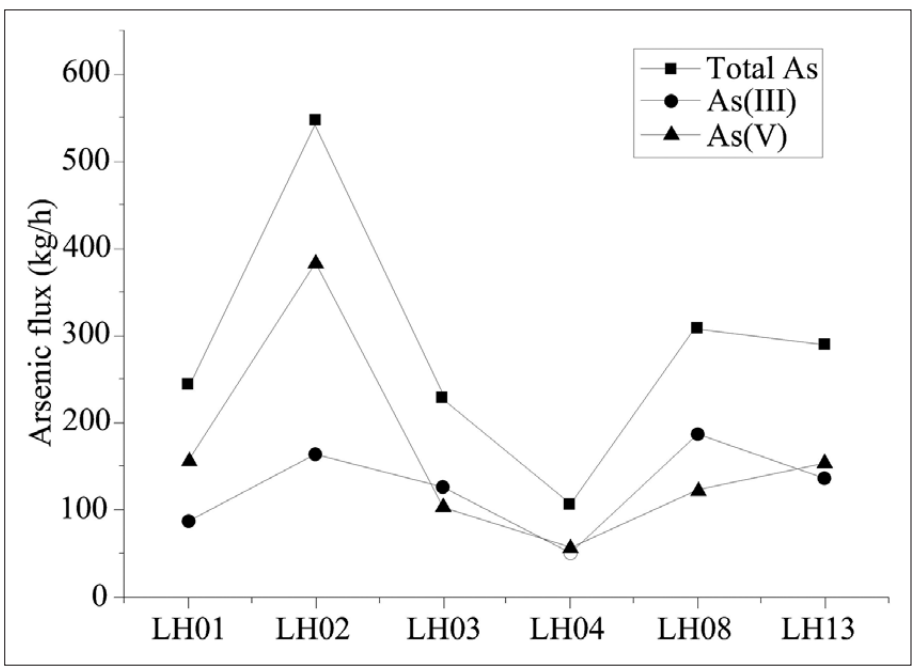

Fig. 3: Variation of inorganic arsenic along the Lihu subterranean stream.

15.10 μg/L and 27.22 μg/L, respectively. Those values are 2.7, 2.0 and 3.2 times higher than that of LH04, and 2.7, 2.1 and 3.3 times higher than that of LH13. The sum fluxes of total As, As(III) and As(V) at upper reaches of LH11, LH10, LH12 and LH08 (Fig. 1) are 589 kg/h, 212 kg/h, 377 kg/h and the fluxes at outlet of Xiaolongdong (LH13) are 290 kg/h, 136 kg/h and 154 kg/h, respectively. The concentrations of those three forms arsenic decreased by 51 %, 36 % and 59 % respectively after a 25.6 km distance in subterranean stream.

DISCUSSION

Compared to the research findings at a non-karst area, calcium and bicarbonate turned out to be the main influence factors for water arsenic adsorption largely because the high calcium and alkaline value in karst water. Therefore, the discussion is mainly focus on those two factors.

CALCIUM FOR ARSENIC ADSORPTION

Generally speaking, the cations such as Fe, Al, Mn have a strong As retention ability and show a remarkable correlation relationships with arsenic (Manning & Goldberg 1997). The Ca can also form complexes with arsenic and then be adsorbed to the sediments surface. Calcium has a promoting effect on arsenic sorption according to Goh and Lim (Goh & Lim 2005). With those ion concentration increases, the sorption function gradually strengthens. Calcium was the most sensitive cations because it can enhance electropositivity at the adsorbent surface. Thus, it strengthens the electrostatic interactions between the arsenic anion, causing more arsenic to be adsorbed. The coexistence of cations consolidate this process (Goh & Lim 2005). Previous research results indicated that the main species of arsenic in water deposits around the Lihu subterranean stream are Fe-As and Ca-As besides residual arsenic (Res-As). The proportion of Ca-As is higher than Al-As and Fe-As (Jian *et al.* 2010), which is different from fluvial sediment in the non-karst area (Cui & Liu 1988, Wei *et al.* 1999). The main lithologic chemical composition in karst area is $CaCO_3$. Carbonate rock can react with arsenic in weak alkaline environment and generate calcium arsenate which precipitates within the stream bottom sediments over time (Bhumbla & Keefer 1994, Jekel & Nriagu 1994).

Compared with the average chemical composition of the Earth's crust, Fe, Al and Mn contents in limestone and dolomite are significantly lower than average crustal elements (only 0.8 % to 21 % of the crustal median). However, the level of calcium and magnesium in karst area is 319 %~738 % of mean value of crust (Tab. 6). Moreover, Fe, Al, Mn contents in calcareous soil is only 0.35 to 1.2 times of red and yellow soil derived from basalt. Yet the corresponding Ca, Mg contents is 3 ~ 89 times higher than that corresponding basalt soil. This may be the reason for increased Ca activities in karst area, and hence it can explain the Ca elements become one of the most important factors on arsenic migration in karst subterranean stream.

BICARBONATE FOR ARSENIC ADSORPTION

The previous research revealed that bicarbonate (HCO_3^-) has a negative relationship with arsenic concentration (Anawar *et al.* 2004, Jay *et al.* 2005, Smith *et al.* 2002, Su *et al.* 2009). They thought that anions such as Cl^-, F^-, SO_4^{2-}, HCO_3^-, $H_2PO_4^-$ and SiO_3^- have prohibitive function on arsenic adsorption, and this prohibitive function would be amplified with the anions concentration increasing (Jay *et al.* 2005, Smith *et al.* 2002; Su *et al.* 2009).

The inhibitional effect of bicarbonate for arsenic adsorption is mainly caused by the competitive adsorption between bicarbonate and arsenic. The higher competitive ability, the more restraining performance. The carbonate weathering by atmospheric CO_2 at karst areas lead to the high bicarbonate concentration in water. The HCO_3^- can be chelated with adsorption sites and consequently hinder arsenic from being adsorbed (Smith *et al.* 1999). Meanwhile, the alkaline environment would slowdown the arsenic adsorption. That is why arsenic concentration in the study area expresses a negative relationship with bicarbonate.

CONCLUSIONS

There are some reasons for arsenic adsorption in karst subterranean stream. According to the study, cations (Fe, Al, Mn, and Ca) and organic matter have acceleration effect on arsenic adsorption, which could separate the ar-

senic from water and reduce the risk of arsenic contamination. Anions (Cl^- SO_4^{2-} and HCO_3^-), especially HCO_3^-, have inhibitory effect on arsenic removal. Calcium and bicarbonate in karst terrain revealed an important role during arsenic transportation and transformation. Therefore, the unique characteristics of karst should be considered during arsenic treatment in karst underground water.

ACKNOWLEDGEMENTS

The work was funded by the Natural Science Fund Project of Guangxi (2013GXNSFBA019218, 2013GXNSFBA019217), and the Project of the China Geological Survey (12120113052500, 12120113005200). We also thank the two anonymous peer-reviewers and the journal editors for their constructive suggestions that improved the manuscript.

REFERENCES

Ahmed, K. M., Bhattacharya, P., Hasan, M. A., Akhter, S. H., Alam, S., Bhuyian, M., Imam, M. B., Khan, A. A. & O. Sracek, 2004: Arsenic enrichment in groundwater of the alluvial aquifers in Bangladesh: an overview.- Applied Geochemistry, 2, 181–200.

Anawar, H. M., Akai, J. & H. Sakugawa, 2004: Mobilization of arsenic from subsurface sediments by effect of bicarbonate ions in groundwater.- Chemosphere, 6, 753–762.

Bhumbla D. K. & R. F. Keefer, 1994: Arsenic mobilization and bioavailability in soils. -In: Hutchinson T.C. & K. M. Meema (eds.) *Lead, Mercury, Cadmium and Arsenic in the Environment.* Scope, pp. 31–51, New York.

Bissen, M. & F. H. Frimmel, 2003: Arsenic-a review. Part II: oxidation of arsenic and its removal in water treatment.- Acta Hydrochimica et Hydrobiologica, 2, 97–107.

Cao, J. & D. Yuan, 2005: *Karst ecosystem of southwest China constrained by geological setting*.- Geological Publishing House, pp. 103, Beijing.

Chen, J., Hong, S., Deng, B. & M. Pan, 1999: Geographical tendencies of trace element contents in soils derived from Granite, Basalt and Limestone of Eastern China.- Soil and Environmental Sciences, 3, 161–167.

Cui, C. & Z. Liu, 1988: Chemical speciation and distribution of arsenic in water, suspended solids and sediment of Xiangjiang River, China.- The Science of the Total Environment, 1, 69–82.

Ford, D.C. & P. W. Williams, 1989: *Karst Geomorphology and Hydrology*.- Academic Division of Unwin Hyman Ltd, pp. 601, London.

Goh, K. H. & T. T. Lim, 2005: Arsenic fractionation in a fine soil fraction and influence of various anions on its mobility in the subsurface environment.- Applied Geochemistry, 2, 229–239.

Guo, H., Wang, Y. & Y. Li, 2003: Analysis of factors resulting in anomalous arsenic concentration in groundwaters of Shanyin, Shanxi province.- Environment Science, 4, 60–67.

Guo, H., Yang, S., Tang, X., Li, Y. Z. & Shen, 2008: Groundwater geochemistry and its implications for arsenic mobilization in shallow aquifers of the Hetao Basin, Inner Mongolia.- Science of the Total Environment, 1, 131–144.

Guo, H., Zhang, B., Li, Y., Berner, Z., Tang, X., Norra, S. & D. Stüben, 2011: Hydrogeological and biogeochemical constrains of arsenic mobilization in shallow aquifers from the Hetao basin, Inner Mongolia.- Environmental Pollution, 4, 876–883.

Han, F. X., Su, Y., Monts, D. L., Plodinec, M. J., Banin, A. & G. E. Triplett, 2003: Assessment of global industrial-age anthropogenic arsenic contamination.- Naturwissenschaften, 9, 395–401.

Jay, J., Blute, N., Lin, K., Senn, D., Hemond, H. & J. Durant, 2005: Controls on arsenic speciation and solid-phase partitioning in the sediments of a two-basin lake.- Environmental Science & Technology, 23, 9174–9181.

Jekel, M. & J. Nriagu, 1994: *Em Arsenic in environment.* Cycling and Characterization, pp 119, New York.

Jian, L., Huang, Z., Liu, Y. & Z. Yang, 2010: Particle size distribution and arsenic partitioning in sediments from a river polluted by mining.- Acta Scientiae Circumstantiae, 9, 1862–1870.

Jian, L., Li, H., Wu, L., Liu, J. & Z. Huang, 2012: Discussion on heavy metal pollution treatment of Diaojiang River.- Environment Science and Management, 148, 108–111.

Kollarits, S., Kuschnig, G., Veselic, M., Pavicic, A., Soccorso, C. & M. Aurighi, 2006: Decision-support systems for groundwater protection: innovative tools for resource management.- Environmental Geology, 6, 840–848.

Li, D. & Y. Luo, 1983: Measurement of carbonate rocks distribution area in China.- Carsologica sinica, 2, 61–64.

Li, L., Zhang, G., Liu, H., Xiang, M., Wei, X. & H. Li, 2010: Distribution and mobility of Sb and As in topsoils and plants in the Dachang multi-metalliferous mine area, Guangxi, China.- Acta Scientiae Circumstantiae, 11, 2305–2313.

Li, X. & Z. Su, 2001: The geochemical characteristics of soil elements of strata in Southwestern Guangxi.- Guangxi Sciences, 4, 301–307.

Manning, B. A. & S. Goldberg, 1997: Adsorption and stability of arsenic (III) at the clay mineral-water interface.- Environmental Science & Technology, 7, 2005–2011.

Ng, J. C., Wang, J. & A. Shraim, 2003: A global health problem caused by arsenic from natural sources.- Chemosphere, 9, 1353–1359.

Nguyet, V. T. M. & N. Goldscheider, 2006: A simplified methodology for mapping groundwater vulnerability and contamination risk, and its first application in a tropical karst area, Vietnam.- Hydrogeology Journal, 8, 1666–1675.

Redman, A., Macalady, D. & D. Ahman, 2001: A preliminary study of various factors influencing arsenic mobility in porous media: Proceedings USGS Workshop on Arsenic in the Environment.-[Online] Available from: http:/wwwbrr.cr.usgs.gov/Arsenic/workshop.htm [Accessed 13rd April 2013].

Savage, K. S., Tingle, T. N., O'Day, P. A., Waychunas, G. A. & D. K. Bird, 2000: Arsenic speciation in pyrite and secondary weathering phases, Mother Lode gold district, Tuolumne County, California.- Applied Geochemistry, 8, 1219–1244.

Segura, R., Arancibia, V., Zúñiga, M. & P. Pastén, 2006: Distribution of copper, zinc, lead and cadmium concentrations in stream sediments from the Mapocho River in Santiago, Chile.- Journal of Geochemical Exploration, 1, 71–80.

Singh, A., Hasnain, S. & D. Banerjee, 1999: Grain size and geochemical partitioning of heavy metals in sediments of the Damodar River–a tributary of the lower Ganga, India.- Environmental Geology, 1, 90–98.

Smedley, P. & D. Kinniburgh, 2002: A review of the source, behaviour and distribution of arsenic in natural waters.- Applied Geochemistry, 5, 517–568.

Smedley, P., Nicolli, H., Macdonald, D., Barros, A. & J. Tullio, 2002: Hydrogeochemistry of arsenic and other inorganic constituents in groundwaters from La Pampa, Argentina.- Applied Geochemistry, 3, 259–284.

Smith, E., Naidu, R. & A. Alston, 1999: Chemistry of arsenic in soils: I. Sorption of arsenate and arsenite by four Australian soils.- Journal of Environmental Quality, 6, 1719–1726.

Smith, E., Naidu, R. & A. M. Alston, 2002: Chemistry of inorganic arsenic in soils: II. Effect of phosphorus, sodium, and calcium on arsenic sorption.- Journal of Environmental Quality, 2, 557–563.

Su, C., Win, H., Wang, Y., Xu, F. & S. Zhang, 2009: Arsenic adsorption behavior and influence factors in sediments of endemic arsenism diseased areas from Datong Basin.- Geological Science and Technology Information, 3, 120–126.

Wang, Y., Sun, C., Xie, X. & Z. Xie, 2010: The genesis of high arsenic groundwater: a case study in Datong basin.- Geology in China, 03, 771–780.

Wei, L. & W. Zhou, 1992: Development of arsenic mineral resources and environment control.- Hunan Geology, 3, 259–262.

Wei, X., Wang, X., Liu, Y. & J. Tan, 1999: The study of the adsoptive behaviour of arsenic in soil and its form distribution.- Journal o Agricultural University of Hebei, 3, 28–30, 55.

Xiao, X., Chen, T., Liao, X., Wu, B., Yan, X., Zhai, L., Xie, H. & L. Wang, 2008: Regional distribution of arsenic contained minerals and arsenic pollution in China.- Geographical Research, 1, 201–212.

Yuan, D. & G. Cai, 1988: *The science of karst environment*.- Chongqing Publishing House, pp. 65, Chongqing.

Zhai, L., Chen, T., Liao, X., Yan, X., Wang, L. & H. Xie, 2008: Pollution of agricultural soils resulting from a tailing spill at a Pb-Zn mine: A case study in Huanjiang Guangxi Province.- Acta Scientiae Circumstantiae, 6, 1206–1211.

COBISS: 1.01

HEAVY MINERALS IN SEDIMENTS FROM THE MOŠNICA CAVE: IMPLICATIONS FOR THE PRE-QUATERNARY EVOLUTION OF THE MIDDLE-MOUNTAIN ALLOGENIC KARST IN THE NÍZKE TATRY MTS., SLOVAKIA

TEŽKI MINERALI V SEDIMENTIH IZ JAME MOŠNICA: IMPLIKACIJE ZA PREDKVARTARNI RAZVOJ SREDNJEGORSKEGA ALOGENEGA KRASA V NIZKIH TATRAH, SLOVAŠKA

Katarína BÓNOVÁ[1*], Pavel BELLA[2], Ján BÓNA[3], Ján SPIŠIAK[4], Martin KOVÁČIK[5], Martin KOVÁČIK[6] & Ľubomír PETRO[5]

Abstract UDC 551.442(437)

Katarína Bónová, Pavel Bella, Ján Bóna, Ján Spišiak, Martin Kováčik, Martin Kováčik & Ľubomír Petro: Heavy minerals in sediments from the Mošnica Cave: Implications for the pre-Quaternary evolution of the middle-mountain allogenic karst in the Nízke Tatry Mts., Slovakia

The cave deposits from the Mošnica Cave located on the northern slope of the Nízke Tatry Mts. were analysed by sedimentological, petrographical and mineralogical methods. Based on mineralogical study the cave sediments are composed of dolomite, quartz, muscovite, amphibole, chlorite, calcite, K-feldspar and plagioclase. Heavy mineral assemblage is formed by garnet, zircon, apatite, monazite, tourmaline, staurolite, rutile, titanite, epidote, sillimanite, allanite, andalusite and barite. Opaque minerals are represented by ilmenite, pyrite, magnetite, Cr-spinel, Fe-oxyhydroxides and chalcopyrite. Detailed research of chemical composition of the heavy minerals points to their source rocks formed by granitoids, amphibolites and amphibolite gneisses representing the crystalline basement and probably by Triassic cover sediments of the Lúžna Formation. Presence of the allochthonous minerals in the cave from metamorphic complex recently occurred on the opposite southern slope of the Nízke Tatry Mts. indicates a past larger catchment area of the allogenic karst of Mošnica Valley on the pre-Quaternary less dissected terrain. A change of watershed boundary leading through the central range of the Nízke Tatry Mts. was probably connected with the tilting of this mountain range

Izvleček UDK 551.442(437)

Katarína Bónová, Pavel Bella, Ján Bóna, Ján Spišiak, Martin Kováčik, Martin Kováčik & Ľubomír Petro: Težki minerali v sedimentih iz jame Mošnica: implikacije za predkvartarni razvoj srednjegorskega alogenega krasa v Nizkih Tatrah, Slovaška

Jamski sediment iz jame Mošnica, ki se nahaja na severnem pobočju Nizkih Tater, so bili analizirani z sedimentološkimi, petrografskimi in mineraloškimi metodami. Na podlagi mineraloških raziskav jamske sedimente sestavljajo dolomit, kremen, muskovit, amfibol, klorit, kalcit, K-glinenec in plagioklaz. Težko mineralno frakcijo predstavljajo granat, cirkon, apatit, monazit, turmalin, staurolit, rutil, titanit, epidot, sillmanit, allanit, andaluzit in barit. Neprozorni minerali so zastopani z ilmenitom, piritom, magnetitom, Cr-spinelom, Fe-oksihidroksidi in halkopiritom. Detajlna analiza kemične sestave težkih mineralov je nakazala njihov izvor iz granitov, amfibolitov in amfibolitnih gnajsov, ki predstavljajo kristalinsko podlago in iz triasnih krovnih sedimentov Lužna formacije. Prisotnost alohtonega materiala iz metamorfnega kompleksa, ki so bili najdeni v jami na nasprotnem južnem pobočju Nizkih Tater nakazuje nekdanje večje območje porečja alogenega krasa v dolini Mošnice na predkvartarnim manj razčlenjenim terenu. Sprememba meje porečja, ki poteka skozi osrednje območje Nizkih Tater je bila verjetno povezana z nagibanjem tega pogorja proti severu zaradi kompresijskega tektonskega režima v času poznega terciarja.

[1] Institute of Geography, Faculty of Science, Pavol Jozef Šafárik University in Košice, Jesenná 5, 040 01 Košice, Slovakia; *e-mail: katarina.bonova@upjs.sk

[2] State Nature Conservancy of the Slovak Republic, Slovak Caves Administration, Hodžova 11, 031 01 Liptovský Mikuláš & Department of Geography, Pedagogical Faculty, Catholic University, Hrabovská cesta 1, 034 01 Ružomberok, Slovakia; e-mail: pavel.bella@ssj.sk

[3] Kpt. Jaroša 780/13, 040 22 Košice, Slovakia; e-mail: janobona@hotmail.com

[4] Department of Geography, Geology and Landscape Ecology, Faculty of Natural Sciences, Matej Bel University, Tajovského 40, 974 01 Banská Bystrica, Slovakia; e-mail: jan.spisiak@umb.sk

[5] State Geological Institute of Dionýz Štúr, Regional centre – Košice, Jesenského 8, 040 01 Košice, Slovakia; e-mail: martin.kovacik@geology.sk, lubomir.petro@geology.sk

[6] State Geological Institute of Dionýz Štúr, Mlynská dolina 1, 817 04 Bratislava, Slovakia; e-mail: mato.kovacik@geology.sk

Received/Prejeto: 19.11.2013

towards the north, in the compression regime during the Late Tertiary.
Key words: cave sediments, slackwater facies, mineral composition, provenance, allogenic karst, Mošnica Cave, Nízke Tatry Mts.

Ključne besede: jamski sedimenti, "slackwater" facies, mineralna sestava, provenienca, alogeni kras, jama Mošnica, Nízke Tatre.

INTRODUCTION

Allochthonous cave sediments prove an important record of sedimentary phases of cave development and paleogeographical evolution of landforms in the adjacent area. Use of heavy mineral associations for the interpretation of source areas in the Western Carpathians performed Kicińska and Głazek (2005) in the karst of Belianske Tatry Mts., Orvošová *et al.* (2006) in the karst of Nízke Tatry Mts., Bónová *et al.* (2008) in the Slovak Karst and Bónová *et al.* (2014) in the karst of Chočské Foothills. The contribution presents the mineralogical-petrological and sedimentological characteristics of allochthonous sediments from the Mošnica Cave as one of the highest-lying subhorizontal caves in the allogenic karst of the Demänová Hills (Nízke Tatry Mts.). The aim of the research is based on the heavy mineral associations and their chemical composition to identify the source rocks and the areas of their transport into the cave, as well as to point out to the importance of the mineralogical and petrological research of cave sediments for the reconstruction of the pre-Quaternary evolution of the middle-mountain allogenic karst on the northern slope of the Nízke Tatry Mts.

LOCATION

The Mošnica Cave is the most important cave in the western part of Demänová Hills that belong to the Ďumbierske Tatry Mts. (geomorphologic subunit of the Nízke Tatry Mts.). The cave is located in the slope of Skoková Valley on the right side of the Mošnica Valley which lies west of the well-known Demänová Valley (Fig. 1A). The Mošnica Valley leads from Bôr (1,887.6 m a.s.l.) to the north and its mouth into the Liptov Basin is at 715 m a.s.l. The main entrance to the Mošnica Cave is at the altitude of 1,060 m, 223 m above the Mošnica river bed.

GEOLOGICAL AND GEOMORPHOLOGIC SETTINGS

The Ďumbierske Tatry Mts. represent the core mountain which consists of crystalline basement and its cover units. The Ďumbier crystalline complex is composed of pre-Mesozoic granitoids, high-grade metamorphic rocks (orthogneisses, granulites, paragneisses), metabasic and metaultramafic rocks (Spišiak & Pitoňák 1990; Biely *et al.* 1992). The metamorphic rocks are intruded by Carboniferous granitoid pluton which consists of several types (Ďumbier, Prašivá and Latiborská hoľa), ranging from tonalite to granite composition. Magmatic rocks occur in the northern part of the area, whereas metamorphic ones form its southern part with a transitional zone of migmatites at their contact (Bezák & Klinec 1983; Fig. 2). Preserved remnants of the sedimentary envelope, in places deeply folded into the crystalline, are built by Lower Triassic (i. e. quartzites), less frequently Middle Triassic rocks (rauhwackes). Western and northern parts of the Tatricum are overlain by Mesozoic units of the Fatricum represented by the Krížna Nappe (Biely *et al.* 1992; Bezák *et al.* 2008).

MOŠNICA VALLEY

The southern part of the valley is formed by Tatricum – crystalline basement with autochthonous sedimentary envelope (Fig. 2). The crystalline rocks are presented mainly by muscovite-biotite granodiorites to granites (Prašivá type), on the left side of the valley with small islet positions of quartz diorite to diorite. Biotite tonalites to granodiorites (Ďumbier type) pass from the neighbouring Demänová Valley (Biely *et al.* 1992). A smoothly

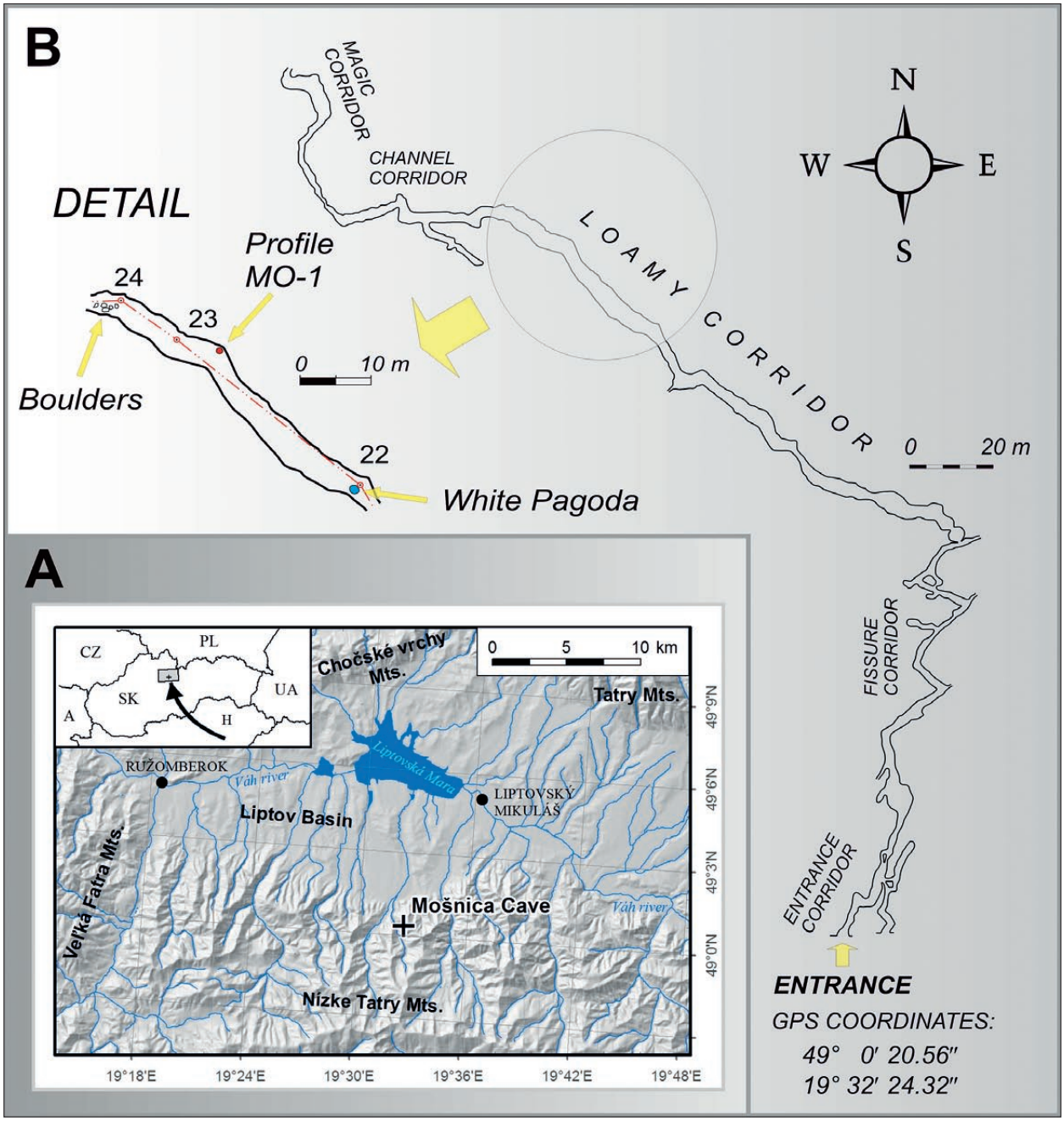

Fig. 1: Mošnica Cave. Location map (A), longitudinal projection (B – measured by Droppa 1950).

modelled relief on the crystalline rocks is partially dissected by glacier landforms from the Late Pleistocene (Škvarček 1978). The Lower Triassic sedimentary envelope performs in a narrow strip on the northern edge of the crystalline basement. Its basal part is represented by Lúžna Formation (Scythian) involves coarse-grained to arkosic sandstones and sandstone quartzites. Werfenian beds (Scythian) consist of less thick strata of colourful shales with rare sandstone inserts. The sedimentary envelope contains also the thick strip of the Middle Triassic rauhwackes (Bujnovský 1975).

The northern part of the Mošnica Valley is build by carbonate complex of Krížna Nappe that consists of Middle Triassic (Anisian) Gutenstein limestones and overlying layered massive dolomites (Ladinian; Fig. 2). The karst of Mošnica Valley presents a karst of monoclinal ridges strongly conditioned by a fault-nappe structure. The narrowest part of the valley presents a karst

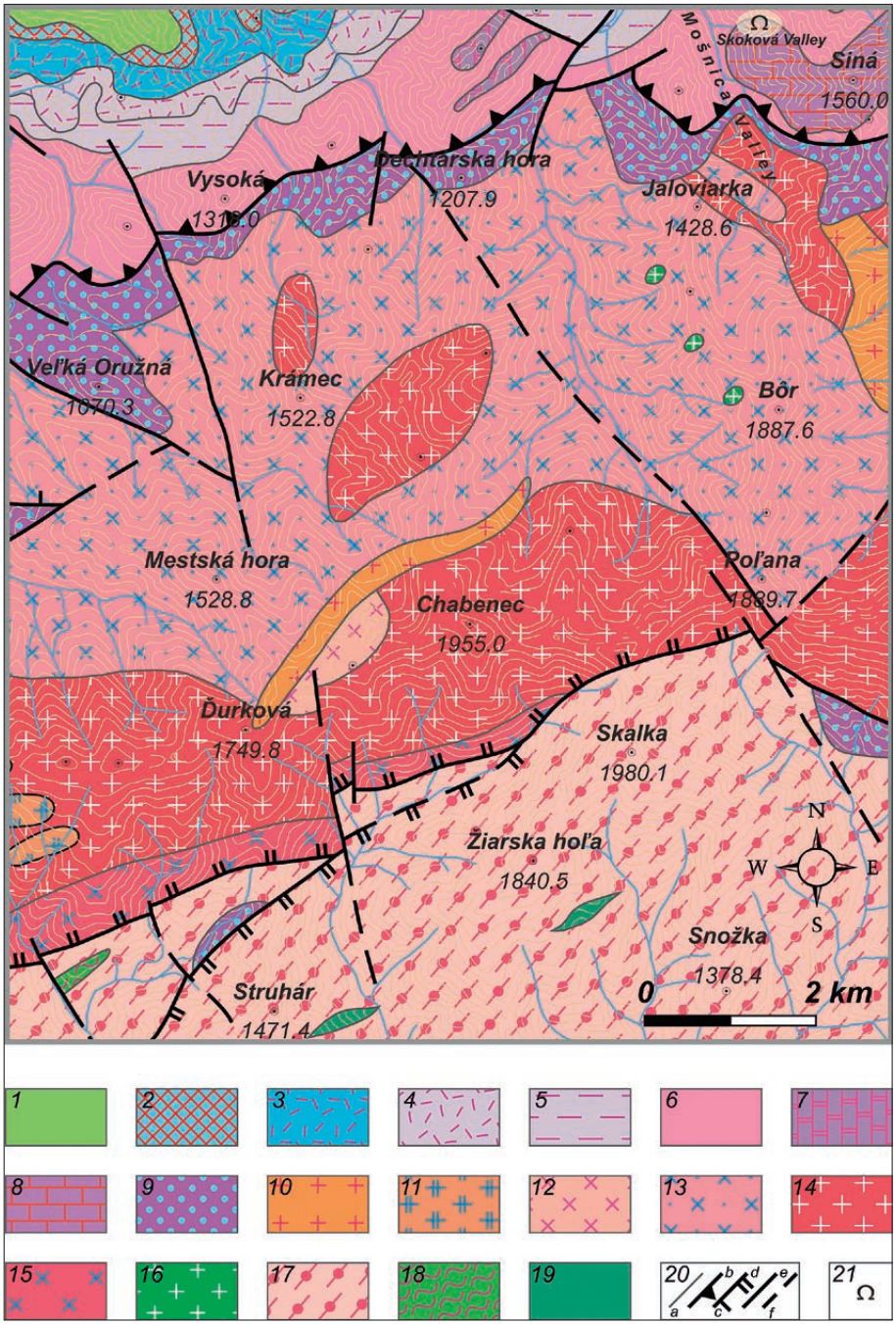

Fig. 2: Geological map of the Mošnica Valley and its surrounding area (according to Bezák et al. 2008, partly modified). Explanations: Fatricum: Jurassic-Cretaceous: 1 – Mraznica Fm.: grey marly limestones, marlstones, marly shales; Osnica Fm.: pale-grey Calpionella limestones, marly shales; Jurassic: 2 – Jasenina Fm.: clayey Sacoccoma-aptychus limestones; Ždiar Fm.: radiolarian limestones and radiolarites; Triassic-Jurassic: 3 – siliceous fleckenmergel, Adnet and Hierlatz limestones, Allgäu Fm., Kopienec Fm., Fatra Fm.; Triassic: 4 – Fatra Fm.: black Lumachella, marly and coral limestones; 5 – Carpathian Keuper; 6 – Ramsau dolomites; 7 – Podhradie limestones; 8 – Gutenstein limestones; Tatricum: T: 9 – Lúžna Fm.: quartzites, quartzose sandstones, greywackes, conglomerates, variegated sandy shales and intercalations of sandstones (Early Triassic); Tatricum crystalline units: Late Devonian-Early Carboniferous: 10 – leucocratic granites, locally porphyritic; 11 – biotite to two-mica granites to granodiorites; 12 – porphyric biotite granites to granodiorites; 13 – porphyric biotite to two-mica granodiorites to granites; 14 – biotite tonalities to granodiorites; 15 – hybridic non-homogenous granodiorites to tonalities; 16 – diorites; Proterozoic?-Paleozoic: 17 – orthogneisses and migmatites with banded and eyed structures with amphibolites and paragneisses layers; 18 – amphibolitic gneisses; 19 – amphibolites; 20 – a) geological boundaries, b) main Paleoalpine tectonic units boundaries, c) partial tectonic units boundaries, d) other tectonic lines, e) unspecified faults, f) assumed faults; 21 – cave.

gorge formed by the incision of allochthonous Mošnica Stream, partly sinking into the underground.

The northernmost part of the valley is formed by Upper Triassic partly silicified stratified dolostones (Carnian–Norian) and the Carpathian Keuper Formation (Norian) consisting of yellowish layered dolostones with interlayers of red and green shales and shales with junk inserts of Keuper-dolostone (Bujnovský 1975). Other upper strata of Krížna Nappe are covered by sedimentary rocks of Central Carpathian Paleogene Basin (Gross *et al.* 1980). Quaternary formations are formed by glacial, glacifluvial, fluvial and deluvial sediments.

BASIC MORPHOLOGICAL FEATURES AND PROBLEMATICS OF CAVE GENESIS

The Mošnica Cave is formed in the Middle Triassic Gutenstein limestones of Krížna Nappe. It reaches a length of 450 m, vertical range about 10 m (Fig. 1B) and dominantly consists of horizontal to subhorizontal corridors (Droppa 1950; Bella 1988; Bella & Urata 2002).

According to Droppa (1950) this cave originated by meteoric waters infiltred though enlarged fissures during intensive precipitations. Based on the sharp-edged particles of fine-grained allochthonous cave sediments he considered their aeolian transport on the surface above the cave from an uplifted and denudated crystalline basement of the central ridge of the Nízke Tatry Mts. and their washing into the cave by rainwaters through enlarged fissures. Droppa (1973) classified the Mošnica Cave as a fissure-corrosion cave.

Oval shapes sculpted by flowing water are visible in the Loamy Corridor and some other parts. The remnant of wall scalloped surface in the Entrance Corridor prove the direction of past water flow into the cave, probably allochthonous waters of the Mošnica paleostream (wall morphology of the corridor was largely remodelled by frost weathering). Primary cavities originated in the phreatic zone (oval corridors, ceiling pockets and irregular hollows; Fig. 3A and B). During younger developmental stage they were remodelled in the shallow phreatic zone after a decrease and following stability of water table (water table wall notches; Fig. 3C). Finally, the rocky floors of Channel and Magic corridors were incised by vadose water flow (meandering floor channel). In the vadose development stage vertical wall grooves originated by corrosion caused by rainwaters seeping along steep fissures, and several varieties of flowstones and dripstones, mainly pagoda-like stalagmites (Fig. 3D), precipitated from the mineralized water solutions. Some cave parts are remodelled by rock breakdown (Bella 1988; Bella & Urata 2002).

Based on oval shapes of several corridors, significantly prevailing horizontal corridors and position in height Bella (1988) considered the Mošnica Cave as an inactive river modelled cave originated during a tectonic stability, probably synchronously with the formation of a planation surface on the north side of Nízke Tatry Mts., remnants of which are of about 1000 m a.s.l. (denudation niveau N-III; Dinev 1942). Its height position more or less corresponds to the Late Pliocene River level that is observed in the Demänová Hills at altitudes of 1000–1050 m, eventually 950–1000 m a.s.l. (Droppa 1972; Bella 2001, 2002).

Considering a developmental correlation of cave levels with terraces of Váh River in the Liptov Basin, Orvoš and Orvošová (1996) rate the Mošnica Cave to the terrace T-XIa (in the relative high of 220–240 m from the recent river bed), which appertain to Reuverian A stage of the North West European stages. Fine-grained clastic sediments in the Loamy Corridor have normal polarity, they were deposited in stagnant water probably during the Gauss paleomagnetic epoch, i.e. before more than 2.588 Ma (Bosák *et al.* 2004; Kadlec *et al.* 2004).

Lower situated cave levels in the valleys of Demänová Hills including the Mošnica Valley) are correlated with the development of Quaternary river terraces (Droppa 1966, 1972; Orvoš & Orvošová 1996; Bella *et al.* 2011).

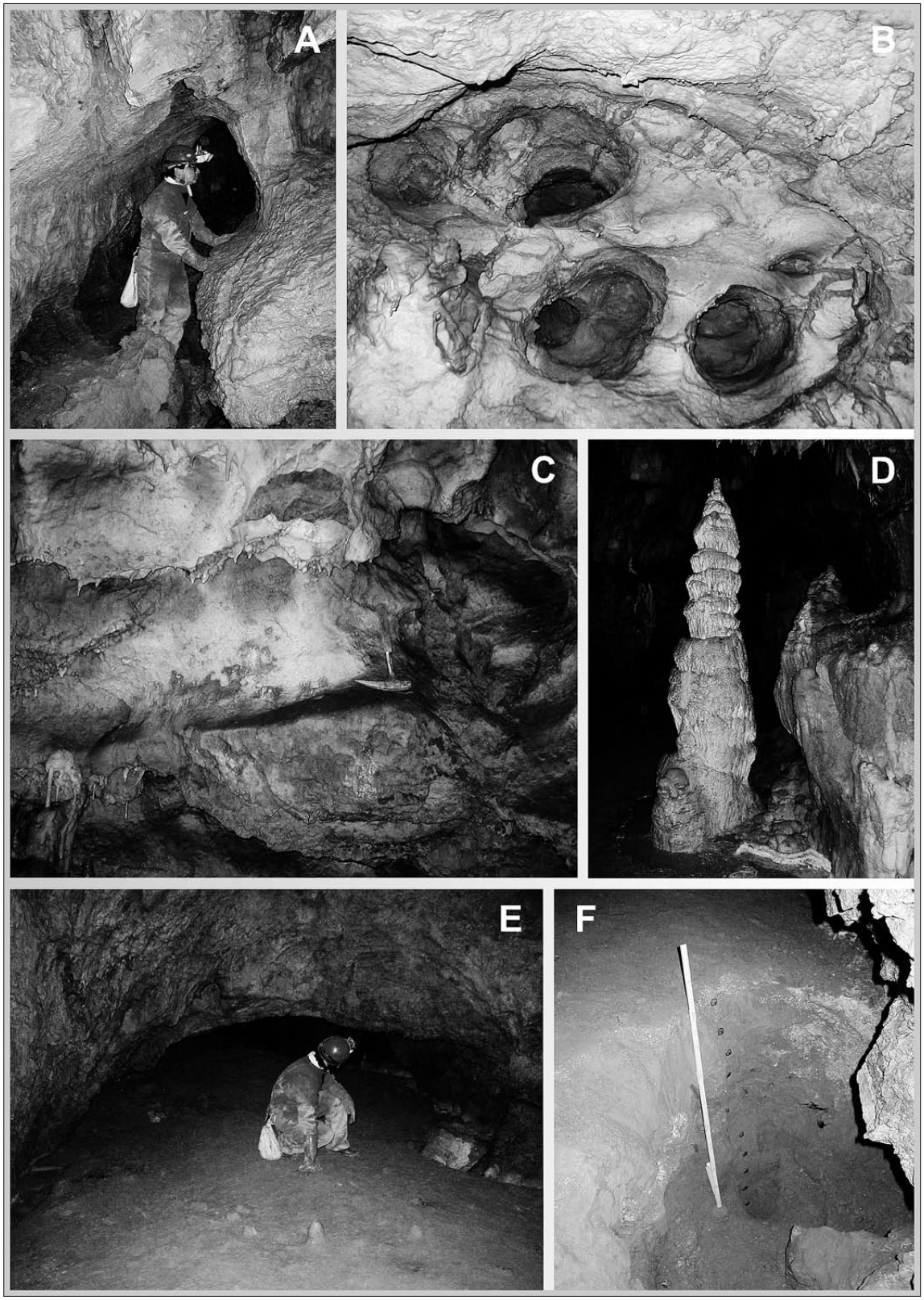

Fig. 3: Mošnica Cave, Loamy Corridor and its north-west adjacent part: A – prevailing phreatic morphology of outflow channel; B – ceiling pockets; C – epiphreatic lateral wall notch; D – stalagmite named the White Pagoda (2.4 m high); E – corridor floor covered by fine-grained sediments; F – studied sedimentary profile (Photo: P. Bella).

MATERIALS AND METHODS

The sedimentological profile located in the Loamy Corridor about 215 m above the bottom of the Mošnica Valley was studied (excavation up 1 m depth; Fig. 1B and 3F). Four samples (MO-1A to MO-1D) weighing 2–3 kg were collected for the granulometric analysis and preparation of the heavy mineral concentrates. Preparation of the samples was carried out in the laboratories of the Department of Applied Technology of Raw Minerals (State Geological Institute of Dionýz Štúr, Regional centre – Košice, Slovakia). Heavy mineral concentrate was obtained by the standard methods from the 0.02 to 0.063 mm size fraction and by the final separating in the heavy liquid, tetrabromethane with D=2.96 g/cm^3. Concentrates were qualitatively and quantitatively evaluated with the focus on translucent heavy minerals. Total of 300 to 350 grains were optically evaluated.

Garnet, amphibole, tourmaline, spinel and Fe-Ti oxides were analysed in a sample of polished thin sections by an electron microanalyzer CAMECA SX 100 (State Geological Institute of Dionýz Štúr, Bratislava) with the WDS method at accelerating voltages of 15 kV, beam current of 20 nA and electron beam diameter of 5 μm. To measure the concentrations of various elements were used following natural and synthetic standards: fluorapatite (P *Kα*), orthoclase (Si *Kα*), TiO_2 (Ti *Kα*), Al_2O_3 (Al *Kα*), Cr (Cr *Kα*), fayalite (Fe *Kα*), rhodonite (Mn *Kα),* forsterite (Mg *Kα*), wollastonite (Ca *Kα*), $SrTiO_3$ (Sr *Kα*), albite (Na *Kα*), LiF (F *Kα*) and NaCl (Cl Kα). Crystallochemical formula of garnet was normalized to 12 oxygens and conversion of an iron valence (Fe^{3+} and Fe^{2+}) according to ideal stoichiometry. Analysed points for tourmaline have been located in the centre, in the rim and on the margin of the grains. Tourmaline structural formula was calculated on the base of 24.5 oxygens (without boron); amphibole structural formula on the basis of 23 oxygens by calculation procedure given in Leake *et al.* (1997). Analyses of spinel were calculated on the basis of 3 cations. Fe^{2+} and Fe^{3+} in spinel were allocated according to the ideal stoichiometry. In Fe-Ti oxides FeO_{tot} was distributed into FeO and Fe_2O_3 *sensu* Dropp (1987) and structural formula was computed on the base of 4 oxygens.

Cathodoluminescence was used for observe the zircon zoning. It was carried out in the same instrument at accelerating voltage of 8 kV and beam current of $1x10^{-3}$ nA.

RESULTS

DESCRIPTION OF THE CAVE DEPOSITS

Two lithofacies have been recorded in the profile (Fig. 4; excavated profile does not attain to the rocky floor): 1) gray silty clay with thickness up to 50 cm, 2) rusty gray silty clay with thickness up to the 10 cm. Both lithofacies alternate in the vertical direction several times and boundaries between them are gradual.

Gray silty clay is lithofacies of standing or stagnant water (slackwater facies, *sensu* Gillieson 1996; Bosch & White 2004). The lithofacies have been created by deposition of fine particles (clay and silt) transported into the cave system as suspended load in muddy floodwater. Rusty gray silty clay is probably the original gray silty clay enriched in Fe-oxyhydroxides originated in oxidative conditions at the time the cave was not flooded and sediments have been subject of weathering. During the sedimentogenesis the clay has been sporadically supplied with speleogene material (e.g. carbonate fragments).

PETROGRAFICAL AND MINERALOGICAL CHARACTERISTICS

Allochthonous cave sediments represent the "cave loams". Based on the results of grain-size analysis they can be classified as a silt fraction (Hlaváč *et al.* 2004).

Dolomite is the main component of the fraction <2 mm (sand fraction) in all samples. Dolomite forms usually the lithic fragments. It is an irregularly limited, transparent to translucent, white to light gray colour. **Quartz** is angular to rounded, usually shows a higher degree of sphericity (Powers 1953; Fig. 5). Very rounded grains of quartz were also observed in non-significant amounts (Fig. 5B). Quartz is usually translucent to white, less transparent, usually bright. Monocrystalline grains predominate over the polycrystalline ones. **Muscovite** has a pearly luster. It forms irregularly limited flakes (rarely pseudohexagonal tables) crumbling under the surface of [001]. **Amphibole** forms the subhedral fragments. It is green to dark green, partially transparent with characteristic cleavage. **Calcite** forms the translucent crystals derived from filling of the carbonate ruptures or lithic fragments which may be derivable from

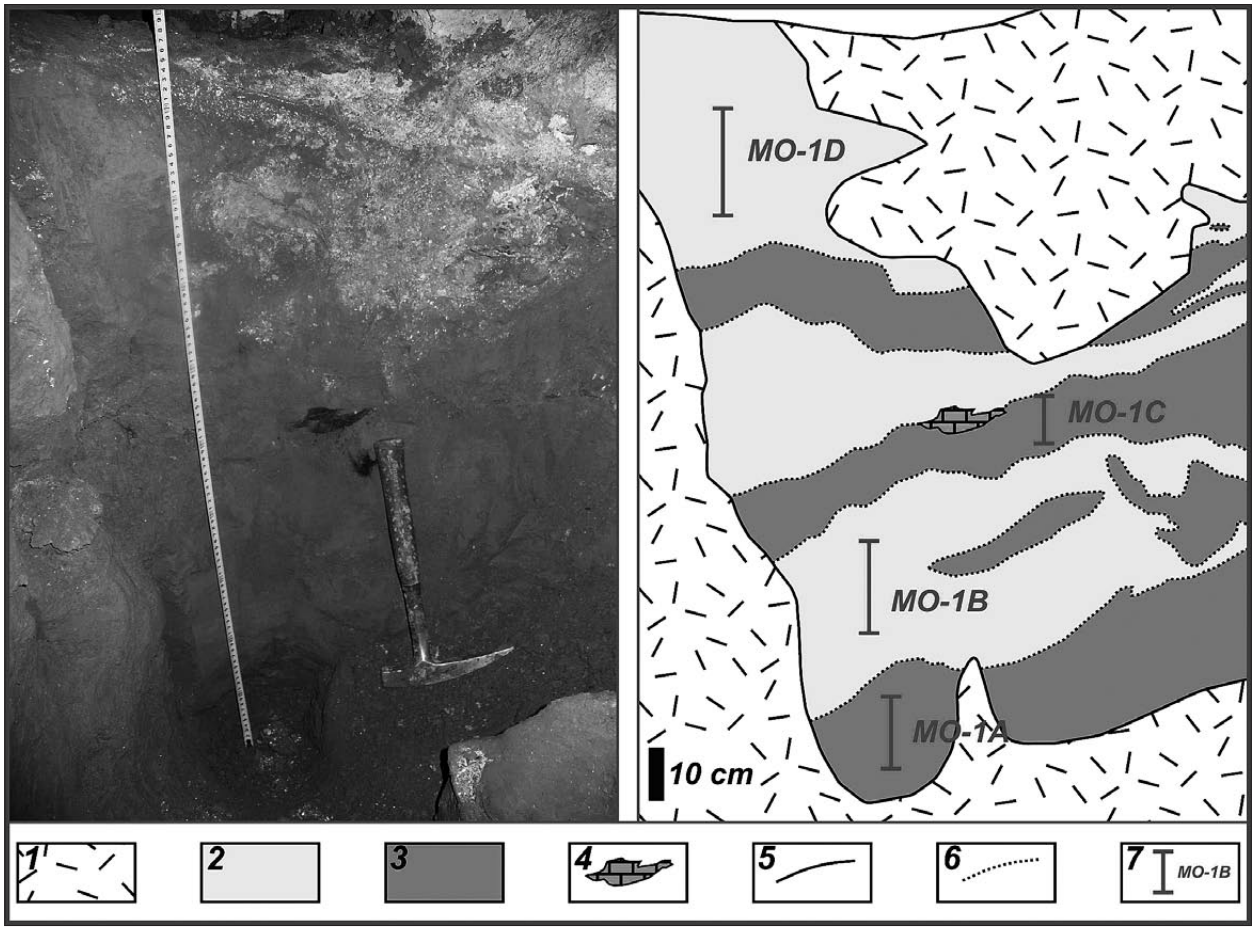

Fig. 4: Profile MO-1, Mošnica Cave: 1 – debris, 2 – gray silty clay, 3 – rusty gray silty clay, 4 – fragment of dark gray carbonate, 5 – sharp boundary between lithofacies, 6 – gradual boundary between lithofacies, 7 – location and identification of samples.

the Gutenstein beds. **K-feldspar (orthoclase)** forms usually pinkish irregularly limited grains or fragments with characteristic cleavage surfaces of [001] and [010]. **Plagioclase** is mostly white, its habitus and cleavage is similar to K-feldspar**. Chlorite** forms flakes crumbling under cleavage of [001]. It has green colour with glass to pearl luster.

The fraction >2 mm (gravel fraction) was noticed in a minor amount and only in MO-1A (5.1 vol. %) and MO-1C (5 vol. %) samples. It is made up of highly angular fragments of carbonates (mainly dolomite) in diameter 5–20 mm. The small crystals of calcite are preserved on the dolomite fragments (MO-1C sample). Individual carbonate fragments show no signs of mechanical transport. Therefore, we consider them to be autochthonous (speleogenous).

HEAVY MINERALS

The percentage abundance of heavy minerals was evaluated from all samples (Tab. 1). Apatite (up to 26.0 vol. %) and amphibole (up to 28.6 vol. %) prevail in the MO-1A, MO-1B and MO-1D samples. In the MO-1C sample zircon predominates over the apatite and amphibole. The quantitative differences can be justified by the differences in the size of the prepared fractions. In addition to apatite, zircon and amphibole, the heavy mineral assemblage is represented by epidote; garnet and tourmaline are found more rarely. The presence of other translucent minerals is given in Tab. 1. The opaque minerals are represented by ilmenite, pyrite, magnetite, Cr-spinel, +/– chalcopyrite and Fe-oxides (limonite, goethite).

Amphibole. All samples are represented mainly by calcic amphiboles with Ti<0.15 and Ca>1.5 *a.p.f.u.* Based on Leake's classification (Leake *et al.* 1997) the magnesiohornblende is predominate (Tab. 2, Fig. 6A). Its chemical composition in the direction of the central zone to grain periphery changes marginally with X_{Mg} [Mg/(Mg+Fe^{2+})] between 0.62 to 0.84. Some hornblendes show rimward Al-enrichment (Tab. 2), pointing to prograde metamorphism. Otherwise, the second group of Mg-hornblendes

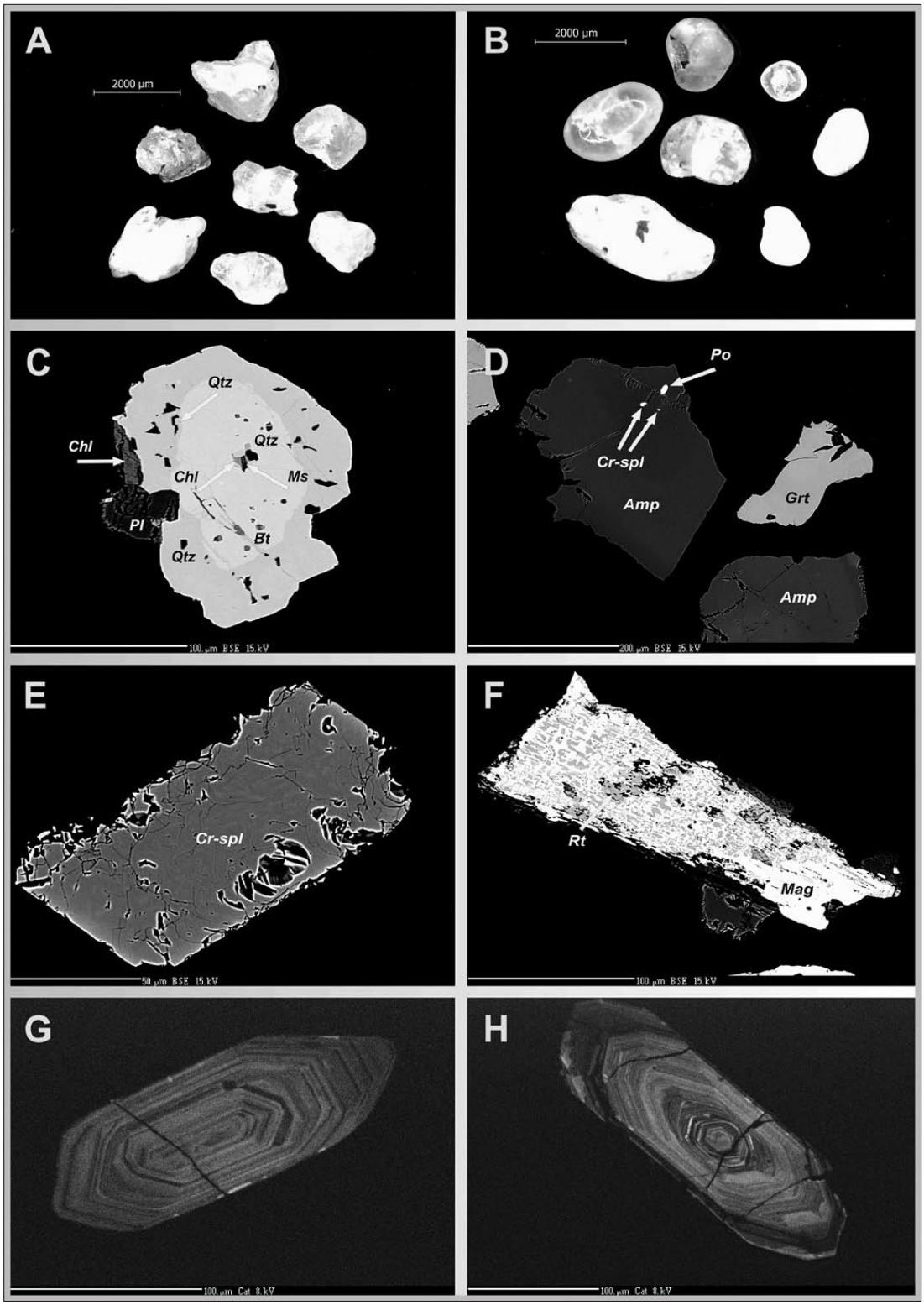

Fig. 5: Quartz: A – Angular to semi-angular clasts with a higher degree of sphericity (MO-1A); B – Rounded to very rounded clasts with the higher and lower degrees of sphericity (MO-1A); Heavy minerals (BSE images): C – inclusions of white mica (Ms), biotite (Bt), chlorite (Chl) and quartz (Qtz) in zonal garnet (MO-1A); D – inclusions of spinels (Cr-spl) and pyrhotite (Po) in hornblende (MO-1A); E – alteration process of chrome-spinel (MO-1C); F – breakdown of Ti-rich magnetite to pure magnetite (Mag) and rutile (Rt), (MO-1C); G, H – internal texture of zircon (CL; MO-1A).

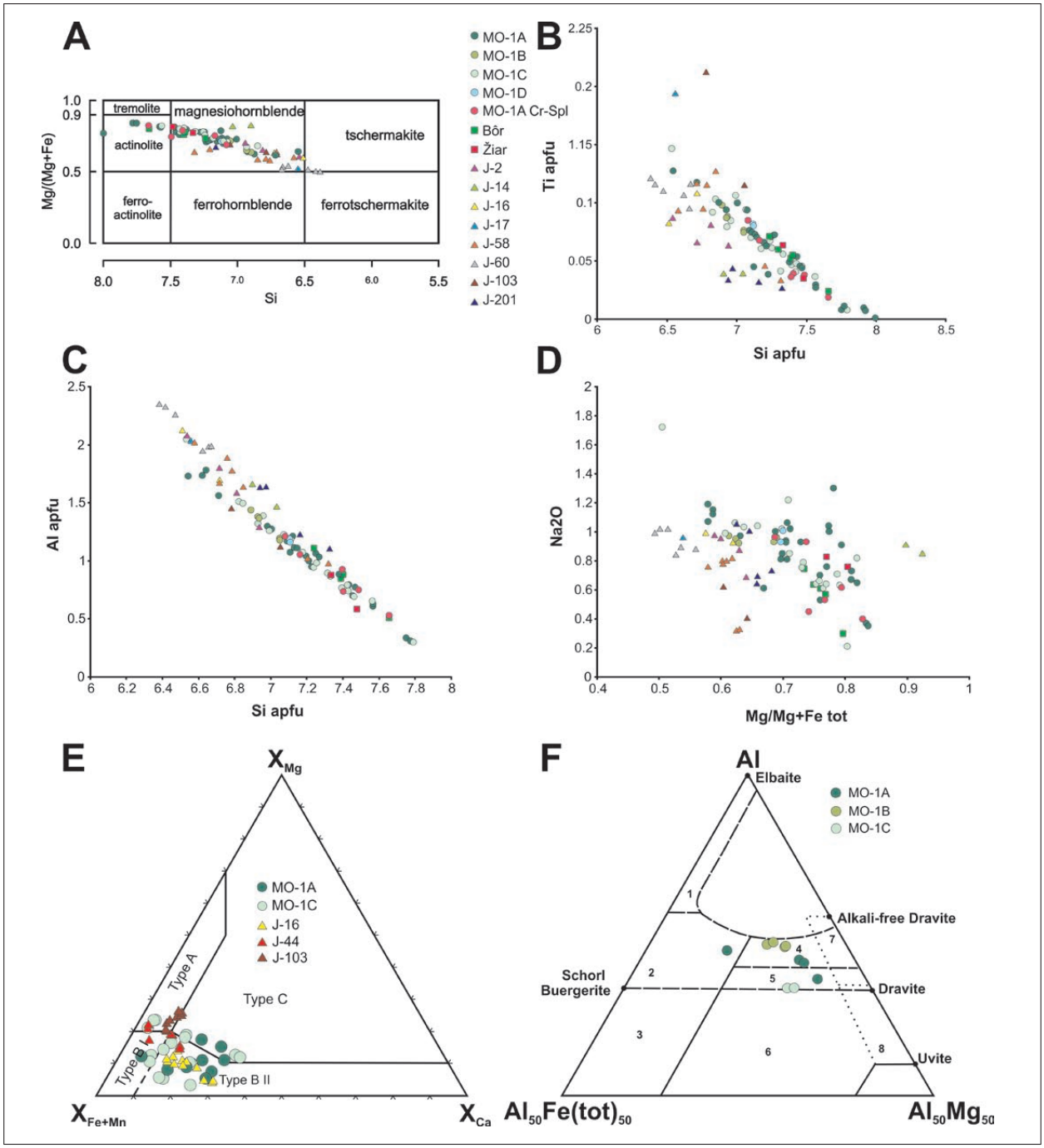

Fig. 6: A – Classification scheme of amphiboles (Leake et al. 1997) from the cave sediments (MO-1A to MO-1D), from diorites (Bôr locality – analyses from this work; Žiar Mts. – analyses from Uher & Miko 1994) and from the different types of amphibolites and amphibolic gneisses (J-2 to J-203); B – Diagram Ti vs. Si (a.p.f.u.) for amphiboles; C – Diagram Al vs. Si (a.p.f.u.) for amphiboles; D – Diagram Na_2O (wt. %) vs. Mg/Mg+Fe (a.p.f.u.) for amphiboles. Locations of the J-2 to J-203 samples are publicated in Pitoňák and Spišiak (1989). E – Composition of detritic garnets in Fe + Mn-Mg-Ca ternary diagram after Morton et al. (2004) from cave sediments (MO-1A, MO-1C) and garnets from amphibolites and amphibolic gneisses (J-16, J-44 and J-103): type A – Grt from granulites; type BI – Grt from intermediate to acid igneous rocks; type B II – Grt from metasediments of amphibolite facies; type C – Grt from metabasites. F – Diagram Al-Fe-Mg for tourmalines (Henry & Guidotti 1985). Explanations: (1) Li-rich granites; (2) Li-poor granites and aplites; (3, 6) Fe^{3+}-rich quartz-tourmaline rocks; (4) metapelites and metapsamites co-existed with Al-rich phases; (5) metapelites and metapsamites not co-existed with Al-rich phases; (7) low-Ca metaultramafites, Cr- and V- rich metasediments; (8) metacarbonates and metapyroxenites.

is shifted into the actinolite with simultaneously increase of Si and decrease of Al. Apatite, chlorite, micrometer-scale wormy Cr-spinel and pyrhotite (Fig. 5D) represent the inclusions. Decreasing content of Al^{IV} and alkalies toward to periphery of the grains indicates the temperature drooping. $Na^{M(4)}$ content in Mg-hornblende reaches a maximum value of 0.02 *a.p.f.u.* indicating a low-pressure environment. These grains are characterized by slightly elevated content of Ti and Al (Fig. 6B, C) and compared to hornblende from igneous rocks also slightly increased content of Na (Fig. 6D). In addition to Mg-hornblende the presence of anthophylite has been observed (MO-1A sample), which is distinctive of the amphibolites and gneisses. Gradual change of edenite (MO-1A and MO-1C samples) to Mg-hornblende from the cores to the rims is accompanied by a decrease of Al content and $(Na+K)_A$ ratio. Edenite is typical of medium-grade metamorphites and/or intermediate plutonic rocks.

Garnet. Detrital grains show variable chemical composition. Grossularite-almandine (Prp_{5-9} $Sps_{6-13}Grs_{14-23}Alm_{64-74}$) indicates the metamorphism in low amphibolite facies conditions. Pyrope-grossularite-almandine garnets with a minimum spessartine component ($Sps_{0-2}Prp_{11-12}Grs_{29-33}Alm_{53-60}$) could originate from the amphibolites. Pyrope-almandine garnets ($Grs_2Adr_2Sps_7Prp_{23}Alm_{66}$) with low Ca component are probably derived from acidic gneisses eventually metagranites. Because of low spessartine in these grains, granites as the source rocks are excluded. Almandine-spessartine garnet ($Adr_3Grs_6Prp_{12}Alm_{38}Sps_{41}$) captured in the MO-1C sample can be considered the granite or granitic pegmatite. Zonal garnets represent a separate group. They are characterised by low grossularite and higher pyrope and almandine components in the central zone ($Sps_6Grs_6Prp_{12}Alm_{77}$). Marginal zone has apparently lower content of pyrope and almandine at the expense of significantly increasing grossularite one ($Sps_3Prp_7Grs_{27}Alm_{63}$). Inclusions of white mica, biotite, chlorite and quartz located mainly in the centre of grains are characteristic. S-shaped trails of quartz and biotite are typical of the rims (Fig. 5C). However, these "inclusions" were probably connected with matrix in parental rock by fractures and these were related to fluid influx during the metamorphic event. The sharp change in the composition of the garnet i.e. increase of grossularite contents (from 6 % in the centre of the grain to 27 % in the margin), as well as in the considerable decrease of Mg content and increase of the Fe/(Fe + Mg) value are significant for retrograde zoned garnets occurring in mica schists and/or gneisses (Korikovsky *et al.* 1988; Méres & Hovorka 1991). We ascribe the metamorphic genesis (probably lower amphibolite facies) for spessartine-almandine garnet (Prp_8Grs_{15} $Sps_{20}Alm_{57}$) in which grossularite component dominates in the peripheral zone ($Prp_5Sps_{18}Grs_{27}Alm_{50}$). REE-epidote and quartz inclusions are restricted to the grain's core, titanite is restricted to its rim. Figure 6E illustrates the chemical composition of the investigated garnets from the cave sediments and the comparative analysis of garnets from amphibolic rocks of the Ďumbier crystalline basement.

Tourmaline. Tourmalines belong to the alkali ones with low to moderate Ca content. They are rather scarce minerals and correspond to a schorl-dravite, rarely dravite. According to the classification indicating the tourmaline origin (Henry & Guidotti 1985), they were derived from metapelites and metapsamites saturated or unsaturated by Al, respectively (Fig. 6F). Zonal character of tourmaline is demonstrated by the decreasing of $\#^{Y}Fe$ ratio and simultaneously increasing of Ca amount towards the marginal zones (Tab. 2). It indicates the progressive metamorphism. There are also reverse zonal grains which may involve a different source rocks or they may represent the grains without the outer rims due to transport. We recorded the inherited core of the schorl composition (MO-1A sample) indicating an origin in Li-poor granitoids (l. c.). Its outer rim originated from the metasedimentary environment. Summarizing, each of tourmalines is most likely of metasedimentary origin.

Spinel group and Fe-Ti oxides. Cr-spinel forms a grain (MO-1C sample) corresponds to alumochromite (Stevens 1944) or chromite (Deer *et al.* 1992) with Cr# = (0.72–0.71), Fe# = (0.52–0.61) and Mg# = (0.48–0.39) from the centre to the rim, respectively. BSE

Tab. 1: Heavy mineral assemblage of cave sediments from the Mošnica Cave. Abbreviations of minerals sensu Kretz (1983).

sample	*Grt*	*Zrn*	*Ap*	*Mnz*	*Tur*	*Sta*	*Amp*	*Rt*	*Ttn*	*Ep*	*Spl*	*Bt+Chl*	*Sill*	*Aln*	*And*	*Op*	*Brt*	*Others*
MO-1A	1.5	15.9	26.0	2.1	0.9	–	24.2	0.3	0.3	10.3	0.3	4.2	–	–	1.8	9.1	2.4	0.9
MO-1B	–	2.3	12.5	–	0.6	0.6	28.6	1.7	–	12.2	–	–	1.5	0.3	–	36.7	0.9	2.0
MO-1C	1.5	42.3	9.6	0.9	0.6	–	8.2	0.6	–	4.4	0.3	–	–	–	–	30.6	–	1.1
MO-1D	2.5	1.3	24.8	–	–	–	23.2	–	–	13.2	–	0.9	–	0.9	–	26.7	3.4	3.1

image illustrates the alteration products of chrome-spinel (Fig. 5E). Dark areas reflect the Mg-rich and Fe-poor composition of the core relative to the light coloured altered rim due to replacement Mg^{2+} by Fe^{2+}. Mn and Zn show no variation from core to rim. High content of TiO_2 (2.74 wt. %) combined with a low proportion of Fe^{2+}/Fe^{3+} = 2.1 indicates its volcanic origin (Lenaz *et al.* 2000). Cr-spinels enclosed in Mg-hornblende exhibit the different character. According to Stevens' (1944) classification these spinels are concerned as ferritchromite with a low Al_2O_3 content (3.57–4.70 wt. %). It may indicate the subsolidus co-precipitation spinel and amphibole, rather than the formation of spinel by exolution from Al-rich amphibole. Within amphibole's profile the Cr_2O_3 content remains unchanged or changes from grain's core to rim, respectively.

Beyond, ferritchromite is usually attributed to the effects of low to medium grade metamorphism up to lower amphibolite facies (Farahat 2008; Xuan Thanh *et al.* 2011). Mn and Zn show high content and introduced into spinel during alteration and metamorphism. Based on very low Mg# = (0.005–0.1) concomitant with high Cr# = (0.83–0.88) ferritchromite is considered to be a metamorphic origin. The altered Cr-spinel data normally have total major elements less than 99 wt. % that is due to containing more or less water component (l. c., Tab. 2).

Several types of Fe-Ti oxides can be observed in the samples: firstly, pure magnetite ($Mag_{99.9}Usp_{0.1}$), which is in the concentrate of heavy minerals the most frequent, further titanomagnetite or magnetite-ulvöspinel s. s. ($Mag_{58}Usp_{42}$) gradually passing into the pure magnetite ($Mag_{97}Usp_3$) in grain's periphery. The break-down of Ti-magnetite is accompanied by the formation of rutile (Fig. 5F). Such a process of disintegration of Fe-Ti oxides has been described in the I-type granitoids from the Nízke Tatry Mts. (Broska & Petrík 2011).

Allanite. Chemical composition of the allanite (MO-1B sample) indicates its magmatic origin which is documented by Al_2O_3 content ranging from 13.47 to 14.22 wt. %. Allanites from primary granitic I-type magmas show around 15 wt. % of Al_2O_3 (Petrík *et al.* 1995).

Zircon. Zircons are characterized by a fine oscillatory zoning often without the signs of resorption. Their regular euhedral habitus indicates a primary magmatic (granitoid) source (Fig. 5G). Some zircons crystallized from the nucleus. The inherited cores in zircons are observed (Fig. 5H). The grains showing the possible metaclastic origin (convolution zoning is indicative of the recrystallization processes) are rather rare in the investigative set of zircons.

DISCUSSION

HEAVY MINERALS AND THEIR POSSIBLE ORIGIN

Shapes of the heavy minerals as well as the minimum proportion of the resistant ones (zircon, tourmaline, rutile) indicate their deposition from the igneous and metamorphic crystalline rocks of the Nízke Tatry Mts. We attribute the igneous origin to the mineral association: zircon, apatite (clear euhedral to subhedral grains), titanite, allanite, ilmenite (containing 47 to 48 wt. % of TiO_2) ± epidote. That mineral association is specific to the I-type granitoids (Broska & Uher 2001). The main rock types are Ďumbier and Prašivá granitoids that form the larger part of the Nízke Tatry pluton (Koutek 1931) and represent typical I-type granitoid suite (Broska & Petrík 1993).

A main source of the tourmaline group of minerals, staurolite, rutile, chlorite, epidote, monazite with an oval to semi-oval habitus, garnet and anhedral apatite are derived mainly from metasediments. Mentioned mineral association may have issued from siliciclastics of the Lúžna Formation and/or from the metamorphites of the Ďumbier crystalline complex.

The heavy mineral association in psammite component of the Lúžna Formation consists of zircon, tourmaline, rutile, apatite, pyrite and leucoxene (Fejdiová 1977a, b). Tourmaline is substantial in the siliciclastics of the Lúžna Formation (Aubrecht 1994; Mišík & Jablonský 2000). Tourmalines of metasedimentary origin (predominantly formed in a low grade clastic metasedimentary rocks) are considered to be exotic, their source is unknown (Aubrecht l. c.). Sporadic occurrence of garnet in the Lúžna sediments is described by Fejdiová (1989) and Aubrecht (1994).

We assume that the amphibole suite comprising the actinolite, Mg-hornblende and anthophyllite in association with epidote, pyrite, Cr-spinel (± ilmenite) and garnet (almandine-grossularite) may originate in metabasites – amphibolites or amphibolitic gneisses, which are an integral part of the Nízke Tatry crystalline complex. Common Ca-amphiboles (Mg-hornblende), actinolite

Tab. 2: Representative microprobe analyses of amphibole, tourmaline, garnet, spinel and Fe-Ti oxides (in wt. %).

mineral	***Amp***										
sample	***MO-1A***								***MO-1C***	***Bôr***	
	1 c	***1 r***	***2 c***	***2 r***	***3 c***	***3 c/r***	***3 r***	***4 c***	***1 c***	***1 c***	***1 r***
SiO_2	49.72	49.22	51.04	50.50	52.91	51.81	53.53	56.47	43.30	50.32	54.11
TiO_2	0.57	0.64	0.67	0.65	0.41	0.45	0.27	0.07	1.29	0.64	0.22
Al_2O_3	5.85	6.45	6.13	6.26	4.61	5.26	3.74	0.97	11.51	6.53	3.04
Fe_2O_3	0.77	1.08	0.00	0.00	0.00	0.00	0.00	0.00	0.00	0.00	0.23
Cr_2O_3	0.13	0.11	0.14	0.07	0.12	0.16	0.12	0.02	0.01	0.12	0.01
MgO	15.48	15.14	17.48	17.36	18.91	18.27	19.12	23.54	9.79	15.82	18.36
CaO	12.35	12.42	11.60	11.58	11.58	11.39	11.90	1.41	11.53	12.22	12.64
MnO	0.33	0.26	0.20	0.25	0.25	0.27	0.21	0.50	0.28	0.32	0.26
FeO	10.83	10.70	9.09	8.98	7.86	8.42	7.50	14.31	17.06	10.26	8.13
NiO	0.02	0.00	0.00	0.02	0.02	0.01	0.05	0.01	0.03	0.00	0.03
Na_2O	0.93	0.81	1.04	1.00	0.73	0.91	0.65	0.12	1.72	0.75	0.30
K_2O	0.48	0.53	0.14	0.11	0.08	0.09	0.05	0.00	0.54	0.46	0.13
Cl	0.03	0.01	0.01	0.03	0.00	0.00	0.02	0.00	0.01	0.03	0.01
F	0.03	0.01	0.01	0.03	0.00	0.00	0.02	0.00	0.01	0.00	0.00
H_2O	2.06	2.06	2.10	2.08	2.12	2.10	2.11	2.14	1.98	2.07	2.11
Σ	99.57	99.43	99.65	98.92	99.60	99.14	99.29	99.56	99.06	99.55	99.58
ek. F, Cl	0.01	0.00	0.00	0.01	0.00	0.00	0.00	0.00	0.00	0.01	0.00
Σ (F,Cl)	99.56	99.43	99.65	98.91	99.60	99.14	99.29	99.56	99.06	99.54	99.58
Si	7.213	7.149	7.271	7.251	7.471	7.381	7.571	7.924	6.535	7.241	7.657
Al^{IV}	0.787	0.851	0.729	0.749	0.529	0.619	0.429	0.076	1.465	0.759	0.343
Σ T	8.000	8.000	8.000	8.000	8.000	8.000	8.000	8.000	8.000	8.000	8.000
Al^{VI}	0.213	0.254	0.301	0.310	0.238	0.265	0.194	0.085	0.583	0.348	0.165
Fe^{3+}	0.084	0.118	0.000	0.000	0.000	0.000	0.000	0.000	0.000	0.000	0.024
Ti	0.062	0.070	0.072	0.070	0.044	0.048	0.029	0.007	0.146	0.070	0.024
Cr	0.015	0.013	0.016	0.008	0.013	0.018	0.013	0.002	0.001	0.013	0.001
Fe^{2+}	1.278	1.268	0.900	0.896	0.725	0.790	0.733	0.000	2.067	1.175	0.914
Mg	3.347	3.278	3.712	3.715	3.980	3.880	4.031	4.905	2.202	3.394	3.872
Σ C	5.000	5.000	5.000	5.000	5.000	5.000	5.000	5.000	5.000	5.000	5.000
Fe^{2+}	0.038	0.035	0.183	0.182	0.204	0.214	0.154	1.699	0.086	0.059	0.049
Mn	0.041	0.032	0.024	0.030	0.030	0.033	0.025	0.059	0.036	0.038	0.031
Ca	1.920	1.933	1.771	1.781	1.752	1.739	1.803	0.211	1.865	1.884	1.917
Na	0.000	0.000	0.022	0.004	0.012	0.014	0.012	0.029	0.010	0.018	0.000
Ni	0.002	0.000	0.000	0.002	0.002	0.001	0.006	0.002	0.004	0.000	0.003
Σ B	2.000	2.000	2.000	2.000	2.000	2.000	2.000	2.000	2.000	2.000	2.000
Na	0.262	0.228	0.265	0.274	0.188	0.237	0.167	0.003	0.494	0.192	0.082
K	0.089	0.098	0.025	0.020	0.014	0.016	0.009	0.001	0.104	0.085	0.023
Σ A	0.350	0.326	0.291	0.295	0.202	0.254	0.176	0.003	0.598	0.277	0.106

Tab. 2. Continued

mineral	***Tur***					***Grt***					
sample	***MO-1A***		***MO-1C***			***MO-1A***		***MO-1C***			
	1c	***1r***	***1c***	***1r***		***1c***	***1r***	***1c***	***1r***	***2c***	***3c***
SiO_2	36.19	36.61	36.70	36.50		37.22	37.84	38.00	38.20	36.93	37.69
TiO_2	0.41	0.88	0.67	0.72		0.00	0.08	0.04	0.04	0.00	0.00
Al_2O_3	32.85	31.56	30.54	30.77		21.25	21.37	21.71	21.85	21.03	21.65
Fe_2O_3						0.00	0.00	1.00	0.50	1.05	0.82
Cr_2O_3	0.00	0.00	0.01	0.00		0.03	0.00	0.01	0.00	0.01	0.00
MgO	3.93	9.22	7.88	8.29		2.91	1.73	3.01	3.14	3.03	5.87
CaO	0.36	1.64	0.58	0.67		2.00	9.44	11.88	11.28	3.01	1.42
MnO	0.02	0.02	0.00	0.02		2.42	1.24	1.08	0.92	17.92	2.87
FeO	10.45	4.34	7.27	6.75		33.83	28.06	23.80	24.55	16.52	29.71
NiO	0.00	0.00	0.00	0.00		0.00	0.00	0.00	0.00	0.00	0.03
Na_2O	1.69	1.85	2.55	2.37		0.03	0.05	0.00	0.04	0.05	0.03
Cl	0.01	0.02	0.00	0.00							
K_2O	0.01	0.02	0.00	0.00		0.00	0.00	0.00	0.00	0.00	0.00
H_2O											
Σ	85.93	86.16	86.20	86.09		99.69	99.81	100.53	100.52	99.56	100.09
ek. F, Cl	0.00	0.00	0.00	0.00							
Σ (F,Cl)	85.93	86.16	86.20	86.09							
Si	6.002	5.928	6.022	5.982	Si	3.000	3.010	2.976	2.985	2.982	2.978
Al_T	0.000	0.072	0.000	0.018	Ti	0.000	0.005	0.002	0.002	0.000	0.000
Σ T	6.002	6.000	6.022	6.000	Al	2.019	2.004	2.004	2.012	2.001	2.016
Al_Z	6.000	5.951	5.904	5.923	Fe^{3+}	0.000	0.000	0.059	0.029	0.064	0.049
Fe_Z	0.000	0.049	0.096	0.077	Cr	0.002	0.000	0.001	0.000	0.001	0.000
Σ Z	6.000	6.000	6.000	6.000	Mg	0.350	0.205	0.351	0.366	0.365	0.691
Al_Y	0.420	0.000	0.000	0.000	Ca	0.173	0.804	0.997	0.944	0.260	0.120
Ti	0.052	0.107	0.083	0.089	Mn	0.165	0.083	0.072	0.061	1.225	0.192
Fe_Y	1.450	0.539	0.902	0.848	Fe^{2+}	2.280	1.867	1.558	1.604	1.116	1.963
Mn	0.003	0.003	0.000	0.003	Ni	0.000	0.000	0.000	0.000	0.000	0.002
Mg	0.972	2.225	1.928	2.025	Na	0.004	0.007	0.000	0.006	0.008	0.005
Ni	0.000	0.000	0.000	0.000	K	0.000	0.000	0.000	0.000	0.000	0.000
Cr	0.000	0.000	0.001	0.000	*Σ*	7.992	7.987	8.020	8.010	8.021	8.016
Σ Y	2.896	2.873	2.913	2.965							
Y vak.	0.104	0.127	0.087	0.035	*Prp*	11.80	6.93	11.80	12.29	12.29	23.30
					Alm	76.81	63.08	52.33	53.92	37.61	66.17
Ca	0.065	0.285	0.102	0.118	*Uv*	0.09	0.00	0.03	0.00	0.03	0.00
Na	0.543	0.581	0.811	0.753	*Grs*	5.73	27.17	30.54	30.29	5.62	1.66
K	0.003	0.005	0.000	0.000	*Sps*	5.57	2.82	2.41	2.05	41.32	6.47
Σ X	0.611	0.871	0.913	0.871	*Adr*	0.00	0.00	2.90	1.46	3.13	2.39
X vak.	0.389	0.129	0.087	0.129							
F	0.000	0.000	0.000	0.000							
Cl	0.002	0.005	0.000	0.000							

Tab. 2. Continued

mineral	***Cr-spl***				***Mag***		
sample	***MO-1A***	***MO-1C***			***MO-1A***	***MO-1C***	
	in Hbl	***1 c***	***1r***		***1c***	***1 c***	***1r***
SiO_2	0.09	0.07	0.03		0.01	0.03	0.12
TiO_2	0.72	2.74	2.65		0.04	13.94	0.87
Al_2O_3	3.57	11.84	11.86		0.10	0.01	0.07
Fe_2O_3	23.04	9.37	9.87		67.50	38.17	62.30
FeO	27.54	17.72	20.50		31.06	42.36	30.04
MnO	1.81	0.33	0.33		0.04	0.12	0.00
MgO	0.07	9.31	7.48		0.00	0.00	0.00
CaO	0.29	0.00	0.00		0.01	0.02	0.03
Cr_2O_3	37.34	44.99	43.53		0.03	0.00	0.01
K_2O	0.00	0.00	0.00		0.00	0.00	0.00
Na_2O	0.00	0.00	0.00		0.00	0.00	0.00
NiO	0.00	0.17	0.18		0.00	0.00	0.00
ZnO	0.90	0.07	0.08		0.00	0.00	0.00
$V2O_5$	0.24	0.22	0.20		0.20	0.06	0.05
Σ	95.61	96.83	96.71		98.98	94.72	93.48
Si	0.003	0.002	0.001		0.000	0.001	0.005
Ti	0.021	0.070	0.069		0.001	0.420	0.027
Al	0.163	0.476	0.483		0.005	0.000	0.003
Fe^{3+}	0.671	0.240	0.257		1.976	1.152	1.929
Fe^{2+}	0.892	0.505	0.593		1.010	1.420	1.033
Mn	0.059	0.010	0.010		0.001	0.004	0.000
Mg	0.004	0.473	0.386		0.000	0.000	0.000
Ca	0.012	0.000	0.000		0.000	0.001	0.001
K	0.000	0.000	0.000		0.000	0.000	0.000
Na	0.000	0.000	0.000		0.000	0.000	0.000
Cr	1.143	1.212	1.190		0.001	0.000	0.000
Ni	0.000	0.005	0.005				
Zn	0.026	0.002	0.002				
V	0.006	0.005	0.005		0.005	0.002	0.001
Σ	3.000	3.000	3.000		3.000	3.000	3.000
Mg#	0.005	0.48	0.39	*Xusp*	0.00	0.42	0.03
Cr#	0.88	0.72	0.71	*Xmag*	1.00	0.58	0.97

Note: *c – core, r – rim (periphery) of the grain. In magnetite FeO_{tot} is distributed between FeO and Fe_2O_3 sensu Dropp (1987).*

hornblende and actinolite were identified in metabasic rocks of the other Tatric core mountains (e. g. Malé Karpaty Mts., Tribeč Mts.; Hovorka & Kováčik 2007). Amphiboles from amphibolitic gneisses and amphibolites of the Ďumbier crystalline complex correspond to Mg-hornblende, or they lie close to Fe-hornblende field (Spišiak & Pitoňák 1990; Fig. 6A). Despite of chrome-spinel inclusions in Mg-hornblende, which could indicate the origin within the altered metaultramafites occur in the Ďumbier crystalline complex (Spišiak & Pitoňák 1990; Biely *et al.* 1992), we do not suppose this provenance because of these rocks have contained only

tremolite (Spišiak *et al.* 1988). Similarly, primitive Mesozoic basalts cutting through the crystalline basement (Hovorka *et al.* 1982; Hovorka & Spišiak 1988; Spišiak *et al.* 1991) could have represented a potential source of Mg-hornblende with Cr-spinel inclusions. However, amphiboles from these rocks are zonal and correspond to kaersutite or low-silicum kaersutite (l. c.). Actinolite and Mg-hornblende occur in lenses of eclogite from the Ďumbier crystalline complex which is overprinted in the granulite facies (Janák *et al.* 2009). Their textural features (symplectites with clinopyroxene and plagioclase, l. c.) do not suppose the amphibole genesis in eclogites. However, this possibility cannot be quite excluded.

Cr-spinel inclusions in amphibole (MO-1A, MO-1C samples) indicate the initial basic protolith of amphibole (basic volcanic or volcano-clastic rock). Ferritchromite inclusions in hornblende can be explained by protolith of amphibolitic rocks. It can be considered a mixture of basic volcanic (to 75 %) and terrigenous sedimentary (up to 25 %) materials (Pitoňák & Spišiak 1988).

On the other hand, the source rock of hornblende could be the quartz diorite to diorite currently existing in the form of the enclaves in Prašivá type granitoids between Bôr (1887.6 m a.s.l.) and Jaloviarka (1428.6 m a.s.l.) (Fig. 2). The chemical composition of amphibole from diorite corresponds to Mg-hornblende with Mg# = (0.73 to 0.78) and Al_{tot} = (0.844 to 1.107 *a.p.f.u.*). Actinolite, Mg-hornblende, tschermakitic hornblende and edenite are known from the identical rocks distributed in the other core mountains (Tatricum; Cambel *et al.* 1981; Uher & Miko 1994; Ivanička *et al.* 1998; Fig. 6A). Diorites from the Ďumbier crystalline complex contain an accessory pyroxene (Biely & Bezák *et al.* 1997). However, pyroxene was neither observed in the heavy mineral assemblage obtained from the cave sediments nor recorded in the recent alluvium sediments of the Mošnica Stream (Bačo *et al.* 2004). Despite this, part of the Mg-hornblende can be attributed to diorite provenance, mainly hornblende having a lower content of Ti, Al_{tot} and perhaps even Na_2O (Fig. 6B-D).

Heterogenous composition and different types of garnet zonality were found in the various metamorphic rocks from the Ďumbier crystalline complex (Spišiak & Pitoňák 1990). The garnets with higher spessartine content have been recorded in the Nízke Tatry crystalline basement. The garnets from granitoid rocks correspond to almandine with significant spessartine (up to 24 mol. % Sps; Petrík & Konečný 2009). The highest MnO recorded from pegmatitic granites (up to 17 wt. %) in the Prašivá massif (Broska *et al.* 2012). These rocks consider to the parental rocks of spessartine garnet found in MO-1C sample.

It follows that the accumulating area of palaeoflow (palaeoflows), which brought the material to the Mošnica Cave was formed mainly by the crystalline rocks – granitoids, gneisses and amphibolites. The specific proportion of the allochthonous material probably originates in the siliciclastics of the Lúžna Formation distributed on the crystalline basement. In crystalline rocks there were described the hydrothermal barite veins (Zuberec *et al.* 2005), whose presence we registered in the investigated samples (Tab. 1), too.

IMPLICATIONS FOR THE PRE-QUATERNARY EVOLUTION OF THE CAVE AND SURROUNDING AREA

Generally, we can conclude that the main source area of allochthonous material of the Mošnica Cave was from the south non-carbonate part of the Mošnica Valley, probably also the metamorphic rocks despite the current position of the metamorphic crystalline complex behind the main ridge of the Nízke Tatry Mts. (cf. Biely *et al.* 1992). The contact of metamorphic rocks and granitoids is indeed tectonic (Biely & Bezák *et al.* 1997; Bezák & Biely 1998).

A fluvial transport of allochthonous material into the cave is probably linked with a past larger catchment area of the allogenic karst of Mošnica Valley on the pre-Quaternary less dissected terrain.

Bella (1988, 2001) supposed the formation of the Mošnica Cave during the Late Pliocene (synchronously with the formation of surrounding planation surface which remnants are currently at about 1000 m a.s.l.). Orvoš and Orvošová (1996) assumed that the Mošnica Cave was formed between 3.2–2.588 Ma. Paleomagnetic record proved the deposition of the cave sediments took place during the Pliocene period (Kadlec *et al.* 2004). In the Western Carpathians the Late Pliocene is considered as a period of tectonic stability with the formation of the river level (Mazúr 1963; Lukniš 1964 and others).

The transport of the clastic material from metamorphic rocks (enriched in amphibole), recently exposed behind the ridge of the mountain range on the southern slopes of the Nízke Tatry Mts., performed probably during the pre-Pliocene period. In this time the metamorphic complex occurred in the northern slopes. A change of watershed boundary leaded through the central range of the Nízke Tatry Mts. can be explained by the tilting of the core mountain around the horizontal or subhorizontal axis (Grecula & Roth 1978) towards the north, in the compression regime during the Late Tertiary (Kováč 2000; Plašienka 2003). The uplift of the Nízke Tatry crystalline basement was induced by transpressional tectonic regime in the Lower Miocene (Kováč *et al.* 1994; Kováč 2000 and others). The relatively rapid uplift of mountain

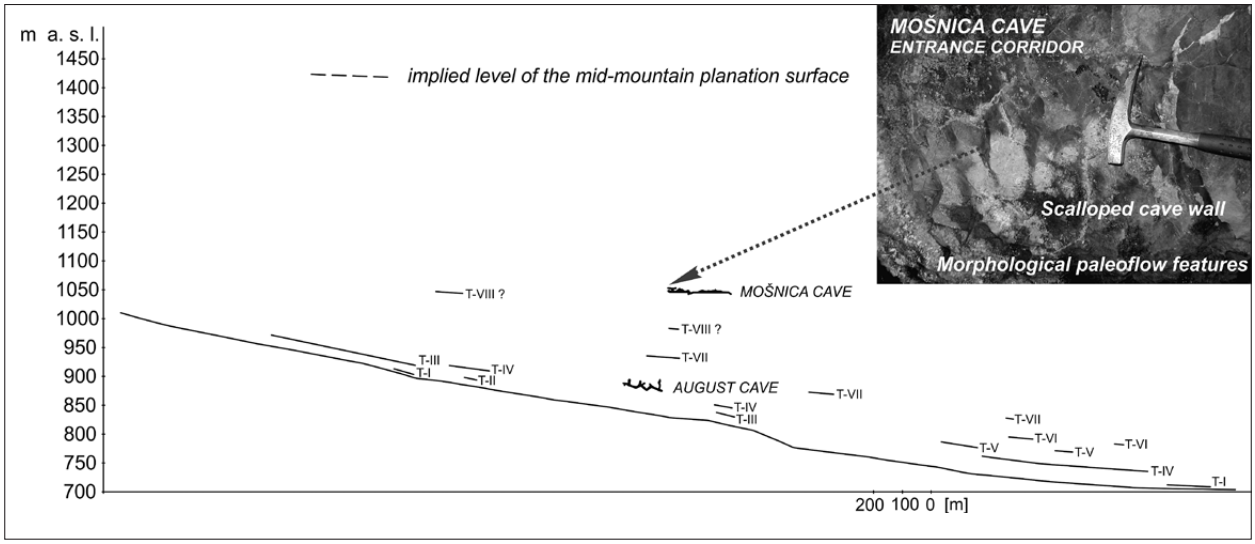

Fig. 7: Longitudinal sections of relief evolution levels in the middle and northern parts of the Mošnica Valley (Bella 1988) including horizontal and subhorizontal caves, and remnants of Pleistocene river terraces T-I to T-VIII.

range occurred over the last stages of its development (Halmešová *et al.* 1992).

The remnant of scalloped rock wall in the Entrance Corridor is a morphological indicator of water flow into the continuing cave parts from the lower entrance (Bella & Urata 2002). This is an evidence of fluvial transport of the allochthonous material into the cave. In accordance with the considerations of Bella (1988) as well as Bella and Urata (l. c.) the underground spaces of the Mošnica Cave was primary originated by water flow with the involvement of the Mošnica palaeoflow. The treatment of the heavy mineral grains and their mineralogical character indicate a close source. The oldest allogenic river network in the Nízke Tatry Mts. elevation confirms the occurrence of the allochthonous sediments in the Ohnište paleokarst (Orvošová *et al.* 2006).

Based on the age of allochthonous sediments older than 2,588 Ma (Bosák *et al.* 2004; Kadlec *et al.* 2004) and their relation with remnants of planation surfaces and river terraces in the valley (Fig. 7) as well as the position of main horizontal cave corridors (at 1,055–1,060 m a.s.l.) in a relative height of 220 m above the recent river bed in the Mošnica Valley, the Mošnica Cave was originated during the pre-Quaternary period, probably in the Pliocene. On the northern part of the Nízke Tatry Mts. remnants the mid-mountain planation surface (Sarmatian–Early Pannonian) are at 1,400–1,450 m a.s.l., the submountain pediment (Pontian?) at 1,225–1,250 m a.s.l. and the river pediment (Late Pliocene) mostly at 1,000–1,050 m a.s.l. (Bella 2002). The relief of the area during a phreatic and epiphreatic development of the cave by allogenic waters was lesser dissected than in the recent.

Droppa (1950) assumed an aeolian transport of allochthonous material on the surface above the Mošnica Cave mainly from Bôr (1887.6 m a.s.l.) and its subsequent washing into the cave by seeping meteoric waters. Based on follow up investigations we tend towards its fluvial transport into the cave by flood waters from a surfaced allogenic paleostream that were slow-moving and ponded mostly in the Loamy Corridor. On the territory of the northern part of Paratethys the warm-temperate humid climate during the Pliocene was not favourable for aeolian processes and appertaining landform sculpturing.

CONCLUSIONS

1. Translucent heavy mineral assemblages reflect no provenance changes.

2. The main source area of the Mošnica Cave was I-type granitoids and probably also the metamorphic rocks despite the current position of the metamorphosed crystalline complex behind the main ridge of the Nízke Tatry Mts.

3. The remnant of scalloped rock wall in the Entrance Corridor (Bella & Urata 2002) and sedimentary features of studied allochthonous sediments indicate

their fluvial transport into the Mošnica Cave. Paleomagnetism research of the sediments (Kadlec *et al.* 2004) and the relative high of the cave above the recent flood plain indicate that the cave originated during the pre-Quaternary period (Pliocene) when a surface morphology (river network) was lesser dissected than the recent relief.

4. The transport of the clastic material from metamorphic rocks performed probably during the pre-Pliocene period, seeing that during Pliocene a tectonic stability in the Nízke Tatry Mts. is considered. In the pre-Pliocene period, the metamorphic complex occurred in the northern slopes.

Acknowledgements. This work was supported by the Slovak Research and Development Agency under contract APVV-0625-11 and APVV-0081-10. Digital graphics of the figure 1A was processed by M. Gallay. We are grateful to Pavel Bosák and anonymous reviewer for constructive comments on this paper.

REFERENCES

Aubrecht, R., 1994: Heavy mineral analyses from "Tatric" units of the Malé Karpaty Mountains (Slovakia) and their consequences for Mesozoic Paleogeography and tectonics.- Mitt. Österr. Geogr. G., 86, 121–132.

Bačo, P., Bačová, N., Bakoš, F., Fodorová, V., Derco, J., Dzurenda, Š., Hricová, M., Hvožďara, P., Kovaničová, Ľ., Križáni, I., Lučiviansky, P., Ondíková, H., Repčiak, M. & J. Smolka, 2004: *Reinterpretation of heavy-mineral concentrates exploration in Slovakia* (in Slovak). MŽP SR, ŠGÚDŠ, pp. 119, Bratislava.

Bella, P., 1988: Speleological research of the Mošnica Valley karst (in Slovak).- Slovenský kras, 26, 87–112.

Bella, P., 2001: To the paleogemorphic development of fluviokarst caves in the Demänová Hills (in Slovak).- Geomorphologia Slovaca, 1, 54–63.

Bella, P., 2002: To the reconstruction of planation surfaces in the Demänová Hills on the northern side of the Nízke Tatry Mts. (in Slovak).- Geographia Slovaca, 18, 13–20.

Bella, P., Hercman, H., Gradziński, M., Pruner, P., Kadlec, J., Bosák, P., Głazek, J., Gąsiorowski, M. & T. Nowicki, 2011: Geochronology of cave levels in the Demänová Valley, Nízke Tatry Mts. (in Slovak).- Aragonit, 16, 64–68.

Bella, P. & K. Urata, 2002: On the paleohydrografical development of the Mošnica Cave (in Slovak).- Slovenský kras, 40, 19–29.

Bezák, V. & A. Klinec, 1983: The new interpretation of tectonic development of the Nízke Tatry Mts. – West part.- Geologický Zborník Geologica Carpathica, 31, 569–575.

Bezák, V. & A. Biely, 1998: Geological-tectonic setting of the Ďumbier part of the Nízke Tatry Mts., parallelism with the study by D. Andrusov *et al.* (1951).- Mineralia Slovaca, 30, 1, 81–82.

Bezák, V., Polák, M., Konečný, V. (eds.), Biely, A. Elečko, M., Filo, I., Hók, J., Hraško, Ľ., Kohút. M., Lexa, J., Madarás, J., Maglay, J., Mello, J., Olšavský, M., Pristaš, J., Siman, P., Šimon, L., Vass, D. & J. Vozár, 2008: *General geological map of Slovak Republic at a scale 1:200,000; Map sheet 36 – Banská Bystrica*.- MŽP SR, ŠGÚDŠ, Bratislava.

Biely, A. (ed.), Beňuška, P., Bezák, V., Bujnovský, A., Halouzka, R., Ivanička, J., Kohút, M., Klinec, A., Lukáčik, E., Maglay, J., Miko, O., Pulec, M., Putiš, M. & J. Vozár, 1992: *Geological map of the Nízke Tatry Mts. at a scale 1: 50 000.*- SGÚ – GÚDŠ, Bratislava.

Biely, A., Bezák, V. (eds.), Bujnovský, A., Vozárová, A., Klinec, A., Miko, O., Halouzka, R., Vozár, J., Beňuška, P., Hanzel, V., Kubeš, P., Liščák, P., Lukáčik, E., Maglay, J., Molák, B., Pulec, M., Putiš, M. & M. Slavkay, 1997: *Explanations to the Geological map of the Nízke Tatry Mts. at a scale 1:50,000* (in Slovak).- GSSR, pp. 232, Bratislava.

Bosák, P., Pruner, P., Kadlec, J., Hercman, H. & P. Schnabl, 2004: Paleomagnetic research of sedimentary fills of selected caves in Slovakia (in Czech). Etapová zpráva č. 4 MS, Geologický ústav AV ČR, pp. 405, Praha.

Bosch, R. F. & W. B. White, 2004: Lithofacies and transport of clastic sediments in karst aquifers.- In: Sasowsky, I. D. & J. Mylroie (eds.) *Studies of Cave Sediments.* Kluwer Academic, pp. 1–22, New York.

Bónová, K., Hochmuth, Z. & J. Derco, 2008: Preliminary results from mineralogical study of fluvial sediments in the Skalistý potok Cave (Slovak Karst) (in Slovak).- Slovenský kras, 46, 277–286.

Bónová, K., Bella, P., Kováčik, M., Bóna, J., Petro, Ľ., Kollárová, V. & Ľ. Kovaničová, 2014: Allochthonous fine-grained sediments and their relation to the genesis of Liskovská Cave (Chočské Foothills, northern Slovakia) (in Slovak).- *Acta Geologica Slovaca,* 6, 2, 145–158.

Broska, I. & I. Petrík, 1993: Tonalite of the Sihla type s. l.: a Variscan plagioclase-biotite I-type magmatite in the Western Carpathians (in Slovak).- Mineralia Slovaca, 25, 1, 23–28.

Broska, I. & P. Uher, 2001: Whole-rock chemistry and genetic typology of the West-Carpathian Variscan granites.- Geol. Carpath., 52, 2, 79–90.

Broska, I. & I. Petrík, 2011: Accessory Fe-Ti oxides in the West-Carpathian I-type granitoids: witnesses of the granite mixing and late oxidation processes.- Miner. Petrol., 102, 1–4, 87–97.

Broska, I., Petrík, I. & P. Uher, 2012: *Acessory mineralsof the Carpathian granitic rocks* (in Slovak).- VEDA, pp. 235, Bratislava.

Bujnovský, A., 1975: Mesozoicum of the northern slopes of the Nízke Tatry Mts. (the area between Križianka and Ľupčianka) (in Slovak).- Vlastivedný zborník Liptov, 3, 83–102.

Cambel, B., Medveď, J. & P. Pitoňák, 1981: Geochemie und Petrogenese dioritischer Gesteine der Kleinen Karpaten.- Geologický Zborník Geologica Carpathica, 32, 189–220.

Deer, W. A., Howie, R. A. & J. Zussman, 1992: *An Introduction to the Rock-Forming Minerals.* Longman, 2-nd. Edition, pp. 696, London.

Dinev, L., 1942: Morphology of the Central Western Carpathians (in Bulgarian).- Izvestija na Bulgarskoto geografsko družestvo, 9, Sofija.

Dropp, G. T. R., 1987: A general equation for estimating Fe^{3+} concentrations in ferromagnesian silicates and oxides from microprobe analyses, using stoichiometric criteria.- Mineral. Mag., 51, 431–435.

Droppa, A., 1950: Mošnica Cave in the Nízke Tatry Mts. (in Slovak).- Krásy Slovenska, 27, 5–8, 182–193.

Droppa, A., 1966: The correlation of some horizontal caves with river terraces.- Studies in Speleology, 1, 186–192.

Droppa, A., 1972: Geomorphological settings of the Demänová Valley (in Slovak).- Slovenský kras, 10, 9–46.

Droppa, A., 1973: Review of investigated caves in Slovakia (in Slovak).- Slovenský kras, 11, 111–157.

Farahat, E. S., 2008: Chrome-spinels in serpentinites and talc carbonates of the El Ideid-El Sodmein District, central Eastern Desert, Egypt: their metamorphism and petrogenetic implications.- Chemie der Erde, 68, 193–205.

Fejdiová, O., 1977a: Development of the Lower Triassic clastics in the Central West Carpathians.- Geologický Zborník Geologica Carpathica, 28, 167–176.

Fejdiová, O., 1977b: Pre-Triassic weathering crust on the Liptovská Lúžna locality (Nízke Tatry Mts.) (in Slovak).- Mineralia Slovaca, 9, 4, 299–302.

Fejdiová, O., 1989: Pre-Triassic weathering crust on the Baláže locality (Nízke Tatry Mts.) (in Slovak).- Regionálna Geológia Západných Karpát, 25, 161–163.

Gillieson, D., 1996: *Caves: Processes, Development and Management.*- Blackwell, pp. 324, Oxford.

Grecula, P. & Z. Roth, 1978: Kinematic model of the Western Carpathians in complete cuts (in Czech).- Sborník geologických věd – geologie, 32, 49–73.

Gross, P., Köhler, E., Papšová, J. & P. Snopková, 1980: Geology and stratigraphy of the inner-Carpathian Paleogene sedimentary rocks (in Slovak).- In: Gross, P., Köhler, E. (eds.) *et al. Geológia Liptovskej kotliny*. GÚDŠ, pp. 22–72, Bratislava.

Halmešová, S., Holzer, R., Marušiaková, D. & L. Pospíšil, 1992: Geodynamic analysis of the Nízke Tatry Mountains based on geophysical and remote sensed data.- Sborník geologických věd, užitá geofyzika, 25, 67–81.

Henry, D. J. & C. V. Guidotti, 1985: Tourmaline as a petrogenetic indicator mineral: An example from the staurolite-grade metapelites of NW Maine.- Am. Mineral., 70, 1–15.

Hlaváč, J., Zimák, J. & J. Štelcl, 2004: "Cave soils" in the show caves of the Nízke Tatry Mts. and Belianske Tatry Mts.- In: Bella, P. (ed.) *Výskum, využívanie a ochrana jaskýň, zborník referátov zo 4. vedeckej konferencie,* 5th–8th October 2003, Tále, 89–94, Liptovský Mikuláš.

Hovorka, D., Chovan, M. & J. Michálek, 1982: Olivine fenokersantite in granodiorite country rock from Dúbrava, Nízke Tatry Mts.- Mineralia Slovaca, 14,1, 85–90.

Hovorka, D. & J. Spišiak, 1988: *Mesozoic volcanism of the Western Carpathians* (in Slovak).- VEDA, pp. 225, Bratislava.

Hovorka, D. & M. Kováčik, 2007: Occurence modes and types of amphibole in Pre-Tertiary metamorphic rocks of the Western Carpathians.- Mineralia Slovaca, 39, 269–282.

Ivanička, J., Hók, J., Polák, M., Határ, J., Vozár, J., Nagy, A., Fordinál, K., Pristaš, J., Konečný, V., Šimon, L., Kováčik, M., Vozárová, A., Fejdiová, O., Marcin, D., Liščák, P., Macko, A., Lanc, J., Šantavý, J. & V. Szalaiová, 1998: *Explanations to the geological map of the Tríbeč Mts. at a scale 1:50,000* (in Slovak).- GSSR, pp. 247, Bratislava.

Janák, M., Mikuš,T., Pitoňák, P. & J. Spišiak, 2009: Eclogites overprinted in the granulite facies from the Ďumbier Crystalline Complex (Low Tatra Mountains, Western Carpathians).- Geol. Carpath., 60, 3, 193–204.

Kadlec, J., Pruner, P., Hercman, H., Chadima, M., Schnabl, P. & S. Šlechta, 2004: Magnetostratigraphy of sediments preserved in caves located in the Nízke Tatry Mts. (in Czech).- In: Bella, P. (ed.) *Výskum, využívanie a ochrana jaskýň, zborník referátov zo 4. vedeckej konferencie,* 5th–8th October 2003, Tále, 15–19, Liptovský Mikuláš.

Kicińska, D. & J. Głazek, 2005: Heavy minerals in deposits of Belianska Cave (in Polish).- In: Gradziński, M. & M. Szelerewicz (eds.) *Materialy 39. Sympozjum Speleologicznego,* 7th–9th October 2005, Starbienino, p. 34, Kraków.

Korikovsky, S. P., Dupej, J., Boronikhin, V. A. & N. G. Zinovieva, 1988: Zoned garnets and their equilibria in mica schists and gneisses of Kohút crystalline complex, Hnúšťa region, Western Carpathians.- Geologický Zborník Geologica Carpathica, 41, 2, 99–124.

Koutek, P., 1931: Geological studies on north-western side of the Nízke Tatry Mts.- Sborník Státního geologického Ústavu ČSR, oddelení geologie, 9, 413–527.

Kováč, M., Kráľ, J., Márton, E., Plašienka, D. & P. Uher, 1994: Alpine uplift history of the Central Western Carpathians: geochronological, paleomagnetic, sedimentary and structural data.- Geol. Carpath., 45, 83–96.

Kováč, M., 2000: *Geodynamic, paleogeographic and structural development of the Carpatho-Pannonian region during the Miocene: new view on the Neogene basins of Slovakia* (in Slovak).- VEDA, pp. 202, Bratislava.

Kretz, R., 1983: Symbols of rock-forming minerals.- Am. Mineral., 68, 277–279.

Leake, B. E., Wooley, A. R., Arps, C. E. S., Birchs, W. D., Gilbert, M. C., Grice, J. D., Hawthorne, F. C., Kato, A., Kisch, H. J., Krivovichev, V. G., Linthout, K., Laird, J., Mandarino, J. A., Maresch, W. V., Nickel, E. H., Rock, N. M. S., Schumacher, J. C., Smith, D. C., Stephenson, N. C. N., Ungaretti, L., Whittaker, E. J. W. & Guo Youzhi, 1997: Nomenclature of amphiboles: report of the Subcommittee on Amphiboles of the International Mineralogical Association, Commission on New Minerals and Mineral Names.- Can. Mineral. 35, 219–246.

Lenaz, D., Kamenetsky, V. S., Crawford, A. J. & F. Princivalle, 2000: Melt inclusion in detrital spinel from the SE Alps, (Italy-Slovenia): a new approach to provenance studies of sedimentary basins.- Contrib. Mineral. Petr., 139, 6, 748–758.

Lukniš, M., 1964: Remains of older surfaces of relief planation in the Czechoslovakian Carpathians (in Slovak).- Geografický časopis, 16, 3, 289–298.

Mazúr, E., 1963: *Žilina Basin and the adjacent mountains* (in Slovak).- SAV, pp. 184, Bratislava.

Méres, Š. & D. Hovorka, 1991: Alpine metamorphic recrystallization of the pre-Carboniferous metapelites of the Kohút crystalline complex (the Western Carpathians).- Mineralia Slovaca, 23, 5–6, 435–442.

Mišík, M. & J. Jablonský, 2000: Lower Triassic quartzites of the Western Carpathians: transport directions, source of clastics.- Geol. Carpath., 51, 4, 251–264.

Morton, A., Hallsworth, C. & B. Chalton, 2004: Garnet composition in Scottish and Norwegian basement terrains: a framework for interpretation of North Sea sandstone provenance.- Mar. Petrol. Geol., 21, 393–410.

Orvoš, P. & M. Orvošová, 1996: Age estimation of the horizontal levels of caves in the Jánska Valley by means of their parallelisation to Váh River terraces (in Slovak).- In: Lalkovič, M. (ed.) *Kras a jaskyne – výskum, využívanie a ochrana, zborník referátov z vedeckej konferencie*, 26th–29th September 1995, Liptovský Mikuláš, 95–101, Liptovský Mikuláš.

Orvošová, M., Uhlík, P. & P. Uher, 2006: Paleokarst of the Ohnište Plateau – research on the filling of the Veľký závrt Doline (Nízke Tatry, Mts., Slovakia) (in Slovak).- Slovenský kras, 44, 71–80.

Petrík, I., Broska, I., Lipka, J. & P. Siman, 1995: Granitoid allanite-(Ce): substitution relations, redox conditions and REE distributions (on an example of I-type granitoids, Western Carpathians, Slovakia).- Geol. Carpath., 46, 79–94.

Petrík, I., & P. Konečný, 2009: Metasomatic replacement of inherited metamorphic monazite in a biotite-garnet granite from the Nízke Tatry Mountains, Western Carpathians, Slovakia: Chemical dating and evidence for disequilibrium melting.- Am. Mineral., 94, 957–974.

Pitoňák, P. & J. Spišiak, 1988: Simple model of paragneisses and amphibole rocks protoliths of the Nízke Tatry Mts. crystalline complex.- Geologický Zborník Geologica Carpathica, 39, 73–86.

Pitoňák, P. & J. Spišiak, 1989: *Mineralogy, petrology and geochemistry of the basic rock types from crystalline basement of the Nízke Tatry Mts.* (in Slovak).- Archív ŠGÚDŠ, pp. 232, Bratislava.

Plašienka, D., 2003: Development of basement-involved fold and thrust structures exemplified by Tatric-Fatric-Veporic nappe system of the Western Carpathians (Slovakia).- Geodinamica Acta, 16, 21–38.

Powers, M. C., 1953: A new roundness scale for sedimentary particles.- J. Sediment. Petrol., 23, 117–119.

Spišiak, J., Pitoňák, P. & M. Petro, 1988: Metaultramafites from the Jasenie-Kyslá area, the Low Tatras (in Slovak).- Mineralia Slovaca, 20, 2, 143–148.

Spišiak, J. & P. Pitoňák, 1990: The Nízke Tatry Mts. crystalline complex – new facts and interpretation (Western Carpathians, Czechoslovakia).- Geologický Zborník Geologica Carpathica, 41, 4, 377–392.

Spišiak, J., Arvensis, M., Linkešová, M., Pitoňák, P. & F. Caňo, 1991: Basanite dyke in granitoids near Dúbrava, Nízke Tatry Mts., Central Slovakia (in Slovak).- Mineralia Slovaca, 23, 339–345.

Stevens, R. E., 1944: Composition of some chromites of the Western Hemisphere.- Am. Mineral., 29, 1–34.

Škvaček, A., 1978: Glaciation of the Mošnica Valley in the Nízke Tatry Mts. (the Western Carpathians).- AFRNUC, Geographica, 16, 177–190.

Uher, P. & O. Miko, 1994: Biotite-amphibole (mela)tonalite – quartz diorite in the Žiar Mts. (Western Carpathians, Slovakia) (in Slovak).- Mineralia Slovaca, 26, 365–366.

Xuan Thanh, N., Trong Tu, M., Itaya, T. & S. Kwon, 2011: Chromian-spinel compositions from the Bo Xinh ultramafics, Northeern Vietnam: Implications on tectonic evolution of the Indochina block.- J. Asian Earth Sci., 42, 258–267.

Zuberec, J., Tréger, M., Lexa, J. & P. Baláž, 2005: *Mineral resources of Slovakia*.- ŠGÚDŠ, pp. 350, Bratislava.

COBISS: 1.01

SEARCHING FOR COLD-ADAPTED MICROORGANISMS IN THE UNDERGROUND GLACIER OF SCARISOARA ICE CAVE, ROMANIA

ISKANJE NA MRAZ PRILAGOJENIH MIKROORGANIZMOV V PODZEMNEM LEDENIKU LEDENE JAMI SCARISOARA (ROMUNIJA)

Alexandra HILLEBRAND-VOICULESCU[1#], Corina ITCUS[2#], Ioan ARDELEAN[2], Denisa PASCU[2], Aurel PERŞOIU[3], Andreea RUSU[2], Traian BRAD[4], Elena POPA[2], Bogdan P. ONAC[5,4] & Cristina PURCAREA[2*]

Abstract UDC 551.444.6:579.26(498)

Alexandra Hillebrand, Corina Itcus, Ioan Ardelean, Denisa Pascu, Aurel Perşoiu, Andreea Rusu, Traian Brad, Elena Popa, Bogdan P. Onac & Cristina Purcarea: Searching for cold-adapted microorganisms in the underground glacier of Scarisoara Ice Cave, Romania

Scarisoara Ice Cave (Romania) hosts one of world's largest and oldest underground glacier. While no studies were carried out on the existence of microorganisms in this cave's ice block, our interest is to investigate the presence of microorganisms and their chronological distribution in the cave's subterranean ice in relationship with past climatic changes. Samples were collected from ice layers of different age (from present to ~900 cal. yrs. BP), and the diversity of embedded microbial communities was assessed by classical cultivation and molecular techniques. The microorganisms from ice-sediments were cultivated at 4 °C and 15 °C, in the presence and absence of light. Epifluorescence microscopy analysis indicates the presence of autotrophic prokaryotes and eukaryotes in sunlight-exposed ice and water samples. Total DNA was isolated from each ice sample and the bacterial and eukaryotic SSU-rRNA genes were amplified by PCR. The chemical composition and organic content of both deeply buried (>10 m inside the ice block) and surface (supra-glacial pond water) habitats were analyzed in relation to their age and organic composition. This study is the first to report on the presence of both prokaryotic and eukaryotic microorganisms in the subterranean ice block of Scarisoara Ice Cave, thriving in both organic-rich ice and clear ice layers. Phototrophic prokaryotes and eukaryotes were identified in sun-exposed recent ice. The compo-

Izvleček UDK 551.444.6:579.26(498)

Alexandra Hillebrand, Corina Itcus, Ioan Ardelean, Denisa Pascu, Aurel Perşoiu, Andreea Rusu, Traian Brad, Elena Popa, Bogdan P. Onac & Cristina Purcarea: Iskanje na mraz prilagojenih mikroorganizmov v podzemnem ledeniku Ledene jami Scarisoara (Romunija)

Študija obravnava pojavnost in časovno porazdelitev mikroorganizmov v jamskem ledu v Ledeni jami Scarisoara (Romunija), v kateri je eden največjih in najstarejših jamskih ledenikov. Pojavnost mikroorganizmov nas zanima predvsem v povezavi s preteklimi klimatskimi spremembami. Vzorčili smo v različnih plasteh ledu, starih od 900 let do recentnih in v njih določevali združbe mikroorganizmov z klasičnim gojenjem in z molekularnimi metodami. Mikroorganizme iz lednih sedimentov smo v temi in na svetlobi gojili na temperaturah 5 °C in 15 °C. Epifluorescentna mikroskopija je pokazala prisotnost avtotrofnih prokariontov in evkariontov v vzorcih ledu in vode, ki so bili izpostavljeni sončnemu obsevanju. Iz ledu smo izolirali celotno DNK ter bakterijske in evkariontske gene male ribosomske podenote (SSU-rRNA) namnožili s polimerazno verižno reakcijo (PCR). Kemično sestavo in organski delež globoko pokopanih (več kot 10 m globoko v ledu) in površinskih (vodni bazen na površini ledu) habitatov smo povezali z njihovo starostjo in organsko sestavo. Študija prva poroča o prokariontskih in evkariontskih mikroorganizmih v podzemnem ledu jame Scarisoara, ki uspevajo tako v organsko bogatih plasteh ledu kot v prosojnem ledu. V ledu, izpostavljenem sončni svetlobi, smo odkrili prisotnost fototrofnih prokariontov in evkariontov. Sestava na mraz prilagojenih mikroorganizmov v ledu se spremi-

[1] Emil Racovita Institute of Speleology, Bucharest, Romania, e-mail: alexandra.hillebrand@iser.ro
[2] Institute of Biology Bucharest, Bucharest, Romania, e-mail: corina.itcus@ibiol.ro, ioan.ardelean@ibiol.ro, denisa.pascu@ibiol.ro, andreea.rusu@ibiol.ro, Elena.popa@ibiol.ro, e-mail: cristina.purcarea@ibiol.ro
[3] Stefan cel Mare University, Suceava, Romania, e-mail: aurel.persoiu@gmail.com
[4] Emil Racovita Institute of Speleology, Cluj-Napoca, Romania, e-mail: brad@biolog.ubbcluj.ro
[5] School of Geosciences, University of South Florida, USA, e-mail: bonac@usf.edu
[#] authors with equal contribution
* Corresponding author: Dr. Cristina PURCAREA, Department of Microbiology, Institute of Biology Bucharest, Romanian Academy, 296 Splaiul Independentei, 060031 Bucharest, Romania, e-mail: cristina.purcarea@ibiol.ro

Received/Prejeto: 20.05.2013

sition of cold-adapted ice embedded microbiota varied with the habitat age and organic content, as resulting from dissimilarities in growth curve profiles at two different temperatures. The presence of bacteria and eukaryotes in all the analyzed samples was asserted by PCR amplification of SSU-rRNA gene fragments. These findings can be further used to reconstruct changes in the microbial diversity over the past approximately 5000 years, in correlation with climatic and environmental changes recorded by the ice block.
Keywords: underground glacier, climate archives, microorganisms, psychrophiles, Scarisoara Ice Cave.

nja s starostjo in organsko sestavo habitata, na kar kaže tudi razlika rastnih krivulj pri dveh različnih temperaturah. Prisotnost bakterij in evkariontov v vseh analiziranih vzorcih smo potrdili tudi z PCR namnožitvijo genskih fragmentov SSU-rRNA. Opisane ugotovitve bodo uporabne za rekonstrukcijo sprememb pestrosti mikroorganizmov v odvisnosti od okoljskih sprememb, zabeleženih v jamskem ledu v zadnjih 5000 letih.
Ključne besede: podzemni ledenik, klimatski arhiv, mikroorganizmi, psihrofili, Ledena jama Scarisoara.

INTRODUCTION

The microbial diversity of cold environments was investigated from a large variety of exposed ice habitats (Priscu *et al.* 2007) such as polar ice sheets (Jungblut *et al.* 2010; Rehakova *et al.* 2010; Varin *et al.* 2010), alpine glaciers (Tscherko *et al.* 2003) and frozen lakes (Felip *et al.* 1995, Dieser *et al.* 2010), and Antarctic permanent lake ice (Priscu *et al.* 1998, Murray *et al.* 2012). Comparative geochemical and microbiological studies of ice cores drilled in polar and high mountain areas (Miteva *et al.* 2009) allowed for the identification of climate biomarkers. In ice layers of different ages from Antarctic (Abyzov *et al.* 1998; Xiang *et al.* 2005) and Alpine (Zhang *et al.* 2006) glaciers, the variation in microbial composition and abundance was correlated with climatic changes. However, very little is known to date about microorganisms communities living in ice deposits from caves, an isolated and light deprived cold environment that ensures advanced species' conservation, and no temporal-dependence studies of these microorganisms diversity were carried out on this type of habitat. Only a few studies report the isolation of bacteria (Margesin *et al.* 2004) and diatom flora (Lauriol *et al.* 2006) from ice caves, whereas the vast majority of ice caves studies targeted their palaeoclimatic information (Racovita & Serban 1990; Yonge & MacDonald 1999; Citterio *et al.* 2004; Kern *et al.* 2004; Holmlund *et al.* 2005; Luetscher 2005; Feurdean *et al.* 2011; Maggi *et al.* 2011). However, unraveling the ice cave biodiversity could complement the palaeoclimate record, in addition to the broad bionanotechnological potential of phychrophilic species isolated from this particular environment.

Among microorganisms commonly found in frozen environments, phototrophic prokaryotes and eukaryotes from light exposed environments play an important role in carbon and nitrogen enrichment of the environment by photosynthetic assimilation of atmospheric nitrogen and CO_2, respectively (Vincent 2007; Morgan–Kiss *et al.* 2006; Jungblut *et al.* 2010; Namsaraev *et al.* 2010; Uetake *et al.* 2010). Their presence and role in perennial ice deposits from caves could be of particular interest for palaeoclimatic reconstruction.

Recently, the discovery of liquid water and ice on Mars (Levin & Weatherwax 2003; Kerr 2010), as well as the theoretical demonstration of the possible existence of ice caves on Mars (Boston 2004; Williams *et al.* 2010), increased the interest for such peculiar terrestrial environments and their biodiversity that mimic extraterrestrial conditions, thus giving an insight on exobiology aspects (Jakosky *et al.* 2003; Rampelotto 2010), but also into possible earlier environments on Earth.

Scarisoara Ice Cave (Romania), containing one of the oldest and largest subterranean ice block (Perşoiu 2011), presents an easily accessible and radiocarbon dated (~1200 cal. Yrs. BP) ice wall, with clear regular horizontal stratification (Fig. 1B) (Holmlund *et al.* 2005; Perşoiu & Pazdur 2011). This cave's ice block constitutes a chronological record of changes in climate and biodiversity embedded in yearly-accumulated ice layers.

A pioneering microbiological study carried out by Pop (1949) on Scarisoara Ice Cave reports the presence of nitrifying bacteria in the calcareous sediments from the Great Reservation. However, no microbiological studies were carried out to date on the underground ice block from this cave.

In this context, this work reports the identification of microorganisms belonging to Bacteria and Eukarya domains, including phototrophs (cyanobacteria and green algae), in recent, 400-years, and 900-years old ice sediments from Scarisoara Ice Cave. This work represents the first microbiological study of ice deposits from this underground glacier, contributing to an integrative characterization of a well-documented cave from geological, chronological, and palaeoclimatic perspectives.

SITE DESCRIPTION

Scarisoara Ice Cave (1,165 m a.s.l., Apuseni Mts., Romania, Fig. 1A) is a short (700 m) and deep (105 m) cave, hosting one of the oldest (>5000 years) and largest (>100.000 m^3) cave glacier in the world (Perşoiu 2011). The ice block formed mainly by the annual freezing in late autumn of ponded drip and rain/snowmelt water, overlapping the ice from previous year (Racovita 1927; Perşoiu *et al.* 2011a). As both rain and drip water carry relatively large amounts of organic matter (*e.g.* soil, pollen, invertebrates), the freezing process resulted in the genesis of a varve-like deposit, comprising both clear ice (1–20 cm thick) and sediment-rich layer, including organic material (Racovita & Onac 2000; Feurdean *et al.* 2011) and cryogenically precipitated calcite (Zak *et al.* 2008). Melting and sublimation due to geothermal heat and cold air circulation led to the gradual retreat of the sides of the ice block, resulting in the development of a vertical wall towards the Little Reservation, where ~1000 years old strata are exposed (Perşoiu & Pazdur 2011) (Fig. 1B).

The climate of the cave is rather stable in the warm period (April–September), the air temperature (T_{air}) remaining constant at 0 °C in the Great Hall, the Church and Little Reservation, and slowly rising (up to 4 °C) towards the deepest parts of the cave (Racovita 1994; Perşoiu *et al.* 2011b). During the cold period (October–March), the air temperature variations in the vicinity of the cave' entrance (the Great Hall) closely (<1 hour delay) follow the external ones, dropping to –14 °C, while in the inner sections of the cave the positive temperatures are preserved. High (>95 %) relative humidity values are recorded in the entire cave throughout the year, with relatively low values occurring in winter in the Great Hall and its surrounding area, when the outside cold and drier air sinks into the cave and replaces the warm and moist air therein.

The ice block is located in the Great Hall at the bottom of the shaft. A reduced section of the ice block surface (~10 m^2) from the Great Hall is exposed to sunlight, thus promoting the development of an abundant popu-

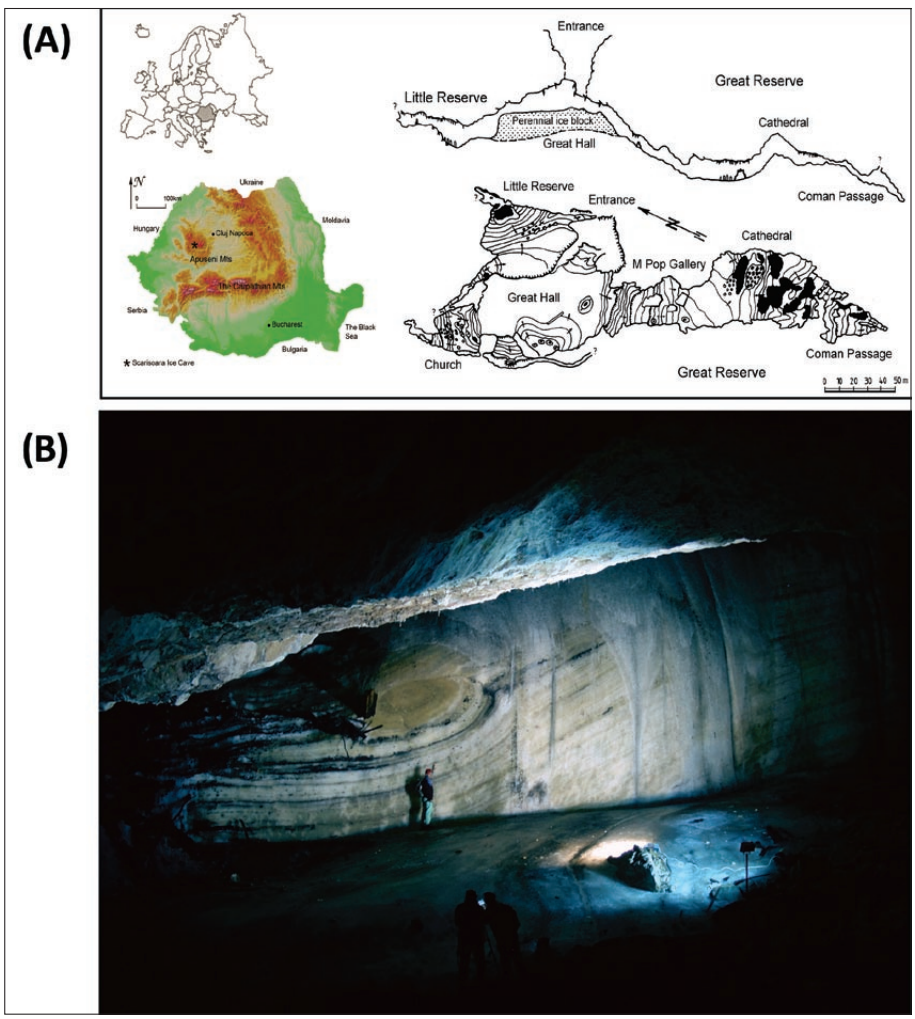

Fig. 1: Scarisoara Ice Cave map and Little Reservation ice wall. (A) Cave's location and map with cross-section. Sampling location (box): Great Hall and Little Reservation; (B) Ice wall of Little Reservation showing horizontal stratification (Photo: A. Perşoiu).

Fig. 2: Ice sampling from Scarisoara Ice Cave. (A) Little Reservation, light-deprived locations. Samples were collected from single layers within the ice wall; (B) Great Hall, light-exposed locations. Samples were collected vertically from one annual-layer of the ice floor; (C) Sterile ice collection in 1-liter flask; (D) sun-exposed supra-glacial pond (SGP) at the entrance of Great Hall containing phototrophic (micro)organisms (green) (Photos: C. Purcarea).

lation of phototrophic (micro)organisms living in the supra-glacial pond at the water-ice interface (Fig. 2D).

SAMPLING

Ice samples were collected during the cold period from five different sites within the glacial part of the cave (Great Hall and Little Reservation, Fig. 1A), corresponding to ice layers of different ages, organic content and light exposure regime (direct sunlight exposure, diffuse light exposure, and darkness).

Samples 1-S and **1-L,** collected from the Great Hall (Fig. 2B), consist of one-year-old ice from two different microclimatic environments: sample **1-S** was collected near the entrance, a less isolated section of the cave, where the ice resulted from the freezing of seepage and rain/snowmelt water accumulated in a sun-exposed lake (Fig. 2D), whereas **sample 1-L** was collected from a similarly formed ice layer located in the central area of the hall, therefore less influenced by the outside environment, where only diffuse light is present. The microclimatic conditions during the ice genesis were similar for these two locations, consisting of an initial phase of water accumulation at constant air temperature of 0 °C, followed by a freezing phase trapping microorganisms and organic matter in the newly formed ice (Perşoiu *et al.* 2011a).

Samples 400-O, 900, and **900-O**, collected from the Little Reservation (Fig. 2A), originate from ice layers of different age and organic matter content. **400-O** and **900-O** were collected from two organic-rich ice layers located at 1125.5 and 1345.4 cm bellow the present-day surface of the ice block, whereas **sample 900** was collected from a layer of clear ice, with no visible organic content, at 1355.4 cm bellow surface. The ages of the two ice layers of **400-O** and **900-O/900** samples are 399 and 887 cal. yrs. BP, respectively (Perşoiu & Pazdur 2011).

Ice samples collection (Fig. 2) was carried out with a manually driven 3 cm diameter auger under sterile conditions, by flaming both the auger and the ice surface with a portable gas burner for 5 s, to avoid contamination with recent microbial species (Fig. 2A and 2C). About 5 cm of ice were removed from the ice block surface in both the sun- and light-exposed areas from the Great Hall (Fig 2B), and the ice samples were collected vertically (Fig 2B) and transferred in the presence of open flame to 1-L sterile flasks (Fig. 2C). Samples collected from the Little Reservation (Fig. 2A) were processed in a similar manner, after removing a deeper ice layer (20 cm) from the surface of the wall, due to a greater contamination risk with recent ice. The drilling was carried out horizontally, parallel to the ice lamination (Fig. 2A). The ice samples were stored at −20 °C.

Water samples (SGP) were also collected under sterile conditions in 1-L flasks from the supra-glacial pond formed during the warm period in a sun-exposed area at the entrance of the Great Hall (Fig. 2D), and stored at 4 °C until processed.

MATERIAL AND METHODS

CHEMICAL ANALYSIS

The chemical analysis of ice and supra-glacial sunlight exposed water samples was performed to determine the organic content, nutrients and salinity of the corresponding habitat of each microenvironment of microbial community. The chemical oxygen demand (COD) and the concentrations (mg L^{-1}) of nitrates, calcium ions, sulfates, and chlorides were determined spectrophotometrically (Clesceri *et al.* 1999) using a Specord 200 spectrophotometer (Analytic Jena). The chemical oxygen demand (COD) was determined by CCOCr volumetric analysis using the small scale tube dichromate method based on the ISO 15705:2002 standard. Chlorides were determined by the argentometric method based on the SR ISO 9297:2001 standard. Sulfates were analyzed by precipitation with barium chloride, using a turbidimetric method (EPA 375.4). The nitrates concentration was measured spectrophotometrically after reaction with sulfosalicylic acid and alkaline treatment (SR ISO 7890-3:2000). Calcium content was determined using the EDTA titration method according to SR ISO 6058:2008.

MICROORGANISMS CULTIVATION

Heterotrophic microorganisms from ice samples were cultivated in Luria-Bertani (LB) liquid medium supplemented with 1 % glucose (**LBG**) (Sambrook & Russell, 2001) at 4 °C and 15 °C. This rich medium favoring bacterial cultivation, also promotes the growth of diverse heterotrophic prokaryotes. Melted ice samples (10 µl) were inoculated in 3-ml liquid medium, and the cultures were incubated for 32 days at the two different temperatures, under static conditions. The microbial communities growth curves were monitored at OD_{600} using a FluStar Omega plate reader (BGM Labtech).

The presence of cultivable phototrophic prokaryotes (cyanobacteria) and eukaryotes (filamentous algae), was investigated by cultivation on BG_{11} liquid medium at 7 °C in the presence of light under static conditions (Rippka *et al.* 1979).

EPIFLUORESCENCE AND LIGHT MICROSCOPY

Heterotrophic and phototrophic microorganisms were analyzed by epifluorescence/light microscopy using AXIO Scope A1 microscope with Axio Cam ERC 5s (Zeiss). The cells were either untreated or stained with SybrGreen (SG) for fluorescence labeling of the entire microbial population, or with ethidium homodimer (HD) (del Giorgio & Gasol, 2008) indicating altered plasmatic membrane (dead cells) for cell viability assessment. SGP water samples were fixed with 2 % formaldehyde immediately after collection, and analyzed by light microscopy using 0.1 % crystal violet staining (Sarchizian & Ardelean 2012).

GENOMIC DNA EXTRACTION AND PCR AMPLIFICATION

The occurrence of bacteria and eukaryotes in ice samples was investigated by PCR amplification of SSU-rRNA specific genes. 200 ml of sediment-rich samples 400-O and 900-O, and 800 ml of 1-S, 1-L, and 900 ice samples were thawed at 4 °C and filtered through 0.22 µm sterile MF-membranes (Millipore) using a vacuum-driven stainless steel filtering system (Millipore) and LaboPort vacuum pump Type N86KN.18 (KNF LAB). The cells collected on the filter were treated with 15 units of mutanolysin (Fermentas) for 1 hour at 37 °C, and the genomic DNA was further isolated using DNeasy Blood and Tissue kit (Qiagen). DNA concentration and purity were measured using the NanoDrop 1000 (Thermo Scientific).

Bacterial 16S-rRNA and eukaryotic 18S-rRNA gene fragments were amplified by PCR using specific primers (Tab. 1). The reaction mixture contained 100 ng genomic DNA, 2 µM or 0.4 µM of each bacterial or eukaryotic primers, respectively, 0.2 mM dNTP, 1 x *Taq* DNA polymerase buffer, 2 mM $MgCl_2$, and 1 unit *Taq* DNA polymerase (Fermentas).

The amplification reaction consisted of (1) initial denaturation at 95 °C for 2 min, followed by 30 cycles of 30 s at 95 °C, 30 s at 60 °C and 90 s at 72 °C, and a final extension step of 5 min at 72 °C for Bacteria, and (2) denaturation at 94 °C for 130 s, followed by 35 cycles of 30 s at 94 °C, 45 s at 56 °C, 130 s at 72 °C, and a final extension step of 7 min at 72 °C for Eukarya. The DNA fragments were analyzed by 1 % agarose gel electrophoresis.

Tab. 1: Primers used for 16S/18S-rRNA gene amplification

Specificity	*Primers*	*Sequence*	*Reference*
Bacteria	B8F 1525R	AGAGTTTGATCCTGGCTCAG AAGGAGGTGATCCAGCCGCA	Roling *et al.* 2001
Eukarya	Euk1A Euk516R-GC	CTGGTTGATCCTGCCAG ACCAGACTTGCCCTCC-#	Diez *et al.* 2001

GC clamp sequence is CGCCCGGGGCGCGCCCCGGGCGGGGCGGGGGCACGGGGGG

RESULTS

CHEMICAL ANALYSIS OF ICE SAMPLES AND SUPRA-GLACIAL POND WATER

The chemical oxygen demand and a partial salinity and nutrients concentrations of supra-glacial pond water (SGP), and 400-O, 900-O and 900 ice samples were determined and analyzed in correlation with the age and organic content of the samples. The results (Tab. 2) showed a decrease of the COD and nitrate content with the age of ice between samples 400-O and 900-O by 4.3-fold and 3.6-fold, respectively. The presence of organic substrate in the 900-O sample is associated with higher COD (6-fold), nitrate (2.4-fold) and calcium (1.8-fold) concentrations than in sample 900 (clear ice). Sulfate and chloride concentrations showed minor variations with the age and organic content of the samples. Meanwhile, SGP exhibited a comparable organic content (COD) with that of sample 900, and slightly higher (1.3-1.7-fold) chloride concentrations than samples 400-O, 900-O, and 900.

CULTIVATION OF HETEROTROPHIC PROKARYOTES FROM ICE SAMPLES

The presence of cold-adapted bacteria in 1-S, 1-L, 400-O, 900 and 900-O ice samples was investigated by cultivation in LBG medium at 4 °C and 15 °C. Under these conditions, the results (Fig. 3) indicated that all samples contained cultivable microorganisms, and that the growth dynamics of the corresponding microbial communities is temperature-dependent.

At 4 °C, the microbial growth curves had different profiles for recent and old ice samples, with a faster growth and a shorter lag time in the cases of 1-L and 400-O (Fig. 3A), while at 15 °C (Fig. 3B), the species from the same samples had relatively more uniform growth profiles (Fig 3A). The cultivable microorganisms at 15 °C (Fig. 3B) from all samples presented a shorter lag time (4–12 days) than the corresponding ones (7–24 days) growing at 4 °C (Fig. 3A). Both microbial communities from 900-O and 900 samples exhibited similar growth profiles, suggesting a relatively homogenous microbiota within this ice layer regardless their organic

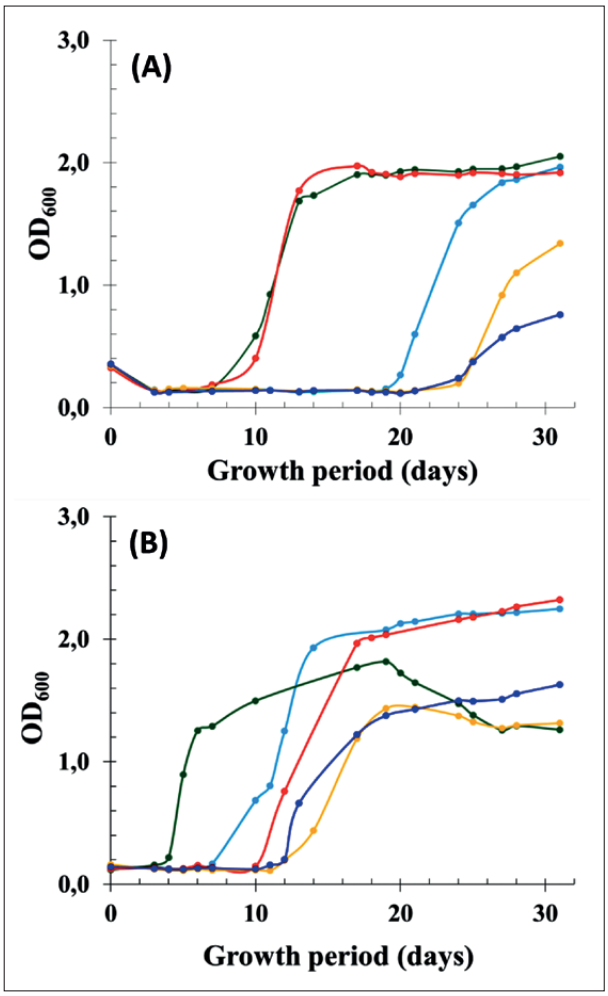

Fig. 3: Growth curves. Ice samples 1-S (light blue), 1-L (green), 400-O (red), 900 (dark blue) and 900-O (yellow) were cultivated for 32 days in LBG medium at (A) 4 °C, and (B) 15 °C.

Tab. 2: Chemical analysis of water and ice samples.

Property / Compound		***Concentration (mg L⁻¹)***			
		SGP	***400-O***	***900-O***	***900***
Organic content	*Chemical oxygen demand (COD)*	30.75	740.88	170.52	28.77
Nutrients	*Nitrates (NO_3^{3-})*	0.937	0.382	0.106	0.044
Salinity	*Calcium ions (Ca^{2+})*	50.9	17.0	16.0	8.9
	Sulfates (SO_4^{2-})	3.6	3.4	3.7	2.8
	Chlorides (Cl^-)	7.2	5.7	5.0	4.3

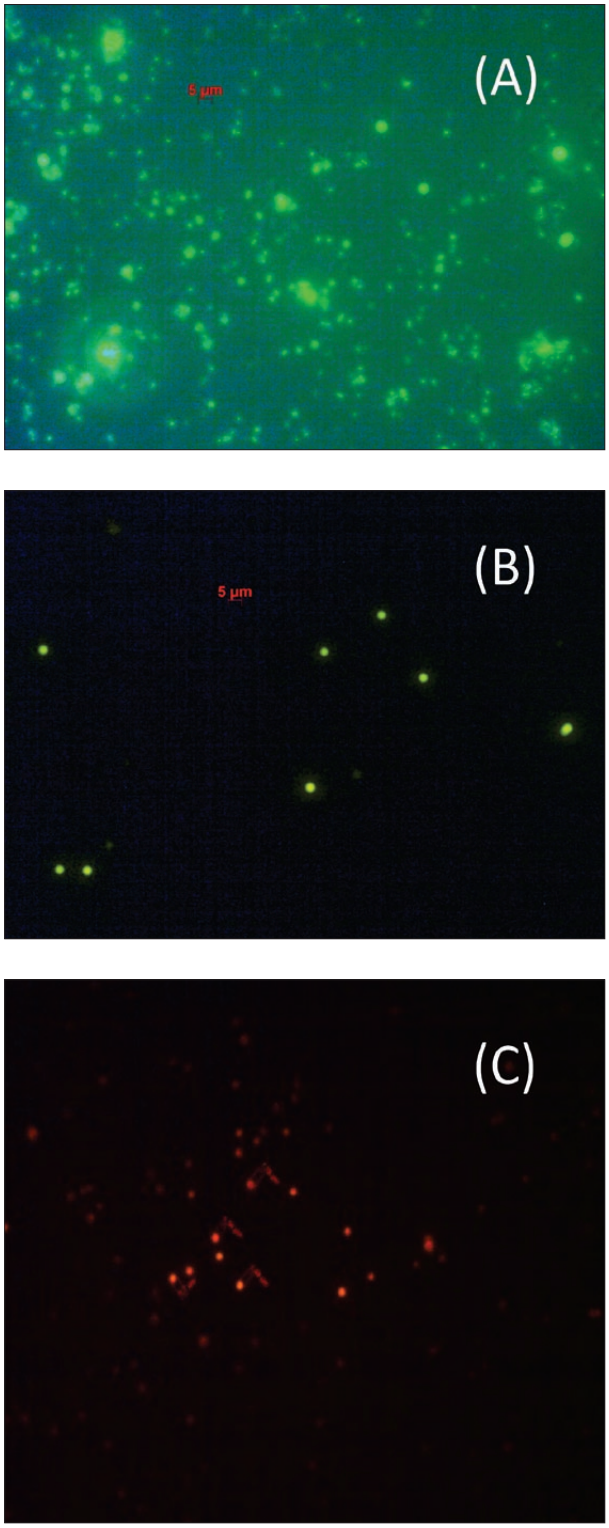

Fig. 4: Epifluorescence microscopy of prokaryotes from 1-S ice sample culture in BG11. Staining with (A) SybrGreen (total cell number); (B) ethidium homodimer (dead cells). (A) and (B) represent the same microscopic field; (C) chlorophyll natural fluorescence (cyanobacteria).

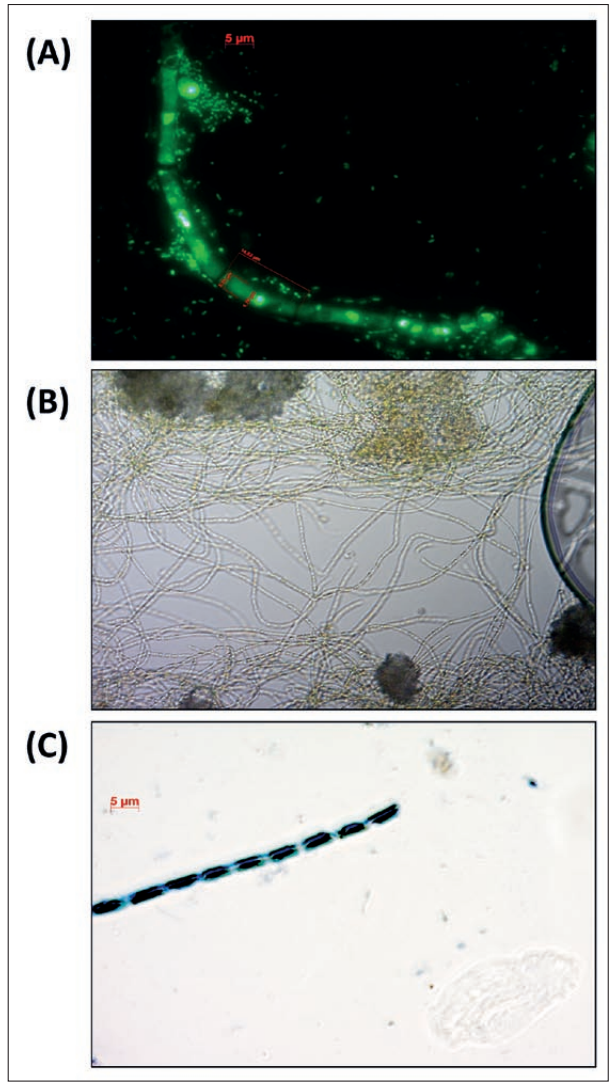

Fig. 5: Filamentous eukaryotic microorganisms from 1-S culture in BG11 and SGP. Cells resulted from cultivation of 1-S ice sample in BG11 at 7 °C for 2 months were analyzed by (A) epifluorescence microscopy using 10xSybrGreen, (B) light microscopy, without staining. (C) SGP water sample fixed with 2 % formaldehyde stained with 0.1 % crystal violet were analyzed by light microscopy.

content. In addition, microbiota from 900 and 900-O presented a slower growth at 4 °C as compared with that of recent and 400-year old ice, indicating a reduced diversity and/or abundance in older strata.

Taken together, the cultivation characteristics of the ice-contained microbiota under different growth conditions suggest differences in the population composition of cold-adapted microbial communities from all the analyzed ice deposits of Scarisoara Ice Cave.

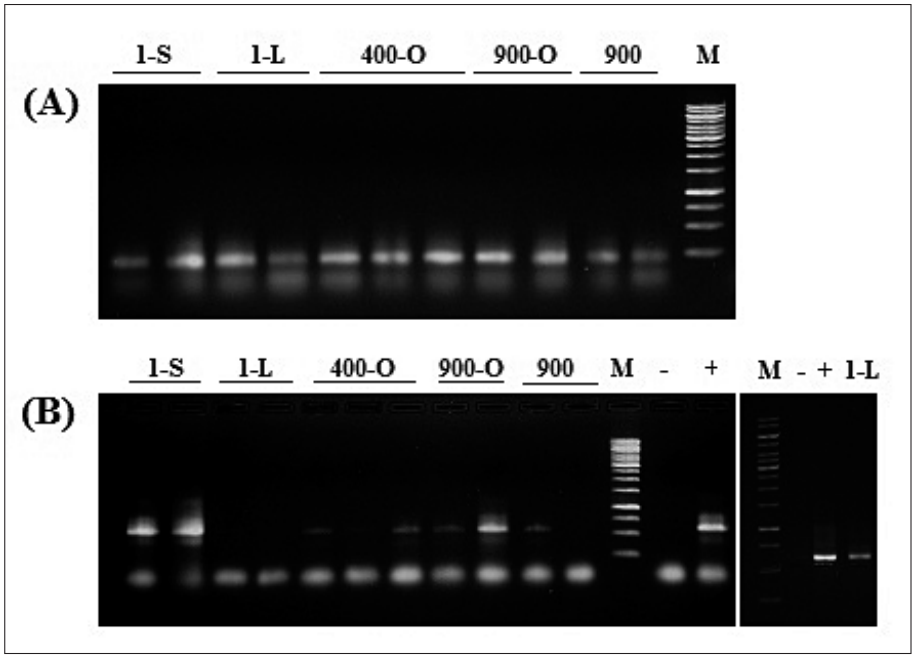

Fig. 6: PCR amplification of SSU-rRNA genes from ice samples. (A) bacterial 16S-rRNA gene fragments using 8F and 1512R primers, (B) eukaryotic 18S-rRNA gene fragments using Euk1A and Euk516R-GC primers.

PRESENCE OF CULTIVABLE PHOTOTROPHIC PROKARYOTES AND EUKARYOTES IN SUNLIGHT EXPOSED ICE

The existence of cultivable phototrophic microorganisms in SGP and 1-S samples collected from the same sunlight-exposed location before and after water freezing, was investigated. 1-S ice samples (10 ml) were incubated with 90 ml BG_{11} liquid medium at 7 °C for up to 2 months in the presence of light and analyzed by epifluorescence microscopy.

In the case of 1-year old sunlight-exposed ice (1-S) cultivated in $BG_{11,}$ the results (Fig. 4) revealed the presence of a high number of prokaryotic cells (Fig. 4A). The majority of these cells are viable, as resulted from the reduced number of dead cells from the same microscopic field (Fig. 4B). Moreover, this culture contains a high number of cyanobacteria exhibiting chlorophyll autofluorescence (Fig. 4C).

In addition to prokaryotic phototrophs, this microbial populations contained cultivable filamentous eukaryotes with clearly visible nuclei (Fig. 5A). Moreover, light microscopy of the untreated cells reveals the presence of chlorophyll-containing filamentous phototrophic eukaryotes in this culture (Fig. 5B). Meanwhile, in the supra-glacial pond at the ice/water interface (SPG), the presence of algae is clearly evidenced (Fig. 5C).

PCR AMPLIFICATION OF SSU-RRNA FROM ICE SAMPLES

The presence of bacteria and eukaryotes in ice layers of different age was assessed by PCR amplification of the corresponding 16S/18S-rRNA gene fragments in all the collected samples. Under these conditions, the results obtained using total DNA extracted from at least two duplicates for each ice sample confirmed the presence of bacterial (Fig. 6A) and eukaryotic (Fig. 6B) species in all the recent and old ice layers investigated. The 18S-rRNA gene amplification, using a GC-clamp eukaryotic primer set (Tab. 1), was further confirmed by DGGE analyses (to be published elsewhere).

DISCUSSION

In this first microbiological study of the biodiversity within the underground ice block from Scarisoara Ice Cave (Romania), we identified the presence of microorganisms thriving in as old as 900 years ice layers of both rich and poor organic content. These microorganisms contain both bacterial and eukaryotic microorganisms.

Epifluorescence microscopy analysis of recent (one year old) ice and supra-glacial water from areas of the cave exposed to sunlight revealed the presence of

prokaryotic and eukaryotic phototrophs, cyanobacteria and filamentous algae, respectively. Bacterial communities from recent, 399 and 887 cal. BP old samples (1-S, 1-L, 400-O, 900-O, and 900), displayed a different composition in cultivable psycrophilic/psychrotolerant microorganisms from ice layers of different age, organic content and sunlight exposure, as resulting from their variable growth curves patterns at 4 and 15 °C.

The chemical composition of the present-day and old habitats of these microorganisms showed major variations with respect to COD, nitrate, and calcium ions concentrations, as a function of both age and organic content of the ice. The substantial decrease of these concentrations between the 399 and 887 cal. BP old ice layers is expected to be associated with a lower microbial content in the latter one. This hypothesis is sustained by the reduced bacterial growth of samples 900 and 900-O as compared to 400-O in LBG at both 4 °C and 15 °C, suggesting a lower representation of psychrophilic / psychrotolerant cultivable strains from microbial communities within the older ice sample than in the more recent ice layers.

While these samples differ by age, there is also a clear distinction in terms of external climate during the deposition of the ice layers from which samples 400-O, 900 and 900-O were collected. Explicitly, samples 900 and 900-O originate from an ice layer deposited during the Medieval Warm Period (MWP), when the significant development of *Fagus sylvatica* forest indicates warmer and drier summers (Feurdean *et al.* 2011). In contrast, sample 400-O was collected from a layer formed during the Little Ice Age (LIA), a colder and wetter period, when *Picea abies* forests (and associated acidic soils) dominated the landscape around the cave's entrance (Feurdean *et al.* 2011). The wetter conditions that prevailed during the LIA over the MWP led to frequent inflow of large volumes of water inside the cave, which carried organic matter and nutrients that could have further improved the habitability of ponded water before freezing, hence favoring an increased biodiversity of the microorganisms' communities.

This study, reporting on the presence of cultivable microorganisms in ~1000-year old subterranean ice from Scarisoara Ice Cave (Romania), and the age-dependent variations of the microbial communities within this habitat, is the first such environmental survey of an ice cave. While, to date, this particular type of ecological niche received a very limited attention, the present study made the first step in unraveling the diversity of microbiota thriving in underground ice deposits from this cave in correlation with past climatic changes.

AKNOWLEDGMENTS

We thank Christian A. Ciubotărescu, president of the "Sfinx" Speleological Association Garda, and Someş-Tisa River Basin Administration – Apele Române Cluj-Napoca S.A. for technical assistance, as well as the Administration of the Apuseni Natural Park for granting sample collecting permits. This study was financially supported by ANCS-UEFISCDI Romania, grant PN-II-ID-PCE-2011-3-0742 (contract nr. 159/28.10.2011).

REFERENCES

Abyzov, S., Mitskevich, I.N. & M.N. Poglazova, 1998: Microflora of the deep glacier horizons of Central Antarctica.- Microbiology, 67, 66–73.

Boston, P.J., 2004: *Extraterrestrial caves.* In Gunn J. (Ed): *Encyclopedia of Cave and Karst Science*, Fitzroy-Dearborn Publishers, pp. 355-358, London.

Citterio, M., Turri, S., Bini, A. & V. Maggi, 2004: Observed trends in the chemical composition, $\delta^{18}O$ and crystal sizes vs. depth in the first ice core from the LoLc 1650 "Abisso sul Margine dell'Alto Bregai" ice cave (Lecco, Italy).- Theoretical and Applied Karstology, 17, 27–44.

Clesceri, L.S., Greenberg, A.E. & A.D. Eaton, 1999: *Standard Methods for the Examination of Water and Wastewater*. American Public Health Association, American Water Works Association, Water Environment Federation.

Del Giorgio, P.A. & J.M. Gasol, 2008: *Physiological structure and single-cell activity in marine bacterioplankton*.- In: Kirchman D.L. (Ed.) Microbial Ecology of the Oceans, WileyBlackwell, NJ, pp. 243–298, Hoboken.

Dieser, M., Nocker, A., Priscu, J.C. & C.M. Foreman, 2010: Viable microbes in ice: application of molecular assays to McMurdo Dry Valley lake ice communities.- Antarctic Science, 22, 470–476.

Diez, B., Pedros-Alio, C., Marsh, T.L. & R. Massana, 2001: Application of Denaturing Gradient Gel Electrophoresis (DGGE) To Study the Diversity of Marine Picoeukaryotic Assemblages and Comparison of DGGE with Other Molecular Techniques.- Applied Environmental Microbiology, 67, 2942–2951.

Felip, M., Sattler, B., Psenner, R. & J. Catalan, 1995: *Highly-Active Microbial Communities In The Ice And Snow Cover Of High-Mountain Lakes*.- Applied Environmental Microbiology, 61, 2394–2401.

Feurdean, A., Perşoiu, A., Pazdur, A. & B.P. Onac, 2011: Evaluating the Palaeoecological Potential of Pollen Recovered from Ice in Caves: A Case Study from Scarisoara Ice Cave, Romania.- Review of Palaeobotany and Palynology, 165, 1–10.

Holmlund, P., Onac, P.B., Hansson, M., Holmgren, K., Morth, M., Nyman, M. & A. Perşoiu, 2005: Assessing the Palaeoclimate Potential Of Cave Glaciers: The Example Of The Scarisoara Ice Cave (Romania).- Geografiska Annaler Series A-Physical Geography, 87A, 193–201.

Jakosky, B.M., Nealson, K.H., Bakermans, C., Ley, R.E. & M.T. Mellon, 2003: Subfreezing activity of microorganisms and the potential habitability of Mars' polar regions.- Astrobiology, 3, 343–350.

Jungblut, A.D., Lovejoy, C. & W.F. Vincent, 2010: Global distribution of cyanobacterial ecotypes in the cold biosphere.- ISME Journal, 4, 191–202.

Kern, Z., Forizs, I., Nagy, B., Kazmer, M., Gal, A., Szanto, Z., Palcsu, L. & M. Molnar, 2004: Late Holocene Environmental Changes Recorded at Gheţarul de la Focul Viu, Bihor Mountains, Romania.- Theoretical and Applied Karstology, 17, 51–60.

Kerr, R.A., 2010: Planetary science. Liquid water found on Mars, but it's still a hard road for life.- Science, 330, 571.

Lauriol, B., Prevost, C. & D. Lacelle, 2006: The distribution of diatom flora in ice caves of the northern Yukon Territory, Canada: relationship to air circulation and freezing.- International Journal of Speleology, 35, 83–92.

Levin, R.L. & J.L. Weatherwax, 2003: *Liquid water on Mars*, Proc. SPIE (Instruments, Methods, and Missions for Astrobiology), 5163, pp. 145–157.

Luetscher, M., 2005: *Processes in ice caves and their significance for paleoenvironmental reconstruction*, Ph.D. thesis, Swiss Institute for Speleology and karst Studies, Switzerland.

Maggi. V., Turri, S., Perşoiu, A., Bini, A., Onac, B.P., Udisti, R. & B. Stenni, 2011: *Two millennia of ice accumulation in Focul Viu Ice Cave, Romania*.- Geophys. Res. Abs., 13, EGU 2011–10142.

Margesin, R., Schumann, P., Sproer, C. & A.M. Gounot, 2004: Arthrobacter psychrophenolicus sp. nov., isolated from an alpine ice cave.- International Journal of Systematic and Evolutionary Microbiology, 54, 2067–2072.

Miteva, V., Teacher, C., Sowers, T. & J. Brenchley, 2009: Comparison of the microbial diversity at different depths of the GISP2 Greenland ice core in relationship to deposition climates.- Environonmental Microbiology, 11, 640–656.

Morgan-Kiss, R.M., Priscu, J.C., Pocock, T., Gudynaite-Savitch, L. & N.P.A. Huner, 2006: Adaptation and acclimation of photosynthetic microorganisms to permanently cold environments.- Microbiology and Molecular Biology Reviews, 70, 222–252.

Murray, A.E., Kenig, F., Fritsen, C.H., Mckay, C.P., Cawleyd, K.M., Edwards, R., Kuhn, E., Mcknight, D.M., Ostrom, N.E., Peng, V., Poncea, A., Priscu, J.C., Samarkin, V., Townsend, A.T., Wagh, P., Young, S.A., Yung, P.T. & P.T. Doran, 2012: Microbial Life at −13 °C in the Brine of an Ice-Sealed Antarctic Lake.- PNAS, 109, 20626–20631.

Namsaraev, Z., Mano, M.J., Fernandez, R. & A. Wilmotte, 2010: Biogeography of terrestrial cyanobacteria from Antarctic ice-free areas.- Annals of Glaciology, 51, 171–177.

Perşoiu, A. & A. Pazdur, 2011: Ice Genesis and Its Long-Term Mass Balance and Dynamics in Scarisoara Ice Cave, Romania.- The Cryosphere, 5, 45–53.

Perşoiu, A., 2011: *Palaeoclimatic Significance of Perennial Ice Accumulations in Caves: an Example from Scarisoara Ice Cave, Romania*, – PhD. Thesis, University of South Florida, USA, http://scholarcommons.usf.edu/etd/3291.

Perşoiu, A., Onac, B.P., Wynn, J.G., Bojar, A.V. & K.Holmgren, 2011a: Stable isotope behavior during cave ice formation by water freezing in Scarisoara Ice Cave, Romania.- Journal of Geophysical Research, 116, D02111.

Perşoiu, A., Onac, B.P. & I. Perşoiu, 2011b: The Interplay Between Air Temperature And Ice Mass Balance Changes In Scarisoara Ice Cave, Romania.- Acta Carstologica, 40, 445–456.

Pop, E., 1949: *Bacterii nitrificante in pestera dela Scarisoara*.- Buletin Stiintific, 1, 901–907.

Priscu, J.C., Fritsen, C.H., Adams, E.E., Giovannoni, S.J., Paerl, H.W., McKay, C.P., Doran, P.T., Gordon, D.A., Lanoil, B.D. & J.L. Pinckney, 1998: Perennial Antarctic Lake Ice: An Oasis for Life in a Polar Desert.- Science, 280, 2095–2098.

Priscu, J.C., Christner, B.C., Foreman, C.M. & G. Royston-Bishop, 2007: *Biological material in ice cores*. In: Ellias S.A., (Ed), Encyclopedia of Quaternary Science, Elsevier, UK, pp. 1156–1167.

Racovita, E.G., 1927: Observations sur la glaciere naturelle dite "Ghețarul de la Scărișoara"- Buletinul Societatii de Stiinte din Cluj, III, 75–108.

Racovita, G. & M. Serban, 1990: *Interprétation en vue d'une reconstitution paleeoclimatique des particularités structurales et dynamiques du dépôts de glace de la grotte de Scarisoara*.- Studia UBB, Geologia, XXXV, 47–61.

Racovita, G., 1994: *Bilan climatique de la grotte glaciere de Scarisoara, dresse sur dix annees d'observations*.- Trav. de L'Institute de Spéologie "Emil Racovitza", XXXIII, 107–158.

Racovita, G. & B.P. Onac, 2000: *Scarisoara Glacier Cave. Monographic study*. Ed. Carpatica, pp. 1–140.

Rampelotto, P.H., 2010: Resistance of microorganisms to extreme environmental conditions and its contribution to astrobiology – Sustainability, 2, 1602–1623.

Rehakova, K., Stibal, M. & J. Rehak, 2010: Survival and colonisation potential of photoautotrophic microorganisms within a glacierized catchment on Svalbard, High Arctic.- Polar Biology, 33, 737–745.

Rippka, R., Deruelles, J., Waterbur, J.B., Herdman, M. & Stanier, R.Y., 1979: Generic assignments, strain histories and properties of pure cultures of cyanobacteria.- Journal of General Microbiology, 111, 1–61.

Roling, W.F.M., Van Breukelen, B.M., Braster, M., Lin, B. & H.W. Van Verseveld, 2001: Relationships between Microbial Community Structure and Hydrochemistry in a Landfill Leachate-Polluted Aquifer.- Applied Environmental Microbiology, 67, 4619–4629

Sambrook, J. & D.W. Russell D.W., 2001*: Molecular Cloning, a Laboratory Manual*. Cold Spring Harbor Laboratory Press, Cold Spring Harbor, NY.

Sarchizian, I. & Ardelean, I.I., 2012: Frequency of dividing cells and growth rates in population of filamentous cyanobacteria isolated from sulphurous mesothermal spring Obanul Mare (Mangalia).- In 12th *International Multidisciplinary Scientific GeoConference & EXPO SGEM 2012,* June 17–23, 2012, 423–430, Albena.

Tscherko, D., Rustemeier, J., Richter, A., Wanek, W. & E. Kandeler, 2003: Functional diversity of the soil microflora in primary succession across two glacier forelands in the Central Alps.- European Journal of Soil Science, 54, 685–696.

Uetake, J., Naganuma, T., Hebsgaard, M.B., Kanda, H., & S. Kohshima, 2010: Communities of algae and cyanobacteria on glaciers in west Greenland.- Polar Science, 4, 71–80.

Varin, T., Lovejoy, C., Jungblut, A.D., Vincent, W.F. & J. Corbeiladin, 2010: Metagenomic profiling of Arctic microbial mat communities as nutrient scavenging and recycling systems.- Limnology and Oceanography, 55, 1901–1911.

Vincent, W.F, 2007: Cold tolerance in cyanobacteria and life in the cryosphere.- In: J. Seckbach (ed.), *Algae and Cyanobacteria in Extreme Environments*, Springer. Pp. 287–301.

Xiang, S., Yao, T., An, L., Xu, B. & J. Wang, 2005: 16S rRNA sequences and differences in bacteria isolated from the Muztag Ata glacier at increasing depths.- Applied Environmental Microbiology, 71, 4619–4627.

Yonge, C. J. & W. D. MacDonald, 1999: The potential of perennial cave ice in isotope palaeoclimatology.- Boreas, 28, 357–362.

Zak, K., Onac, B.P. & A. Perşoiu, 2008: Cryogenic carbonates in cave environments: a review.- Quaternary International, 187, 84–96.

Zhang S., Hou, S., Ma, X., Qin, D. & T. Chen, 2006: Culturable bacteria in Himalayan ice in response to atmospheric circulation.- Biogeosciences Discussions, 3, 765–778.

Williams, K.E., McKay, C.P., Toon, O.B. & J.W. Head, 2010: Do ice caves exist on Mars?- Icarus, 209, 358–368.

COBISS: 1.01

SURVIVAL OF THE EPIGEAN DENDRODRILUS RUBIDUS TENUIS (OLIGOCHAETA: LUMBRICIDAE) IN A SUBTERRANEAN ENVIRONMENT

PREŽIVETJE POVRŠINSKEGA DEŽEVNIKA DENDRODRILUS RUBIDUS TENUIS (OLIGOCHAETA: LUMBRICIDAE) V PODZEMELJSKEM OKOLJU

Tone NOVAK[1 *], Csaba CSUZDI[2], Franc JANŽEKOVIČ[1], Tanja PIPAN[3,5], Dušan DEVETAK[1] & Saša LIPOVŠEK[1, 4]

Abstract UDC 595.142:551.442(497.4Huda luknja)

Tone Novak, Csaba Csuzdi, Franc Janžekovič, Tanja Pipan, Dušan Devetak & Saša Lipovšek: Survival of the epigean Dendrodrilus rubidus tenuis (Oligochaeta: Lumbricidae) in a subterranean environment

The peregrine earthworm *Dendrodrilus rubidus tenuis* was regularly sampled in a percolating water drip originating in a habitat inaccessible to humans in the Huda luknja pri Doliču cave, Slovenia. The reconstruction of this habitat includes both a larger passage with bat colonies supplying wet bat guano sediments, on which the earthworms feed, and narrow channels, which drain water from this passage into the sampling drip. Fresh guano is deposited in autumn shortly before the earthworms become inactive. Then, it is exploited by moulds and additionally depleted by water washing out the nutrients before the earthworms reactivate in spring. Thus, this is a rather poor food resource for the earthworms. Despite this, and apart from their short size and delayed maturation, no other disturbance or damage was found caused by malnutrition, which was confirmed in individuals submitted to starvation in captivity. We suggest that *Dd. r. tenuis,* which shows neither disturbance from nor adaptation to living in a subterranean environment, can subsist there because of its euryoecious character. Nevertheless, in temperate climates, this is rather a harsh habitat for this earthworm.

Keywords: dripping water, earthworms, karstic cave.

Izvleček UDK 595.142:551.442(497.4Huda luknja)

Tone Novak, Csaba Csuzdi, Franc Janžekovič, Tanja Pipan, Dušan Devetak & Saša Lipovšek: Preživetje površinskega deževnika Dendrodrilus rubidus tenuis (Oligochaeta: Lumbricidae) v podzemeljskem okolju

V vzorcih curka prenikajoče vode v Hudi luknji pri Doliču je bila peregrina vrsta deževnika *Dendrodrilus rubidus tenuis* redno prisotna. Curek doteka iz neznanega, človeku nedostopnega habitata. Na osnovi zbranih podatkov sklepamo, da sestoji ta habitat iz dveh habitatnih tipov. Prvi je večji rov s kolonijami netopirjev, ki proizvajajo gvano, s katerim se deževniki hranijo. Drugi je sistem ozkih kanalov, po katerih odteka voda iz tega rova v vzorčevani curek. Netopirji proizvedejo sveže gvano jeseni, malo preden deževniki prenehajo z aktivnostjo. Nato gvano izkoristijo plesni, dodatno se osiromaši zaradi kapljajoče vode, ki iz njega izpere nutriente, preden se spomladi deževniki reaktivirajo. To je torej zanje dokaj reven vir hrane. Kljub temu razen njihove kratke dolžine in poznega spolnega dozorevanja ne kažejo nobene motnje ali poškodbe, ki bi bile posledica slabe prehrane; enako smo ugotovili pri osebkih v ujetništvu. Predlagamo razlago, da lahko *Dd. r. tenuis,* ki ne kaže niti motenj niti prilagoditev na življenje v podzemeljskem okolju, tam preživi zaradi svojega evriekega značaja. Kljub temu so razmere v podzemeljskem okolju v območjih z zmernim podnebjem za to vrsto dokaj ostre.

Ključne besede: deževniki, kraška jama, prenikajoča voda.

[1] Department of Biology, Faculty of Natural Sciences and Mathematics, University of Maribor, Koroška cesta 160, SI-2000 Maribor, Slovenia, e-mail: tone.novak@um.si; franc.janzekovic@um.si; dusan.devetak@um.si

[2] H-2081 Piliscsaba, Kenderesi str. 13, Hungary, e-mail: csuzdi01@gmail.com

[3] Karst Research Institute, Scientific Research Centre of the Slovenian Academy of Sciences and Arts, Titov trg 2, SI-6230 Postojna, Slovenia, e-mail: pipan@zrc-sazu.si

[4] Medical Faculty, University of Maribor, Taborska ulica 8, SI-2000 Maribor, Slovenia, e-mail: sasa.lipovsek@uni-mb.si

[5] University of Nova Gorica, Vipavska 13, Rožna dolina, SI-5000 Nova Gorica, Slovenia

Received/Prejeto: 11.03.2013

INTRODUCTION

A dozen lumbricid species have been reported exclusively from caves, such as *Allolobophora cryptocystis* Černosvitov, 1935, *Helodrilus kratochvili* (Černosvitov, 1935), and *H. mozsaryorum* (Zicsi, 1974), mostly as single finds. Some have later been recognized as accidental individuals of epigean species (Černosvitov 1939, Pop 1968, Zicsi 1974, Dumnicka & Juberthie 1994). In central and northern Slovenia, 17 lumbricid species and one subspecies have been occasionally recorded in caves and artificial tunnels (Mršić 1990a, 1990b; Novak 2005). These are *Allolobophora leoni* (Michaelsen, 1891), *Aporrectodea rosea* (Savigny, 1826), *Ap. smaragdina* (Rosa, 1892), *Dendrobaena byblica* (Rosa, 1893), *D. octaedra* (Savigny, 1826), *Dendrodrilus r. rubidus* (Savigny, 1826), *Dd. r. tenuis* (Eisen, 1874), *Eisenia lucens* (Waga, 1857), *E. spelaea* (Rosa, 1901), *Eiseniella t. tetraedra* (Savigny, 1826), *Lumbricus castaneus* (Savigny, 1826), *L. r. rubellus* Hoffmeister, 1843, *Octodrilus transpadanus* (Rosa, 1884), *O. meroandricus* Mršić, 1985, *Octodriloides kamnensis* (Baldasseroni, 1919), *O. zupancici* Mršić, 1987, *Octolasion l. lacteum* (Örley, 1881) and *Proctodrilus antipae* (Michaelsen, 1891). Zicsi (1974) declared *H. mozsaryorum* from the famous Hungarian cave Baradla to be a troglobiotic aquatic species, although he did not exclude the possibility of its finding in surface habitat in the future. However, despite the intensive research carried out in the Aggtelek karstic region, *H. mozsaryorum* has not been found in surface habitats; therefore, the troglobiotic nature of this species was later corroborated (Zicsi *et al.* 1999). Beside this species, no other exclusively cavernicolous lumbricid earthworm is known so far (Dumnicka *in lit.*).

Hypogean communities of epigean earthworm species can always be found in caves among accumulations of various types of organic matter, like torrential deposits and the sediments of underground watercourses and guano (Dumnicka & Juberthie 1994; Sambugar & Sket 2004; Dumnicka 2005). After the discovery of the importance of epikarst for subterranean biota (Pipan 2005), intensive investigations of this habitat started in Slovenia and the USA (Pipan *et al.* 2006, 2008; Pipan & Culver 2005, 2007a, 2007b; Culver & Pipan 2008, 2014). During similar investigation of the fauna in percolating water drips in a cave in northern Slovenia, we found a viable population of *Dendrodrilus rubidus tenuis* (Lumbricids in Pipan *et al.* 2008). Cave-dwelling, troglophile populations of this species have also been reported from other caves (McAlpine & Reynolds 1977; Reeves *et al.* 1999). Our present scope is to analyze the main parameters allowing this epigean earthworm species to survive in a subterranean habitat, and to reconstruct the environmental features of this hypogean habitat inaccessible to humans. For this purpose, we considered both the dripping water data, and the physical condition of the *Dendrodrilus* specimens found in the drip. We hypothesized a rich food resource supply in the habitat, which is crucial for the survival of the earthworms.

MATERIAL AND METHODS

Systematic monthly sampling of water from 12 trickles was carried out in the Medvedji rov passage in the Huda luknja pri Doliču cave (Fig. 1; entrance 46°24′53″ N, 15°10′44″ E, altitude 508 m) from November 2005 till October 2006 (details in Pipan *et al.* 2008). These trickles provided different types of percolating water: a tiny permanent current (min ca. 0.5 dL day^{-1}), constant dripping water (0.05–0.2 dL sec^{-1}) and drips immediately reacting to precipitation (up to 1.5 dL sec^{-1}). Water drips were collected using a funnel 30 cm in diameter into a 15 cm high container of 10 cm diameter, with side overflow holes covered with net (mesh size 60 μm) to retain the animals and solid particles. The water temperature was measured in situ; concentrations of Na^+, K^+, Ca^{2+}, Mg^{2+}, Cl^-, NO_3^- and SO_4^{2-} ions as well as Ca- and total hardness, and conductivity were determined using Standard Methods for the Examination of Water and Wastewater (1989) in the laboratory. The samples of fauna were fixed *in situ* with formaldehyde to a final concentration of 2–3 %. After extraction, the organisms were stored in 70 % ethanol. To provide further information on earthworms, each bat guano accumulation in the cave and the "lumbricid-trickle" in control were additionally inspected for lumbricids 14 times between 2006 and 2009. The fauna of the small water pools formed in guano piles by trickling water was sampled using a spoon.

For light microscopy, three earthworms were treated immediately with gut contents intact, and two were kept alive on a water-gelatine gel, analogous to the water-agar gel method (Pokarzhevskii *et al.* 2000), for four days at 8 °C until the gut content was voided. The earthworms were fixed in 2.45 % glutaraldehyde and

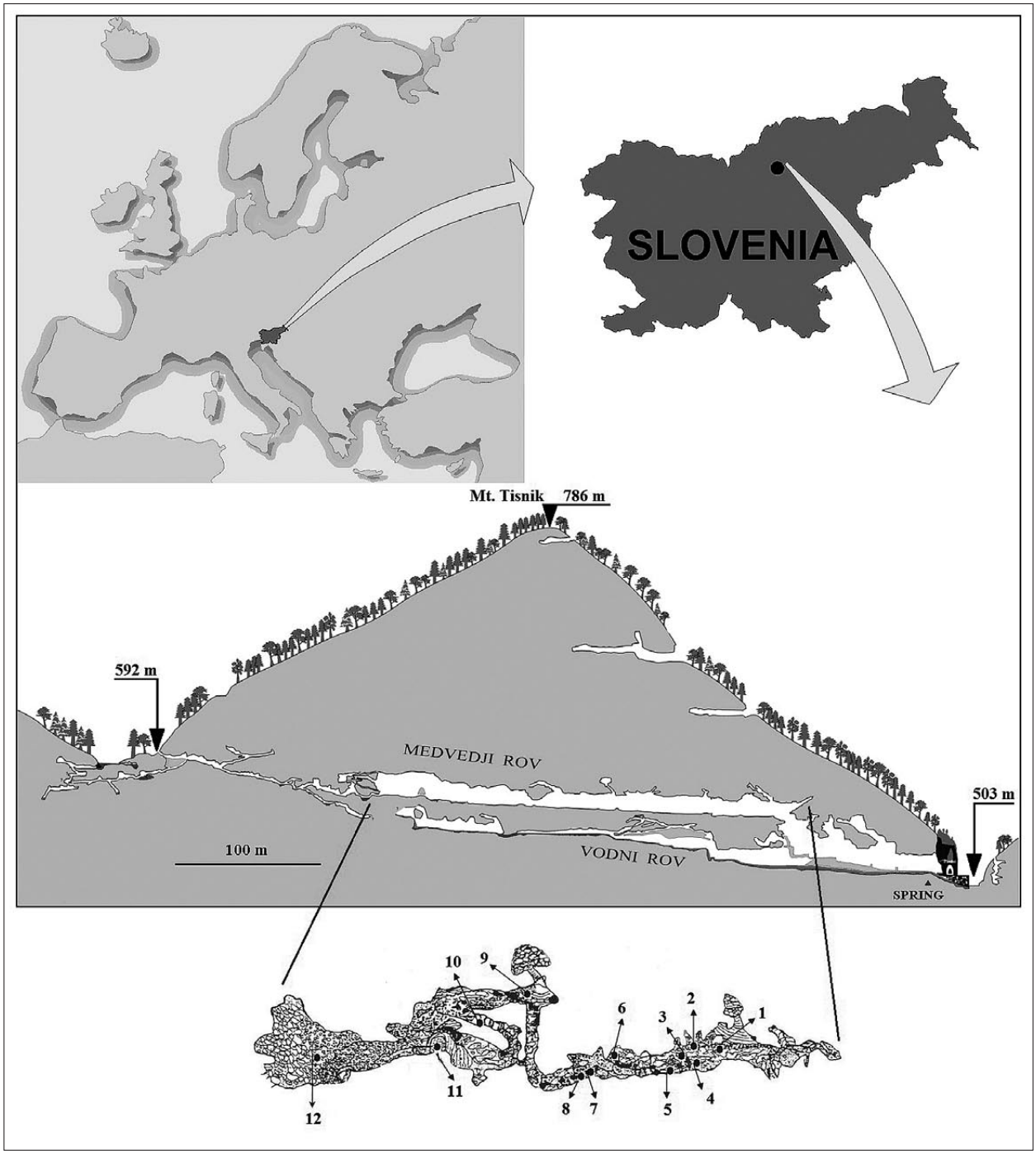

Fig. 1: Geographical location and the longitudinal section of the Huda luknja cave system with the ground plan of the Medvedji rov passage; from Pipan et al. (2008), partly modified. Courtesy Acta Carsologica.

2.45 % paraformaldehyde in a 0.1 M sodium cacodylate buffer (pH 7.3), at room temperature for 3 hrs, and at 4 °C for 12 hrs. The samples were washed in a 0.1 M sodium cacodylate buffer (pH 7.3), at room temperature for 3 hrs, postfixed with 2 % OsO_4, at room temperature for 2 hrs and dehydrated in a graded series of ethanol (50, 70, 90, 96, 100 %, each for 30 min at room temperature). Tissue samples were embedded in TAAB epoxy resin (Agar Scientific Ltd., Essex, England). Semi-thin sections (5 µm) were cut and stained with 0.5 % tolui-

dine blue in aqueous solution. After staining, the tissue was analyzed with a Nikon Eclipse E800 microscope. 22 individuals were measured for their length, width and number of segments.

Additionally, from February 26th till June 25th 2007, seven earthworms were kept in a refrigerator at 8 °C to provide information about their behavior. The specimens were kept in a 1.5 dL vessel with 2 cm deep water from the trickle, and with a piece of folded toilet paper, half of it projecting above the water surface. No food was added. The worms were inspected once a week (14 observations in total) for their placement selection in or outside the water, and their gregariousness, controlling at the same time their condition to cease the observation immediately, if any sign of disturbance would appear.

Descriptive statistics was used to evaluate the physical and chemical characteristics of the drips, as well as the main morphological characteristics of the worms. A t-test for independent samples was used in testing the differences between the drip with and those without *Dendrodrilus* for each physical and chemical parameter (Legendre & Legendre 2012). The program SPSS 21.0 for Windows was used in the statistical procedures.

RESULTS

During one-year monthly sampling, we found *Dendrodrilus* specimens in only one of the 12 trickles sampled (No. 3 in Fig. 1) from April till October with an abundance peak in June, while they were absent during winter. Trickle No. 3 (hereinafter *Dendrodrilus* drip) and two other trickles (No. 6, 10) had similar permanent discharge slightly varying throughout the year (ca. 0.05–0.1 dL sec^{-1}), but they differed in other parameters (details in Pipan *et al.* 2008). Ca- and total hardness (TH), and conductivity (con.) in the *Dendrodrilus* drip were constantly significantly higher with respect to other drips (Ca: t=16.10, TH: t=17.49, con.: t=6.33, df=276, p<0.0001) (Fig. 2) in every month of the worm's activity in the hypogean habitat. In other parameters these differences either alternated between the *Dendrodrilus* drip and the other drips (temperature, K^+, Ca^{2+}, SO_4^{2-}), or did not differ significantly (pH, Na^+, Mg^{2+}). Besides, in the *Dendrodrilus* drip, NO_3^- values drastically increased from August till October, and Cl^- values in September and October (Fig. 2); these values were both significantly different from the other drips (NO_3^- t=4.84, Cl^- t=4.61, df=276, p<0.0001).

In the relatively pure water collected in the vessel during continuous percolation, all specimens were alive. During dry periods, a few of them died because the water in the vessel was polluted with fresh bat droppings. Those earthworms that escaped and crawled up the vessel walls above the water survived. After 2006 we collected nine juveniles from the *Dendrodrilus* drip. On May 16, 2009, for the first time, two individuals–one of them adult–were found in a little pool eroded by trickling water in a guano pile a few meters from the trickle, and one juvenile was observed on June 17, 2009 (Fig. 3). Only in this guano accumulation *Dendrodrilus* were found.

In the trickle, 22 individuals measured 15.0±1.7 (12.1–17.0) mm in length and were 1.8±0.2 (1.6–2.0) mm wide, counting 96 (79–105) segments. The adult worm found on 29.5.2007 was 28.0 mm long and had 99 segments.

In the refrigerator, all specimens crept into the submerged, tightly folded paper and were permanently crowded together, with the exception of one or two individuals 1–3 cm away. Whenever the paper was turned upside down, i.e., the immersed earthworms were turned to the air, they crawled into the lower, immersed folds within a minute. While stretching parts of their body, the earthworms elongated these parts 4–5-times their entire length and became correspondingly thinner. They fed on the paper, and all survived four months without any evident disturbance or damage. All specimens were fully fed and of normal appearance with simple, low and wide typhlosole (Fig. 4).

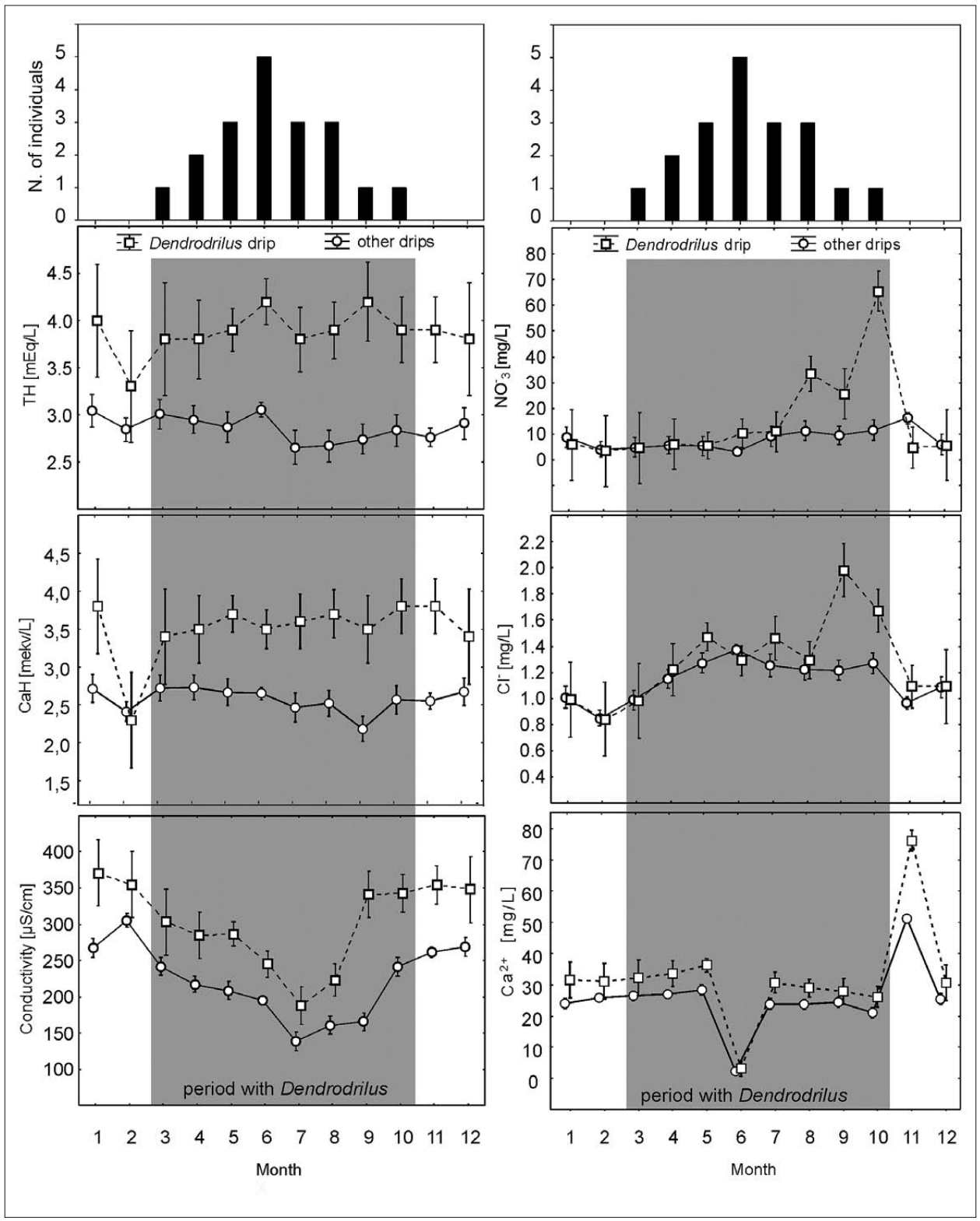

Fig. 2: Total (TH) and calcium hardness (CaH), conductivity, nitrate (NO_3^-), chloride (Cl^-) and calcium (Ca^{2+}) in the Dendrodrilus *drip vs. other drips.*

Fig. 3: Pits made by dripping water in a bat guano pile, where an adult Dendrodrilus rubidus tenuis *was found.*

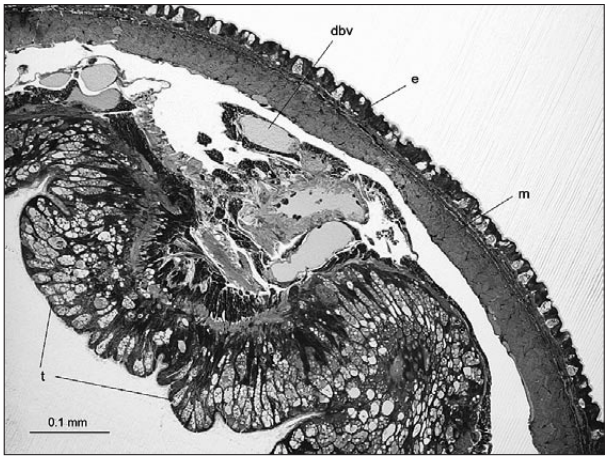

Fig. 4: Dendrodrilus rubidus tenuis, *typhlosole in the 40th segment of a representative specimen. e epidermis, m longitudinal muscle layer, dbv dorsal blood vesel, t typhlosole.*

DISCUSSION

Individuals of *Dd. r. tenuis* retrieved from the dripping water had drifted there from an unknown subterranean habitat above the sampling passage. This terrestrial species most likely preferred a substrate soaked with water. According to chemical analysis of the trickling water, this habitat has two specific properties that are distinct from the other seeps without earthworms. First, it is supplied by annually fluctuating, large quantities of fresh organic matter, the volume of which starts to rise in August, culminating in October. This is evident from the NO_3^- and Cl^- increases, which perfectly match the defecation and urination patterns of the progressively enlarging colony of the Bent-wing Bat, *Miniopterus schreibersii* (Kuhl, 1817), up to 2000 individuals. Most of these bats then suddenly moved to an unknown passage to overwinter and roost; most probably, the trickling water flows from there. Second, the particular drip is characterized by the highest values of Ca- and total hardness as well as conductivity. There could be a few reasons for higher values: 1. Water flowing from the sites with overwintering bats passes through narrow spaces with relatively high CO_2 pressure, which in turn enhances the water's dissolving capacity. 2. Longer residence time of the water caught underground for a long period in contact with the limestone bedrock provided higher saturation state, and hence higher values of both hardnesses and conductivity. 3. Presence of other ions such as Cl^- and NO_3^- caused higher equilibrium and consequently higher conductivity. Any of these or their combination could be the reason.

Theoretically, the hypogean characteristics of lumbricid species in carbonate rocks are their small size and a reduction in a number of organs, like testicles, spermathecae etc. (Dumnicka 1986; Dumnicka & Juberthie 1994), the hindrance or reduction of reproductive seasonality and its internal regulation (Rozen 2006), and, presumably, intensive activity of the calciferous glands (Robertson 1936, Canti & Pearce 2003). However, in this case, the reduction of the genital organs could also be due to the well-known parthenogenetic reproduction of *Dd. r. tenuis*. Besides, as a consequence of feeding on poor food resources, more extensive branching of the typhlosole may be expected in specialized hypogean species. Since fresh guano was deposited in the period when *Dendrodrilus* were carrying out their annual activity, they were able to exploit this resource to a limited extent. Later, the guano was exploited by moulds, while percolating water additionally washed out soluble compounds, leaving behind an energy-poor resource for the earthworms in spring. In this population of *Dd. r. tenuis*, small size and the large ratio of immature individuals are considered the direct consequence of malnutrition caused by such impoverishment of the substrate, while no hindrance in development, enlargement of the typhlosole and malformation of or damage to other organs was noticed. Moreover, surviving a four-month period of starvation in captivity without damage demonstrates that *Dd. r. tenuis* – reported to inhabit litter and organically enriched surface soil layers (Hendrix & Bohlen 2002) – is well adapted to poor food resources,

as well. Additionally, the capacity for extreme elongation and narrowing may be an adaptation for living in systems consisting of narrow spaces, as can be expected in the rhizosphere and epikarst (Culver & Pipan 2009; Novak *et al.* 2012), or might be an adaptation to exploit more efficiently the water-solved oxygen. Their ability to crawl out of the water demonstrates that *Dd. r. tenuis* can leave an inappropriate habitat, and search for an appropriate microhabitat. Adult *Dd. r. tenuis* do not survive temperatures below 0 °C and do not overwinter in cold climates (Berman *et al.* 2010), while the adult found in May suggests that the species may overwinter in hypogean habitats. This is likely to be the case in Central Europe, where earthworms overwinter deeper in the soil. It is thus either death or overwintering that caused their absence from the samples during winter. All these denote that *Dd. r. tenuis* is a euryoecious rather than a specialized species, which helps in an understanding of its invasive character (cf. Global Invasive Species Database).

CONCLUSIONS

Most likely, the reconstruction of this sampling site with *Dendrodrilus rubidus tenuis* is as follows: an undiscovered passage with bat guano accumulation somewhere above this particular passage is settled by the earthworms, from where water passes through narrow channels and drips into the passage under investigation. The narrow channels with percolating water function as merely a connecting habitat between the spacious habitat providing the guano and the sampling site in the gallery being investigated. *Dendrodrilus* shows a high tolerance to such energy-poor food resource, but no special adaptation to or damage from living in a subterranean habitat. Although this represents rather a harsh habitat for these earthworms, they can survive in such habitats with bat guano deposits and a permanent water supply.

ACKNOWLEDGEMENTS

We are indebted to the staff of the chemical laboratory of the Šoštanj Steam Power Station where the chemical analyses were carried out, especially to Mrs. G. Srnovršnik. We are grateful to V. Navodnik, V. Ocvirk and L. Slana Novak who helped with the field work, and to the cavers of the Speleos–Siga Cavers' Club in Velenje for the support in the investigations. We sincerely thank two anonymous referees for insightful comments and suggestions, and Michelle Gadpaille for valuable improvements to the language. The study was partly supported by the Slovenian Research Agency within the Biodiversity Research Programme (P1-0078).

REFERENCES

Berman, D.I., Meshcheryakova, E.N. & A.N. Leirikh, 2010: Egg cocoons of the earthworm *Dendrodrilus rubidus tenuis* (Lumbricidae, Oligochaeta) withstand the temperature of liquid nitrogen.- Doklady Biological Sciences 434, 347–350.

Canti, M.G. & T.G. Pearce, 2003: Morphology and dynamics of calcium carbonate granules produced by different earthworm species.- Pedobiologia 47, 511–521.

Culver, D.C. & T. Pipan, 2008: Superficial subterranean habitats – gateway to the subterranean realm?- Cave and Karst Science 35, 5–12.

Culver, D.C. & T. Pipan, 2009: *The Biology of Caves and Other Subterranean Habitats*. Oxford University Press, 256 pp., Oxford, New York.

Culver, D.C. & T. Pipan, 2014: *Shallow Subterranean Habitats*. Oxford University Press, 258 pp., Oxford, New York.

Černosvitov, I., 1939: Etudes biospéologiques – X(1). Catalogue des Oligochètes hypogés.- Buletin du Museum Royal de Histoire Naturelle de Belgique 15, 1–92.

Dumnicka, E., 1986: Naididae (Oligochaeta) from subterranean waters of West Indian Islands; distribution, taxonomic remarks and description of a new species.- Bijdrage Dierk 6, 267–281.

Dumnicka, E., 2005: Worms.- In: Culver, D. C. & W. B. White (eds.): *Encyclopaedia of Caves*. Elsevier, pp. 614–618.

Dumnicka, E. & C. Juberthie, 1994: Aphanoneura et Oligochaeta.- In: Juberthie, C. & V. Decu (eds.), *Encyclopaedia biospeologica*, pp. 67–75, Société de Biospéologie, Moulis – Bucarest.

Global Invasive Species Database-[Online] Available from: http://www.issg.org/database/welcome/ [Accessed 3rd June 2014.]

Hendrix, F.P. & P.J. Bohlen, 2002: Exotic Earthworm Invasions in North America: Ecological and Policy Implications.- BioScience 52, 801–809.

Legendre, P. & J. Legendre, 2012: Numerical Ecology. Elsevier, 990 pp., Amsterdam.

McAlpine, D.F. & J.W. Reynolds, 1977: Terrestrial Oligochaeta of some New Brunswick Caves with remarks on their ecology.- Canadina Field-Naturalist 91, 360–366.

Mršić, N., 1991a: *Monograph on earthworms (Lumbricidae) of the Balkans I.* Opera SAZU 31, pp. 1–355, Ljubljana.

Mršić, N., 1991b: *Monograph on earthworms (Lumbricidae) of the Balkans II.* Opera SAZU 31, pp. 356–757, Ljubljana.

Novak, T., 2005: Terrestrial fauna from cavities in northern and central Slovenia, and a review of systematically ecologically investigated cavities.- Acta Carsologica 34,169–210.

Novak, T., Perc, M., Lipovšek, S. & F. Janžekovič, 2012: Duality of terrestrial subterranean fauna.- International Journal of Speleology 41, 181–188.

Pipan, T., 2005: *Epikarst – a promising habitat*.- Carsologica, Založba ZRC SAZU, 101 pp., Ljubljana,

Pipan, T., Blejec, A. & A. Brancelj, 2006: Multivariate analysis of copepod assemblages in epikarstic waters of some Slovenian caves.- Hydrobiologia 559, 213–223.

Pipan, T. & D.C. Culver, 2005: Estimating biodiversity in the epikarstic zone of a West Virginia cave.- Journal of Cave and Karst Studies 67, 103–109.

Pipan, T. & D.C. Culver, 2007a: Copepod distribution as an indicator of epikarst system connectivity.- Hydrogeology Journal 15, 817–822.

Pipan, T. & D.C. Culver, 2007b: Regional species richness in an obligate subterranean dwelling fauna – epikarst copepods.- Journal of Biogeography 34, 854–861.

Pipan, T., Navodnik, V., Janžekovič, F. & T. Novak, 2008: Studies of the fauna of percolation water of Huda luknja, a cave in isolated karst in Northeast Slovenia.- Acta Carsologica 37, 141–151.

Pokarzhevskii, A.D., Van Straalen, N.M. & A.M. Semenov, 2000: Agar as a medium for removing soil from earthworm guts.- Soil Biology & Biochemistry 32, 1315–1317.

Pop, V., 1968: Les Lumbricides cavernicoles de la Collection Biospeologica.- Archives de Zoologie Éxperimentale et Générale 109, 229–256.

Reeves, W., Reynolds, K., & J. Warren, 1999: New records of cave-dwelling earthworms (Oligochaeta: Lumbricidae, Megascolecidae and Naididae) and other annelids (Aeolosomatida, Branchiobdellida and Hirudinea) in the Southeastern United States, with notes on their ecology.- Megadrilogica 7, 65–71.

Robertson, J.D., 1996: The function of the calciferous glands of earthworms.- Journal of Experimental Biology 13, 279–297.

Rozen, A., 2006: Internal regulation of reproduction seasonality in earthworm *Dendrobaena octaedra* (Savigny, 1826) (Lumbricidae, Oligochaeta).- Soil Biology & Biochemistry 38, 180–182.

Sambugar, B. & B. Sket, 2004: Annelida.- In: Gunn, J. (ed.), *Encyclopaedia of Caves and Karst Science*, pp. 66–68, Taylor & Francis.

SPSS 21.0 for Windows.

Standard Methods for the Examination of Water and Wastewater, 17th ed., APHA-AWWA-WPCF (1989), 1088 pp.

Zicsi, A., 1974: Ein neuer Höhlen-Regenwurm (Oligochaeta: Lumbricidae) aus Ungarn.- Acta zoologica Academiae Scientiorum Hungaricae 20, 227–232.

Zicsi, A., Dózse-Farkas, K. & Cs. Csuzdi, 1999: Terrestrial Oligochaetes of the Aggtelek National Park.- In: Mahunka, S. (ed.): *The Fauna of the Aggtelek National Park*, Hungarian Natural History Museum, pp. 39–43, Budapest.

DAVID C. CULVER AND TANJA PIPAN: SHALLOW SUBTERRANEAN HABITATS. ECOLOGY, EVOLUTION AND CONSERVATION

Oxford University Press, 2014, 1st Impression, pp. 258.

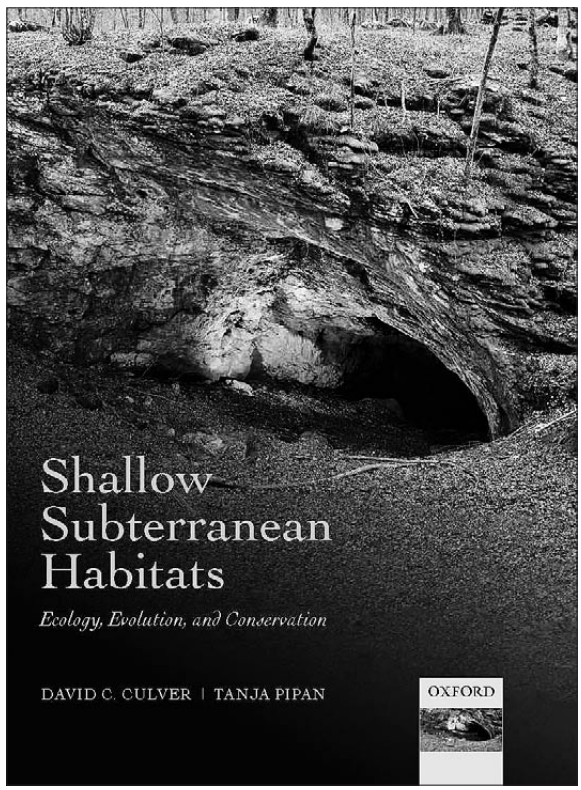

Five years after publishing their book *The Biology of Caves and Other Subterranean Habitats* (Oxford University Press, 2009), the Authors offer up the first modern review of the shallow, previously called superficial, subterranean habitats (SSHs). These habitats are pragmatically determined as a group of aphotic and partly twilight habitats down to 10 m below the surface. Their diameter most usually does not exceed 10 cm, or 10 m in the case of lava tubes. Particular SSHs are characterized for their particular combination of the environmental circumstances and biota. The Authors distinguish between strict sense and broad sense SSHs. These include hypotelminorheic habitat with their supplying seepage springs, epikarst, shallow calcrate aquifers, intermediate-sized terrestrial and aquatic SSHs, soil and lava tubes. In the 16 chapters, the Authors discuss the SSHs referring to 550 papers and make careful conclusions. They explain that SSHs appear in either karstic regions, yielding about 15 % of the earth's surface or non-karstic areas, or in both. All these habitats interact with the surface, with the possible exception of the calcrate aquifers, and harbor, among others, the troglobiotic species.

The hypotelminorheic habitats, typically up to half a meter deep, are considered the shallowest aquatic SSHs. The epikarst, yielding about 12.5 % of the earth's surface, constitutes a soil–rock interface and provides highly dynamic species distributions. The intermediate-sized terrestrial SSHs–consisted of spaces of up to about 10 cm–are screes and taluses, milieu souterrain superficiel (MSS), shallow fissured rock and lava clinker, each of them with a specific combination of the environmental conditions. The aquatic interstitial SSHs comprise lake bottoms, hyporheic and parafluvial areas, which represent a lotic ecotone between the main water body and the ground water. The calcrate aquifers are distinctive of deserts and specific for their salinity and patchy, isolated distribution. Soils are discussed as a type of SSH, because they host a range of troglomorphic species. Lava tubes are special for their proximity with the surface and, in many of them, roots as the main source of food. Besides, short caves and any cave entrances are ecotones between

the surface and deep subterranean habitats. The Authors exhaustively discuss similarities and differences between the treated habitats with respect to all of these features. Somehow travertine escaped the Authors' attention. This chemically-precipitated porous limestone habitat is an ecotone between surface, mostly current water, and a vadose or occasionally shallow phreatic environment (Pentecost 2005). It is known to harbor also troglomorphic taxa at least in North America (*Caecidotea stygia*; Pentecost 2005) and Slovenia (*Iglica* and *Paladilhiopsis* species were found by the malacologist France Velkovrh).

The Authors systematically deal with many aspects of the SSHs: their geographic distribution and morphology, variation, hydrology, geology, habitat chemical and physical characteristics and dynamics. As for fauna, they deal with ecology, and morphological characteristics of animals, species diversity, richness and distributions, principles of colonization and adaptation to the subterranean environment, convergent and divergent evolution and speciation rates, phylogeny, roles of the environmental factors (light, physical factors, organic carbon, nutrients, environmental fluctuations and stresses) on biota, circadian and annual cycles as response to environmental cyclicity, convergent and divergent selective pressures, the body and appendages size and shape in relation to (micro)habitat properties, and conservation and protection problems. The Authors expose fields of highly incomplete knowledge and appeal to research these gaps. All these are based on a variety of case studies exposing puzzling facts and terminological inconsistencies as well.

Briefly, this book is the first overall review of the shallow subterranean habitats. Information on travertine is expected if the book reprints, and one would welcome a more detailed presentation of the seashore interstitial habitats and a discussion of possible SSH ecosystem services. Three points are refreshing in the ecology and biology of the subterranean habitats: the inclusion of soils into the SSHs and the debate on troglomorphy and terminology. The Authors argue that the rotten bedrock soil horizon, i. e., the regolith, and spaces in rhizosphere are often inhabited by troglobionts. Further they explain that troglomorphic characteristics may evolve in the subterranean as well as in any other totally dark and twilight habitat, like leaf litter. Finally, they appeal to return to use a general evolutionary terminology. This book is strongly recommended to anybody, especially biologists and ecologists, dealing with any point of the aquatic or terrestrial habitats, rocks and soils down to the depth of 10 m. And, who doesn't?

Tone Novak

Pentecost, A., 2005: *Travertine*.-Springer-Verlag, Berlin, Heidelberg, pp. 445.

DOUGLAS W. KIRKLAND: ROLE OF HYDROGEN SULFIDE IN THE FORMATION OF CAVE AND KARST PHENOMENA IN THE GUADALUPE MOUNTAINS AND WESTERN DELAWARE BASIN, NEW MEXICO AND TEXAS

National Cave and Karst Research Institute. Special Paper 2, (2 un-numbered pages) + vii + 77pp., National Cave and Karst Research Institute, Carlsbad NM, 2014.

In the Foreword to this A4-format paperback book the Managing Editor, Lewis Land, notes that, "*… this publication will serve as an important source book and milestone for future research in the Delaware Basin region for many years to come.*" The present reviewer is of the opinion that the book is much more. As with the first edition of the NCKRI Special Paper (Alexander Klimchouk: Hypogene Speleogenesis: Hydrogelogical and Morphogenetic Perspective.), the current one presents a milestone in the general development of ideas related to speleogenesis. If twentieth-century karst science examined the karst from three slightly different viewpoints, i.e. karst hydrogeology, speleology and karst geomorphology, Kirkland's present work introduces novel aspects, which return to the basics of general sedimentology and (bio)geochemistry in a broad sense The actual state of the karst underground in the studied area is not merely a "karstified (whatever that expression might mean) rocky mass" but an obvious stage in the diagenesis of the carbonate-sulphate-halite body that, during geological time, has been exposed to both hypogene and epigene water. Individual caves are scarcely mentioned – the focus remains upon development in the "Cave Belt" as a whole and its geoenvironment.

Kirkland's work is the *dénouement* of almost 20 years of research in south-eastern New Mexico and western Texas, at the same time summarizing, discussing and incorporating decades of research by previous workers combined with his new ideas. Though sulfide speleogenesis remains the central point of concern, development of the parent rocks (from sedimentation up until the present), including local tectonic effects, had to be broadly considered. From this point of view the book presents an example of how different branches of the earth sciences should be involved in physical karst science studies in the future. The study was made more challenging by the area's unusual geological history, particularly the complex history of diagenesis; undoubtedly those with a grounding in modern oil geology will find the text easier to understand.

The book's contents are arranged into three sections, covering the main foci of the research. Its scientific core is preceded by, *Foreword, Contents List of Figures* (63 in total), and *Abstract*. At the end are *Summary and Conclusions*, *Acknowledgments*, and *References Cited* (228 in total). Chapters and sections are not numbered. The main section titles speak for themselves: *Introduction* (Objectives and Purpose of the investigation), *Sulfidic Origin of Caves of the Guadalupe Mountains, Origin of Major Deposits of Native Sulfur,* and *Methane as Microbial Foodstuff.*

Further, the sections are split into chapters, and the main one (*Sulfidic Origin …*) also into sub-chapters. Its chapters and sub-chapters (shown in brackets below) are as follows: *Geographic and Stratigraphic Setting of Caves, Peculiar Qualities and Unusual Origin of Caves, Role of Sulfuric Acid in Cave Formation, Attributes of Hydrogen Sulfide Transported to the Caves (Curious Sulfur Isotopic Composition, Microbial Derivation, Immense Quantity), Sources and Pathways of Hydrogen Sulfide: Previous Models (The Existing Shelfal Model, The Existing Basinal Model*, *Modified Basinal Model: Source of Hydrogen Sulfide and its Pathway to Caves (Beginning of Intense Cavern Formation, Formation of Basinal Hydrologic Pathways, Generation and Migration of Methane in Late Tertiary of Western Delaware Basin, Reaction between Methane and Sulfate Anions in Late-Tertiary of Western Delaware Basin, Transit of Hydrogen Sulfide-Charged Water through Conduits within Castile Halite into Capitan Formation, Progressive Oxidation of Hydrogen Sulfide from Southwest to Northeast along the Cave Belt and from Higher to Lower Elevations within Individual Caves), Dissolution of Castile and Salado Halite and Gypsum by Epigenic Groundwater.* (Sub-subchapters, if they exist, are omitted from this list.)

The text is clear though very compact. Statements are concise and well founded, based either upon the author's original findings, or upon extensive, partly quite specialized, literature. Figures (mostly drawings) are clear, without irrelevant padding. A parallel product of the paper is the introduction of some less widely known geomorphic terms, such as *castile*, which have become important in discussions of evaporite karst.

The complexity of the central issue and the main ideas may be exposed by a few citations from the Summary. "*An immense weight (millions of metric tons) of microbial hydrogen sulfide (H_2S) moved into caves of the Guadalupe Mountains during the late Miocene and early Pliocene (~12–4 million years ago). The H_2S reacted with O_2 chiefly within subaerial water of condensation to form sulfuric acid (H_2SO_4) - the primary cave-forming agent ... The caves formed within … reefal limestone … and within adjacent, time-equivalent, shelfal carbonates ...*" (p.61); "*… the H_2S involved in speleogenesis was probably transported into the evolving caves from the adjoining Delaware Basin through upwardinclined pathways within Castile halite ...*" (pp. 61); "*Two approximately coeval Late Tertiary events superimposed on the consistent Castile stratigraphic framework resulted in intense H_2S-H_2SO_4 speleogenesis in the Guadalupe Mountains. These events were • high-heat flow, …, and • eastward tilting of the paleo-Guadalupe tectonic block, ...*" (pp. 61); "*The free convective process resulted in chambers being dissolved vertically upward within the Halite I Member until they contacted the intact base of the next overlying bed of anhydrite …, which dipped uniformly eastward over thousands of square kilometers. Then, by the same process of convective dissolution, but in an abrupt change in dip (from ~90° to < ~1°) and in direction of dip (from upward to westward), anhydrite-capped voids advanced up the slight homoclinal slope for up to several tens of kilometers. The solvent, nearly saturated with $CaSO_4$, no longer readily dissolved anhydrite. The conduits, …, were confined to halite. The width of dissolution conduits is inferred to have been narrow (< ~30 m); their height, low (< ~2 m); and their length, long (up to tens of kilometers).*" (pp. 61-62); "*Halite dissolved most actively … where solutionally aggressive groundwater directly contacted halite. Here, the convectively flowing groundwater abruptly and diametrically changed direction. Just beneath rising aggressive water (in a two-way stream), brine saturated with NaCl flowed easterly within conduits directly down the slight slope of the homocline, and passed through fractures, breccias, and voids within the Anhydrite I Member and drained into sandstone of the Bell Canyon Formation. Growing conduits continuously advanced westerly up the homoclinal slope as the ascending, aggressive groundwater dissolved halite. Many conduits eventually contacted the steep face of the reef or the steep face of the forereef; here Castile halite was flush against Capitan carbonates.*" (pp. 62); "*The "cave belt" of the Guadalupe Mountains, a six-kilometer-wide band parallel to and including the Capitan reef, has a northeast-southwest trend across the uniformly eastward dipping, Guadalupe tectonic block. Because of this configuration, on uplift of the homoclinal tectonic block the highest elevation of the cave belt was to the southwest. Erosion, which generally progressed down the tectonic block from west to east, probably initially removed the stratal cover … from the most elevated southwestern part of the cave belt. In step with intermittent uplifts, erosional removal of the evaporitic cover from the cave belt probably progressed to the southeast over millions of years.*" *(pp. 62); "A primary control over both H_2S–H_2SO_4 speleogenesis in the Guadalupe Mountains and H_2S–S genesis in the Delaware Basin was availability of O_2. Abundant H_2S … charged the sluggishly moving*

groundwater in the lower part of the ancestral Capitan aquifer, which over much of its extent coincided (in plan) with the cave belt. O_2 was dissolved within groundwater in the upper part of the aquifer in meager concentrations, and generation of minor quantities of aqueous H_2SO_4 at a pycnocline may have resulted in incipient caves. Intense speleogenesis began only when atmospheric O_2 became available to these initially formed caves." (pp. 62); "*… during an interval of ~8 Ma - with additional episodes of uplift, descent of the water table, and erosion of the cover- speleogenesis descended progressively in steps both within the slightly inclined (<0.5°) northeast-trending cave belt and within individual caves.*" (pp. 62); "*A genetic and geographic relationship exists between caves of the Guadalupe Mountains and large deposits of native sulfur … beneath the adjacent Gypsum Plain. The deposits and the caves probably formed at about the same time, and they probably both owe their existence to a coincidence of essentially the same stratigraphic, thermal, biogenic, and tectonic events.*" (pp. 62+).

Kirkland's work has shed a quite new light upon the understanding of speleogenesis in general and is an essential "must read" for every serious, 21st century, karstologist. The present reviewer presumes that the (listed) peer reviewers would share this opinion.

The book is distributed by the National Cave and Karst Research Institute, 400-1 Cascades Ave., Carlsbad, NM 88220, USA; www.nckri.org. The file can be downloaded at http://nckri.org/about_nckri/nckri_publications.htm.

France Šušteršič

9th INTERNATIONAL SYMPOSIUM OF SUBSURFACE MICROBIOLOGY ISSM 2014

October 5-10, 2014, Pacific Grove, California, USA

The 9th International Symposium on Subsurface Microbiology in Pacific Grove, California, attracted 228 scientists, engineers, and students from 25 countries and 5 continents. The symposium offered four plenary sessions, ten regular sessions and two poster sessions. Since the last meeting in 2011, a great deal of new knowledge was adopted and for this reason the organizers decided to combine contributions into the following topics: Biomes, Chemistry, Contaminants, Ecology, Fate and Methods. A special session within Biomes was also dedicated to Cave, Karst, and Fractured Rock Microbiology.

Recent developments, especially in metagenomics, facilitated scientists to stretch their research above the general question "who is there" towards the question "what do they do". Nevertheless, proper and quantitative DNA isolation is the most critical step to obtain the relevant results in downstream applications. It was emphasized that physical proximity of microbial communities in the subsurface is not necessarily related to the similarity among these communities. Surface sediments were found less diverse than the subsurface ones. Such understudied environments offer a great potential for isolation of microbes of biotechnological importance, for example those which can resist high ionic conditions.

New borders of our knowledge on microbial habitability have been drawn. For example, the largest aquifer on the planet is the ocean crustal aquifer, where hydrothermal vents are typically found, and the environmental conditions can be highly varying, e.g. pressure from 150 to 500 bar and temperature from 4 to 350 °C. On the other hand, large datasets of bacterial diversity can help "to predict" geochemical characteristics. It seems that microbial structure has "memory" of past environmental conditions. Diverse microbes were found in the Precambrian rock, can we consider these rocks the oldest habitat on Earth?

Microbial metabolism was the focus of several oral and poster presentations. Abundant polysaccharide biofilms in the form of reduced sugars can act as an "electron sink". However, sometimes the environmental conditions, such as the presence of clays, can make microbial to uptake of essential nutrients, such as nitrogen, more difficult. Microbial conversions of dissolved organic matter can occur faster than previously thought in underground karst rivers. Going deeper into the subsurface, autotrophy can in some cases notably exceed heterotrophy. On the other hand, serpentinization, which results in formation of H_2 as an energy source, does not always increase microbial biomass because CO_2 can be a limiting factor.

Electromicrobiology is a rather novel microbiological subdiscipline which has lately attracted more scientific attention. Microbes are able to transport electrons directly from minerals, using nanowires or along cell filaments. It was proven that electric current can be produced on pyrite. Filamentous bacteria, also called "cable bacteria", can produce an electric field when the circuit of electrons is coupled with the circuit of ions. Microbial activity on the sea floor gives approximately 20 mW/m^2.

Biodegradation and remediation of contaminated sites is a very challenging topic for microbiologists. It was recently proven that biodegradation of oil occurs with the minimum presence of water. Namely, the presence of an electron acceptor, i.e. sulphate, is in such systems crucial for biodegradation. Radioactive contaminated sites in the U.S. (Manhattan project from the WWII) and Russia (Karachay Lake with more than 42,000 mg of NO_3^- per liter) are especially challenging in terms of microbial metabolism and diversity. The impact of hydraulic fracturing which introduces organic C and allocthonous microbes in the subsurface is not studied enough.

Water quality and pollution is a global urgent issue, with the respect of water usage increase of 1% annually. New developed tools to predict scenarios of fecal pollution are thus highly welcome. An important global issue related with climate changes is the release of organic C from permafrost.

The new president of the society became Reiner U. Meckenstock and the next ISSM symposium will in 2017 in New Zealand.

Janez Mulec

Acta carsologica

43, 2-3 (2014)

Izdala in založila / Published by
Slovenska akademija znanosti in umetnosti / Slovene Academy of Sciences and Arts
in / and
Znanstvenoraziskovalni center SAZU / Scientific Research Centre of the SASA
v Ljubljani / in Ljubljana

Grafična priprava in tisk / Layout and print
Inženiring grafičnih storitev, d.o.o., Ljubljana

Naklada 500 izvodov / Printed in 500 copies

Organizacija Združenih narodov za izobraževanje, znanost in kulturo

United Nations Educational, Scientific and Cultural Organization

Slovenska nacionalna komisija za UNESCO

Slovenian National Commission for UNESCO

ACTA CARSOLOGICA
ISSN 0583-6050 · LETNIK/ VOLUME 43 · ŠTEVILKA/NUMBER 2–3 · LJUBLJANA 2014

ISSN 0583-6050
9 770583 605015